UNIVERSITY OF SOUTHAMPTON

FACULTY OF ENGINEERING, SCIENCE AND MATHEMATICS

School of Mathematics

Mathematical Modelling of MEMS Viscometers and Densitometers

by

Kelly Anne Ronaldson

Thesis for the degree of Doctor of Philosophy
April 2006

UNIVERSITY OF SOUTHAMPTON

ABSTRACT

FACULTY OF ENGINEERING, SCIENCE AND MATHEMATICS

SCHOOL OF MATHEMATICS

Doctor of Philosophy

MATHEMATICAL MODELLING OF MEMS VISCOMETERS AND DENSITOMETERS

by Kelly Anne Ronaldson

Measurements of the density and viscosity of fluids are required to determine optimal production strategies in the exploitation of fossil fuel reservoirs and the monetary value of the fluid produced. In this work, we consider the analysis of two different designs of Micro Electrical Mechanical Systems (MEMS) that have been developed to determine both density and viscosity of fluids in situ.

The first device is a transversely oscillating plate, known as the spider. It is about 1.6 mm wide, 2.4 mm long and 20 μm thick. It is suspended from a 0.4 mm thick support by 24 square cross-section legs each of length 0.5 mm. Mathematical models have been produced for the plate operating in either forced or transient mode, intended for use in both Newtonian and non-Newtonian fluids. We only consider the general case of incompressible fluids, using the one dimensional diffusion equation to model Newtonian fluid motion and a reduced form of Maxwell's equations for viscoelastic fluid motion.

The second MEMS device is based on a vibrating plate clamped along one edge, with dimensions of the order of 1 mm and a mass of ≈ 0.1 mg. The plate is set in motion when an alternating current is passed through the coil mounted on the plate in the presence of a magnetic field. At resonance, the plate motion is observed using a strain gauge. Mathematical models have been used in different limiting cases to analyse the behaviour of the device. Densities in the range (1 to 1800) kg m^{-3} and viscosities in the range (10 to 300000) Pa·s were determined experimentally with the vibrating plate in argon, methane, nitrogen, n-octane, methylbenzene and heptane.

Contents

List of Figures

Unless otherwise stated, all diagrams were produced by the author. Photographs were taken by Miss Claire Jakeways at Schlumberger Research Cambridge.

List of Tables

Nomenclature

chapter 2

ρ	density of fluid mass (kg/m^3)	q	component of fluid velocity (m/s)
V	volume of fluid (m^3)	p	pressure (Pa)
τ	stress (Pa)	τ_y	yield stress (Pa)
γ	shear rate (1/s)	K, n	constants in Herschel-Bulkley
κ_T	compressibility (1/Pa)		formulation (Pa·s^k),(-)

chapter 3

Torsional decay

$\alpha(\tau)$	angular displacement (-)	ω_0	angular frequency (1/s)
T_0	period of oscillation (s)	τ_0	dimensionless time (-)
Δ_0	logarithmic decrement (-)	I	moment of inertia (kg·m^2)
$m(\tau)$	torque (kg·m^2/s^2)	$S, \hat{S}$	complex roots (-)
D	Laplace transform of torque (kg·m^2/s^2)	ω	frequency (1/s)

Oscillating disc

ϕ, φ	angular amplitudes (-)	T	period of oscillation (s)
ρ	fluid density (kg/m^3)	δ	boundary layer thickness (m)
μ	fluid dynamic viscosity (kg/m/s)	β	dimensionless separation (-)
σ	complex circular frequency (-)	R	disc radius (m)
b	harmonic mean distance (m)		

Quartz-crystal

M	mass (kg)	S	surface area (m^2)
f	resonant frequency (1/s)	Δ_{fluid}	damping due to fluid (-)
ν	viscosity (kg/m/s)		

Concentric-cylinders

T	torque (kg·m^2/s^2)	Ω	angular velocity (1/s)
l	immersion depth (m)		

Vibrating wire

R	radius (m)	T	tension (kg/s^2)
D_b	drag force (kg/m/s)	D_0	coef. of internal damping (kg/m/s)
ω	angular frequency (1/s)	ρ_s	rod density (kg/m^3)
F	force (kg/s^2)	I	2nd moment of area (m^4)
E	Young's modulus (kg/m/s^2)	m_s	rod mass (kg/m)
m_b	added mass (kg/m)	y_0	max initial displacement (m)
$\phi_j(\zeta)$	eigenvectors (-)	ξ_j	displacement (-)
g_m	amplitude of transient force (-)	$\epsilon\Omega$	Reynolds number (-)
ϵ	max amplitude of motion (-)	c	sonic velocity (m/s)
Ma	Mach number (-)	K_0, K_1	modified Bessel functions (-)
k, k'	parameters (-)	ζ	distance (m)
$2l$	length of wire (m)		

chapters 4-5

$\mathbf{B}$	magnetic field (A/m)	I	alternating current (A)
Q	quality factor ($\frac{f_{res}}{2g}$)	f_{res}	resonant frequency (1/s)
ν	kinematic fluid viscosity (m^2/s)	ρ	fluid density (kg/m^3)
$\mathbf{F}_{er}$	elastic restoring force ($kg/m/s^2$)	l	leg length (m)
d	plate/leg thickness (m)	E	Young's modulus ($kg/m/s^2$)
A	amplitude of motion (m)	M_p, m	plate mass (kg)
a	plate length (m)	B	plate width (m)
ω_v	undamped/vacuum frequency (1/s)	N	number of legs (-)
c_p	specific heat capacity ($m^2/s^2/K$)	ρ_s	plate density (kg/m^3)
L	approx amplitude of oscillation (m)	U	approx plate speed (m/s)
μ	dynamic fluid viscosity (kg/m/s)	k	spring constant (kg/s^2)
R	resistance in wire ($m^2 \cdot kg/s^3/A^2$)	I	current in wire (A)
δ	depth of wave penetration (m)	ω	frequency of oscillation (1/s)
T	temperature (K)	y	distance from plate (m)
t	time (s)	q	plate velocity (m/s)
U_p	plate velocity in x-direction (m/s)	U_0	arbitrary initial velocity (m/s)
$\mathbf{v}$	fluid velocity (m/s)	p	pressure ($kg/m/s^2$)
h	height of added plate (m)	G	shear modulus of fluid (GPa)
θ	$= \frac{\mu}{G}$ (s)	γ	$= \arctan \frac{1}{\omega\theta}$ ($GPa \cdot s^2/m^2$)
σ	stress (Pa)	S	frictional force ($kg/m/s^2$)
P	power ($kg \cdot m^2/s^3$)	r	internal damping (kg/s)
ω_0	initial frequency (1/s)	ω_m	max recorded frequency (1/s)
A	$= \frac{r}{\rho_s B d a}$ (1/s)	B	$= \frac{k^2}{\rho_s B d a}$ ($1/s^2$)
C	$= \frac{2}{d\rho_s}$ (m^2/kg)	E	$= \mathsf{C}\sqrt{\mu\rho}$ ($1/s^{\frac{1}{2}}$)
W	weight of plate (kg)	X	initial displacement (m)
$\tilde{t}$	non-dimensionalised time ($\frac{k}{\sqrt{W}}t$) (-)	Δt	time-step (s)
$\tilde{x}$	non-dimensionalised distance ($\frac{x}{X}$) (-)	α	damping coefficient ($\frac{r}{k\sqrt{W}}$) (-)
β	damping coefficient ($\frac{2\sqrt{\mu\rho}Ba}{\sqrt{k\pi}W^{\frac{3}{4}}}$) (-)	ς_1, ς_2	constants in equation (5.9)
ϖ_1, ϖ_2	constants in equation (5.16)	ϑ	constant in equation (5.52)
φ_1, φ_2	constants in equation (5.69)	Υ_1, Υ_2	constants in equation (5.82)
Γ	gamma function	p	stability polynomial

chapter 6

D	flexural rigidity ($\frac{Ed^3}{12(1-\sigma^2)}$) ($kg \cdot m^2/s^2$)	$\mathbf{F}$	force normal to plate surface ($kg \cdot m/s^2$)
σ	Poisson ratio (-)	E	Young's modulus ($kg/m/s^2$)
A_0	arbitrary initial amplitude (m)	b_f	$\sqrt{\omega_n}\left(\frac{\rho_s d}{D}\right)^{\frac{1}{4}}$ (1/m)
ω_n	natural frequency of oscillation (1/s)	ϵ	perturbation quantity (m)
S	$= \sinh(ba) + \sin(ba)$ (-)	C	$= \cosh(ba) + \cos(ba)$ (-)
f	frequency ($\frac{\omega}{2\pi}$) (1/s)	$q(x,z,t)$	displacement of plate (m)
Φ	potential (m^2/s)	Ψ	stream function (m^2/s)
$\mathbf{x}$	arbitrary point in fluid (x, y, z)	$\boldsymbol{\gamma}$	stokeslet position $(\gamma_1, \gamma_2, \gamma_3)$
h	distance from plane $z = 0$ (m)	F_k	point force ($kg \cdot m/s^2$)
r	$= \lvert\mathbf{x} - \boldsymbol{\gamma}\rvert$ (m)	R	$= \lvert\mathbf{x} - \boldsymbol{\gamma}'\rvert$ (m)
$\boldsymbol{\gamma}'$	$= (\gamma_1, \gamma_2, -h)$	ξ_1, ξ_2	constants in equation (6.87) (-)

Acknowledgements

I should like to extend my sincere appreciation to my supervisors, Prof. A. D. Fitt and Prof. W. Wakeham, and my advisor, Prof. C. P. Please, for their continuous advice, encouragement and guidance throughout this research.

I am also grateful to my industrial advisor Dr. A. R. H. Goodwin, for his valuable contributions on technical issues, Schlumberger Research Cambridge, for providing the resources and laboratory facilities, Maria Manrique de Lara for the finite element calculations using ANSYS and Miss Claire Jakeways for carrying out the majority of the experiments.

Finally, I am deeply grateful to my husband, Luke, for his patience and support over the last three years.

Chapter 1

Introduction

The main aim of this thesis is to understand the mathematical modelling behind oscillating body viscometers and then use this understanding to model new viscometers intended for use with fluids. In particular, the instruments will be used experimentally in the oil industry, testing the fluids present while drilling for oil.

We begin by describing viscosity and different fluid properties, in particular those of oil, with a brief discussion of other reservoir fluids. Newtonian and non-Newtonian fluids will be described and mathematical equations and models will be specified for the use of each. We will then give a description of some previously modelled viscometer designs ranging chronologically from falling body viscometers, through oscillating bodies, to vibrating wires. The limits to the success of each will be discussed in an attempt to determine their usefulness as down-hole *in situ* viscometers.

We will then consider the analysis of two new viscometer designs that take the form of oscillating plates, fabricated from silicon using the methods of Micro-Electro-Mechanical-Systems (MEMS). We will describe oscillating MEMS devices intended for use with down-hole fluids such as crude oil or brine. The viscometers are needed to measure the thermo-physical properties of fluids *in situ*, to determine optimal production strategies and exploit the value of the fluids in the well. We recognise that a trade-off may have to be made between accuracy and the ability to withstand hostile environments and measure fluid properties over a wide range of conditions. It will be shown that conventional viscometers are currently unsuitable for measurements *in situ* for a number of reasons, suggesting that the development of a new viscometer that will both remain sufficiently accurate in hostile conditions and reflect both Newtonian and non-Newtonian fluid motion would be advanta-

geous in this field.

This work has been carried out in co-operation with Schlumberger Research Cambridge. Their research into the production of MEMS sensors commenced a number of years before this thesis was written. With their extensive knowledge of the oil industry, Schlumberger have provided valuable information regarding down hole drilling, methods of oil analysis, the production of MEMS sensors and the industry in general. An aim of this work is to analyse and optimise the performance with respect to uncertainty of Schlumberger's existing viscometers and to aid in the design of future MEMS sensors.

Chapter 2

Fluid viscosity

2.1 The properties of oil

The analysis of oil is carried out for a wide range of fuel applications. Industrial hydraulic oils, turbine oils, and diesel and gasoline engine oils all undergo a series of laboratory tests. Technological advances in both machinery and instrumentation has made the testing considerably more cost effective. Numerous different tests can be used to evaluate lubricants. The choice of these is dependent on the information required and a comparison of time, cost and accuracy necessary to complete each individual test. Testing is required to measure physical properties of the oil, the most common tested properties being viscosity, acidity and alkalinity.

It is also valuable to know the level of contamination of oil, particularly in determining machinery wear rates for hydraulic oils. Therefore oil is also tested by particle count, water content and wear metal analysis. A particle count quantifies the levels of particles at various sizes in a fluid sample. The particles can damage machinery components, so high levels need to be reduced. The presence of metallic elements is determined using a technique such as Spectrometric Analysis, Infrared Analysis (FT-IR) or Rotrode Filter Spectroscopy (a spectroscopic method using a rotating carbon disc electrode spectometer). Serious wear problems can occur from high levels of copper, lead, iron, aluminium or tin. The presence of water is also not desirable. Excessive amounts destroy lubricity and promote corrosion of metal parts. Measuring the total acid number (TAN) and total base number (TBN) can also determine a fault in the oil sample. The total base number is a measure of the oils' ability to neutralise acid and the total acid number is a measure of the acid and acid-like material in the oil. Alkalinic additives that enhance lubricity can become depleted or acidic

by-products may be formed that are corrosive to metals.

The effective analysis of oil is extremely beneficial. In the case of hydraulic fuels this can increase production efficiency and component life, and shorten equipment downtime. For engine oils the result is prolonged engine life due to extended oil change intervals. This is increasingly important since the future availability of engine oils is currently being questioned and the prices continue to rise. Viscosity is undoubtedly the most important of the lubricant's physical properties. In the fuel industry it is essential to know an accurate value for viscosity because this data determines the necessary temperatures for pumping, injection and storage of the fuel. Residual fuels can be classified by their kinematic viscosity. Kinematic viscosity is a gauge of the degradation of the lubricant, measured in m^2s^{-1} (SI units) at a specified temperature. The break down of a hydraulic fuel or petroleum based engine oil is indicated by an increase in viscosity. This is also true to a lesser extent for synthetic or partially synthetic based engine oils. The viscosity of the lubricant is projected to increase with use but a rapid jump can indicate a more serious problem such as a cooling system failure. A decrease in viscosity is often more severe and could be an indication of contamination or fuel dilution.

The viscometers that we will be modelling are intended for, but not limited to, use with down-hole fluids such as crude oil or brine. In oil exploration, the viscosity can indicate the mobility of the reservoir fluid, its flow characteristics and the commercial value of the reservoir fluid. Currently, samples are collected from the reservoir and later analysed at the surface in a laboratory. It would be more useful if samples could be taken on a more frequent basis and the properties determined down-hole. The fluid properties and composition of a reservoir will change during its lifetime making it hard to simulate reservoir conditions in a laboratory. A typical hydrocarbon reservoir exhibits temperatures between (323 to 448) K at pressures of (10 to 200) MPa [1]. These conditions can be recreated but it is difficult to replicate other effects such as fluid contamination and solid deposition. Evidently the production of a small-scale viscometer that can be used down-hole would be advantageous in this field.

2.2 The Notion of Viscosity

Viscosity describes the internal friction of a moving fluid and its adhesive/cohesive or frictional properties. The internal molecular resistance within the fluid produces a frictional drag effect. A high viscosity means greater internal friction, so the fluid is more inclined to resist motion. A low viscosity results in less friction during motion so the fluid flows easily. Viscosity can also be defined as a transport property because momentum is transported across a velocity gradient. [2] describes viscosity thus:-

The resistance arising from the want of lubricity in parts of a fluid is, other things being equal, proportional to the velocity with which the parts of the fluid are separated from one another

The proportionality constant referred to above is the viscosity. It is a function of molecular mass, temperature, and collision diameter. This basic idea of absolute viscosity is termed "dynamic viscosity" however kinematic viscosity, that is the ratio of the absolute viscosity to the density, may also describe a fluid.

2.3 Viscosity of Newtonian Fluids

For our simple fluid model, we will assume that the fluid does not contain a mix of oil and non-Newtonian drilling muds. Instead we assume that the fluid is a homogeneous liquid with one density and one viscosity value. The classical theory of viscous fluids is based upon two equations, one for momentum and a continuity equation. The principle of conservation of mass produces the continuity equation [3],

$$\frac{\partial \rho}{\partial t} + \nabla.(\rho \mathbf{q}) = 0$$

where ρ is the density of the fluid mass and $\mathbf{q}$ is the velocity. Under the assumption of incompressibility, i.e. constancy of mass density (ρ), this reduces to

$$\nabla.\mathbf{q} = 0.$$

The conservation of momentum equation states that the rate of change of momentum for any volume $V(t)$ of fluid is equal to the force exerted on the fluid in V. Assuming that the only forces acting on $V(t)$ are at its boundary due to the viscous forces exerted by the surrounding fluid, and assuming the viscosity (ν) is constant, this equation becomes

(2.1). These two equations combine to give the Navier-Stokes equations for the motion of an incompressible Newtonian fluid [3]:

$$\mathbf{q_t} + (\mathbf{q}.\nabla)\mathbf{q} = -\frac{1}{\rho}\nabla p + \nu\nabla^2\mathbf{q} \tag{2.1}$$

$$\nabla.\mathbf{q} = 0 \tag{2.2}$$

where p is the pressure. Fluids are Newtonian if the first equation holds and thus obey Newton's law of viscosity. Such fluids have a constant viscosity and density at a constant temperature and pressure. The governing equations for stress and velocity distribution in an incompressible Newtonian fluid can be fixed for any flow system from the values of these two material constants.

2.4 Non-Newtonian Fluids

Non-Newtonian fluids have a variable viscosity at a constant temperature. The viscosity can vary with the rate of shear and hence is referred to as "shear-rate dependent" viscosity. Fluids that show decreasing viscosity with increasing shear rate are described as shear thinning or pseudoplastic. This effect can be quite dramatic and viscosity can reduce by a factor of 10^2 to 10^3 [4]. Some shear thinning fluids are shampoo, slurries, fruit juice concentrates and ketchup. A fluid is shear thickening or dilatant if viscosity increases with increasing shear rate, for example wet sand. The viscosity of a viscoplastic fluid increases proportionally with shear stress and rate of shear but does not start to flow until a certain critical shear stress called the yield-stress has been exceeded. Below this critical value, flow becomes negligible. Examples of such fluids would be certain greases. The plastic property is the fact that the fluid has a so-called yield value. Some plastic fluids are tomato paste, toothpaste and hand cream. Most fluids can be divided into one of the following three categories; a viscous fluid, an elastic fluid or a viscoelastic fluid. In a purely viscous fluid all energy added is dissipated into heat, whereas in a completely elastic fluid all the energy added is stored in the fluid and stress is directly proportional to strain. Stress is the force per unit area acting on the fluid causing it to change its dimensions and strain is the percentage deformation of the fluid when subjected to a load. A viscoelastic fluid exhibits both viscous and elastic behaviour. If a stress-strain curve is drawn for a viscoelastic fluid there are two notable points of interest. The proportional limit is the point where derivation from a linear relationship occurs. The elastic limit is the point at the maximum stress the

fluid can absorb and still return to its original dimensions.

For each of these types of non-Newtonian fluid, Newton's law of viscosity is not a suitable description. We can measure density in an incompressible non-Newtonian fluid but we have no analogous equation for the shear stress. Viscosity can no longer be assumed constant and shear stress must also be measured. Unlike a Newtonian fluid, experiments yield a number of material functions that can depend on time, frequency, shear rate and a host of other variables.

When testing is carried out during drilling for oil, it must be recognised that some of the additives to the drilling fluids are also non-Newtonian. One example is sodium bentonite, added to increase the density of the drilling mud. The properties of such muds can change after interaction with soil or water, and exhibit different rheological behaviours. One such behaviour is to reach a yield stress then come into a Bingham phase. Alternatively a Herschel-Bulkley law is often an adequate description [5]. Increasing the concentration of bentonite in the suspension in either case seems to lead to an increase in viscosity.

2.5 Herschel-Bulkley Fluids

The Herschel-Bulkley model is a general mathematical model for viscosity that may be used to express non-Newtonian characteristics. Its formulation is

$$\tilde{\tau} = \tau_y + K\tilde{\gamma}^n \tag{2.3}$$

where $\tilde{\tau}$ is the stress, τ_y is the yield stress, $\tilde{\gamma}$ is shear rate, and K and n are constants. In the special case when $n = 1$ and $\tau_y = 0$, the fluid is Newtonian and K is the Newtonian viscosity μ. For shear-thinning fluids $n < 1$ and for shear thickening fluids $n > 1$. When $n = 1$ (2.3) is reduced to the Bingham model.

$$\tilde{\tau} = \tau_y + K\tilde{\gamma} \tag{2.4}$$

In this case, K is constant and represents the plastic viscosity of the fluid. A minimum application of stress (τ_y) is required to cause a flow and once this has been reached the fluid behaves as a Newtonian fluid. A plot of shear stress and shear rate for each of the described models is shown in figure (2.1). Another property of non-Newtonian fluid motion is its relation with time. Previously mentioned models all apply to the motion of time-

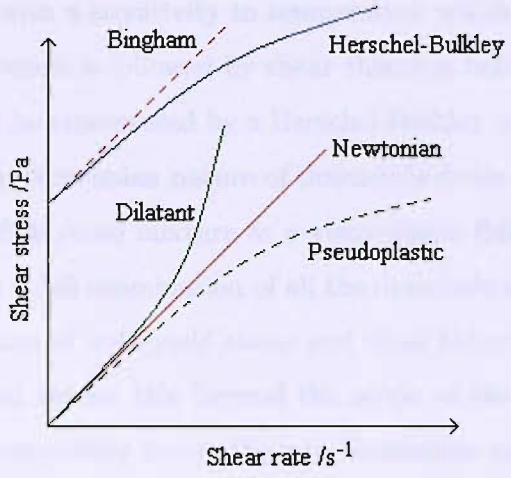

Figure 2.1: Non-Newtonian fluid behaviour

independent fluids, the viscosity is not influenced by the time of applied shear. In some fluids a dependency on the time subjected to a shear force can be seen. A fluid whose apparent viscosity decreases with the time of shearing and then recovers its original viscosity after a period of rest is referred to as 'thixotropic' or time thinning. An example would be yoghurt or paint. Fluids that are time thickening, also known as rheopectic, are less common. One example of a fluid exhibiting such behaviour is gypsum paste. A fluid is known as rheopectic if the apparent viscosity increases with time of shearing and again reverts to the original viscosity after rest. Throughout this work we shall consider time-dependent non-Newtonian fluid motion.

At present the rheology of reservoir fluids is usually measured at ambient surface conditions. These results are then later extrapolated to down-hole conditions. This requires a good model of how fluids are affected by temperature and pressure down-hole, an area which is still not fully understood. This could be due to the inadequacy of using two parameter equations, such as the Bingham model, to make measurements of shear rheology. Some experimental evidence exists that appears to show that down-hole fluids may be modelled as Bingham fluids. The difficulties involved with Bingham fluid formulation unfortunately mean that analytical techniques are extremely challenging to pursue. The rheology of reservoir muds such as bentonite is influenced by many factors such as temperature, pressure, composition and shear history, and it is difficult to isolate the effects of each. Schlumberger have carried out rheological tests on a number of water-based muds, such as may be present in an oil reservoir, at temperatures up to 403 K and pressures to 100 MPa [6]. From these results it has been deduced that muds have a largely pressure

independent yield stress with a sensitivity to temperature which increases with increasing temperature. This yield stress is followed by shear thinning behaviour. It was found that this behaviour could best be represented by a Herschel-Bulkley model. Many authors have discussed the possible non-Newtonian nature of down-hole fluids. [6] suggests that it may be reasonable to treat a fluid/mud mixture as a visco-elastic fluid. As far as this thesis is concerned, we realise that a full examination of all the downhole properties of drilling muds should include consideration of both yield stress and shear thinning effects. Unfortunately the complications involved render this beyond the scope of the current work. However, since we do not wish to completely ignore the non-Newtonian nature of drilling muds, we will give some attention to visco-elastic models, which by their nature preserve the linearity of the governing equations.

2.6 Maxwell Fluids

A visco-elastic fluid possesses both viscous and elastic properties and it is useful to have a single equation combining the two. We can define visco-elastic fluid motion using Maxwell's equations

$$\mathbf{v}_t + (\mathbf{v}.\nabla)\mathbf{v} = -\frac{1}{\rho}\nabla p + \nabla.\sigma \tag{2.5}$$

$$\nabla.\mathbf{v} = 0 \tag{2.6}$$

with the stress tensor, σ_{ij}, given by

$$\sigma_{ijt} + (\mathbf{v}.\nabla)\sigma_{ij} - \frac{\partial v_i}{\partial x_k}\sigma_{kj} - \frac{\partial v_j}{\partial x_k}\sigma_{ki} + \frac{1}{\theta}\sigma_{ij} = \frac{\nu}{\theta}\left(\frac{\partial v_i}{\partial x_j} + \frac{\partial v_j}{\partial x_i}\right) \tag{2.7}$$

where $\mathbf{v}$ is the fluid velocity, $\theta = \frac{\mu}{G}$ and G is the shear modulus of the fluid. We can simplify these equations if we assume that $\mathbf{v}$ is of the form $\mathbf{v} = [u(y,t), 0, 0]$ and all of the stresses are functions of y and t alone, so that motion is thus independent of x. If this is the case, a number of terms vanish from (2.7) leaving the simplified equations

$$\sigma_{11t} - 2u_y\sigma_{21} + \frac{1}{\theta}\sigma_{11} = 0 \tag{2.8}$$

$$\sigma_{22t} + \frac{1}{\theta}\sigma_{22} = 0 \tag{2.9}$$

$$\sigma_{12t} - u_y\sigma_{22} + \frac{1}{\theta}\sigma_{12} = \frac{\nu}{\theta}u_y \tag{2.10}$$

$$\sigma_{21t} - u_y\sigma_{22} + \frac{1}{\theta}\sigma_{21} = \frac{\nu}{\theta}u_y. \tag{2.11}$$

Since $\sigma_{ij} = \sigma_{ji}$ by symmetry of the stress tensor, we have $\sigma_{21} = \sigma_{12}$ so equation (2.11) does not supply any extra information. From (2.9), we find that $\sigma_{22} = A(y)e^{-\frac{t}{\theta}}$, where $A(y)$ is an arbitrary function of y. Assuming that $\sigma_{22} = 0$ at $t = 0$, we find that $\sigma_{22} \equiv 0$ is a solution. (2.8) decouples as σ_{11} does not appear elsewhere, so we are left with the single equation

$$\sigma_{12t} + \frac{1}{\theta}\sigma_{12} = \frac{\nu}{\theta}u_y. \tag{2.12}$$

In a similar way, (2.5) is reduced to

$$u_t = \sigma_{12y}. \tag{2.13}$$

Differentiating (2.12) with respect to y and substituting (2.13) the resulting equation for fluid motion is

$$\frac{\partial^2 u}{\partial t^2} + \frac{1}{\theta}\frac{\partial u}{\partial t} = \frac{\nu}{\theta}\frac{\partial^2 u}{\partial y^2}. \tag{2.14}$$

We will use this equation further in a later chapter when considering the MEMS in viscoelastic fluids.

2.7 Stokes flow

With MEMS devices, due to their dimensions, it is typical to find Stokes flow. Stokes flow is a type of flow where the viscous forces are much larger than the inertial forces. The flow is described by the Navier-Stokes equations (2.1) with the inertial and body force terms equal to zero. The Reynolds number of a flow is a ratio of inertial forces, $U\rho$, to viscous forces, $\frac{\mu}{L}$. If flow has a small Reynolds number ($Re << 1$) it can therefore be considered Stokes flow. We can calculate an approximate value of the Reynolds number for the MEMS sensor by considering the equation

$$Re = \frac{LU}{\nu}$$

where L is an appropriate length scale, U a comparable speed and $\nu = \frac{\mu}{\rho}$ is the kinematic viscosity of the fluid. In this case we will use the amplitude of the plate oscillations for L, assuming that they are similar to the oscillations of the fluid close to the plate, and for U we will use the speed of these oscillations. Taking appropriate values for the sensor gives

$$Re = \frac{10^{-6} \times 10^{-2}}{\frac{10^{-3}}{10^3}} = 10^{-2} << 1$$

so the flow has a small Reynolds number and can be considered stokes flow. In the work of chapter 6 we will assume stokes flow throughout.

2.8 Viscosity of reservoir fluids

Liquids commonly encountered in oil reservoirs are chemically and compositionally complex. This means that despite existing correlations that relate viscosity to other fluid properties, these are not sufficiently accurate. For reservoir fluids there is a third parameter, other than temperature or pressure, which affects viscosity. This is the amount of gas in solution in the fluid. A decrease in temperature will cause the liquid viscosity to rise. An increase in pressure should cause an increase in viscosity however the higher the pressure, the more gas is in solution. An increase in the amount of gas in solution should cause a decrease in viscosity [7].

[7] suggests that reservoir fluids are compressible and defines the isothermal compressibility at constant reservoir temperature as

$$\kappa_T = -\frac{1}{V}\left(\frac{\partial V}{\partial P}\right)_T \tag{2.15}$$

where V is the original volume, P is the pressure and κ_T is the compressibility. Gas is considerably more compressible than the other reservoir fluids such as liquid hydrocarbons or water. The general order of magnitude of compressibility can be seen below.

Fluid	κ_T /psi^{-1}	Fluid	κ_T /psi^{-1}
Reservoir saline waters	3×10^{-6}	Gas at 1450 psi	689×10^{-6}
Undersaturated black oils	17×10^{-6}	Gas at 5800 psi	172×10^{-6}

These factors affect the volume of liquid collected at the surface. The volume of liquid will be less at the surface than at reservoir conditions due to changes in the three parameters. A pressure reduction will increase the volume but a temperature reduction will decrease the volume. The most significant factor is that a pressure reduction will decrease the solubility of gas causing a large decrease in fluid volume.

To summarise, for our simple fluid model, we are assuming that the fluid is a homogeneous liquid. When modelling non-Newtonian fluid motion we will consider fluids to be time-dependent such that the viscosity is affected by the time of applied shear. Despite the

complexity introduced by gas in the down-hole solution, the compressibility of the fluids are small so the amount of gas in solution will have negligible effect on viscosity in comparison to other important parameters such as temperature. For this reason we will be modelling the general case of incompressible fluids.

Chapter 3

Viscometers

In the previous chapter, some of the different properties of fluids were considered. We are now going to discuss the main topic of the thesis, namely the instruments used in the measurement of viscosity. The main purpose of this chapter is to analyse designs and methods for the measurement of viscosity that have been tried in the past. Let us start by briefly mentioning some early viscometer methods. The first set of devices to be discussed in more detail are torsionally oscillating body viscometers. Here we plan to describe the development from a cylindrical body to a flat metal disc and then finally to a quartz disc. From here, the progression to transversely oscillating wire viscometers will be shown. The chapter will conclude with a summary table in chronological order describing a selection of previously modelled instrument designs.

3.1 Early Methods

3.1.1 Falling body viscometers

This method mainly uses relative viscosity measurements although absolute measurements are possible [8]. In these instruments viscosity is determined by allowing a solid of revolution to fall through a sample fluid [9] [10]. The main assumptions behind the working equations are:

1. the body falls at constant terminal velocity,
2. the flow is fully developed,
3. the flow is laminar axial,
4. the flow is cylindrically symmetric.

The ideas behind this method continue to be brought up to date. In recent years a falling-needle has been used to incorporate the advantages of slender-body theory to simplify calculations of drag coefficients [11]. Although such methods are quite accurate, the free moving parts involved in such viscometers make them unsuitable for use down-hole.

3.1.2 Capillary viscometers

This type of instrument can be used as an absolute viscometer [8]. The main body is a small capillary tube of known length. The fluid is forced through by applying a pressure differential across the tube. The fluid viscosity (ν) is expressed in terms of the tube radius (r), pressure drop along the tube (P), length of tube (l) and volumetric flow rate (Q). The working equations are based upon the Hagen-Poiseuille equation of fluid dynamics [12].

$$Q = \frac{\pi P r^4}{8\nu l} \tag{3.1}$$

This equation implies that the flow rate is directly proportional to the radius^4 and is inversely proportional to the length of the tube, so greater flow is seen in shorter, wider capillary tubes. The suitability of this type of viscometer for down-hole use is in doubt for a number of reasons. Firstly there is the need for a device to produce constant fluid flow. Also, at high pressures, an external pressure will be needed to balance the internal one to prevent distortions occurring in the tube. In down-hole fluids, scale deposition problems are also possible.

3.2 Oscillating Body Viscometers

All of the viscometers discussed will contain the basic structural idea of a main oscillating body though they will all appear in slightly different forms. By evaluating the advantages and disadvantages of a selection of such devices it is hoped that the limits to the success of each can be determined. It will also be shown that some of the instruments have been used successfully in practical applications. However the accuracy is often reduced by assumptions in the mathematical modelling of the instrument or the physical constraints at non-ambient conditions, such as high temperatures and pressures. The information gathered suggests that a change to both the mechanical design of the viscometer and the mathematical equations supporting it is needed to model an accurate instrument for measuring non-Newtonian fluid viscosity. This suggests the development of a new viscometer that will both remain precise in hostile conditions and accurately reflect non-Newtonian fluid motion.

3.3 Torsionally Decaying Oscillators

Torsionally oscillating bodies have been used successfully in a number of viscometer designs. Accurate measurements are accomplished by observing the decay of oscillations of the axially symmetric body whilst suspended from an elastic strand. Once immersed in a liquid, the surrounding fluid causes torque on the body surface that increases the effective moment of inertia. This can be observed in one of two ways, by an increase in the logarithmic decrement of the amplitude of angular displacement and by an increase in the period of oscillation. Various devices have been used experimentally with fluid both internal and external to the oscillator, see figure (3.1). A typical radius for such a body would be 35 mm [15].

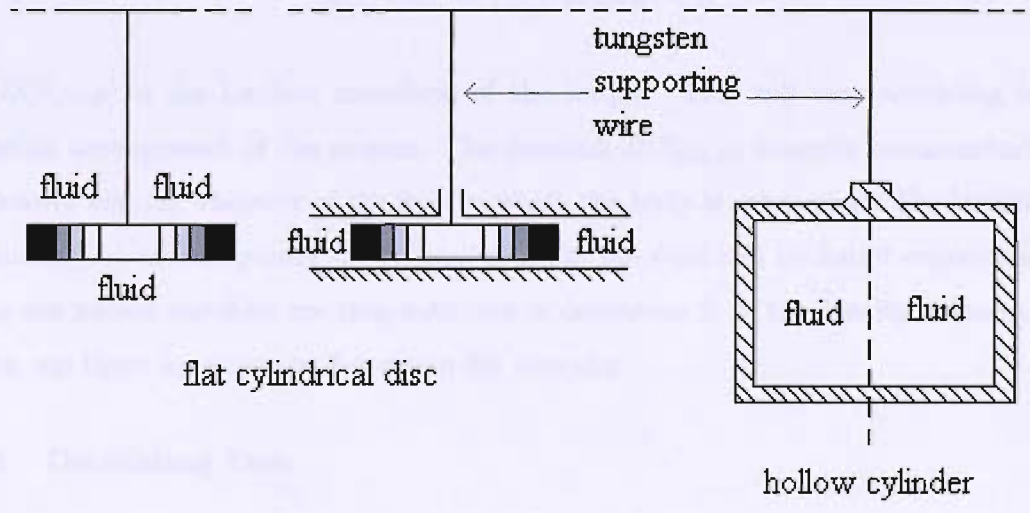

Figure 3.1: Oscillating body viscometer designs: a flat cylindrical disc in an infinite fluid, a flat cylindrical disc between parallel plates and a hollow cylinder with fluid internal

3.3.1 Theory of Torsional Decay

The motion of a torsionally oscillating body suspended in a sample fluid is described by the equation [12]

$$I\omega_0^2[\frac{d^2\alpha(\tau)}{d\tau^2} + 2\Delta_0\frac{d\alpha}{d\tau} + (1+\Delta_0{}^2)\alpha(\tau)] = m(\tau) \quad . \tag{3.2}$$

Here $\alpha(\tau)$ is angular displacement, $\omega_0 = \frac{2\pi}{T_0}$ is the natural angular frequency of oscillation in vacuum, T_0 is the period of oscillation in vacuum, $\tau_0 = \omega_0 t$ is a dimensionless time,

$\triangle_0$ is the logarithmic decrement in vacuum, I is the moment of inertia of the oscillating system and $m(\tau)$ is torque exerted by the fluid on the body. The logarithmic decrement is the logarithm of the ratio of angular amplitudes over a period. Equation (3.2) may be regarded as a statement of the fact that a torsionally oscillating body moves in a manner similar to a simple linear spring but with damping provided by both the body itself and the fluid that surrounds it. It is in the $m(\tau)$ term that all the fluid dynamics is contained. The sequential development of this equation for an oscillating disc by Kestin and Persen [13] and then Newell [14] is briefly explored later in this chapter. The working equation (i.e. the equation that will be used for calculation purposes) is written

$$S, \bar{S} = \frac{\omega(-\triangle \pm \imath)}{\omega_0} \tag{3.3}$$

where S and $\bar{S}$ are two complex roots of the characteristic equation

$$(S + \triangle_0)^2 + 1 + D(S_J\mu, \rho) = 0 \tag{3.4}$$

and $D(S_J\mu, \rho)$ is the Laplace transform of the torque. This will vary according to the geometric arrangement of the system. The function $D(S_J\mu, \rho)$ depends parametrically on the density and the viscosity of the fluid in which the body is submerged. The logarithmic decrement ($\triangle$) and frequency (ω) of oscillation in the fluid can be found experimentally. These two known variables are then sufficient to determine S. If the density is known then we can use these equations to determine the viscosity.

3.3.2 Oscillating Disc

We will now discuss two different forms of the oscillating disc model. The operation of torsionally oscillating bodies in an assumed infinite space had proved to be fairly inaccurate. Three-dimensional vortex-like flow patterns would appear to form at the surface of the disc [16]. An exact theory from first principles was initially derived by Kestin and Person [13] for a thin disc between two plates, based upon the ideal case of an infinitely thin disc of infinite radius. The instrument was calibrated in vacuum to find the natural period of oscillation (T_0) of the disc, and the decrement of damping ($\triangle_0$) using (3.5):

$$\triangle_0 = \frac{1}{2\pi m} \ln \frac{\phi_n + \psi_n}{\phi_{n+m} + \psi_{n+m}} \quad . \tag{3.5}$$

Here ϕ and ψ denote the angular amplitudes of motion on the two sides of the position at rest. $Amplitude_n$ is taken n full cycles from an arbitrary zero and $amplitude_{n+m}$ taken m

full cycles later. With the exception of early transient motion and the last phases at very small amplitude, the motion is damped harmonically. The motion is isochronous, sequential oscillations have a constant phase relationship, and the period T in the fluid is larger than that in vacuum, so that

$$\theta = \frac{T}{T_0} > 1 \qquad . \tag{3.6}$$

The complex circular frequency, determined using

$$\sigma = \frac{-\triangle + \imath}{\theta} \qquad , \tag{3.7}$$

is equal to the complex root (s) of a characteristic equation. The characteristic equation used by Kestin and Persen took the form:

$$(s + \triangle_0)^2 + 1 + \frac{\pi R^4 \rho \delta s^{\frac{3}{2}}}{I} \coth(\beta s^{\frac{1}{2}}) = 0 \qquad . \tag{3.8}$$

Here $\beta = \frac{b}{\delta}$ is a dimensionless separation and I is the moment of inertia of the system. The density ρ is found from other sources leaving only one unknown δ, the boundary layer thickness. For Newtonian fluids this was shown to be

$$\delta = (\frac{\mu T_0}{2\pi\rho})^{\frac{1}{2}} \qquad . \tag{3.9}$$

From (3.9) the viscosity is extracted. This theory requires the boundary layer to be large compared to the plate separation, yet assumes that the plate separation and the disc thickness are both small in comparison with the disc radius R. The theory is based on a portion of the radius R of an infinite, but infinitely thin disc. This assumption ignores the effect of the finite radius of a real disc and neglects any contribution from the small, finite cylindrical circumference.

The following characteristic equation introduced by Newell is a result of an expansion of the hyperbolic cotangent in equation (3.8).

$$(s + \triangle_0)^2 + 1 + \frac{\pi R^4}{bI\omega_0}\mu s(C_N + \frac{1}{3}s\beta_1\beta_2 - \frac{1}{90}s^2((\beta_1)^3(\beta_2)^3)\beta +$$

$$\frac{1}{945}s^3((\beta_1)^5(\beta_2)^5)\beta + ...) = 0 \tag{3.10}$$

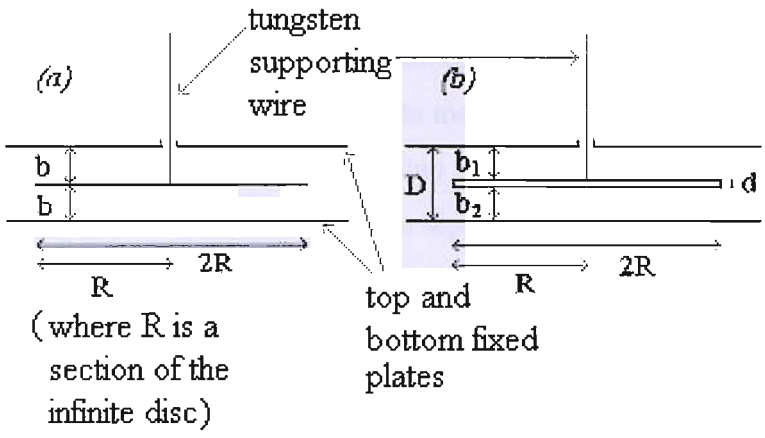

Figure 3.2: (a) Kestin and Persen's model [13] (b) Newell's model [14]

where

$$C_N = 1 + \frac{8}{\pi}\frac{b}{R}[\cosh\gamma \log(\cosh\gamma + 1) - (\cosh\gamma - 1)\log\sin\gamma] + 2(\frac{b}{R})^2(1 + 3\frac{d}{b}) \tag{3.11}$$

$$\gamma = \cosh^{-1}(1 + \frac{d}{2b}) \tag{3.12}$$

β assumed small and b is the harmonic mean distance calculated using the distances between the plates and the disc, b_1 and b_2.

The effects of the disc edges and the finite thickness of the disc is contained in the section following unity of (3.11) for C_N. Putting the complex circular frequency values (3.7) into this characteristic equation and then taking the imaginary part and neglecting terms of order higher than $\triangle^2$, reduces C_N to the equation

$$C_N = [\frac{2I}{\pi\rho b R^4}(\frac{\triangle}{\theta} - \triangle_0) + a\frac{\triangle}{\theta}]\beta^2 + f\frac{3\triangle^2 - 1}{\theta^2}\beta^4 + h\frac{\triangle(\triangle^2 - 1)}{\theta}\beta^6 \tag{3.13}$$

where $a = \frac{1}{6}[(k+1) + (\frac{1}{k} + 1)]$, $f = \frac{1}{720}[(k+1)^3 + (\frac{1}{k} + 1)^3]$, $h = \frac{1}{7560}[(k+1)^5 + (\frac{1}{k} + 1)^5]$ and $k = \frac{b_1}{b_2}$. C_N is independent of fluid properties and depends only on the geometry of the system. Using the above equations β^2 can be determined and using the relation $\delta^2 = \frac{b^2}{\beta^2}$ this value can be substituted into (3.9) for the boundary layer thickness to extract a viscosity.

The equations produced by Newell [15] are only valid if $b_1 + b_2 + d \ll R$ and $b_1 + b_2 + d \ll \delta$. The use of an expansion means that the equation breaks down for a boundary layer thickness δ when β is too large for convergence. Accuracy also suffers due to the limited number of terms kept in the equation. Numerically, this method involves a lot of work and realistically should be carried out computationally. Due to the strict dependence on the system's geometry, effort is needed to measure the plate separation distances and the disc thickness accurately. Another difficulty arises in ensuring all the faces of the instrument are perfectly flat. Good alignment is essential for parallelism. An example of the layout of such an oscillating disc viscometer can be seen in figure (3.3).

3.3.3 Analysis of the Decay Method

In obtaining the working equations for oscillating-body viscometers certain assumptions are commonly made:

1. the amplitude and frequency are sufficiently small for secondary flows to be neglected,
2. we can apply the linearised Navier-Stokes equations for an incompressible fluid,
3. the suspension strand is perfectly elastic,
4. the body weight is chosen to keep the axial tension on the strand to a desired minimum.

A common cause of failure of the early design of torsionally oscillating viscometer was its inability to function at conditions far from ambient such as very high or low temperatures or in corrosive atmospheres. High pressure environments were particularly problematic. Oscillating body viscometers containing fluid are unsuitable for operation at high pressures. It is inevitable that distortions in the dimensions of the body will occur. Only the disc form with external fluid is consistent with the volume of sample acceptable for use at high pressures. However the damping effect on the disc induced by liquids at such conditions is often so large that the mass of disc required cannot be supported by any available method. Also, the oscillating disc experiments require careful measurement of the natural decay time of the system. For the case of the oscillating disc between parallel plates, errors can occur if the spacing is not sufficiently comparable with the boundary-layer thickness. Gases with boundary-layer thickness of order 0.1 to 5 cm require that the spacing must not exceed 1 to 5 mm. At high temperatures thermal expansion of the system will influence the magnitude of this gap.

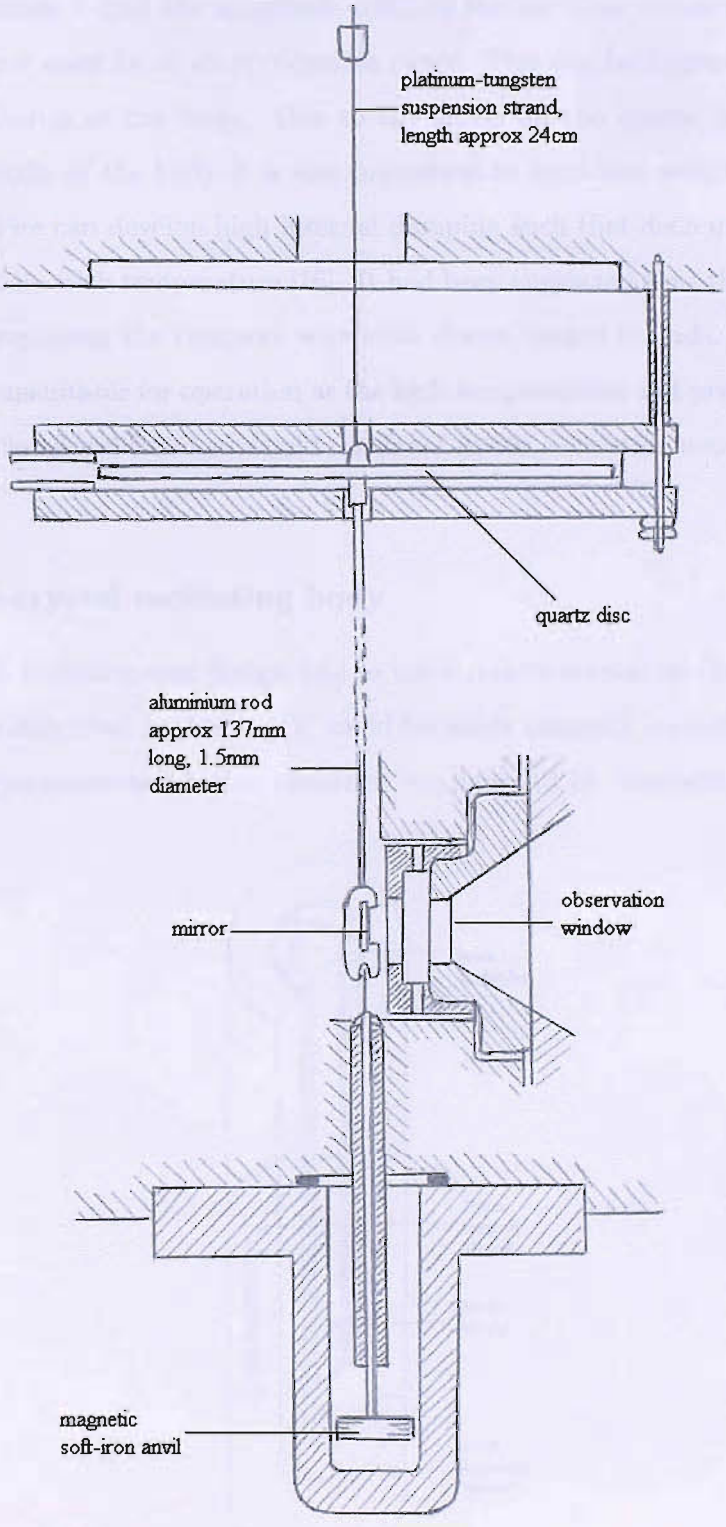

Figure 3.3: Instrument with disc between parallel plates, drawn by hand, reproduced from [15]

For an instrument to be successful at very high pressures it must conform to specific design criteria. The amplitude and frequency of oscillation must be kept small enough so that viscous torque is not affected by secondary flows. It is necessary to measure a practical number of oscillations before the amplitude restricts further observation therefore the logarithmic decrement must lie in an appropriate range. This can be improved by increasing the moment of inertia of the body. Due to the stress on the elastic suspension strand caused by the weight of the body it is also important to keep this weight to a minimum. The supporting wire can develop high internal damping such that decrement $\triangle_0$ increases almost exponentially with temperature [16]. It had been suggested that this problem could be overcome by replacing the tungsten wire with drawn quartz strands. Generally, these early devices are unsuitable for operation at the high temperatures and pressures commonly found in down hole oil wells and so would not be of use in such circumstances.

3.3.4 Quartz-crystal oscillating body

Another variation in instrument design was to use a quartz-crystal oscillating body. Such an instrument as described by Diller [17] could be made compact enough to measure viscosity at low temperatures and higher pressures, see figure (3.4). Viscosities accurate to 0.5

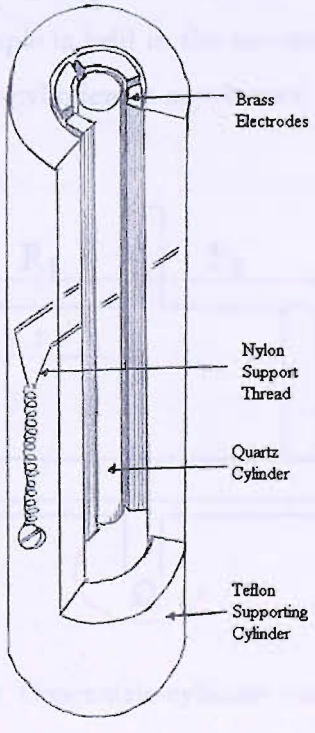

Figure 3.4: Quartz crystal oscillator, drawn by hand, reproduced from [17]

% were determined in temperatures of 14-100 K at pressures up to 35 MPa. No calibration was necessary so absolute viscosity was measured. The first design used a torsionally oscillating right circular natural quartz cylinder that was 5 cm in length and 0.5 cm in diameter.

Calculations were made using (3.14), relating viscosity with the logarithmic decrement of the oscillations.

$$(\nu\rho)_{fluid} = (M/S)^2(f/\pi)\triangle^2_{fluid} \tag{3.14}$$

where M is the mass, S is the surface area and f is the resonant frequency of the crystal in the fluid. $\triangle_{fluid}$ is damping resulting from the fluid and can be found by subtracting damping that occurs in vacuum from the total.

$$\triangle_{fluid} = [\triangle_{total} - \triangle_{vacuum}] \tag{3.15}$$

More precise results can be obtained if the crystal is forced to oscillate near its resonant frequency.

3.3.5 Concentric-cylinder (Couette) viscometer

An alternative form of the oscillating disc viscometer is the concentric-cylinder geometry [18], shown in figure (3.5). The first practical coaxial cylinder viscometer was devised by Couette in 1890. The fluid sample is held in the annulus between the cylinder surfaces. The laminar flow between the two cylinders is now known as Couette flow.

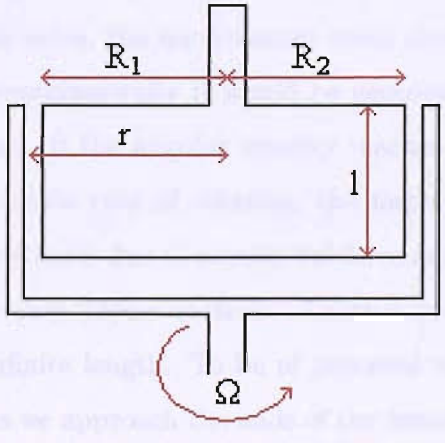

Figure 3.5: Concentric-cylinder viscometer

The design of these viscometers can vary, with either the inner, outer or both cylinders rotating. They can occur in a number of configurations as shown in figure (3.6), each one

aimed at improving an aspect of the viscosity measurement.

(a) The double gap design has a much larger surface area to measure low viscosity fluids.

(b) The cone ended design is intended to reduce end effects.

(c) The serrated inner cylinder is aimed at reducing slip.

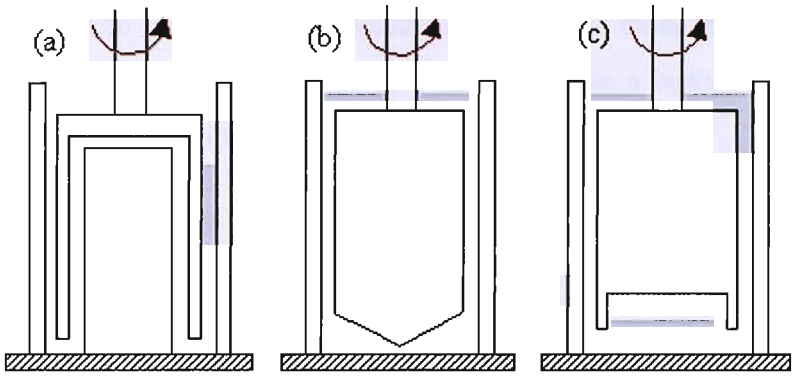

Figure 3.6: Coaxial cylinder designs: (a) double gap, (b) cone ended and (c) serrated inner cylinder

The viscosity of a Newtonian fluid is found using the Margules equation [18]:

$$\mu = \frac{T}{2\pi l \Omega} \frac{R_2 - R_1}{R_2 {R_1}^2} \tag{3.16}$$

where T is the torque, l is the immersion depth and Ω is the angular velocity.

There are a number of issues that arise with the coaxial cylinders viscometer. One problem is the dependence of viscosity on temperature. If the fluid tested is very viscous and tests are carried out at high shear rates, the temperature could rise significantly due to viscous heating. This means that experimentally it would be necessary to find a way to retain a known, constant temperature. If the angular velocity reaches too high a speed, turbulent flow can occur. Above a certain rate of rotation, the faster moving fluid tries to move from the inner to the outer cylinder due to centripetal force and the flow becomes complex. Local circulation occurs forming Taylor vortices. Another problem is that the equations are based on cylinders of infinite length. To be of practical use, the device must contain cylinders of finite length. As we approach the ends of the inner cylinder the velocity gradient becomes non-radial so the torque per unit length decreases. The ends themselves will also produce additional torque, so the equation needs to be changed to allow for this. One way to overcome this problem would be to perform calibration in a known fluid to negate the end effects.

3.3.6 Cone and plate viscometer

The final torsionally oscillating body viscometer that design we will discuss is the "cone and plate" viscometer. This viscometer is often used for fluids with a high viscosity. In commercial instruments, the geometry usually involves an angle α of between 0.5 and 8 degrees [4]. When measuring viscosity as a function of shear stress or shear rate, this set up causes the shear rate to be close to a constant value [18]. In most theoretical models, the analysis makes use of the fact that α is small enough to allow a lubrication approximation to be applied to flow in the gap.

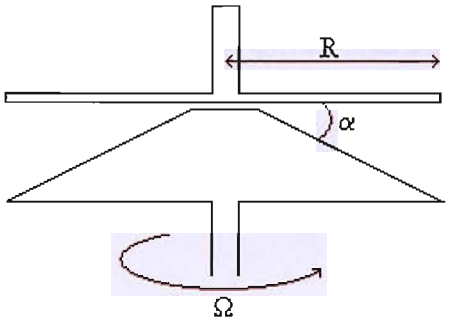

Figure 3.7: Cone and plate viscometer, where R is the plate radius, α is the angle between the cone and the plate, and Ω is the angular velocity

The cone is rotated about the central axis with angular velocity Ω, and the torque T on the fixed plate is measured. The viscosity can then be found in terms of the diameter R, angle α, angular velocity Ω and the measured value of torque T [4], using

$$\mu = \frac{3T\alpha}{2\pi R^3 \Omega} \quad . \tag{3.17}$$

The cone and plate viscometer also has its problems. It is not particularly useful for particulate fluids. The particles contained in the suspension can undergo a grinding action and interfere with the tip of the cone. This can be solved by removing the very end of the tip. As with the Couette flow viscometer, viscous heating effects mean that the temperature in the gap between the cone and plate may not be uniform, and secondary flows can occur for fast rotations and large values of α.

3.4 Vibrating Viscometers

A later step in viscometer design was to use a long cylindrical rod or wire. The idea was introduced from Stokes theory [19] about a cylinder in fluid undergoing damped oscilla-

tions. Stokes reasoned that an element of a cylindrical rod oscillating as a pendulum would experience resistance nearly equivalent to a similar element of an infinite cylinder oscillating linearly with the same velocity. He derived a set of working equations for the infinite cylinder oscillating perpendicular to its axis in an infinite mass of fluid. He stated that near the ends of the finite length rod this representation would lead to errors but argued that this would be negligible if the diameter of the rod was small in comparison with its length. This method was developed by Tough et al [20] in 1963. Instead of measuring torsional oscillations, the body was made to vibrate transversely. The wire is stretched taut in a magnetic field. An outline of the apparatus used is shown in figure (3.8). A direct current is passed through the wire to initiate a deflection and is switched off once a steady deflection is achieved. As the oscillations decay, an alternating voltage is induced. The usual way of measuring this signal was to magnify it and then display it on an oscilloscope. The frequency was deduced from photographs of the oscilloscope traces and could be used in plots to find the decay constant τ. An example of a semilog plot of this type is shown in figure (3.10).

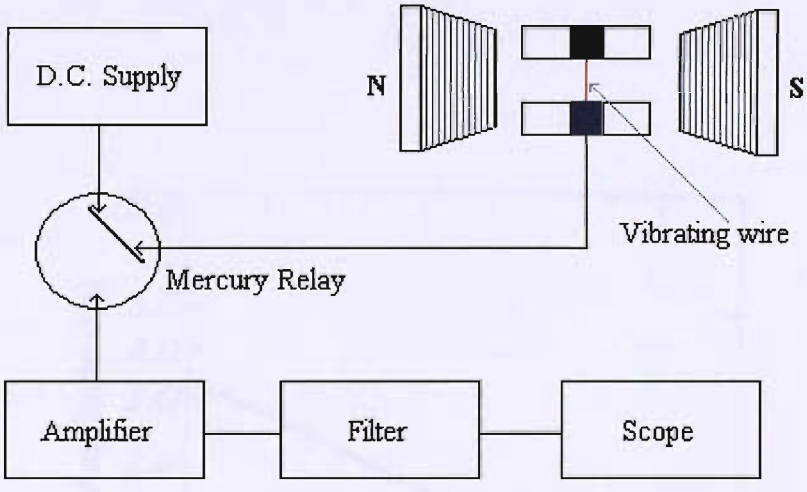

Figure 3.8: Equipment set up for vibrating wire viscometer

Inaccuracies appearing in results from using torsionally oscillating bodies at extreme physical conditions were reduced with this new viscometer design. The simple and compact measurement cell was much more appropriate for conditions far from ambient. In 1978, Karnus et al [21] described an instrument that could be used at pressures up to 15 MPa and temperatures from (14 to 300) K. The accuracy obtained was within ± 2 % of the true viscosity. This instrument was only tested in samples of low viscosity, mainly gases. It was more difficult to obtain results from the oscillogram in a higher viscosity fluid due

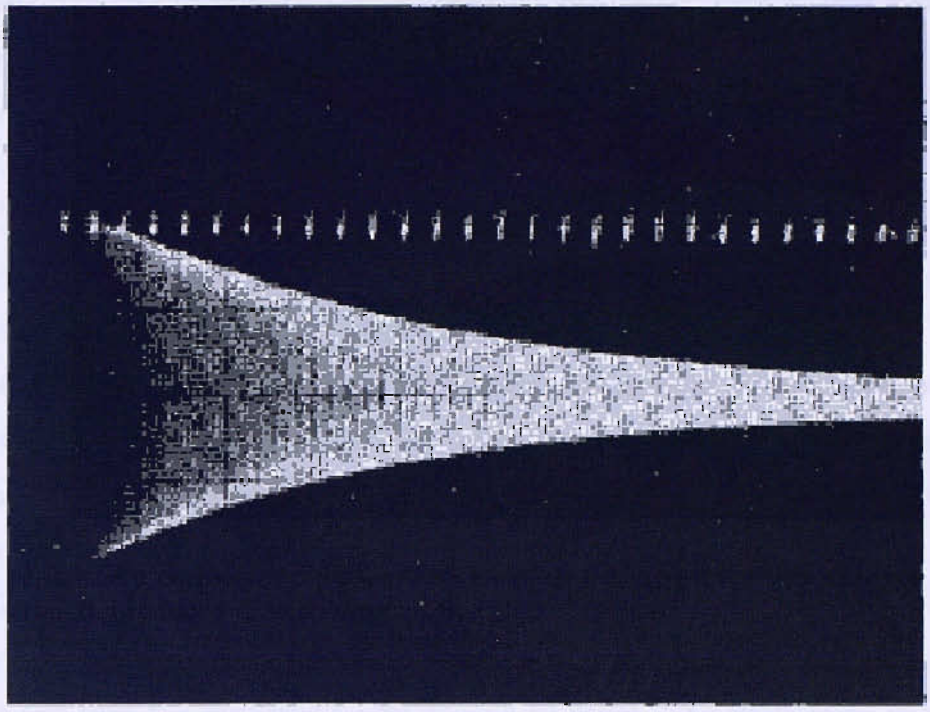

Figure 3.9: An oscilloscope photograph showing the frequency and exponential decay of the wire. Reproduced directly from [20]

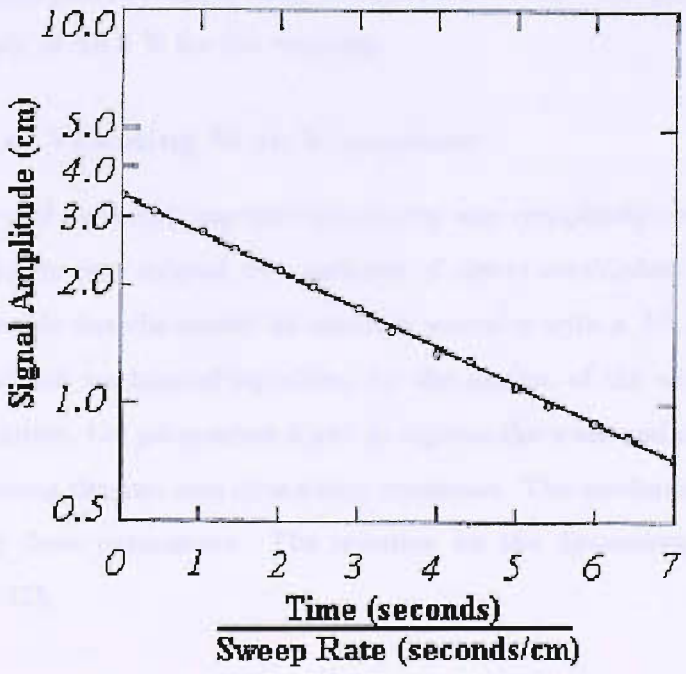

Figure 3.10: Semi-log plot showing data from (fig 3.9). Reproduced directly from [20]

to the reduced number of free oscillations of the body. The range of viscosities that the instruments could measure needed to be widened. Tough et al did not publish any results for the tests that were claimed to have been in water. In 1980, Charles et al [22] presented a vibrating wire viscometer for liquids with viscosities up to 0.5 cPa·s. Again the accuracy recorded was around ±2 %.

As developments were made to the physical design of the instrument and new technology arrived to ease observations and measurements, the accuracy and range of the vibrating wire viscometer improved yet further. Measuring viscosities of fluids at pressures above 40 MPa while still maintaining an accuracy comparable to that achievable at atmospheric conditions proved to be extremely problematic. By 1988, Van der Gulik et al [23] had introduced an instrument that produced results for temperatures of (80 to 310) K at pressures up to 1 GPa. The basic method involved was similar to that described [20] in 1963. A taut tungsten wire was forced to vibrate close to its resonant frequency by passing through a DC pulse and then the oscillations were allowed to decay. The oscilloscope was replaced by a microprocessor to store the signal produced. A photograph was no longer necessary, this signal could be Fourier transformed and fitted to the Lorentz curve, a function of the cumulative distribution of ordered data. The wire was attached to an aluminium-oxide holder using metal clamps. It was able to work in hostile conditions because the vibrating wire body was electrically insulated from the pressure vessel. The published results [23] claimed an accuracy of ±0.5 % for the viscosity.

3.4.1 Theory of Vibrating Wire Viscometer

In 1986, the theory of the vibrating-wire viscometer was completely reworked by Retsina et al. [24]. The theory was subject to a number of newly established instrument design constraints that enable the viscometer to measure viscosity with a ±0.1 % accuracy. The fluid equations and the mechanical equations for the motion of the wire were considered separately. In the latter, the parameters k and k' express the mass and added damping due to the fluid, combining the two sets of working equations. The mechanics can be analysed without specifying these parameters. The notation for the dimensions of the model are shown in figure (3.11).

The mechanical equations follow simple beam theory with the wire being modelled as a solid cylindrical rod clamped at both ends and subject to a tension T. Due to the specification

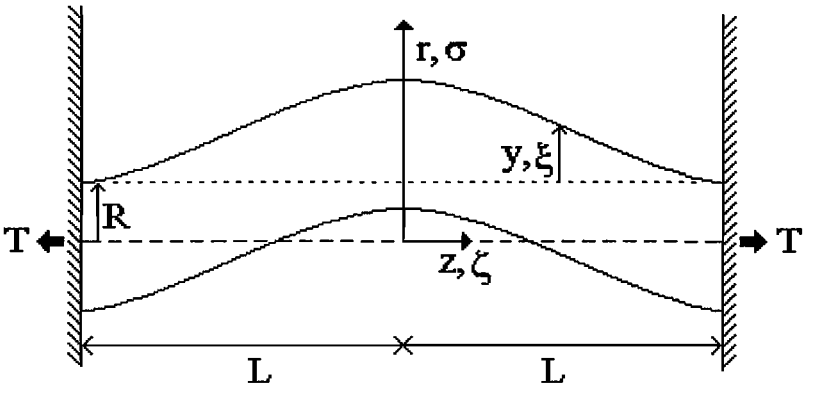

Figure 3.11: Model of vibrating rod

that transverse displacements and amplitude of oscillations will be small, linear theory can be adopted. The rod motion is described by the equation

$$EI\frac{\partial^4 y}{\partial z^4} - Ty\frac{\partial^2 y}{\partial z^2} + (m_s + m_b)\frac{\partial^2 y}{\partial t^2} + (D_b + D_0)\frac{\partial^2 y}{\partial t^2} = F(z,t) \tag{3.18}$$

where $I = \frac{1}{4}\pi R^4$ is the second moment of area, $m_s = \rho_s \pi R^2$ is the mass per unit length of solid rod, $m_b = \rho\pi R^2 k$ is the added mass per unit length of external fluid, $D_b = \rho\pi R^2\omega k'$ is the drag force of the fluid and $D_0 = 2\rho_s\pi R^2\omega\triangle_0$ is the coefficient of internal damping. E is the Young's modulus for the rod material, ρ_s is the rod density, ρ is the fluid density, ω is the angular frequency, $\triangle_0$ is the logarithmic decrement in vacuo and F represents a force per unit length acting on the rod, which becomes negligible for large times.

Motion is started by an initial displacement of the rod at time $t = 0$. The beam oscillates in one mode in the plane containing the beam axis and perpendicular to it. The rod and the fluid are both initially at rest. The theory deals with the transient decay of free oscillations so (3.18) is solved subject to the following boundary and initial conditions [24]

$$y = 0 \quad \text{and} \quad y_z = 0 \quad \text{at} \quad z = \pm L$$

$$y(z,t) = y_0 f(z)$$

$$y_t = 0 \quad \text{at} \quad t = 0$$

where y_0 is the maximum initial displacement of the beam and f is an arbitrary function of z with $|f| \leq 1$. The general solution to a non-dimensionalised form of (3.18) in any single

mode, j is given by

$$\xi_j(\zeta,t) = A_j\phi_j(\zeta)e^{(\imath-\triangle)\omega_j t} + \sum_{m=1}^{\infty} g_m\phi_m(\zeta)e^{-\upsilon_m\omega_m t} \tag{3.19}$$

where ξ_j is the displacement of each point at distance ζ from the origin, g_m is the amplitude of transient force and $\phi_j(\zeta)$ are eigenvectors of the normal modes of oscillation. The first term in (3.19) conveys damped harmonic motion in one mode and the remaining term represents a simple decaying displacement due to initial transient in the fluid motion. With further progression [24] this is reduced to a complex working equation which can be expressed in real and imaginary parts as

$$\triangle = \frac{(\rho/\rho_s)k' + 2\triangle_0}{2(1+(\rho/\rho_s)k)} \tag{3.20}$$

$$\frac{\omega^2}{\omega_0^2}\{[1+(\rho/\rho_s)k][\triangle^2-1] - \triangle((\rho/\rho_s)k' + 2\triangle_0)\} + 1 + \triangle_0^2 = 0 \quad . \tag{3.21}$$

The fluid behaviour is analysed by solving the Navier-Stokes equations subject to the following boundary and initial conditions

$$\upsilon_r = (\imath-\triangle)\omega\epsilon Re^{(\imath-\triangle)\omega t}cos\theta$$

$$\upsilon_\theta = -(\imath-\triangle)\omega\epsilon Re^{(\imath-\triangle)\omega t}sin\theta$$

$$\text{at} \quad r = \epsilon Re^{(\imath-\triangle)\omega t} + R(1-\epsilon^2 e^{2(\imath-\triangle)\omega t}sin^2\theta)^{\frac{1}{2}}$$

$$\text{and} \qquad \upsilon_r = \upsilon_\theta = 0 \qquad \text{as} \qquad r \to \infty.$$

These conditions state that the fluid is initially at rest and there is no fluid motion far from the rod. The geometry used to derive these can be seen in figure (3.12).

The solution is obtained for an infinite volume of an incompressible liquid implying that the Mach number is small. Thus

$$Ma = (1+\triangle^2)^{\frac{1}{2}}\omega\epsilon R/c \ll 1 \quad . \tag{3.22}$$

Owing to the assumed small transverse displacements, the non-linear inertial terms are neglected so that

$$\epsilon \ll \rho\omega R^2/\mu = \Omega \ll 1/\epsilon^2 \tag{3.23}$$

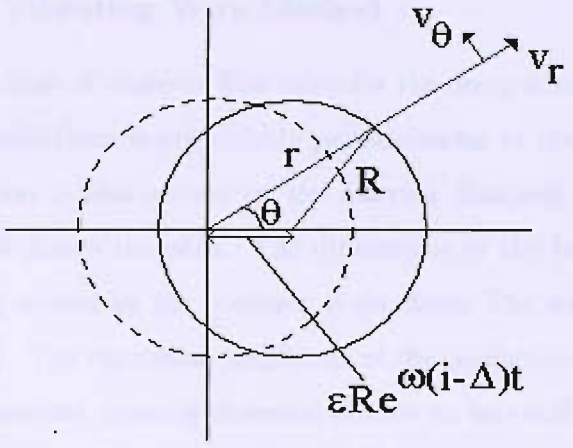

Figure 3.12: Symbols defined for the r, θ plane

where c is the sonic velocity in the fluid, ϵ is the maximum amplitude of the motion and $\epsilon\Omega$ is the Reynolds number of the flow. The motion is also assumed to be isochronous with a frequency ω. From the fluid analysis, Retsina et al [24] derive working equations to express the parameters k and k' in the form

$$A = (\imath - \triangle)/\left[1 + \frac{2K_1([(\imath - \triangle)\Omega]^{\frac{1}{2}})}{[(\imath - \triangle)\Omega]^{\frac{1}{2}}K_0([(\imath - \triangle)\Omega]^{\frac{1}{2}})}\right] \tag{3.24}$$

$$k = -1 + 2Im(A) \tag{3.25}$$

$$k' = 2Re(A) + 2\triangle Im(A) \quad . \tag{3.26}$$

Here K_0 and K_1 are modified Bessel functions. If the rod material properties are known then (3.24), (3.25) and (3.26) combined with either (3.21) or (3.20) provide a complete set of working equations to find the viscosity of the fluid. Measurement of the frequency of oscillations and the logarithmic decrement allow either the density or the viscosity of the fluid to be determined. Equation (3.20) is the preferred choice in practice because it is more sensitive to the measurement of viscosity.

Assael et al [25] describe two viscometer designs that follow these principles. They operate in a range of pressures from 80 to 300 MPa and at temperatures between 270 and 370 K. Over this range of conditions it is estimated that the accuracy of the reported viscosity is ±0.5 %. This is influenced by any inaccuracies in the values of the wire material properties and the error in the fluid density. The instruments were estimated to measure the decrement of oscillations to a precision of approximately ±0.1 % and the frequency to ±0.01 %.

3.4.2 Analysis of Vibrating Wire Method

Errors can arise from a host of sources. The value for the decay-time constant will be erroneous if the plane of oscillations is not strictly perpendicular to the magnetic field. Decay in the vibrational motion is also caused by the internal damping of the wire. The wire used most often is hard-drawn tungsten. The dimensions of the body must be chosen to emphasise the damping caused by the presence of the fluid. The wire diameter is required to be small (≈ 100 μm). The maximum amplitude of the oscillations is also specified to be small relative to the diameter, causing observed motion to be small (≈ 10 μm). A typical wire used by Tough et al was 5 cm in length and 25 μm in diameter, and would oscillate at an amplitude of about four times the diameter. Errors also arise from differences in the theory of the instrument and its actual physical geometry. The corrections at the ends and edges of the body can be quite large. In reality, the ends do not follow an ideal case and are neither perfectly clamped nor hinged so errors occur when a choice of these is made for the hydrodynamic equations.

The validity of the equations derived by Retsina et al [24] impose necessary instrument design constraints so that certain conditions are met. For a chosen range of ρ and μ for the fluid, limits should be placed on the radius of the wire (rod) and the frequency of oscillation. The conditions given by (3.23), (3.22), and the condition $\epsilon \ll 1$, require that

$$\omega \ll \mu/\epsilon^2 \rho R^2 \tag{3.27}$$

$$\omega \gg \mu\epsilon/\rho R^2 \tag{3.28}$$

$$\omega \ll c/\epsilon R \tag{3.29}$$

It is apparent from these inequalities that the smallest realistic value for ϵ will be the most beneficial, where $\epsilon = \zeta_{max}/R$ is the maximum amplitude of the wire motion in terms of the beam radius.

A further restriction is imposed because the Navier-Stokes equations were used to evaluate the parameters k and k'. This is only permitted if the fluid tested is Newtonian. A further assumption made is that the total temperature rise in the fluid sample is negligible. The temperature near the surface of the beam will differ from that of the surrounding fluid owing to viscous dissipation. Inaccuracy will also occur as a result of the assumption that there is an infinite volume of fluid. It has been shown [23] that this error is approximately

proportional to $(a/a_v)^2$ where a is the radius of the wire and a_v is the radius of the fluid container. This is said to be less than 0.05 % for $a_v = 100a$. Other corrections need to be considered for the non-uniformity of the wire, in particular its cross section.

3.5 Summary

This analysis indicates that conventional viscometers are currently unsuitable for measurements in situ for a host of reasons. Falling body viscometers contain free moving parts and capillary viscometers need not only a device to produce a constant fluid flow but also an external pressure to balance the internal pressure to prevent distortions occurring in the tube. Torsional oscillating-body viscometers containing fluid can perform poorly at high pressures, since it is inevitable that distortions in the dimensions of the body will occur. The damping effect on the discs of disc viscometers induced by liquids at such conditions is often so large that the mass of disc required cannot be supported by any available method. The simple and compact measurement cell used in vibrating wire viscometers is more appropriate for the far from ambient conditions that are found down-hole. It is able to work in hostile conditions because the wire body is electrically insulated from the pressure vessel [23]. Unfortunately, the vibrating wire viscometer is limited by the equations used to evaluate the parameters in its mathematical model. By applying the Navier-Stokes equations, the model is only representative if the fluid tested is Newtonian.

The information presented suggests that a change to both the mechanical designs of the viscometers and the mathematical equations supporting them are needed to model an accurate instrument for measuring fluid viscosity in oil/gas wells in situ. This prompts the development of a new viscometer that will both remain sufficiently accurate in hostile conditions and reflect both Newtonian and non-Newtonian fluid motion. We recognise that a trade-off may have to be made between extreme accuracy and the ability to withstand hostile conditions and measure a wide range of fluids. We conclude that the production of a novel type of small-scale viscometer that can be used down-hole would be advantageous in this field.

Table 3.1: Comparison of past designs in chronological order (For the method of detection, E:=electromagnetic, P:=piezoelectric, Oo:=optical using oscilloscope photographs and Op:=optical using photodiodes.)

Geometry	Method	Det.	Freq. /kHz	Viscosity Range /mPa.s	Pressure Range /MPa	Temp Range /K	Other Limitations
Hollow disc pendulum [26]	Torsional free decay. Resonant frequency and damping measurement.	E	0.2 −2.3	0.5 − 50			Lack of exact knowledge of temperature of the pendulum.
Cylindrical wire [20]	Transverse oscillations. Free decay, resonant frequency and damping measurement.	Oo	0.475 −3.34	0.0013 −0.0027		1.1 −2.5	Imperfections in the wire. Claimed uncertainty 2.1 %
Quartz Crystal cylinder [27]	Torsional crystal method. Resonant frequency and damping measurement.	P			0.1 −34.5	14 −100	Claimed uncertainty 0.5 %
Immersed Plate [28]	Electromagnetic resonant frequency and resistance measurement.	E	0.1	1 − 600		283 −323	
Cylindrical multiple lump resonator [29]	Multiple lump resonator. Forced torsional oscillations. Resonant frequency and damping measurement (bandwidth).	Op	0.1 −8.3	0.5 − 50			Onset of modal coupling at high viscosity. Claimed uncertainty 0.5 %
Cylindrical wire [21]	Transverse oscillations. Free decay, resonant frequency and damping measurement.	E			0.1 − 15	14 −300	Oscillations must be strictly perpendicular to magnetic field. Claimed uncertainty 2 %

Table 3.2: Comparison continued

Geometry	Method	Det.	Freq. /kHz	Viscosity Range /mPa.s	Pressure Range /MPa	Temp Range /K	Other Limitations
Cylinder [30]	Torsional free decay. Resonant frequency and damping measurement.	Op		< 1		to 1473	Uncertainty in cylinder radius. Claimed uncertainty 0.5 – 1 %
Cylindrical wire [31]	Transverse oscillations. Transient decay. Resonant frequency and damping measurement.	E	1	$0.3 - 0.53$	$0.1 - 80$		Uncertainty in wire density. Claimed uncertainty 0.5 %
Cylindrical wire [25]	Resonant frequency and logarithmic decrement of free transverse oscillations.	E	1	$0.1 - 10$	0.1 −300	270 −370	Uncertainty in wire density. Claimed uncertainty 0.2 %
Cylinder [32]	Torsional free decay. Resonant frequency and damping measurement.	P	20 −500	$1 - 500$			
Cylindrical wire and solid sinker buoy [33]	Forced transverse oscillations. Resonant frequency and damping of 1.5 % measurement. (uncertainty for viscosities < 7 mPa·s)	E		$5 - 45$	$0 - 100$	197 −350	Loss of accuracy at viscosity over 15 mPa.s. Claimed uncertainty max 2.5 %
Rectangular membrane [34]	Vibrational modes and impedance measurement.	E	263 −1050	Density only			Sensitive to environmental influences that affect membrane tension.
Immersed plate [35]	Forced transverse oscillations. Resonant frequency, phase shift and attenuation measurement.	P	1400 −2400	to 1000		293 −303	Discrepancies at higher order modes.
Tube [36]	Resonant torsional oscillations.	E	5.6	$0.3 - 500$			

Chapter 4

MEMS Fabrication Process

The new vibrating viscometer designs described here are MEMS (Micro-Electro-Mechanical-Systems). Ultimately the MEMS sensors will be used in situ in oil exploration. The sensors are intended to be integrated into existing tools used down-hole. This is placed into the hole, suspended by an electric cable. Its first task is to probe the reservoir formation and carry out pressure tests at varying depths. This defines the transition zones between the different fluids in the reservoir. Simultaneously, fluid samples are taken for chemical analysis. Individually, tools for down-hole use are extremely expensive so an integrated device will help to minimise costs.

Such tools can be up to 30 m in length and they can travel a few kilometres below the surface. The temperature at this depth can easily reach 448 K. The tools must be extremely robust to withstand down-hole conditions. Some oilfields have temperatures as high as 498 K and in places such as Alaska, storage temperatures at the surface can be as low as 218 K. The equipment must also be capable of withstanding severe shocks and vibrations generated during transportation and deployment, and the fluid tested may be corrosive. If the sensors are to be incorporated into future logging tools, they must reflect this robustness in their own design.

4.1 Materials

The dimensions of the sensors are extremely small, with both thickness and amplitude of motion typically being measured in micro-meters [37]. The devices have both electrical and mechanical components. One viscometer that will be discussed in detail in a later chapter

employs an oscillating plate which is a mechanical element that can be set in motion by the force between an electric current flowing through the plate and an externally-applied magnetic field.

Such devices are produced using integrated circuit techniques, and are fabricated by a structure of layers, using material deposition and etching onto a silicon wafer. A fusion-bonded Silicon on Insulator (SOI) wafer is used, with a 4 inch diameter. This is made up of three layers, 350 μm mono-crystalline silicon, 0.5 μm SiO_2 and 20 μm mono-crystalline silicon (Si). An advantage of this wafer is that the thickness of the final plate can be chosen at will. The bulk of the sensor will be anisotropic single crystal silicon with crystalline direction $< 100 >$. We therefore assume that the mass and mechanical properties of the device will correspond to silicon only. To simplify the model the silicon is considered to be isotropic. Material properties in certain crystalline directions can be calculated from basic crystal properties. For silicon in the $< 100 >$ plane, the isotropic values that best reflect the aniostropic behavior are given by Spiering et al [38] and Petersen [39]. These are summarised in table (4.1).

Table 4.1: Silicon properties

Young's modulus /GPa	150
Poisson ratio	0.17
Density /kgm^{-3}	2330
Compression yield strength /MPa	7000
Tensile yield stress /MPa	300

The device also contains significantly smaller layers of different materials. These are deposited and removed from the wafer in a clean room by a series of etching steps using photolithography. The relative thickness and function of these materials are given in table (4.2). The final step in the process is to use a back-etching process to remove the 350 μm bulk mono-crystalline silicon layer. Figure (4.1) shows a cross sectional view of the plate, indicating the various material layers.

The addition of different materials to the top surface of the sensor creates an unevenness that could affect the fluid flow around the plate. The magnitude of these undulations is estimated to be equal in magnitude to the viscous penetration depth of the fluid. The

Table 4.2: Material components of the MEMS sensor

Material	Function	% total thickness
Silicon	Bulk structural material	94.06
Silicon	Device	5.37
Silicon oxide	Etch stop layer	0.13
Silicon nitride	Passivation layer	0.11
Aluminium	Conductors and wire-bonding pads	0.22
Polysilicon	Strain gauges Integrated resistance thermometer (RTD)	0.11

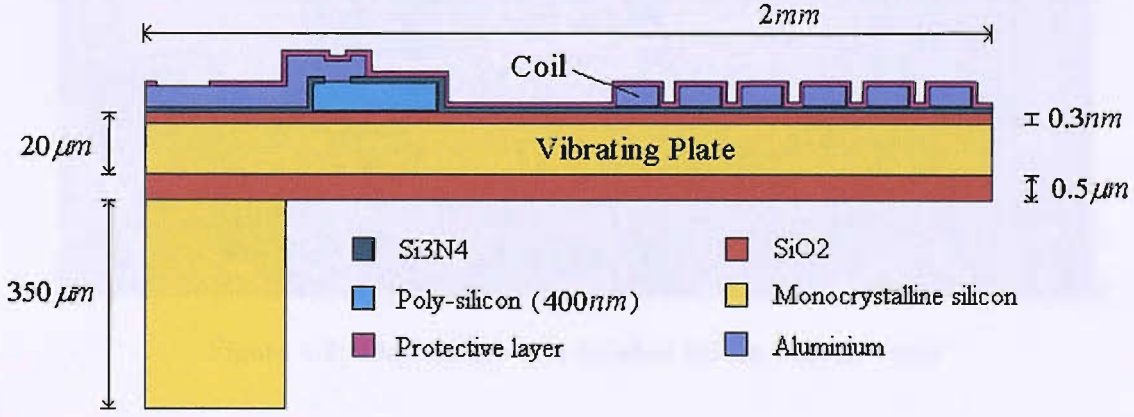

Figure 4.1: Cross section of plate [37] (not to scale)

viscous penetration depth $\delta = \sqrt{\frac{2\nu}{\omega}}$ is defined as the depth at which, for the flow of an unbounded viscous fluid with kinematic viscosity ν above an infinite plate oscillating with frequency ω, the fluid velocity falls to $\frac{1}{e}$ of the original value at the plate surface. This is explained for the MEMS devices in following chapters. The top surface is covered with an even protective layer. This layer is approximately 2 μm thick. Both the top layer and the underneath silicon layer are optically polished for a smooth finish, leaving a smooth but non-level surface. The protective layer is also an important addition in that it helps prevent corrosion on the plate, an important consideration in the harsh reservoir conditions.

After the wafer has been etched and micro-machined, it is diced to release the individual sensors. The photograph in figure (4.2) shows a finished MEMS wafer. It contains approximately 140 individual sensors with dimensions 4 mm x 8 mm, some of which have been removed.

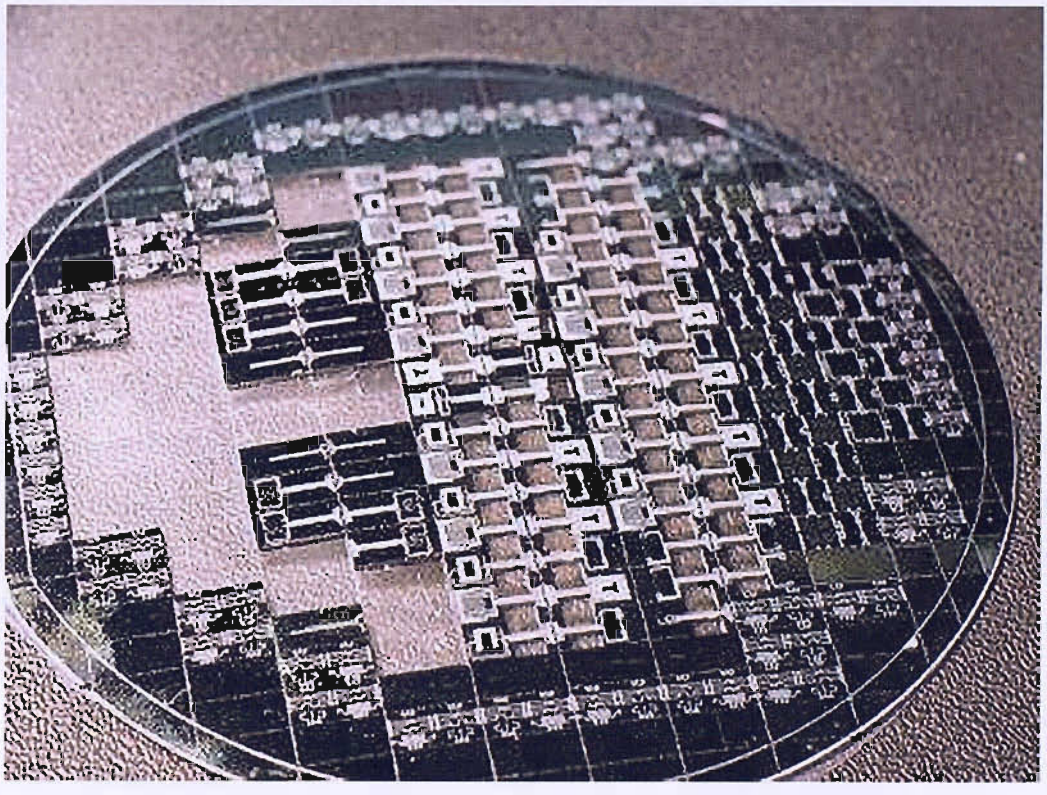

Figure 4.2: Photograph of a finished silicon MEMS wafer

4.2 Actuator and Detector

The motion of the MEMS sensors is activated electromagnetically. The viscometers are set in motion using an alternating current through a conductor held in a magnetic field.

This produces a Lorentz driving force. This force can be altered by changing one of two things, either the current or the intensity of the magnetic field. In a previous chapter, we discussed earlier viscometers that used different actuator methods. These were considered for MEMS but were ruled out for various reasons. Thermal excitation, injecting a periodic current into a resistor, and piezoelectric methods have both proven to be less precise than measurements electromagnetically. Piezoelectric materials were also considered to pose a higher contamination risk.

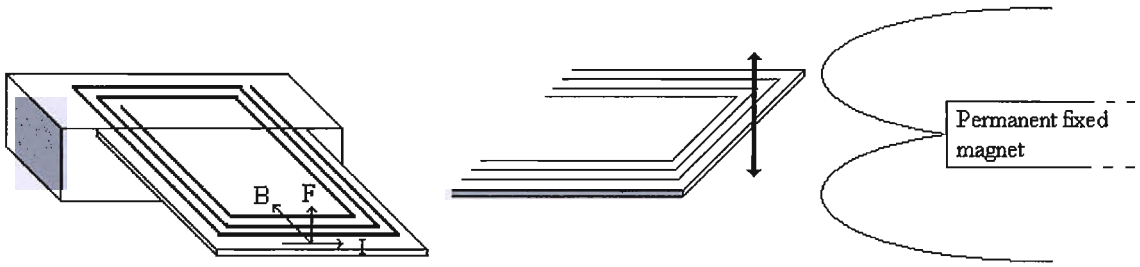

Figure 4.3: Electro-magnetic actuation, where **B** is the constant magnetic field, I is the alternating current in the coil and **F** is the force produced

The electromagnetic principle used is shown diagramatically in figure (4.3). An external electromagnet, or a fixed permanent magnet, holds the plate in a constant magnetic field, **B**. The alternating current, I, is injected into the wire coil that is fabricated onto the sensor. This produces corresponding alternating Lorentz forces, **F**, that force the plate to oscillate. When the current reaches the first natural frequency of the sensor, the plate will oscillate at the maximum amplitude in the first bending mode at resonant frequency. It was found experimentally that the modes for both of the MEMS sensors considered are well separated, both *in vacuo* and in fluid. These modes differ for each MEMS design and will be discussed for the individual sensors in a later chapter.

The conductor and magnetic field that together make up the actuator have no interaction with the detector. It was originally suggested that the two should be coupled. This preferred method would be done by measuring motional EMF. This was not possible due to the large impedence of the coil on the sensor, roughly 300 Ω. The detectors used in the MEMS devices are polysilicon piezoresistive strain gauges. These are placed at the points where the maximum and minimum strain occur and form a Wheatstone bridge. The optimum positioning for each different MEMS design was found using finite element analysis with the standard finite element package ANSYS [40]. On the cantilever plate this optimum placement was found to be near to where the plate was clamped.

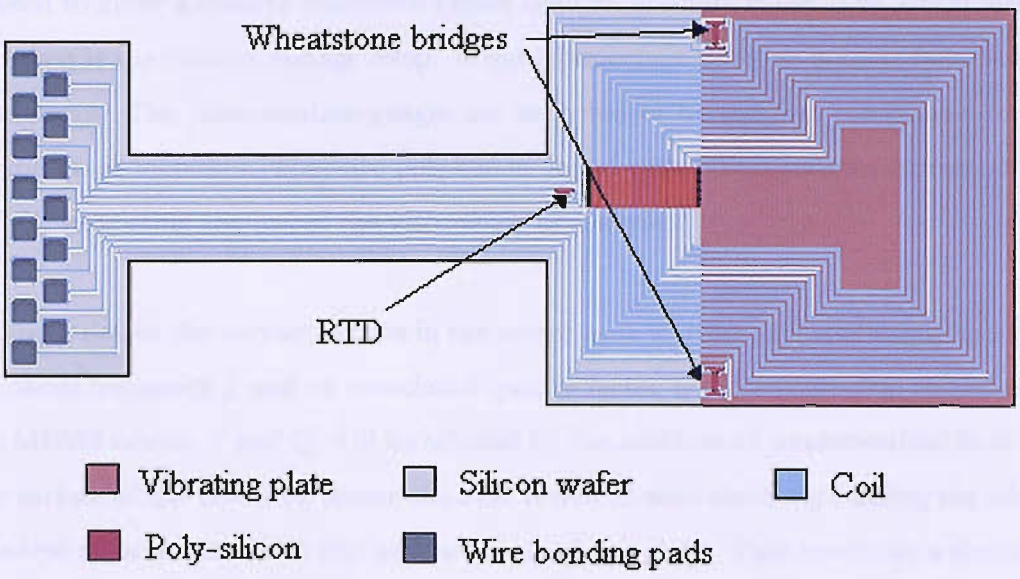

Figure 4.4: Schematic of the top surface of a flexural plate MEMS

This is not the same for the transversely oscillating plate sensor, which we will refer to as the "Spider". Here, the Wheatstone bridge is formed from the first six wire "legs" on each side, closed by wire-bonding. There are 24 legs in total on each side.

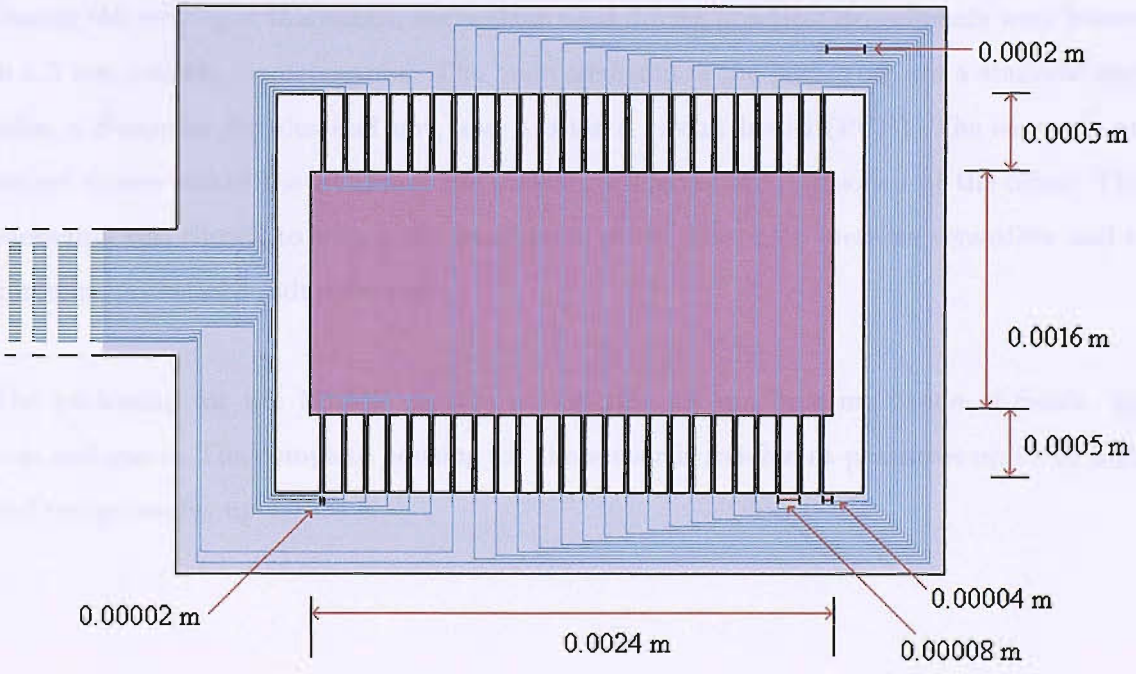

Figure 4.5: Transversely oscillating MEMS: the "Spider"

There are some problems with the strain gauges. They are not completely stable. Their

resistance fluctuates with temperature and pressure. This can in part be ignored since we only need to know a relative resistance rather than an absolute value. The actual measurement taken is the relative voltage drop. A more important problem is their failure at high temperatures. The piezoresistive gauges are expected to be the first component to break as temperature increases. They are polysilicon doped with boron and are estimated to fail at 493 K, restricting the use of the viscometer as a whole.

The gauges detect the varying strains in the sensor as it vibrates and enable one to measure a resonance frequency f and an associated quality factor Q. The resonance characteristics of the MEMS device, f and Q, will be affected by the addition of a surrounding fluid. Near to the surface of the vibrating sensor the fluid is moved with the body causing the addition of effective mass or inertia to the intrinsic mass of the plate. This results in a decrease in f. Q also decreases from the value in vacuum since viscous energy is lost to the shearing motion of the fluid around the sides of the plate. Therefore knowing values of f and Q for a sensor in a fluid allows us, in principle, to obtain the viscosity ν and density ρ of the fluid.

4.3 Packaging

During the writing of this thesis, the sensors used during practical experiments were housed in a 3 mm outside diameter tube. The main elements of the packaging are a stainless steel tube, a Swagelok ferrules and nut, and a printed circuit board (PCB). The sensor is attached to one end of the PCB and the pads for soldering are positioned at the other. This packaging was chosen to match the small scale of the sensor, to increase versatility and to minimize potential production costs.

The packaging for the MEMS devices is designed for use in a multitude of fluids, liquids and gases. The complete housing for the sensor is reliable at pressures up to 70 MPa and temperatures up to 423 K.

4.4 Laboratory procedure - Experimental equipment

The MEMS sensors have been undergoing a number of experimental tests. These have been carried out by myself and others [40] at the Schlumberger Research centre in Cambridge. Despite carrying out tests on the sensors in tolurene, the results from these tests were not comprehensive enough to include here. Instead, I will refer to results taken from experiments carried out by Claire Jakeways. The basic set-up for the experiments can be seen in the figures (4.6) and (4.7). Some pieces of equipment have been upgraded since the photographs were taken.

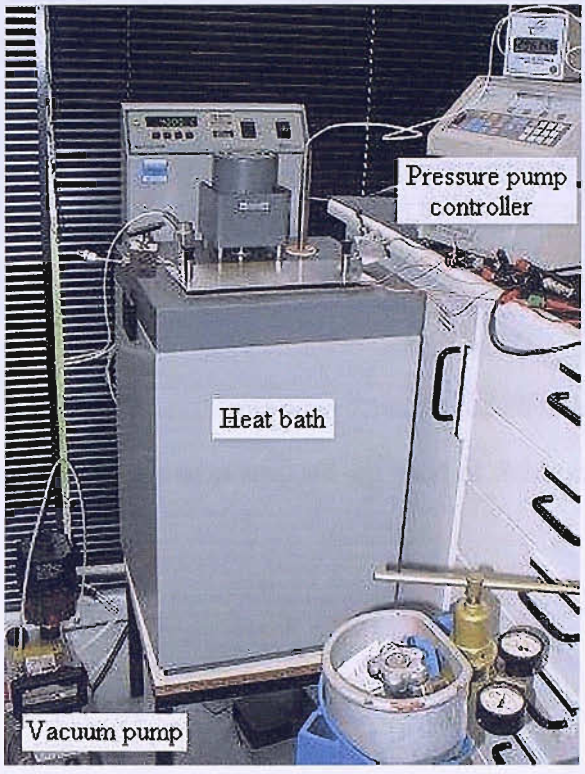

Figure 4.6: Heat bath containing the MEMS sensor and fluid sample

The first stage is to check that the sensors resonate correctly in air. The sensors are wired into the configuration shown in figure (4.8). A sinusoidal current is injected by the wave generator into the coil on the sensor using a typical voltage of 50 mVp-p. The plate is vibrated by placing a permanent magnet near the sensor creating a magnetic field of the order 0.1 T. A dc power supply feeds the Wheatstone bridge with 0.5 V dc. A preamplifier is attached between the output of the Wheatstone bridge and the lock-in amplifier. This allows the lock-in amplifier to compare the reference signal from the wave generator with the signal from the preamplifier. The lock-in amplifier then computes the phase difference and amplitude for every frequency.

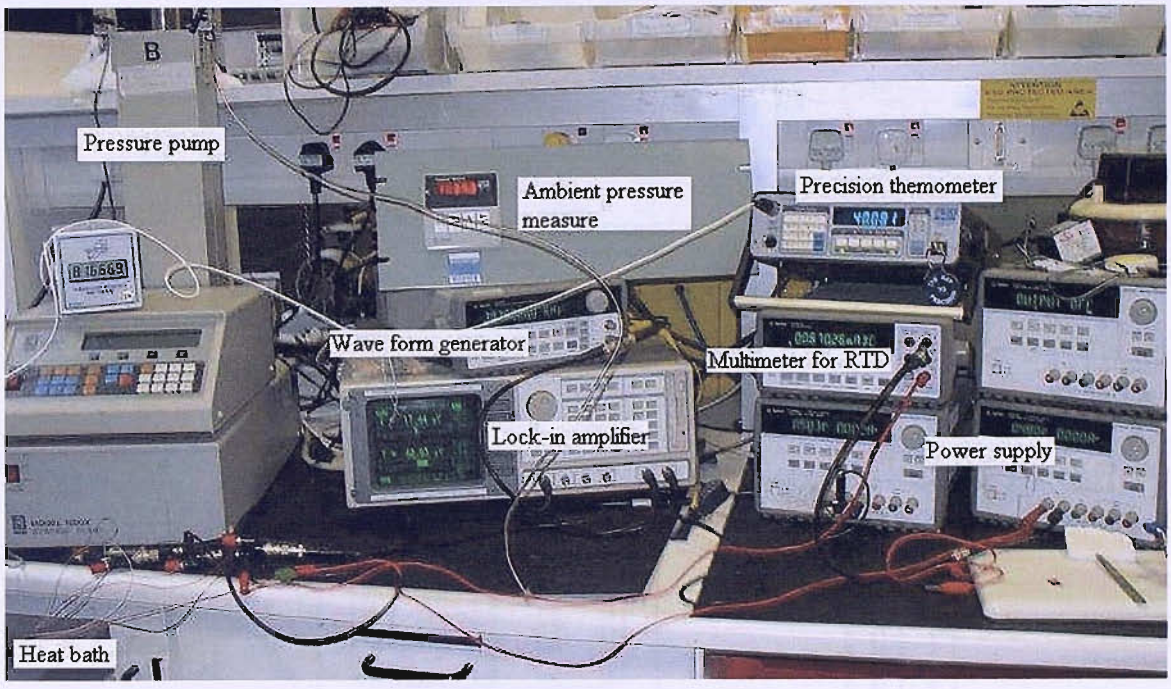

Figure 4.7: Example of the experimental set-up used at Schlumberger Cambridge

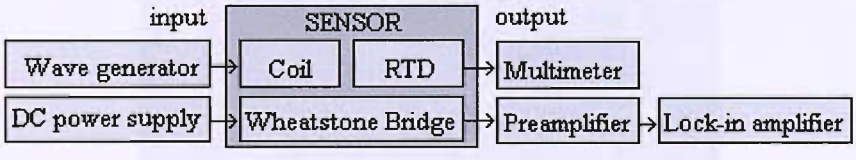

Figure 4.8: Equipment and wiring schematic [40]

Measurements are then taken in vacuum. This is done in the pressure system shown in figure (4.11). At this stage the structure can break in resonance owing to a dramatic increase in the quality factor. To prevent this occurring, the amplitude of the voltage in the coil is reduced.

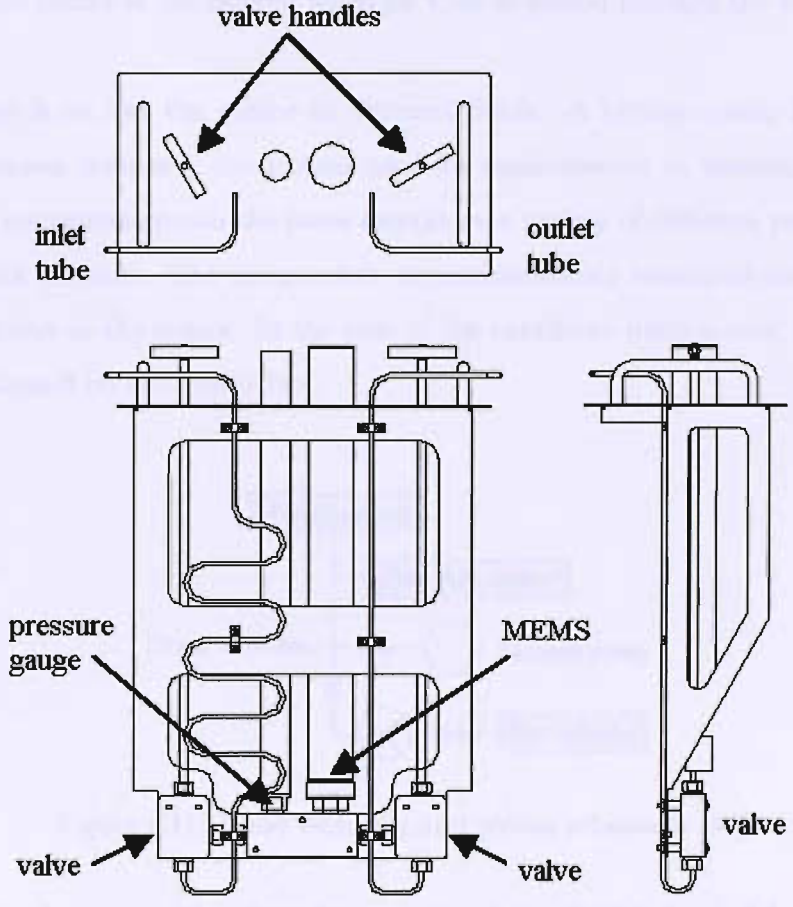

Figure 4.9: Schematic of apparatus submerged in fluid bath. Reproduced directly from [37]

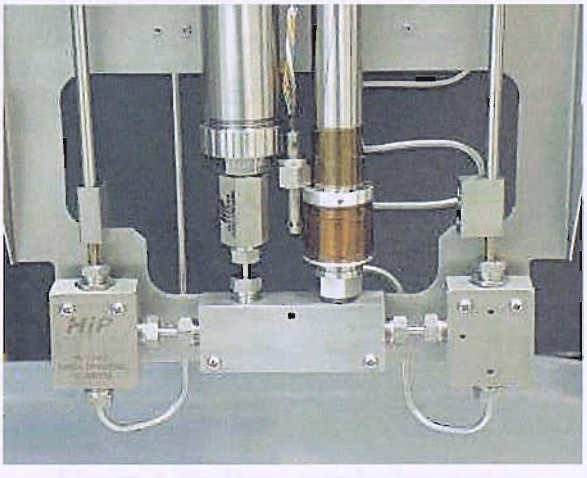

Figure 4.10: Photograph of apparatus in figure (4.9)

The MEMS is inserted into an adaptor which fits into the top of a block containing a port for the pressure gauge and tubes at each end for the fluid to be flushed through, see figure (4.9). The volume between the two valves is approximately 2 cm^3. The electromagnet is formed in an aluminium bobbin, containing about 700 turns of polyimide coated copper wire, and is mounted outside the protective tube. A magnetic field, with a flux of 0.1 T, is produced at the centre of the bobbin when 25 V dc is passed through the copper coil.

The final stage is to test the sensor in different fluids. A syringe pump injects a small sample of a known fluid into the system used for measurement in vacuum. This system can carry out measurements on the same sample at a variety of different pressures, beginning at ambient pressure. The temperature is simultaneously measured using a platinum thermometer close to the sensor. In the case of the cantilever plate sensor, the RTD thermometer is situated on the sensor face.

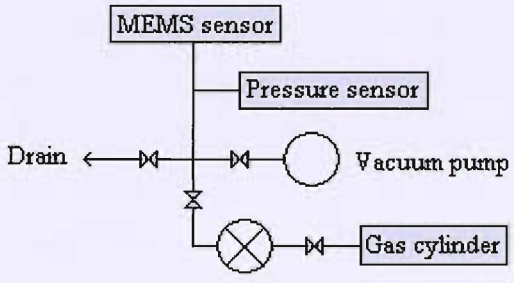

Figure 4.11: Fluid handling and piping schematic [40]

Once the required measurements have been obtained, the fluid is drained from the system, or vented into a fume cupboard in the case of gases. Between samples, the apparatus is evacuated to a pressure below 13 mPa. The apparatus, set at a temperature of 373 K between fluids, is then cooled to 323 K and flushed three times with the next fluid to be measured. The equipment is evacuated for about 12 hours between different fluid samples.

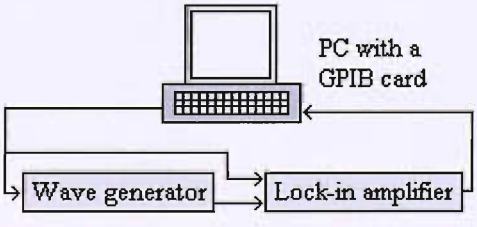

Figure 4.12: Data acquisition system

The temperature and pressure of the system is controlled manually using the heat bath and pressure pump controller, both shown in figure (4.6). The precision thermometer is accurate to 10 mK. The set-up in figure (4.12) is used for automating the remaining data acquisition. The PC is installed with an 82350A Agilent GPIB card. The settings for the wave generator and lock-in amplifier are controlled with a HT-Basic program. This controls the scanning of frequencies and reads the output of the lock-in amplifier to give the resonance frequency and the quality factor, as required.

Chapter 5

The Spider

5.1 The transversely oscillating MEMS device

We model the plate in each of the MEMS devices as an elastic solid oscillating in a fluid. The spider takes the form of an oscillating plate, fabricated from silicon using the methods of Micro-Electro-Mechanical-Systems (MEMS). The plate is about 1.6 mm wide, 2.4 mm long and 20 μm thick. It is suspended from a 0.4 mm thick support by 48 square cross-section legs each of length 0.5 mm with width and depth of 20 μm. The process of lithography is used to deposit layers atop the silicon that can be formed into resistors and metallic tracks. The latter traverse the supporting legs to provide connections between the plate and external electronics. The oscillating plate is a mechanical element that can be set in motion by the force between an electric current flowing in the plate and an externally applied magnetic field, producing corresponding alternating Laplace forces, which force the plate to oscillate. The viscometer can be operated in either forced or transient mode and is intended for use in both Newtonian and non-Newtonian fluids. The device is named the "spider" owing to the legs that connect the transversely oscillating plate to the viscometer support and interconnecting body.

Two different mathematical models for the determination of viscosity will be discussed. The "forced" model is time-independent, with the plate oscillating at a fixed forced frequency. We will then analyse the "plucked" problem, considering the transient or time-dependent behaviour, where the amplitude of oscillation varies in time, decaying gradually after an initial perturbation. We will consider the general case of incompressible fluids, using the Navier-Stokes equation to model Newtonian fluid motion and a reduced form of Maxwell's equations for viscoelastic fluid motion.

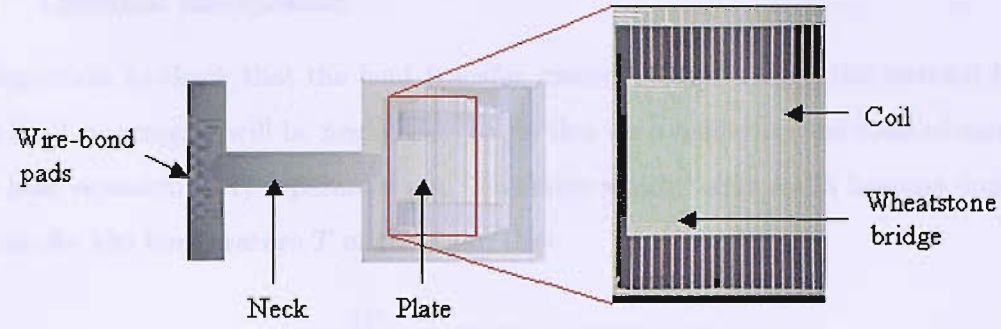

Figure 5.1: Photograph of the upper surface of the 'spider'

As discussed previously, the plate will oscillate at the maximum amplitude in the first bending mode at resonant frequency when the current reaches the first natural frequency of the sensor. Theoretically an armature will possess an infinite number of modes of vibration and so give a complex interaction with the surrounding fluid. Generally, several of the modes will be measurable. To obtain a description of the fluid-armature interaction that we will be able to model we will assume these modes are well separated and that each mode may be described by a linear simple harmonic oscillator. The various modes for the spider sensor are shown in figure (5.2). These diagrams were reproduced from analysis carried out by Maria Manrique at Schlumberger Research using the finite element package ANSYS. The mode of interest for this MEMS device is the 3rd, with the plate oscillating in a plane, reducing the problem to two dimensions.

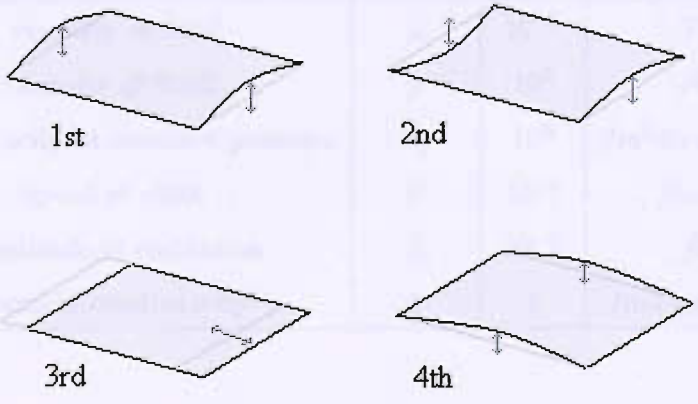

Figure 5.2: Various modes of oscillation of the 'spider': 1st mode at 16.9 kHz, 2nd mode at 20.6 kHz, 3rd mode at 34.5 kHz and 4th mode at 40 kHz

5.1.1 Thermal dissipation

It is important to check that the heat transfer caused by dissipation, the internal friction due to fluid movement, will be negligible. To do this we consider typical sizes of each term of the heat equation (5.1) separately and determine which terms could become dominant. We have, for the temperature T of the fluid, that

$$\rho c_p(\frac{\partial T}{\partial t} + (\mathbf{q}.\nabla)T) = k\nabla^2 T + \mu\Theta \tag{5.1}$$

with

$$\Theta = \frac{\partial q_i}{\partial x_j}\frac{\partial q_i}{\partial x_j}$$

where c_p is the specific heat capacity of the fluid, ρ is the density of the fluid, k is the thermal conductivity of the fluid and we assume that suitable boundary conditions may be posed at the surface of the plate.

For this analysis and throughout this work, unless otherwise stated, we will use values for the variables as given in table (5.1). Here we use them to obtain order of magnitude estimates for each of the terms in equation (5.1).

Table 5.1: Assumed values for variables

Proprty	Symbol	Value	Units
viscosity of fluid	μ	10^{-3}	/Pa·s
density of fluid	ρ	10^{3}	/Pa
heat capacity at constant pressure	c_p	10^{3}	/m^2·kg·s^{-2}·K^{-1}
speed of plate	U	10^{-2}	/m·s^{-1}
amplitude of oscillation	L	10^{-6}	/m
thermal conductivity	k	1	/m·kg·s^{-3}·K^{-1}

The first term, corresponding to advection, can be written

$$\frac{\rho c_p \triangle T U}{L}$$

We are using typical experimental values for ρ and c_p. The length scale L is chosen to represent the amplitude in meters of oscillation of the plate, and U is an approximation

of the speed of the plate in seconds found experimentally. The temperature T can change during down-hole drilling and we will consider a change of anywhere up to 300 K. This gives us an approximate value for the first term of

$$\frac{10^3 \times 10^3 \times 300 \times 10^{-2}}{10^{-6}} \approx 3 \times 10^{12} \text{kg·m}^{-1}\text{·s}^{-3}$$

The next term in (5.1) is associated with heat diffusion. This term is written as

$$\frac{k\triangle T}{L^2}$$

with k being of order 1 for most solids. This second term also has an approximate value of

$$\frac{1 \times 300}{10^{-6} \times 10^{-6}} \approx 3 \times 10^{12} \text{kg·m}^{-1}\text{·s}^{-3}$$

The third term in (5.1) corresponds to heat dissipation. The order of magnitude of this term is written

$$\frac{\mu U^2}{L^2}$$

where μ is the fluid viscosity. This gives a value of order 10^7, a significantly smaller value than the contribution from either of the previous two terms. Even in a fluid of greater viscosity it is extremely unlikely that the dissipation term will ever become dominant.

To accurately analyse the heat balance for the whole of the plate you would also have to consider heating associated with the electrical energy in the coil of wires on the plate surface. Experimentally, the current through the wires in liquid, I, has been recorded to be around 1×10^{-3} A. The resistance in the wires, R, is approximately 300 Ω. The heating due to the circuitry will cause a negligible heat increase on the plate and so need not be worried about.

This analysis shows that the advection term will normally be the most dominant of the four contributing terms in equation (5.1). Therefore for the purpose of this work we will assume that temperature change is negligible and as such do not need to worry about a heating term.

5.1.2 Introducing viscosity

The spider is a uni-directional device. As the sensor oscillates in a fluid, fluid layers form around the surface of the moving plate. These layers of fluid must move with the plate and in effect the mass of the fluid within the layers is added to the mass of the plate (the so called "added mass" effect). The plate now has to work harder to oscillate at the same speed, to compensate for this added mass. This increase in work will be proportional to the viscosity and density of the surrounding fluid.

The plate itself has extremely small dimensions and its mass reflects this. This means that the addition of the fluid's mass will be much more significant than it would be to a larger sensor, making the device more sensitive to the fluid properties. In theory the plate could be made even thinner to reduce mass yet further but this will make the device less robust and more prone to breakage. The sensor must also be able to survive and operate in down hole conditions.

5.2 Forced oscillations

5.2.1 The mechanics of the infinite plate

For a simplified model, the plate is assumed to be infinite in both the x and z directions and lie initially in the x-z plane. The surface of the plane bounds an incompressible fluid, at first considered to flow in the region $y > 0$. The plane is forced to oscillate in the x direction with simple harmonic motion, confined to the x-z plane. The velocity of the plate can thus be defined as $\mathbf{q} = [U_p(y,t), 0, 0]$ with

$$U_p = U_0 e^{-i\omega t}$$

where ω is the frequency of oscillation and U_0 is the amplitude.

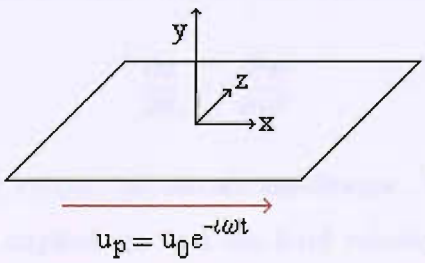

Figure 5.3: Plane oscillating in the x-direction, U_p is the plate velocity in this direction

Newtonian viscous Flow

We first consider the plate oscillating in an infinite volume of liquid and then discuss what happens when there is a second stationary plate at a height $y = +h$ from the first. A second plate is a practical consideration by Schlumberger as a measure of preventing larger particles of rock and dirt from reaching the oscillating plate and potentially damaging it. We assume the viscous fluid bounded by the plane has a plane parallel shear flow [44] with motion of the form

$$\mathbf{v} = \begin{pmatrix} u(y,t) \\ 0 \\ 0 \end{pmatrix}$$

For an incompressible fluid, the motion can be described by the equation of continuity and the Navier-Stokes equations. Acceleration caused by gravity, $g \approx 10$, is small in comparisson to the acceleration of the plate, $u_t \approx 10^2$, so neglecting gravity these are reduced to

$$\nabla.\mathbf{v} = 0 \tag{5.2}$$

$$\frac{\partial u}{\partial t} = -\frac{1}{\rho}\frac{\partial p}{\partial x} + \nu\frac{\partial^2 u}{\partial y^2} \tag{5.3}$$

$$\frac{\partial p}{\partial y} = \frac{\partial p}{\partial z} = 0. \tag{5.4}$$

The first of these is automatically satisfied because u is independent of x hence $\mathrm{div}(\mathbf{v}) = \frac{\partial u}{\partial x} = 0$. Rearranging (5.3), $\frac{\partial p}{\partial x}$ is the difference between two terms. Each of these terms is independent of x therefore p_x can be only a function of t. We assume there is no applied pressure gradient and define p to be a linear function of x with equal pressures at $x = \pm\infty$. Since p_x is independent of x, it follows that

$$\frac{\partial p}{\partial x} = 0.$$

Substituting this into (5.3) we are left with the one-dimensional diffusion equation

$$\frac{\partial u}{\partial t} = \nu\frac{\partial^2 u}{\partial y^2}. \tag{5.5}$$

We now need to solve (5.5) subject to certain conditions. When no stationary plate is present, the only conditions implied are that the fluid velocity at the plate surface will be equal to the velocity of the plate at each instant and the fluid has zero velocity far from

the plate. Thus

$$u = U_p = U_0 e^{-i\omega t} \qquad \text{on} \qquad y = 0, \tag{5.6}$$

$$u \to 0 \qquad \text{as} \qquad y \to \infty. \tag{5.7}$$

We assume that the solution will take the form

$$u = f(y)e^{-i\omega t}. \tag{5.8}$$

This is substituted into (5.5) to obtain

$$\frac{\partial^2 f}{\partial y^2} + \frac{i\omega}{\nu} f = 0.$$

This can be solved for $f(y)$ and has the solution

$$f = \varsigma_1 e^{\lambda_1 y} + \varsigma_2 e^{\lambda_2 y} \tag{5.9}$$

where ς_1 and ς_2 are constants to be determined and $\lambda = \sqrt{\frac{-i\omega}{\nu}}$ so that

$$\lambda_1 = \sqrt{\frac{\omega}{2\nu}}(i-1) \qquad \text{and} \qquad \lambda_2 = \sqrt{\frac{\omega}{2\nu}}(1-i).$$

To satisfy the boundary conditions (5.6) and (5.7), we need

$$\varsigma_1 = U_0 \qquad \text{and} \qquad \varsigma_2 = 0$$

Substituting $f(y)$ into (5.8) the velocity becomes

$$u = Re\left(U_0 e^{-\frac{y}{\delta}} e^{i(\frac{y}{\delta} - \omega t)}\right) \tag{5.10}$$

where $\delta = \sqrt{\frac{2\nu}{\omega}}$ is the viscous penetration depth. Taking real parts only we reduce (5.10) to

$$u = U_0 e^{-\frac{y}{\delta}} \cos(\frac{y}{\delta} - \omega t). \tag{5.11}$$

The fluid flow (u) can be plotted using known material properties of the plate, figure (5.4). It can be seen that as the plate oscillates, a corresponding wave is formed in the fluid propagating from the plate surface. The oscillations of this wave decrease as it moves further from the plate. This is what we would expect to happen physically, the fluid being dragged with the plate due to the resistance on the no-slip surface and the viscosity of the

fluid.

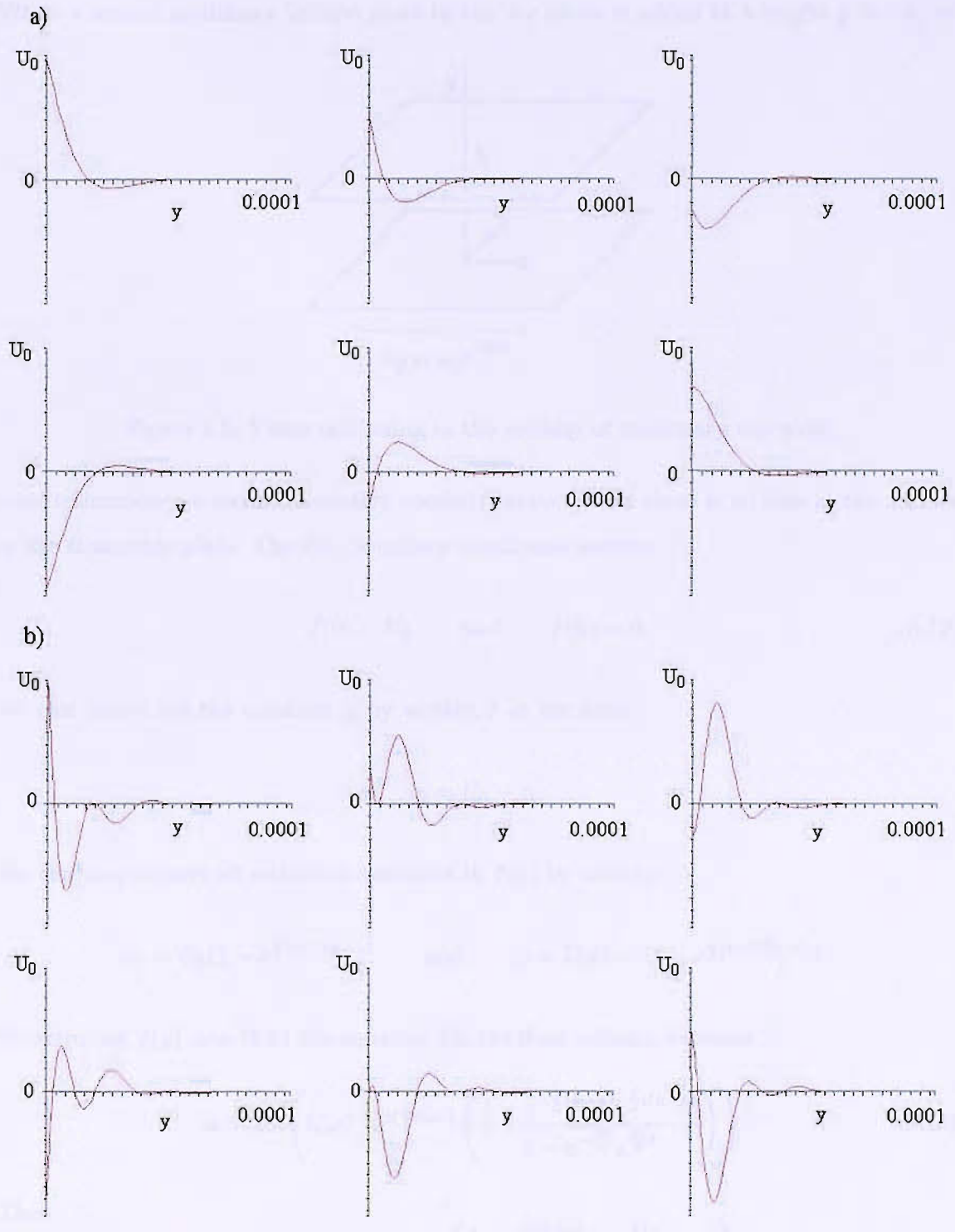

Figure 5.4: (a) Newtonian viscous flow in an infinite volume of liquid (one complete period) (b) Newtonian viscous flow bounded by a stationary plate at $h = 0.0001$ m (In all plots, y is shown between 0 and 0.0001 m

Newtonian viscous flow bounded by a stationary plate

When a second stationary infinite plate in the x-z plane is added at a height $y = +h$, we

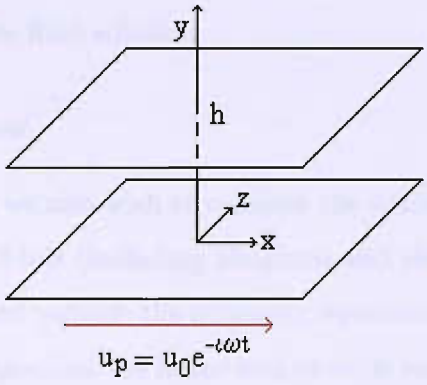

Figure 5.5: Plane oscillating in the vicinity of stationary top plate

need to introduce a second boundary condition stating that there is no flow at the surface of the stationary plate. The two boundary conditions become

$$f(0) = U_0 \qquad \text{and} \qquad f(h) = 0. \tag{5.12}$$

We can cancel out the constant ς_2 by writing it in the form

$$\varsigma_2 = U_0 - \varsigma_1.$$

We can now remove all unknown constants in $f(y)$ by writing

$$\varsigma_1 = U_0(1 - e^{\frac{2}{\delta}(i-1)h})^{-1} \qquad \text{and} \qquad \varsigma_2 = U_0(1 - (1 - e^{\frac{2}{\delta}(i-1)h})^{-1}).$$

Substituting $f(y)$ into (5.8) the equation for the fluid velocity becomes

$$u = Re\left(U_0 e^{-\frac{y}{\delta}} e^{i(\frac{y}{\delta} - \omega t)} \left(\frac{1 - e^{-\frac{2}{\delta}(h-y)} e^{\frac{2}{\delta}i(h-y)}}{1 - e^{-\frac{2h}{\delta}} e^{\frac{2h}{\delta}i}}\right)\right). \tag{5.13}$$

Thus

$$u = U_0 e^{\frac{y}{\delta}} \cos\left(\frac{y}{\delta} + \omega t\right) \left(\frac{1 - e^{\frac{2}{\delta}(h-y)} \cos\frac{2}{\delta}(h-y)}{1 - e^{\frac{2h}{\delta}} \cos\frac{2h}{\delta}}\right). \tag{5.14}$$

When the flow (u) is plotted, figure (5.4), we see a similar propagating wave in the fluid caused by the oscillations of the plate. As previously mentioned, the second plate is to protect the oscillating plate from particles of rock and dirt, so for this reason we need h to be small. With the stationary plate positioned at a height of $h = 0.0001$ m from the moving

plate, there appear to be more oscillations than in the infinite fluid case. This makes sense physically since the wave has less distance in which to decay and must have zero velocity at the stationary plate due to the no-slip condition applied there. As h increases, the fluid flow will approach the infinite fluid solution.

5.2.2 Visco-elastic Flow

As discussed in chapter two, we also wish to consider the spider sensor in a non-Newtonian fluid. For Herschel-Bulkley fluids (including Bingham and shear-thinning fluids), matters become extremely complicated because the necessary equations are non-linear. For a visco-elastic fluid, the governing equations are linear and so some analytic progress can be made. For this reason we chose to model the fluid as a Maxwell fluid.

We first return to the single plate model. In a similar way to the Newtonian case we substitute the assumed form of the solution (5.8) into the equation for Maxwell fluid motion (2.14) to produce an equation to be solved for $f(y)$ in the form

$$\frac{\partial^2 f}{\partial y^2} - \frac{\omega}{\nu}(-i - \omega\theta)f = 0. \tag{5.15}$$

This has the solution

$$f = \varpi_1 e^{\lambda_1 y} + \varpi_2 e^{\lambda_2 y} \tag{5.16}$$

where ϖ_1 and ϖ_2 are constants to be determined and

$$\lambda_1 = i\sqrt{\frac{\omega}{\nu}}(1+\omega^2\theta^2)^{\frac{1}{4}}\left[\cos(\frac{\gamma}{2}) + i\sin(\frac{\gamma}{2})\right]$$

$$\lambda_2 = i\sqrt{\frac{\omega}{\nu}}(1+\omega^2\theta^2)^{\frac{1}{4}}\left[\cos(\frac{\gamma}{2}+\pi) + i\sin(\frac{\gamma}{2}+\pi)\right]$$

with $\gamma = \arctan\frac{1}{\omega\theta}$. We require that the real part of λ satisfies $Re(\lambda) < 0$ and to satisfy the boundary condition (5.6), we need

$$\varpi_1 = U_0 \qquad \text{and} \qquad \varpi_2 = 0.$$

Substituting $f(y)$ into (5.8) the velocity becomes

$$u = Re\left(U_0 e^{-\sqrt{\frac{\omega}{\nu}}(1+\omega^2\theta^2)^{\frac{1}{4}}\sin(\frac{\gamma}{2})y} e^{i(\sqrt{\frac{\omega}{\nu}}(1+\omega^2\theta^2)^{\frac{1}{4}}\cos(\frac{\gamma}{2})y - \omega t)}\right). \tag{5.17}$$

Taking the real parts only we reduce (5.17) to

$$u = U_0 e^{-\sqrt{\frac{\omega}{\nu}}(1+\omega^2\theta^2)^{\frac{1}{4}}\sin(\frac{\gamma}{2})y}\cos\left(\sqrt{\frac{\omega}{\nu}}(1+\omega^2\theta^2)^{\frac{1}{4}}\cos(\frac{\gamma}{2})y - \omega t\right). \tag{5.18}$$

When the plate oscillates in the visco-elastic fluid, a corresponding wave will be formed. By plotting the fluid flow with various values of θ, figure (5.6), it is shown that an increase in the shear modulus of the fluid (a decrease in θ) results in a decrease in the number of oscillations of the propagating wave.

Visco-elastic flow bounded by stationary plate

It is again of interest to study the problem with the addition of a second stationary infinite plate in the x-z plane at a height $y = +h$. We impose two boundary conditions,

$$f(0) = U_0 \qquad \text{and} \qquad f(h) = 0. \tag{5.19}$$

The first corresponds to the fluid and plate velocities being equal in the plane $y = 0$ and the second states that there is no flow at the surface of the stationary plate. Applying the boundary conditions as in the previous three examples we achieve the following equation for $f(y)$:

$$f(y) = U_0 e^{py}\left(\frac{1 - e^{2p(h-y)}}{1 - e^{2ph}}\right) \tag{5.20}$$

where $p = i\sqrt{\frac{\omega}{\nu}}(1+\omega^2\theta^2)^{\frac{1}{4}}\cos\frac{\gamma}{2} - \sqrt{\frac{\omega}{\nu}}(1+\omega^2\theta^2)^{\frac{1}{4}}\sin\frac{\gamma}{2}$.

Substituting $f(y)$ into (5.8) the equation for the fluid velocity becomes

$$u = U_0 e^{-\sqrt{\frac{\omega}{\nu}}(1+\omega^2\theta^2)^{\frac{1}{4}}\sin\frac{\gamma}{2}y} e^{i[\sqrt{\frac{\omega}{\nu}}(1+\omega^2\theta^2)^{\frac{1}{4}}\cos\frac{\gamma}{2}y - \omega t]} \times \tag{5.21}$$

$$\left[\frac{1 - e^{2i(h-y)\sqrt{\frac{\omega}{\nu}}(1+\omega^2\theta^2)^{\frac{1}{4}}\cos\frac{\gamma}{2}} e^{-2(h-y)\sqrt{\frac{\omega}{\nu}}(1+\omega^2\theta^2)^{\frac{1}{4}}\sin\frac{\gamma}{2}}}{1 - e^{2ih\sqrt{\frac{\omega}{\nu}}(1+\omega^2\theta^2)^{\frac{1}{4}}\cos\frac{\gamma}{2}} e^{-2h\sqrt{\frac{\omega}{\nu}}(1+\omega^2\theta^2)^{\frac{1}{4}}\sin\frac{\gamma}{2}}}\right].$$

When this fluid velocity is plotted, figure (5.6), we once again see a propagating wave in the fluid caused by the oscillations of the plate. From the plots we can see that as the stationary plate comes within 0.00001 m of the oscillating plate, the wave becomes unable to produce a complete cycle. This tells us that to allow for a reasonable number of oscillations in the fluid flow we should keep the stationary plate at a height of $h > 0.0001$ m.

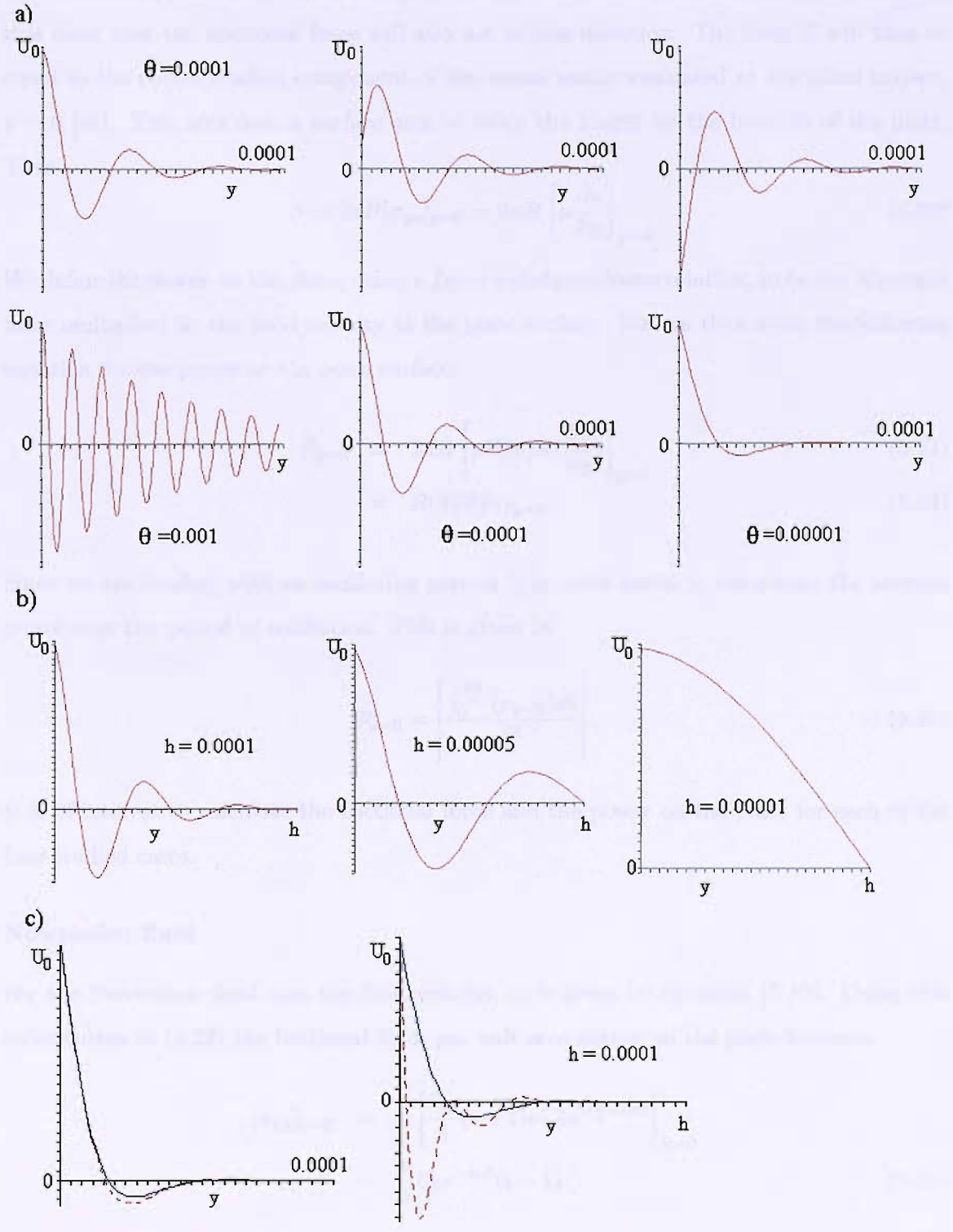

Figure 5.6: (a) Visco-elastic flow in an infinite volume of liquid, with different values of θ /GPa and y shown between 0 and 0.0001 m (b) Visco-elastic flow bounded by a stationary plate at various heights (h /m) (c) Comparisson between Newtonian (dashed lines) and visco-elastic flow (full lines)

5.2.3 Frictional force and Power on the plate

The oscillating plate only has a non-zero velocity component in the x-direction therefore it is clear that the frictional force will also act in this direction. The force S will thus be equal to the corresponding component of the stress tensor evaluated at the plate surface, $y = 0$ [43]. This acts over a surface area of twice the length by the breadth of the plate. Thus

$$S = 2aB[\sigma_{yx}]_{y=0} = 2aB\left[\mu\frac{\partial u}{\partial y}\right]_{y=0}. \tag{5.22}$$

We define the power on the plate, using a $force \times distance/time$ relation, to be the frictional force multiplied by the fluid velocity at the plate surface. We can thus write the following equation for the power at the plate surface:

$$\begin{aligned} P_{y=0} &= 2aB\left[\mu\Re(u)\Re(\frac{\partial v}{\partial y})\right]_{y=0} && (5.23)\\ &= \Re(S)\Re(u)_{y=0}. && (5.24) \end{aligned}$$

Since we are dealing with an oscillating system it is more useful to determine the average power over the period of oscillation. This is given by

$$P_{y=0} = \left|\frac{\int_0^{\frac{2\pi}{\omega}}(p_{y=0})dt}{\frac{2\pi}{\omega}}\right|. \tag{5.25}$$

It is of interest to calculate the frictional force and the power on the plate for each of the four studied cases.

Newtonian fluid

For the Newtonian fluid case the fluid velocity, u, is given by equation (5.10). Using this substitution in (5.22) the frictional force per unit area acting on the plate becomes

$$\begin{aligned} [\sigma_{yx}]_{y=0} &= \mu\left[\frac{U_0}{\delta}(i-1)e^{-\frac{y}{\delta}}e^{i(\frac{y}{\delta}-\omega t)}\right]_{y=0}\\ &= \frac{\mu}{\delta}U_0e^{-i\omega t}(i-1). && (5.26) \end{aligned}$$

Assuming that U_0 is real we take the real part of (5.26) to obtain

$$\Re(S_y) = -2aB\sqrt{(\omega\mu\rho)}U_0\cos(\omega t + \frac{1}{4}\pi). \tag{5.27}$$

The velocity of the oscillating plate is $U_p = U_0 \cos \omega t$, hence we observe a phase difference between this velocity and the frictional force. To find the power we also need to determine the real part of the fluid velocity at the plate surface, found by evaluating equation (5.11) at $y = 0$:

$$\Re(u)_{y=0} = U_0 \cos(\omega t). \tag{5.28}$$

The relevant substitutions can now be made into equation (5.23) to give

$$P_{y=0} = -2aBU_0 \cos(\omega t)\sqrt{(\omega\mu\rho)}U_0 \cos(\omega t + \frac{\pi}{4}) \tag{5.29}$$

which results in a time averaged power of

$$|P_{y=0}| = \frac{1}{\sqrt{2}} aBU_0{}^2\sqrt{\omega\mu\rho}. \tag{5.30}$$

We can now rearrange this formula to get an equation for viscosity or density in terms of power and initial velocity.

$$\mu = \frac{2}{\omega\rho}\left[\frac{|P_{y=0}|}{aBU_0{}^2}\right]^2 \tag{5.31}$$

Addition of stationary top plate

With the added top plate at $y = h$ we obtained an equation for u given by (5.13) which can be rewritten as

$$u = U_0 e^{-i\omega t}\left(\frac{\sin\frac{1+i}{\delta}(h-y)}{\sin\frac{1+i}{\delta}h}\right) \tag{5.32}$$

In this case the frictional force per unit area on the oscillating plate is given by

$$S_{1y} = \mu\left(\frac{\partial u}{\partial y}\right)_{y=0}. \tag{5.33}$$

Substituting (5.32) into the above we obtain

$$S_{1y} = -\sqrt{(\frac{1}{2}\omega\mu\rho)}(1+i)U_0 e^{-i\omega t}\cot\left(\frac{1+i}{\delta}\right)h. \tag{5.34}$$

The frictional force per unit area acting on the stationary plate is found using

$$\begin{aligned} S_{2y} &= \mu(\frac{\partial u}{\partial y})_{y=h} \\ &= \sqrt{(\frac{1}{2}\omega\mu\rho)}(1+i)U_0 e^{-i\omega t} cosec\left(\frac{1+i}{\delta}\right)h. \end{aligned} \tag{5.35}$$

Assuming U_0 is real we take the real part of (5.34) to be

$$\begin{aligned}\Re(S_{1y}) &= \sqrt{\frac{\omega\mu\rho}{2}}U_0 h(\cos\omega t\sin(\tfrac{1}{\delta})\cos(\tfrac{1}{\delta}) - \sin\omega t\sinh(\tfrac{1}{\delta})\cosh(\tfrac{1}{\delta}) \\ &\quad + \cos\omega t\sinh(\tfrac{1}{\delta})\cosh(\tfrac{1}{\delta}) + \sin\omega t\sin(\tfrac{1}{\delta})\cos(\tfrac{1}{\delta}))/(\cos(\tfrac{1}{\delta})^2 - \cosh(\tfrac{1}{\delta})^2).\end{aligned} \tag{5.36}$$

The real part of (5.35) can be written

$$\begin{aligned}\Re(S_{2y}) &= \sqrt{\frac{\omega\mu\rho}{2}}U_0 h(-\cos\omega t\sin(\tfrac{1}{\delta})\cosh(\tfrac{1}{\delta}) + \sin\omega t\sinh(\tfrac{1}{\delta})\cos(\tfrac{1}{\delta}) \\ &\quad - \cos\omega t\sinh(\tfrac{1}{\delta})\cos(\tfrac{1}{\delta}) - \sin\omega t\sin(\tfrac{1}{\delta})\cosh(\tfrac{1}{\delta}))/(\cos(\tfrac{1}{\delta})^2 - \cosh(\tfrac{1}{\delta})^2).\end{aligned} \tag{5.37}$$

The real part of equation (5.32) when evaluated at the plate surface reduces to

$$\Re(u)_{y=0} = U_0\cos(\omega t). \tag{5.38}$$

Equations (5.38) and (5.36) can now be substituted into the equation for average power over time, evaluated at the plate surface, resulting in the following expression for $P_{y=0}$

$$P_{y=0} = \sqrt{\frac{\omega\mu\rho}{2}}aBh\frac{{U_0}^2}{\omega^2}\left(\frac{\sin\frac{1}{\delta}\cos\frac{1}{\delta} + \sinh\frac{1}{\delta}\cosh\frac{1}{\delta}}{\cosh\frac{1}{\delta}^2 - \cos\frac{1}{\delta}^2}\right). \tag{5.39}$$

Once again we can rearrange this formula to derive an expression for viscosity or density.

$$\mu\rho = \frac{2}{\omega}\left[\frac{|P_{y=0}|\omega^2}{{U_0}^2 aBh}\left(\frac{\cosh\frac{1}{\delta}^2 - \cos\frac{1}{\delta}^2}{\sin\frac{1}{\delta}\cos\frac{1}{\delta} + \sinh\frac{1}{\delta}\cosh\frac{1}{\delta}}\right)\right]^2. \tag{5.40}$$

Visco-elastic fluid

For the visco-elastic fluids described earlier, the fluid velocity was found to be (5.17). As in the Newtonian case, the frictional force per unit area S_y on the oscillating plate is obtained by the substitution of (5.17) into (5.26) evaluated at $y = 0$. This gave

$$\begin{aligned}S_y &= \mu\frac{\partial}{\partial y}\left[U_0 e^{-i\omega t}e^{i\sqrt{\frac{\omega}{\nu}}(1+\omega^2\theta^2)^{\frac{1}{4}}\cos(\frac{\gamma}{2})y - \sqrt{\frac{\omega}{\nu}}(1+\omega^2\theta^2)^{\frac{1}{4}}\sin(\frac{\gamma}{2})y}\right]_{y=0} \\ &= \mu U_0 e^{-i\omega t}\left[i\sqrt{\frac{\omega}{\nu}}(1+\omega^2\theta^2)^{\frac{1}{4}}\cos(\frac{\gamma}{2}) - \right. \\ &\quad \left.\sqrt{\frac{\omega}{\nu}}(1+\omega^2\theta^2)^{\frac{1}{4}}\sin(\frac{\gamma}{2})\right].\end{aligned} \tag{5.41}$$

Assuming U_0 is real we take the real part of (5.41), giving

$$\Re(S_y) = \mu U_0 \frac{\sqrt{2}}{\delta}(1+\omega^2\theta^2)^{\frac{1}{4}}\left(\sin\omega t\cos\frac{\gamma}{2} - \cos\omega t\sin\frac{\gamma}{2}\right). \tag{5.42}$$

The fluid velocity at the surface of the plate can be found by evaluating equation (5.17) at y=0. The real part of this gives us the boundary condition

$$\Re(u)_{y=0} = U_0\cos(\omega t). \tag{5.43}$$

We can substitute equations (5.42) and (5.43) into (5.23) to give us the average power at $y = 0$ in the form

$$P_{y=0} = \sqrt{(\omega\mu\rho)}aB\frac{{U_0}^2}{\omega^2}(1+\omega^2\theta^2)^{\frac{1}{4}}\sin\frac{\gamma}{2}. \tag{5.44}$$

When rearranged this expression gives the following equation for viscosity or density:

$$\mu\rho = \frac{1}{\omega}\left[\frac{|P_{y=0}|\omega^2}{aB{U_0}^2(1+\omega^2\theta^2)^{\frac{1}{4}}\sin\frac{\gamma}{2}}\right]^2 \tag{5.45}$$

Addition of stationary top plate

With the addition of the top plate at $y = +h$ we can rewrite the fluid velocity equation (5.21) as

$$u = \frac{U_0 e^{-i\omega t}}{1-e^{2hk_1}}(e^{k_1 y} - e^{2hk_1}e^{-k_1 y}) \tag{5.46}$$

where $k_1 = i\sqrt{\frac{\omega}{\nu}}(1+\omega^2\theta^2)^{\frac{1}{4}}\cos(\frac{\gamma}{2}) - \sqrt{\frac{\omega}{\nu}}(1+\omega^2\theta^2)^{\frac{1}{4}}\sin(\frac{\gamma}{2})$.
We can substitute this velocity into the following equations to find the frictional force per unit area on each of the plates. For the oscillating plate we get

$$\begin{aligned} S_{1y} &= \mu\left(\frac{\partial u}{\partial y}\right)_{y=0} \\ &= \mu U_0 e^{-i\omega t}(k_1)\left(\frac{1+e^{2h(k_1)}}{1-e^{2h(k_1)}}\right). \end{aligned} \tag{5.47}$$

For the stationary plate we obtain

$$\begin{aligned} S_{2y} &= -\mu\left(\frac{\partial u}{\partial y}\right)_{y=h} \\ &= -\mu U_0 e^{-i\omega t}(k_1)\left(\frac{2e^{h(k_1)}}{1-e^{2h(k_1)}}\right). \end{aligned} \tag{5.48}$$

The real component of S_{1y} can be written

$$\begin{aligned}\Re(S_{1y}) &= \frac{-\mu U_0 k_2}{1+e^{-4hk_2\sin\frac{\gamma}{2}}-2e^{-2hk_2\sin\frac{\gamma}{2}}\cos\left(2hk_2\cos\frac{\gamma}{2}\right)} \\ &\quad \left[(1-e^{-4hk_2\sin\frac{\gamma}{2}})\sin(\omega t+\frac{\gamma}{2})-2e^{-2hk_2\sin\frac{\gamma}{2}}\sin 2hk_2\cos\frac{\gamma}{2}\cos(\omega t+\frac{\gamma}{2})\right]\end{aligned}$$

with

$$k_2 = \sqrt{\frac{\omega\rho}{\mu}}(1+\omega^2\theta^2)^{\frac{1}{4}}. \tag{5.49}$$

As in each of the previous three cases, the real part of the fluid velocity at the surface of the plate can be reduced to

$$\Re(u)_{y=0} = U_0\cos(\omega t). \tag{5.50}$$

Once again, these expressions can be substituted into equation (5.23) for the average power at the surface $y=0$.

$$P_{y=0} = k_2\mu aB\frac{{U_0}^2}{\omega^2}\left|\frac{\sin\frac{\gamma}{2}-\sin\frac{\gamma}{2}e^{4hk_2\sin\frac{\gamma}{2}}+4e^{2hk_2\sin\frac{\gamma}{2}}\cos\frac{\gamma}{2}\sin hk_2\cos\frac{\gamma}{2}\cos hk_2\cos\frac{\gamma}{2}}{4\cos(hk_2\cos\frac{\gamma}{2})^2e^{2hk_2\sin\frac{\gamma}{2}}-1-e^{4hk_2\sin\frac{\gamma}{2}}-2e^{2hk_2\sin\frac{\gamma}{2}}}\right| \tag{5.51}$$

Unfortunately, since k_2 appears both within and outside the exponential functions in (5.51), we are unable to isolate $\mu\rho$.

We now have theoretical expressions for the frictional force and power on the oscillating plate for both the Newtonian and the visco-elastic fluid cases. These are closed form solutions and for the first three cases can be easily rearranged to give an expression for viscosity or density in terms of power and the initial velocity of the plate.

5.2.4 Experimental incompatability

The Newtonian inviscid fluid solution that we have found determines viscosity or density so that one is determined when we know the other. The solution is a function of the initial plate velocity and the power in the plate. The problem that arises in experimentation is that these two parameters are not always measured. The functions that are actually recorded by Schlumberger are the in-phase and quadrature voltage of the system. This means that we can determine the frequency and the 'Q' of the system. Q is defined by the following expression

$$Q = \frac{f_{res}}{2g}$$

where f_{res} is the resonance frequency of the plate in fluid, or the frequency which produced the highest recorded amplitude of plate motion, A_{max}, and g is described in diagram (5.7).

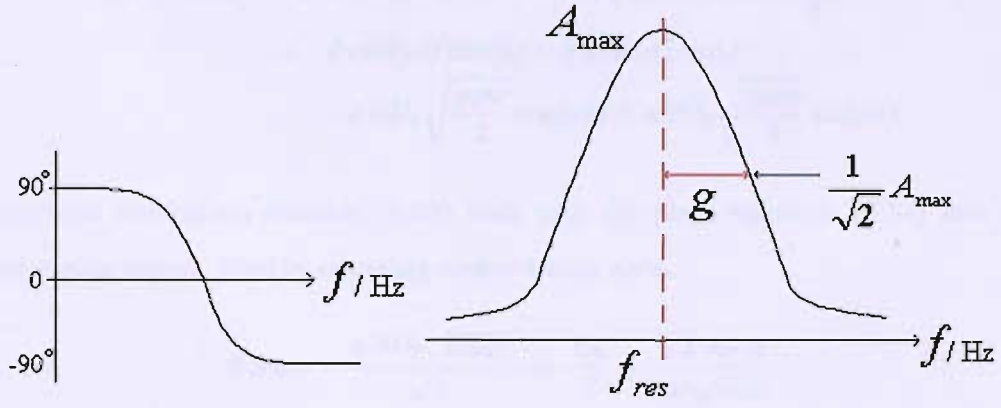

Figure 5.7: Examples of graphs produced from experiments, showing the in-phase and quadrature voltage respectively.

Plate equation

To find a solution that can be more easily compared to experimental results we need to define a different modelling strategy. First we re-pose the plate equation:

$$m\ddot{x} + mk^2x = \vartheta \cos(\omega t) - \mu v_y \tag{5.52}$$

Here m denotes the mass of the plate and k represents the spring constant, both dependent on the mechanical properties of the plate. x is the displacement of the plate from its stating position. On the right hand side of the equation is the external force on the plate, the first term relating to the uniform driving force and the second term relating to the viscous drag due to the surrounding fluid. ϑ is the magnitude of the driving, an unknown constant to be determined. We expand this by assuming that we know the solution after a long time, which is that the plate is moving at a known velocity.

$$\dot{x} = U_0 \cos(\omega t) \qquad t \to \infty. \tag{5.53}$$

We know that in this case the viscous drag term per unit area for a Newtonian fluid acting on the plate is given by equation (5.27). What is not certain is to what extent the driving force will be in phase with the plate vibrations. We can try to drive it at frequency ω, but as a result the plate may oscillate at a different frequency due to the retarding force of the surrounding fluid. We introduce a ϕ component into the driving force term to allow for a

phase difference. Putting these back into the plate equation we obtain:

$$\begin{aligned} m\ddot{x} + mk^2x &= \vartheta\cos(\omega t + \phi) - aBU_0\sqrt{\mu\rho\omega}\cos(\omega t + \frac{\pi}{4}) \\ &= \vartheta\cos(\omega t)\cos(\phi) - \vartheta\sin(\omega t)\sin(\phi) \\ &\quad -aBU_0\sqrt{\frac{\mu\rho\omega}{2}}\cos(\omega t) + aBU_0\sqrt{\frac{\mu\rho\omega}{2}}\sin(\omega t). \end{aligned} \tag{5.54}$$

We substitute the known solution (5.53) back into the plate equation (5.54) and equate sine and cosine terms. Firstly, equating cosine terms gives:

$$\vartheta\cos\phi = \frac{aBU_0\sqrt{\omega\mu\rho}}{\sqrt{2}} \Longrightarrow \frac{U_0}{\vartheta} = \frac{\sqrt{2}\cos\phi}{aB\sqrt{\omega\mu\rho}}. \tag{5.55}$$

Equating sinusoidal terms:

$$-m\omega U_0 + mk^2\frac{U_0}{\omega} = -\vartheta\sin\phi + \frac{aBU_0\sqrt{\omega\mu\rho}}{\sqrt{2}} \tag{5.56}$$

From (5.55) we have that $\vartheta = \frac{aBU_0\sqrt{\omega\mu\rho}}{\sqrt{2}\cos\phi}$. Substituting this into (5.56) and applying the relation $\cos\phi\tan\phi = \sin\phi$, produces the following expression for ϕ, our first working equation:

$$\phi = \arctan\left(1 + \frac{m\sqrt{2\omega}}{aB\sqrt{\mu\rho}} - \frac{mk^2\sqrt{2}}{aB\sqrt{\mu\rho}\omega^{\frac{3}{2}}}\right) \tag{5.57}$$

We can now substitute the equation for ϕ back into (5.55) to give us our second working equation:

$$\frac{U_0}{\vartheta} = \frac{\sqrt{2}}{aB\sqrt{\omega\mu\rho}} \frac{1}{\sqrt{1 + \left(1 + \frac{m\sqrt{2\omega}}{aB\sqrt{\mu\rho}} - \frac{mk^2\sqrt{2}}{aB\sqrt{\mu\rho}\omega^{\frac{3}{2}}}\right)^2}} \tag{5.58}$$

The result is thus two working equations which when plotted, correspond to the two graphs produced experimentally in figure (5.7). k, μ and ρ are now the only unknowns on the right hand side of equation (5.58).

If we let $\frac{U_0}{\vartheta} = H$, then the curve defined by (5.58) is found by plotting H against ω. If ω_m is the maximum recorded frequency, then this will correspond to the maximum point on the curve, when $\frac{dH}{d\omega} = 0$. Differentiating (5.58) with respect to ω and then equating this to zero we can rearrange the result to get:

$$\sqrt{\mu\rho} = \frac{m}{4aB{\omega_m}^6}\left(-{\omega_m}^{\frac{9}{2}}\sqrt{2}k^2 - 3\sqrt{2}{\omega_m}^{\frac{13}{2}} \pm \sqrt{34{\omega_m}^9k^4 + 12{\omega_m}^{11}k^2 - 14{\omega_m}^{13}}\right) \tag{5.59}$$

We consider the device oscillating in vacuum, $\sqrt{\mu\rho} = 0$, at a vacuum frequency of $\omega_v = f_v 2\pi$. Substituting this into (5.57) gives

$$m\sqrt{2\omega_v} = \frac{mk^2\sqrt{2}}{\omega_v{}^{\frac{3}{2}}}$$

which simplifies down to

$$k = \omega_v.$$

Substituting this value for k and $m = aBd\rho_s$ back into (5.59), we can simplify the solution to

$$\mu\rho = \frac{d^2{\rho_s}^2}{8{\omega_m}^3}\left({\omega_v}^2 + 3{\omega_m}^2 - \sqrt{17{\omega_v}^4 + 6{\omega_m}^2{\omega_v}^2 - 7{\omega_m}^4}\right)^2 \tag{5.60}$$

Having found a solution for the spider forced at a constant driving force, we will now consider the problem for the sensor without an external driving force so that the oscillations of the moving plate are allowed to decay.

5.3 Decaying oscillations

We consider the device to be a damped harmonic oscillator with a corresponding decay rate. When placed in a fluid, the decay in amplitude of oscillation is then hoped to be proportional to the viscosity and density of the fluid. To allow us to obtain a reasonable amount of data, we must ensure that the plate can oscillate a number of times in the fluid before the oscillations decay completely. It is possible we will also need to reject the early oscillations which could exhibit irregular transient behaviour. In a very viscous fluid this is made more difficult.

We will consider two cases of the 'spider' with decaying oscillations. In the first case, the experiment is started with the plate transversely oscillating in the x-z plane with a speed of $U_0 \cos(\omega_0 t)$. The plate is first made to oscillate for a length of time to allow the system to reach a state of steady oscillations at a constant speed. The external power input and initial frequency (ω_0) needed to maintain this speed are recorded. To begin the measurements the external power supply is switched off and the plate oscillations are allowed to decay.

In the second case, which we will consider in more detail and try to solve fully, the plate is given an arbitrary displacement and held there by an external force. Measurements begin

when the external force is removed and the plate is released with an initial velocity of 0. In effect, the 'spider' is 'plucked'. In both cases it is assumed that the legs around the edge of the plate provide resistance, r, and that plate motion is also retarded by the shear stress of the viscous fluid ($\mu u_y|_{y=0}$), acting over the surface area of the plate, top and bottom ($2aB$).

The fluid flow, $u(y,t)$, is defined by (5.5)

$$u_t = \nu u_{yy} \tag{5.61}$$

We describe the motion of the plate by the following equation

$$\rho_s dBa\frac{d^2x}{dt^2} + r\frac{dx}{dt} + k^2x = 2Ba(\mu u_y|_{y=0}) = F(t) \tag{5.62}$$

where ρ_s is the plate density, d is the plate depth, a is the plate length, B is the plate breadth and k is the spring constant. This governing equation is essentially identical to (5.52) save for the facts that (i) the plate is no longer driven and (ii) the damping of the plate legs has been included.

5.3.1 Decaying from steady oscillations

At time $t = 0$ the speed of the plate is U_0. It was shown in section (5.2.1) that a plate oscillating with a velocity of $U_p \cos(\omega t)$ produces a fluid motion $u(y,t) = U_p e^{-ky}\cos(ky - \omega t)$ with $k = (\frac{\omega\rho}{2\mu})^{\frac{1}{2}}$. This gives two initial conditions for the fluid motion, namely

$$u = U_p = U_0 \qquad \text{at} \qquad y = 0, t = 0 \tag{5.63}$$

$$u = U_0 e^{-k_0 y}\cos(k_0 y) \qquad \text{with} \qquad k_0 = (\frac{\omega_0\rho}{2\mu})^{\frac{1}{2}} \qquad \text{at} \qquad y > 0, t = 0. \tag{5.64}$$

For our two boundary conditions we have that the fluid velocity is equal to the velocity of the plate at the oscillating surface and that the fluid velocity will decrease to zero with increasing y. Thus

$$u = U_p \qquad \text{at} \qquad y = 0 \tag{5.65}$$

$$u = 0 \qquad y \to \infty. \tag{5.66}$$

As we will now show, (5.61) and (5.62) can be solved using Laplace transforms, coupling the plate and fluid motion equations into a single equation which may then be solved and analysed.

Solving the problem using Laplace transforms

We now recast the partial differential equation for $u(y,t)$ (5.61) as an ODE for $\hat{u}(y,s)$ by taking a Laplace transform in time. Equation (5.61) becomes

$$\hat{u}_{yy} - (\frac{1}{\nu})[s\hat{u} - u(y,0)] = \hat{u}_{yy} - (\frac{1}{\nu})[s\hat{u} - \dot{x}(0)] = 0. \tag{5.67}$$

We can also find the Laplace transform of the boundary condition, that the plate motion equals the fluid motion at the plate surface. We choose to define the initial velocity of the plate as U_0.

$$\hat{u} = s\hat{x} - x(0) \qquad \text{on} \qquad y = 0. \tag{5.68}$$

At time $t = 0$ the plate is assumed to be at zero amplitude and have velocity U_i so we can make the following substitutions:

$$x(0) = 0 \qquad \text{and} \qquad \dot{x}(0) = U_0.$$

A solution is then

$$\hat{u}(y,s) = \varphi_1(s)e^{y\sqrt{\frac{s}{\nu}}} + \varphi_2(s)e^{-y\sqrt{\frac{s}{\nu}}} + \frac{U_0}{s}, \tag{5.69}$$

where φ_1 and φ_2 are constants to be determined. Since it is necessary that as real s tends to ∞, $y\sqrt{\frac{s}{\nu}}$ also tends to ∞, we can simplify (5.69) by defining

$$\varphi_1(s) = 0.$$

Applying condition (5.68) we find

$$\varphi_2(s) = s\hat{x} - \frac{U_0}{s},$$

so that the fluid solution can be written

$$\hat{u}(y,s) = (s\hat{x} - \frac{U_0}{s})e^{-y\sqrt{\frac{s}{\nu}}} + \frac{U_0}{s}. \tag{5.70}$$

The Laplace transform of the plate equation (5.62) gives

$$s^2\hat{x} - sx(0) - \dot{x}(0) + s\mathsf{A}\hat{x} - \mathsf{A}x(0) + \mathsf{B}\hat{x} = \mathsf{C}\mu\hat{\mathbf{v}}_y|_{y=0} \tag{5.71}$$

where $\mathsf{A} = \frac{r}{\rho_s B d a}$, $\mathsf{B} = \frac{k^2}{\rho_s B d a}$ and $\mathsf{C} = \frac{2Ba}{\rho_s B d a}$.

Since we know the plate amplitude and velocity at time $t = 0$, we can re-write this as

$$(s^2 + \mathsf{A}s + \mathsf{B})\hat{x} - U_0 = \mathsf{C}\mu\hat{\mathbf{v}}_y|_{y=0}. \tag{5.72}$$

To couple our equations we need to differentiate our fluid solution with respect to y and evaluate this at $y = 0$.

$$\hat{\mathbf{v}}_y|_{y=0} = \left[-\left(s\hat{x} - \frac{U_0}{s}\right)\sqrt{\frac{s}{\nu}}e^{-y\sqrt{\frac{s}{\nu}}}\right]|_{y=0} = -\sqrt{\frac{s}{\nu}}\left(s\hat{x} - \frac{U_0}{s}\right) \tag{5.73}$$

This can then be substituted back into the plate equation (5.72).

$$(s^2 + \mathsf{A}s + \mathsf{B})\hat{x} - U_0 = -\mathsf{C}\mu\sqrt{\frac{s}{\nu}}\left(s\hat{x} - \frac{U_0}{s}\right) \tag{5.74}$$

We are now left with an equation just in terms of $\hat{x}$ and s, so we can take the inverse Laplace transform of this function to produce the desired solution. Here we make the substitution $\nu = \mu\rho$. We find that

$$x = U_0 L^{-1}\left[\frac{1 + \mathsf{C}\sqrt{\mu\rho}s^{-\frac{1}{2}}}{s^2 + \mathsf{C}\sqrt{\mu\rho}s^{\frac{3}{2}} + \mathsf{A}s + \mathsf{B}}\right]. \tag{5.75}$$

5.3.2 The 'plucked spider'

In the case of the 'plucked spider', the fluid equation (5.61) must be solved subject to the following boundary conditions:

$$u(t) = \frac{dx}{dt} \qquad \text{at} \qquad y = 0 \tag{5.76}$$

$$u = 0 \qquad y \to \infty. \tag{5.77}$$

As in the previous example, these correspond to the plate having equal velocity to the fluid at the plate surface and the fluid having no velocity far from the plate. In this case however, the initial condition states that both the fluid and the plate are at rest at time $t = 0$, so that

$$u = 0 \qquad \text{at} \qquad t = 0. \tag{5.78}$$

Owing to the mutual dependence of the fluid and plate velocities, we again need to couple the two equations of motion.

Solving the problem using Laplace transforms

Once again we can use Laplace transforms to define our partial differential equation for $u(y,t)$ (5.61) as an ODE for $\hat{u}(y,s)$. Equation (5.61) and the two boundary conditions become

$$s\hat{u} - \nu\hat{u}_{yy} = 0 \tag{5.79}$$

$$\hat{u}(0,s) = s\hat{x} - x(0) \tag{5.80}$$

$$\hat{u}(\infty,s) = 0. \tag{5.81}$$

The solution is

$$\hat{u}(y,s) = \Upsilon_1(s)e^{y\sqrt{\frac{s}{\nu}}} + \Upsilon_1(s)e^{-y\sqrt{\frac{s}{\nu}}} \tag{5.82}$$

where Υ_1 and Υ_1 are constants to be determined. We first apply condition (5.81). In the same way to the previous case, since it is necessary that as real s tends to ∞, $y\sqrt{\frac{s}{\nu}}$ also tends to ∞, we can simplify (5.82) by defining

$$\Upsilon_1(s) = 0$$

Applying condition (5.80) we find

$$\Upsilon_2(s) = \hat{G}(s) = s\hat{x} - x(0)$$

so that (5.82) can be written

$$\hat{u}(y,s) = (s\hat{x} - x(0))e^{-y\sqrt{\frac{s}{\nu}}} \tag{5.83}$$

Since the plate velocity is 0 at time $t = 0$, we can re-write the Laplace transform of the plate equation (5.71) as

$$(s^2 + \mathsf{A}s + \mathsf{B})\hat{x} - (s + \mathsf{A})x(0) = \mathsf{C}\mu\hat{\mathbf{v}}_y|_{y=0} \tag{5.84}$$

We can differentiate our fluid solution (5.83) with respect to y and evaluate this at $y = 0$ to get

$$\hat{u}_y|_{y=0} = \left(-\sqrt{\frac{s}{\nu}}(s\hat{x} - x(0))e^{-y\sqrt{\frac{s}{\nu}}}\right)|_{y=0} = -\sqrt{\frac{s}{\nu}}(s\hat{x} - x(0)) \tag{5.85}$$

which can then be substituted back into (5.84) to get

$$(s^2 + As + B)\hat{x} - (s + A)x(0) = -C\mu\sqrt{\frac{s}{\nu}}(s\hat{x} - x(0)) \tag{5.86}$$

As in the model starting in motion, we are once again left with an equation just in terms of x and s, so we can take the inverse Laplace transform of this function to find our required solution.

$$x = x(0)L^{-1}\left[\frac{s + A + C\sqrt{\mu\rho s}}{s^2 + As + B + C\sqrt{\mu\rho}s^{\frac{3}{2}}}\right] \tag{5.87}$$

Solving the inverse Laplace problem for the plucked model

To find our solution for x we could apply the standard formula for inverse Laplace transforms to (5.87):

$$x(t) = \frac{x(0)}{2\pi i}\int_{y-i\infty}^{y+i\infty} e^{st}f(s)ds \tag{5.88}$$

where $f(s) = \frac{s+A+E\sqrt{s}}{s^2+As+B+Es^{\frac{3}{2}}}$ and $E = C\sqrt{\mu\rho}$. However, this particular problem is complicated by the numerous singularities in f(s). To solve the integral we must first analyse these singularities and then define a contour to integrate along that excludes these points.

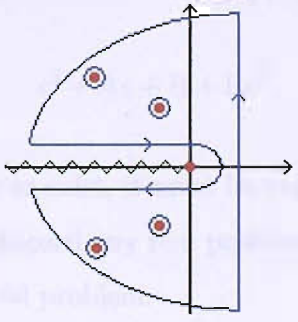

Figure 5.8: Contour excluding singular points

By multiplying $f(s)$ by its conjugate, $f(s)$ can be rewritten to give two terms which show the singularities more clearly.

$$\begin{aligned} f(s) &= \left[\frac{s + A + E\sqrt{s}}{s^2 + As + B + Es^{\frac{3}{2}}}\right]\left[\frac{s^2 + As + B - Es^{\frac{3}{2}}}{s^2 + As + B - Es^{\frac{3}{2}}}\right] \\ &= \frac{(s + A)(s^2 + As + B) - E^2s^2}{(s^2 + As + B)^2 - E^2s^3} + \frac{EB\sqrt{s}}{(s^2 + As + B)^2 - E^2s^3} \end{aligned} \tag{5.89}$$

Here we can see that four pole residues will occur due to the quartic polynomial on the base of each of the two fractions. It can be assumed that the poles will be complex conjugates

and must have negative real parts for decay to occur. The poles are determined by finding the roots of the quartic polynomial equation:

$$s^4 + (2A - E^2)s^3 + (2B + A^2)s^2 + 2BAs + B^2 = 0 \tag{5.90}$$

A further branch cut is introduced by the square root in the second term.

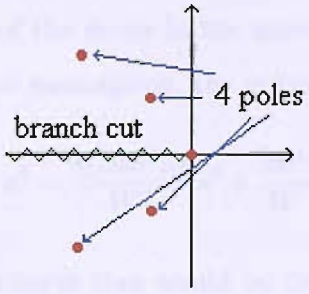

Figure 5.9: Poles and branch cut

Having multiplied $f(s)$ by its conjugate, we must be careful to rule out any poles resulting from our analysis which are also roots of the conjugate equation $s^2 + As + B - Es^{\frac{3}{2}}$. If we look back at the original polynomial on the base of $f(s)$,

$$s^2 + As + B + Es^{\frac{3}{2}},$$

we can see that if a real root was to exist, it must be negative since A,B and E are positive by definition. We can therefore discard any real positive roots from our analyis since they can not be solutions to the original problem.

The full solution to the inverse Laplace transform should have three main contributing terms, an exponential term for each complex conjugate pair and an algebraic term due to the branch cut.

Quartic polynomial analysis

We are now going to investigate the poles involved in our inverse Laplace problem. We do this by analysing the quartic polynomial (5.90) and then finding the roots. Using $A = \frac{r}{W}$, $B = \frac{k^2}{W}$ and $E = \frac{2Ba\sqrt{\mu\rho}}{W}$, where $W = \rho_s Bda$ is the weight of the plate, r represents the damping of the legs and k the simple harmonic motion of the legs, we may write the

polynomial as

$$\begin{aligned} s^4 + (2\mathsf{A} - \mathsf{E}^2)s^3 + (2\mathsf{B} + \mathsf{A}^2)s^2 + 2\mathsf{BA}s + \mathsf{B}^2 &= 0 \\ \Rightarrow s^4 + \left(\frac{2r}{W} - \frac{4(Ba)^2\mu\rho}{W^2}\right)s^3 + \left(\frac{2k^2}{W} + \frac{r^2}{W^2}\right)s^2 + \frac{2rk^2}{W^2}s + \frac{k^4}{W^2} &= 0. \end{aligned}$$

No damping case

In an attempt to simplify the problem we will assume that the interaction with the surrounding fluid provides most of the decay in the motion and that the damping of the legs is negligible ($r = 0$). Using this assumption, the polynomial becomes

$$f(s) = s^4 - \frac{4(Ba)^2\mu\rho}{W^2}s^3 + \frac{2k^2}{W}s^2 + \frac{k^4}{W^2} = 0. \tag{5.91}$$

We now choose to analyse the curve that would be drawn by plotting the polynomial f(s). By calculating the derivative of $f(s)$ with respect to s and then equating this to zero, we can work out where the turning points in the curve $f(s)$ will occur.

$$f'(s) = 4s^3 - 12\frac{(Ba)^2\mu\rho}{W^2}s^2 + 4\frac{k^2}{W}s = 0 \tag{5.92}$$

One solution will be $s = 0$. The two remaining turning points are found from the solution to the quadratic equation

$$4s^2 - 3\mathsf{E}^2 s + 4\mathsf{B} = 0 \Rightarrow s^2 - \frac{3}{4}\mathsf{E}^2 s + \mathsf{B} = 0.$$

Solving the quadratic equation to find the two roots of s we get

$$\begin{aligned} s &= \frac{\frac{3}{4}\mathsf{E}^2 \pm \sqrt{\frac{9}{16}\mathsf{E}^4 - 4\mathsf{B}}}{2} \\ \Rightarrow s &= \frac{3\mathsf{E}^2}{8} \pm \frac{\sqrt{9\mathsf{E}^4 - 64\mathsf{B}}}{8} \end{aligned}$$

This leads to three possible cases. First, if $9\mathsf{E}^4 = 64\mathsf{B}$, there will be repeated roots resulting in one other turning point, an inflection at $s = \frac{3\mathsf{E}^2}{8}$. When $9\mathsf{E}^4 - 64\mathsf{B} > 0$, there will be two real roots giving an additional two turning points. Finally we could have $9\mathsf{E}^4 - 64\mathsf{B} < 0$ which gives no real roots so will lead to no extra turning points. In this last case, where there is only one turning point at $s = 0$, we would get four complex roots for $f(s)$. We can

determine the value of k needed for the turning points to be real

$$\begin{aligned} 9\mathrm{E}^4 - 64\mathrm{B} &> 0 \\ \Rightarrow 9\left(\frac{4(Ba)^2\mu\rho}{W^2}\right)^2 - 64\frac{k^2}{W} &> 0 \\ \Rightarrow \frac{9(Ba)^4(\mu\rho)^2}{4W^3} - k^2 &> 0 \end{aligned} \tag{5.93}$$

Since k^2 and $\frac{(Ba)^4(\mu\rho)^2}{W^3}$ are both strictly positive values, for real roots to occur we need that

$$k^2 < \frac{9(Ba)^4(\mu\rho)^2}{4W^3}$$

If (5.93) is true, we will get three real turning points at $s = 0$, $s = s_1$ and $s = s_2$. Substituting known values into the relation (5.93) we can determine the necessary viscosity for the relation to hold true.

We know that the weight of the plate is $W = 1.789 \times 10^{-7}$ kg, the length is $a = 0.0024$ m and the breadth is $B = 0.0016$ m. We assume that a spring constant per unit mass of $k = 1$ kg/s^2 would be a reasonable assumption and that a realistic fluid density could be $\rho = 1000$ kg/m^3. For example, an atomic force microscopes cantilever has a spring constant of 0.1 kg/s^2 and a Slinky spring has a spring constant of 1 kg/s^2 [42]. Using these values the relation is reduced to

$$\mu > 5.18 \times 10^{-13}\text{Pa·s} \tag{5.94}$$

This is extremely likely and will be true for all fluids we wish to investigate, indicating that there will in fact be three real turning points.

The next step is to work out the behaviour of the turning points. We can do this by differentiating (5.92) again with respect to s to get

$$f''(s) = 12s^2 - 24\frac{(Ba)^2\mu\rho}{W^2}s + 4\frac{k^2}{W} = 0$$

We now need to evaluate the second derivative at each of the three turning points. At the point $s = 0$, we are left with $f''(0) = 4\mathrm{B}$ which by definition must be a positive number. This indicates that this turning point of the curve described by the quartic polynomial $f(s)$ will be a minimum. Using (5.91) we can also see that when $s = 0$ the curve $f(s)$ will be at B^2, also a positive value. We have plotted the shape of f(s) for the no damping case with

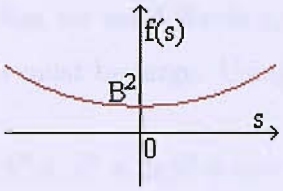

Figure 5.10: $f(s)$ with only one turning point

only one turning point at $s = 0$, see figure (5.10).

At the points $s_1 = \frac{3E^2}{8} + \frac{\sqrt{9E^4-64B}}{8}$ and $s_2 = \frac{3E^2}{8} - \frac{\sqrt{9E^4-64B}}{8}$, we get

$$f''(s_1) = \frac{9}{8}E^4 - 8B + \frac{3}{8}\sqrt{9E^4 - 64B}$$

$$f''(s_2) = \frac{9}{8}E^4 - 8B - \frac{3}{8}\sqrt{9E^4 - 64B}$$

Using the relation (5.93), we know that $\frac{9}{8}E^4 - 8B > 0$, hence $f''(s_1) > 0$. This means that the turning point s_1 is also a minimum. Since we have two minimum points, this implies that the third turning point s_2 must be a maximum and must occur between s_1 and $s = 0$. We can determine $f(s)$ for each of the turning points $s = 0$, $s = s_1$ and $s = s_2$.

$$\begin{aligned} f(0) &= B^2 \\ f(s_1) &= \frac{E^2}{512}\left(-27E^6 - 9E^4\sqrt{9E^4 - 64B} + 288BE^2 + 64B\sqrt{9E^4 - 64B}\right) \\ f(s_2) &= \frac{E^2}{512}\left(-27E^6 + 9E^4\sqrt{9E^4 - 64B} + 288BE^2 - 64B\sqrt{9E^4 - 64B}\right) \end{aligned} \quad (5.95)$$

This tells us that the curve must cross the axis an even number of times, either twice or not at all and thus will have two or zero real roots respectively.

Simplification using asymptotic analysis

Although it is valuable to have the exact solutions above (and in most cases the expressions may easily be evaluated) some simplifications may occur when the existence of small parameters is exploited.

Making the substitution $s = S\frac{k}{\sqrt{W}}$, (5.91) becomes

$$\begin{aligned} \frac{k^4}{W^2}S^4 - \frac{4(Ba)^2\mu\rho}{W^2}\frac{k^3}{W^{\frac{3}{2}}}S^3 + \frac{2k^4}{W^2}S^2 + \frac{k^4}{W^2} &= 0 \\ \Rightarrow S^4 + \alpha S^3 + 2S^2 + 1 &= 0 \end{aligned} \quad (5.96)$$

where $\alpha = \frac{-4(Ba)^2\mu\rho}{kW^{\frac{3}{2}}}$. We know that for most fluids $\mu\rho$ is of order 1 and believe k to be small. Given $W^{\frac{3}{2}} = 7.57 \times 10^{-7}$, α must be large. Using this, we can rewrite (5.96) as

$$\varepsilon S^4 + S^3 + 2\varepsilon S^2 + \varepsilon = 0 \tag{5.97}$$

with $\varepsilon = \frac{1}{\alpha} \ll 1$. The S^3 term appears to dominate indicating that the equation will have three normal roots, found by regular pertubation, and one singular root. To find approximate roots of this quartic polynomial we will use the fact that $\varepsilon \ll 0$ and use asymptotic approximations of S. For the three regular roots we use the following expansion of S

$$\begin{aligned} S &= \sum_{i=0} \varepsilon^{\frac{i}{3}} S_i \\ &= S_0 + \varepsilon^{\frac{1}{3}} S_1 + \varepsilon^{\frac{2}{3}} S_2 + \varepsilon S_3 + \dots \end{aligned} \tag{5.98}$$

Substituting (5.98) into the polynomial (5.97), we can evaluate the S_i terms by solving the equation for each order of ε, starting with ε^0, until each S_i term has been determined. For example

$$O(\varepsilon^0): \quad {S_0}^3 = 0$$
$$S_0 = 0$$

$$O(\varepsilon^{\frac{1}{3}}): \quad 3{S_0}^2 S_1 = 0$$
$$S_0 = 0$$

$$O(\varepsilon^{\frac{2}{3}}): \quad S_0(2S_0S_2 + {S_1}^2) + 2{S_1}^2 S_0 + S_2{S_0}^2 = 0$$
$$S_0 = 0$$

Substituting the values of S_i back into (5.98) we get our three regular roots:

$$S = \begin{cases} -\varepsilon^{\frac{1}{3}} - \frac{2}{3}\varepsilon + \dots \\ e^{i\frac{\pi}{3}}\varepsilon^{\frac{1}{3}} - \frac{2}{3}\varepsilon + \dots \\ e^{-i\frac{\pi}{3}}\varepsilon^{\frac{1}{3}} - \frac{2}{3}\varepsilon + \dots \end{cases}$$

In a similar way, we can find the singular root by using a different expansion of S, as follows,

and substituting this new expansion into (5.97).

$$S = \frac{S_{-1}}{\varepsilon} + S_0 + \varepsilon S_1 + \varepsilon^2 S_2 + \dots \tag{5.99}$$

This will give us the following equation

$$\varepsilon(\frac{S_{-1}}{\varepsilon} + S_0 + \varepsilon S_1 + \varepsilon^2 S_2)^4 + (\frac{S_{-1}}{\varepsilon} + S_0 + \varepsilon S_1 + \varepsilon^2 S_2)^3 + 2\varepsilon(\frac{S_{-1}}{\varepsilon} + S_0 + \varepsilon S_1 + \varepsilon^2 S_2)^2 + \varepsilon = 0$$

As before, we can evaluate the S_i terms by solving the equation for each order of ε, this time starting with $O(\varepsilon^{-3})$, then substitute these S_i terms into (5.98) to find our fourth, singular root:

$$S = -\frac{1}{\varepsilon} + 2\varepsilon + \dots$$

With $\varepsilon = \frac{1}{\alpha}$ and $\alpha = -\frac{4(Ba)^2\mu\rho}{kW^{\frac{3}{2}}}$ we can write our four roots together. To find the roots of the original polynomial (5.91), we need to use the relation $s = \frac{k}{\sqrt{W}}S = kW^{-\frac{1}{2}}S$.

$$S = \begin{cases} \left(\frac{kW^{\frac{3}{2}}}{4(Ba)^2\mu\rho}\right)^{\frac{1}{3}} + \frac{2kW^{\frac{3}{2}}}{12(Ba)^2\mu\rho} + \dots \\ e^{2i\frac{\pi}{3}}\left(\frac{kW^{\frac{3}{2}}}{4(Ba)^2\mu\rho}\right)^{\frac{1}{3}} + \frac{2kW^{\frac{3}{2}}}{12(Ba)^2\mu\rho} + \dots \\ e^{-2i\frac{\pi}{3}}\left(\frac{kW^{\frac{3}{2}}}{4(Ba)^2\mu\rho}\right)^{\frac{1}{3}} + \frac{2kW^{\frac{3}{2}}}{12(Ba)^2\mu\rho} + \dots \\ \frac{4(Ba)^2\mu\rho}{kW^{\frac{3}{2}}} - \frac{2kW^{\frac{3}{2}}}{4(Ba)^2\mu\rho} + \dots \end{cases} \rightarrow s = \begin{cases} \left(\frac{k^4}{4(Ba)^2\mu\rho}\right)^{\frac{1}{3}} + \frac{2k^2W}{12(Ba)^2\mu\rho} + \dots \\ e^{2i\frac{\pi}{3}}\left(\frac{k^4}{4(Ba)^2\mu\rho}\right)^{\frac{1}{3}} + \frac{2k^2W}{12(Ba)^2\mu\rho} + \dots \\ e^{-2i\frac{\pi}{3}}\left(\frac{k^4}{4(Ba)^2\mu\rho}\right)^{\frac{1}{3}} + \frac{2k^2W}{12(Ba)^2\mu\rho} + \dots \\ \frac{4(Ba)^2\mu\rho}{W^2} - \frac{2k^2W}{4(Ba)^2\mu\rho} + \dots \end{cases}$$

Using possible values of k, ρ and W, we can see what form the roots will take by plotting their position as we vary the value of μ (appendix A). We can compare the roots we would get from solving the polynomial exactly with the roots found with the asymptotic analysis. As mentioned earlier, we can discard any positive real roots since they are likely to have appeared due to the conjugate introduced to simplify $f(s)$ and can not be solutions. As is shown by the following diagrams, both methods result in a pair of complex conjugate roots. In both cases the complex roots have negative real parts, necessary for decay to occur.

If r is non-zero, we would expect similar results but with more damping. For example, we would anticipate the negative real parts of the complex roots to be more negative so that decay occurs more quickly.

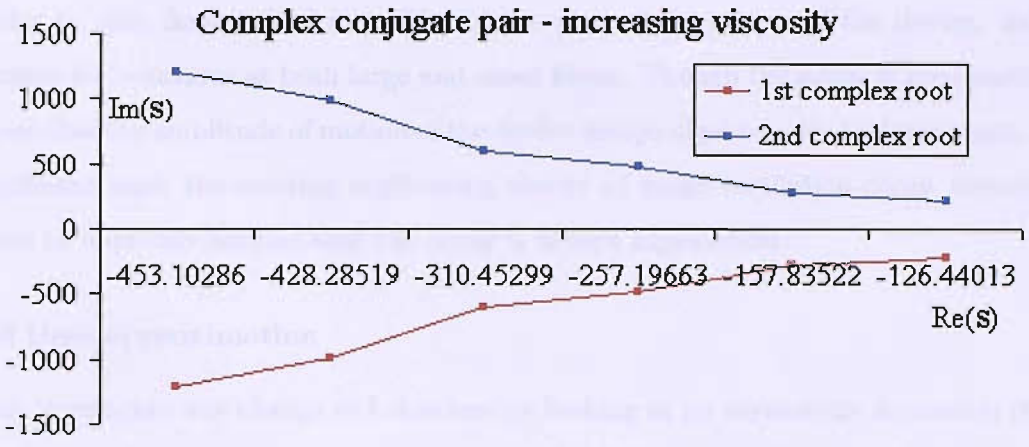

Figure 5.11: Roots of the polynomial evaluated exactly using values in table (5.1), with k=1. Shows a complex conjugate pair with imaginary parts approaching zero with increasing viscosity.

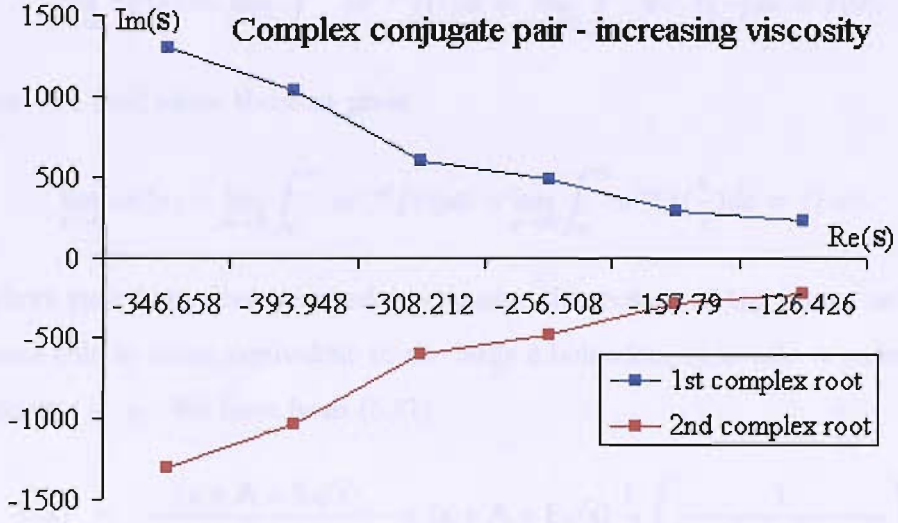

Figure 5.12: Roots of the polynomial found with asymptotic analysis, using values in table (5.1), with k=1. Shows the complex conjugate pair with imaginary parts approaching zero with increasing viscosity.

We can approximate the solution to our inverse Laplace problem by considering the behaviour at different time periods. At small time there will be transient decay. At intermediate time there will be regular, measurable oscillations which cross the axis. At large time the branch cut contribution will dominate and decay will be algebraic. Overall we expect to see the oscillations decay exponentially but the mean displacement to decay algebraically. In the next section we consider the behaviour of the solution in each of these time periods using asymptotic of $f(s)$.

5.3.3 Large and small time behaviour

In order to gain further understanding of the general properties of the device, we now determine its behaviour at both large and small times. Though the latter is predictable, we shall see that the amplitude of motion of the device decays algebraically for large times. This is significant since the existing engineering theory of many oscillation-decay viscometers appears to implicitly assume that the decay is always exponential.

Small time approximation

We can investigate any change in behaviour by looking at an asymptotic expansion of $f(s)$ for short time (large s) or long time (small s). This follows since the behaviour of the time function $f(t)$ for small t is governed by the behaviour of the Laplace transform $sF(s)$ for large s. The initial value theorem states that given a limit exists then

$$\lim_{s\to\infty} sF(s) = \lim_{s\to\infty} \int_0^\infty se^{-st}f(t)dt = \lim_{s\to\infty} \int_0^\infty e^{-v}f(\frac{v}{s})dv = f(0).$$

Conversely, the final value theorem gives

$$\lim_{s\to 0} sF(s) = \lim_{s\to 0} \int_0^\infty se^{-st}f(t)dt = \lim_{s\to 0} \int_0^\infty e^{-v}f(\frac{v}{s})dv = f(\infty).$$

For the short time behaviour we need to consider the motion of the sensor as $t \to 0$. We approximate this as being equivalent to the large s behaviour thus take a series expansion of $f(s)$ about $s = \infty$. We have from (5.87)

$$\begin{aligned}
f(s) &= \frac{(s+\mathsf{A}+\mathsf{E}\sqrt{s})}{s^2+\mathsf{E}s^{\frac{3}{2}}+\mathsf{A}s+\mathsf{B}} = (s+\mathsf{A}+\mathsf{E}\sqrt{s})\frac{1}{s^2}\left(\frac{1}{1+\frac{\mathsf{A}}{s}+\frac{\mathsf{E}}{\sqrt{s}}+\frac{\mathsf{B}}{s^2}}\right) \\
&= \frac{(s+\mathsf{A}+\mathsf{E}\sqrt{s})}{s^2}\left[1+\frac{\mathsf{A}}{s}+\frac{\mathsf{E}}{\sqrt{s}}+\frac{\mathsf{B}}{s^2}\right]^{-1} \\
&= \frac{(s+\mathsf{A}+\mathsf{E}\sqrt{s})}{s^2}\sum_{r=0}^{\infty}(-1)^r\left[\frac{\mathsf{E}}{\sqrt{s}}+\frac{\mathsf{A}}{s}+\frac{\mathsf{B}}{s^2}\right]^r \\
&= \frac{(s+\mathsf{A}+\mathsf{E}\sqrt{s})}{s^2}\sum_{r=0}^{\infty}(-1)^r\frac{\mathsf{E}^r}{s^{\frac{r}{2}}}\left[1+\frac{\mathsf{A}}{\mathsf{E}\sqrt{s}}+\frac{\mathsf{B}}{\mathsf{E}s^{\frac{3}{2}}}\right]^r \\
&= \frac{(s+\mathsf{A}+\mathsf{E}\sqrt{s})}{s^2}\sum_{r=0}^{\infty}(-1)^r\frac{\mathsf{E}^r}{s^{\frac{r}{2}}}\sum_{p=0}^{\infty}\frac{r!}{p!(r-p)!}\left[\frac{\mathsf{A}}{\mathsf{E}\sqrt{s}}+\frac{\mathsf{B}}{\mathsf{E}s^{\frac{3}{2}}}\right]^p \\
&= \frac{(s+\mathsf{A}+\mathsf{E}\sqrt{s})}{s^2}\sum_{r=0}^{\infty}(-1)^r\frac{\mathsf{E}^r}{s^{\frac{r}{2}}}\sum_{p=0}^{\infty}\frac{r!}{p!(r-p)!}\frac{\mathsf{A}^p}{\mathsf{E}^p s^{\frac{p}{2}}}\left[1+\frac{\mathsf{B}}{\mathsf{A}s}\right]^p
\end{aligned}$$

$$
\begin{aligned}
f(s) &= \frac{(s+\mathsf{A}+\mathsf{E}\sqrt{s})}{s^2}\sum_{r=0}^{\infty}\sum_{p=0}^{r}\frac{(-1)^r\mathsf{E}^r\mathsf{A}^p r!}{s^{\frac{r+p}{2}}\mathsf{E}^p p!(r-p)!}\left[1+\frac{\mathsf{B}}{\mathsf{A}s}\right]^p \\
&= \frac{(s+\mathsf{A}+\mathsf{E}\sqrt{s})}{s^2}\sum_{r=0}^{\infty}\sum_{p=0}^{r}\frac{(-1)^r\mathsf{E}^r\mathsf{A}^p r!}{s^{\frac{r+p}{2}}\mathsf{E}^p p!(r-p)!}\sum_{q=0}^{\infty}\frac{q!}{q!(p-q)!}\left[\frac{\mathsf{B}}{\mathsf{A}s}\right]^q \\
&= \frac{(s+\mathsf{A}+\mathsf{E}\sqrt{s})}{s^2}\sum_{r=0}^{\infty}\sum_{p=0}^{r}\sum_{q=0}^{p}\frac{1}{s^{\frac{r+p}{2}+q}}\left[\frac{(-1)^r\mathsf{E}^r\mathsf{A}^p r!p!\mathsf{B}^q}{\mathsf{E}^p\mathsf{A}^q p!q!(r-p)!(p-q)!}\right] \\
&= \frac{1}{s}-\frac{\mathsf{B}}{s^3}+\frac{\mathsf{BE}}{s^{\frac{7}{2}}}+\mathsf{B}\frac{\mathsf{A}-\mathsf{E}^2}{s^4}+\frac{\mathsf{B}(\mathsf{E}^3-2\mathsf{EA})}{s^{\frac{9}{2}}}\ldots \quad . \qquad (5.100)
\end{aligned}
$$

We are now able to take the term by term inverse Laplace transform of $f(s)$ in this new form.

$$
L^{-1}[f(s)] = 1-\frac{\mathsf{B}}{2}t^2+\frac{8\mathsf{BE}}{15\sqrt{\pi}}t^{\frac{5}{2}}+\mathsf{B}\frac{\mathsf{A}-\mathsf{E}^2}{6}t^3-\frac{32\mathsf{BEA}}{105\sqrt{\pi}}t^{\frac{7}{2}}+\ldots \qquad (5.101)
$$

Substituting this into equation (5.87) gives us a solution for the small time behaviour of the motion:

$$
x(t) = x(0)\left[1-\frac{\mathsf{B}}{2}t^2+\frac{8\mathsf{BE}}{15\sqrt{\pi}}t^{\frac{5}{2}}+\mathsf{B}\frac{\mathsf{A}-\mathsf{E}^2}{6}t^3-\frac{32\mathsf{BEA}}{105\sqrt{\pi}}t^{\frac{7}{2}}+\ldots\right]. \qquad (5.102)
$$

Using this solution we can analyse the behaviour of the plate at $t=0$. The main dependence in the first two terms seems to be on the variable B, with $\mathsf{B}=\frac{\text{spring constant of plate}}{\text{weight of plate}}$. This suggests that the small time behaviour only depends on the mechanical properties of the plate and not on the surrounding fluid. It is interesting to note that the viscosity does not appear at all in the first two terms of the expansion. This implies that experimentally the oscillations must continue for a more significant length of time to ensure that viscosity is being measured.

We note also that

$$
x'(t) = x(0)\left[-\mathsf{B}t+\frac{4\mathsf{BE}}{3\sqrt{\pi}}t^{\frac{3}{2}}+\mathsf{B}\frac{\mathsf{A}-\mathsf{E}^2}{2}t^2-\frac{16\mathsf{BEA}}{15\sqrt{\pi}}t^{\frac{5}{2}}+\ldots\right]
$$

thus at $t=0$ we have $x'(0)=0$, so the slope of the curve is linear. We also find that

$$
x''(t) = x(0)\left[-\mathsf{B}+\frac{2\mathsf{BE}}{\sqrt{\pi}}t^{\frac{1}{2}}+\mathsf{B}(\mathsf{A}-\mathsf{E}^2)t-\frac{8\mathsf{BEA}}{3\sqrt{\pi}}t^{\frac{3}{2}}+\ldots\right].
$$

At $t=0$ we therefore have $x''(t)=-\mathsf{B}x(0)$. We know that $\mathsf{B}=\frac{k^2}{W}$ is positive so $x''(0)<0$ indicating that the slope at time $t=0$ then approaches the t-axis as time increases.

Large time approximation

For the large time behaviour, assuming that none of the poles have a positive real part, the main contribution comes from the integral occurring due to the branch cut. If the poles have positive real parts, this would result in increasing motion, thus not allowing for the decaying motion which is expected physically. A requirement for the real parts of the poles to be negative is that the s^3 coefficient in the polynomial (5.90) is negative also. This corresponds to the sum of the real parts of the polynomial's roots. Since our poles will be conjugate pairs this then corresponds to the sum of the roots themselves. In our case this gives us the following inequality to be satisfied:

$$(2\mathsf{A} - \mathsf{E}^2) < 0$$

With $\mathsf{A} = \frac{r}{\rho_s d B a}$ and $\mathsf{E} = \frac{2Ba\sqrt{\mu\rho}}{\rho_s d B a}$, where B is the breadth of the plate, this reduces to:

$$\frac{\mu}{r} > \frac{\rho_s d}{2\rho B a} \tag{5.103}$$

The branch cut lies on the origin so at large time we look at the end points of the integral with contributions coming from $s = 0$. We start be taking a binomial series expansion of $f(s)$ about $s = 0$. We find that

$$\begin{aligned} f(s) &= \frac{(\mathsf{A} + \mathsf{E}\sqrt{s} + s)}{\mathsf{B}} \left[1 + \left(\frac{\mathsf{A}}{\mathsf{B}}s + \frac{\mathsf{E}}{\mathsf{B}}s^{\frac{3}{2}} + \frac{1}{\mathsf{B}}s^2\right)\right]^{-1} \\ &= \frac{\mathsf{A}}{\mathsf{B}} + \frac{\mathsf{E}}{\mathsf{B}}\sqrt{s} + \frac{\mathsf{B} - \mathsf{A}^2}{\mathsf{B}^2}s - \frac{2\mathsf{AE}}{\mathsf{B}^2}s^{\frac{3}{2}} + \frac{\mathsf{A}^3 - 2\mathsf{AB} - \mathsf{E}^2\mathsf{B}}{\mathsf{B}^3}s^2 + \frac{3\mathsf{A}^2\mathsf{E} - 2\mathsf{EB}}{\mathsf{B}^3}s^{\frac{5}{2}} + \dots \end{aligned} .$$

This form of $f(s)$ can now undergo an inverse Laplace transform. The first term has no contribution to the large time behaviour since $L^{-1}\left[\frac{\mathsf{A}}{\mathsf{B}}\right] = \frac{\mathsf{A}}{\mathsf{B}}\delta(t)$. The delta function $\delta(t)$ has a value of zero for all t except at time $t = 0$, when $\delta(0) = \infty$. Physically this is similar to the plate getting a big hit at an earlier time. Taking the inverse Laplace of this series shows us that terms containing integer powers of s will also not contribute to behaviour at large time since they are multiples of the delta function. This leaves us with

$$\begin{aligned} L^{-1}[f(s)] &= L^{-1}\left[\frac{\mathsf{E}}{\mathsf{B}}\sqrt{s} - \frac{2\mathsf{AE}}{\mathsf{B}^2}s^{\frac{3}{2}} + \frac{3\mathsf{A}^2\mathsf{E} - 2\mathsf{EB}}{\mathsf{B}^3}s^{\frac{5}{2}} + \dots\right] \\ &= \frac{\mathsf{E}}{\mathsf{B}}\frac{\sqrt{\pi}}{t^{\frac{3}{2}}} - \frac{\mathsf{AE}}{\mathsf{B}^2}\frac{\sqrt{\pi}}{t^{\frac{5}{2}}} + \frac{(3\mathsf{A}^2\mathsf{E} - 2\mathsf{EB})}{\mathsf{B}^3}\frac{3\sqrt{\pi}}{4t^{\frac{7}{2}}} + \dots \end{aligned} . \tag{5.104}$$

Putting this back into equation(5.87) gives us a solution for the large time behaviour of the motion:

$$x(t) = x(0)\left[\frac{\mathsf{E}}{\mathsf{B}}\frac{\sqrt{\pi}}{t^{\frac{3}{2}}} - \frac{\mathsf{AE}}{\mathsf{B}^2}\frac{\sqrt{\pi}}{t^{\frac{5}{2}}} + \frac{(3\mathsf{A}^2\mathsf{E} - 2\mathsf{EB})}{\mathsf{B}^3}\frac{3\sqrt{\pi}}{4t^{\frac{7}{2}}}\right]. \tag{5.105}$$

We can analyse this solution by considering the limit as $t \to +\infty$.

$$\lim_{t\to\infty} x(t) = \lim_{t\to\infty}\left[x(0)\left(\frac{\mathsf{E}}{\mathsf{B}}\sqrt{\pi}\left(\frac{1}{t}\right)^{\frac{3}{2}} - \frac{\mathsf{AE}}{\mathsf{B}^2}\sqrt{\pi}\left(\frac{1}{t}\right)^{\frac{5}{2}} + \frac{3(3\mathsf{A}^2\mathsf{E} - 2\mathsf{EB})}{4\mathsf{B}^3}\sqrt{\pi}\left(\frac{1}{t}\right)^{\frac{7}{2}} + \ldots\right)\right] = 0.$$

Hence $x(t)$ approaches 0 as time approaches infinity. The approach to 0 represents the oscillations decaying to a stop. Decay occurs algebraically, like $t^{\frac{3}{2}}$, indicating that the oscillations decay more slowly than they would for any exponential terms arising from the poles. As mentioned above this algebraic decay is regarded as somewhat non-standard for oscillation-decay viscometers, which are normally assumed to decay exponentially.

Also we know that as $t \to \infty$, the terms after the first term will converge to 0 much faster making the first term dominant at large time. The first term is

$$x(0)\frac{\mathsf{E}\sqrt{\pi}}{\mathsf{B}t^{\frac{3}{2}}} = x(0)\frac{2Ba\sqrt{\mu\rho\pi}}{k^2t^{\frac{3}{2}}}.$$

$x(t)$ therefore approaches 0 from the positive direction whenever $x(0) > 0$.

Exact evaluation of the branch cut

The branch cut provided by the $\sqrt{s}$ term in equation (5.89) has a branch point at $s = 0$. The integral around the branch cut will be an algebraic expression as opposed to the exponential terms from the integrals around the poles. Since algebraic terms decay at a much slower rate than exponentials, the branch cut provides the dominant contribution for the long time behaviour of the plate motion, so we can evaluate the solution of $L^{-1}[f(s)]$ for long time by considering only the $\sqrt{s}$ term.

The inverse Laplace of this term can be found by integrating around the branch cut along the contour c (with $c = c_1 + c_2$).

Let $I_c = L^{-1}\left[\frac{\mathsf{EB}\sqrt{s}}{(s^2+\mathsf{A}s+\mathsf{B})^2-\mathsf{E}^2s^3}\right]$, then

$$\begin{aligned} I_c &= \frac{\mathsf{EB}}{2\pi i}\int_c \frac{e^{st}\sqrt{s}ds}{(s^2+\mathsf{A}s+\mathsf{B})^2-\mathsf{E}^2s^3} \\ &= \frac{\mathsf{EB}}{2\pi i}\int_{c_1} \frac{e^{st}\sqrt{s}ds}{(s^2+\mathsf{A}s+\mathsf{B})^2-\mathsf{E}^2s^3} + \mathsf{EB}\int_{c_2} \frac{e^{st}\sqrt{s}ds}{(s^2+\mathsf{A}s+\mathsf{B})^2-\mathsf{E}^2s^3}. \end{aligned} \tag{5.106}$$

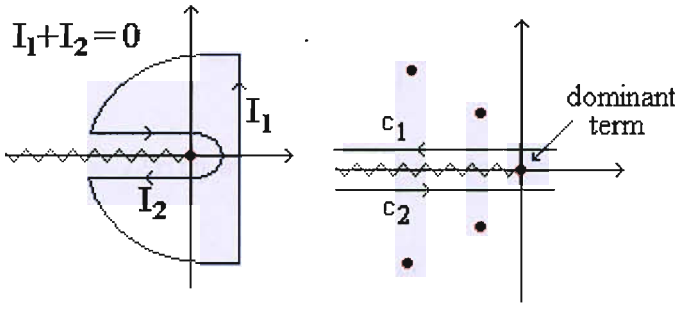

Figure 5.13: Contours to exclude the branch cut singularity

We now make a change of variables. Along the contour c_1 we let $s = ze^{i\pi}$ and along the contour c_2 we let $s = ze^{-i\pi}$, with $-\pi < arg(s) < \pi$. Our integral now becomes:

$$\begin{aligned} I_c &= \frac{\mathsf{EB}}{2\pi i}\int_0^\infty \frac{dze^{i\pi}e^{ze^{i\pi}t}(ze^{i\pi})^{\frac{1}{2}}}{((ze^{i\pi})^2+\mathsf{A}ze^{i\pi}+\mathsf{B})^2-\mathsf{E}^2(ze^{i\pi})^3} \\ &\quad + \frac{\mathsf{EB}}{2\pi i}\int_\infty^0 \frac{dze^{-i\pi}e^{ze^{-i\pi}t}(ze^{-i\pi})^{\frac{1}{2}}}{((ze^{-i\pi})^2+\mathsf{A}ze^{-i\pi}+\mathsf{B})^2-\mathsf{E}^2(ze^{-i\pi})^3} \\ &= -\frac{\mathsf{EB}}{2\pi}\int_0^\infty \frac{e^{-zt}z^{\frac{1}{2}}dz}{(z^2-\mathsf{A}z+\mathsf{B})^2+\mathsf{E}^2z^3} - \frac{\mathsf{EB}}{2\pi}\int_0^\infty \frac{e^{-zt}z^{\frac{1}{2}}dz}{(z^2-\mathsf{A}z+\mathsf{B})^2+\mathsf{E}^2z^3} \\ &= -\frac{\mathsf{EB}}{\pi}\int_0^\infty \frac{e^{-zt}z^{\frac{1}{2}}dz}{(z^2-\mathsf{A}z+\mathsf{B})^2+\mathsf{E}^2z^3}. \end{aligned} \tag{5.107}$$

This shows that the large time solution can be written as an integral in closed form which although not simple should now be solvable.

5.3.4 Solving the plucked spider problem numerically

Since it is not straightforward to solve the decaying oscillations problem analytically due to the complications from the pole and branch cut singularities, the next step is to try and determine a numerical solution. From equation (5.83) we can see that the solution to the fluid equation in Laplace form is

$$\hat{u}(x,y,s) = \hat{G}(s)e^{-y\sqrt{\frac{s}{\nu}}} \tag{5.108}$$

We now consider the convolution theorem:

$$\begin{aligned} J(s)K(s) &= L(j*k) \\ \Rightarrow L^{-1}\left[J(s)K(s)\right] &= \int_0^t j(s)k(t-s)ds \end{aligned} \tag{5.109}$$

Letting $K(s) = e^{-y\sqrt{\frac{s}{\nu}}}$ so that

$$k(s) = L^{-1}\left[e^{-y\sqrt{\frac{s}{\nu}}}\right] = \frac{ye^{-\frac{y^2}{4\nu t}}}{2\sqrt{\pi\nu}t^{\frac{3}{2}}}$$

and taking $J(s) = \hat{G}(s) = L[\dot{x}(t)]$ such that $j(s) = \dot{x}(s)$, we can use (5.109) to write our solution as

$$u(x,y,t) = \int_0^t \dot{x}(s)\frac{ye^{-\frac{y^2}{4\nu(t-s)}}}{2\sqrt{\pi\nu}(t-s)^{\frac{3}{2}}}ds \tag{5.110}$$

The plate equation $Wx_{tt} + rx_t + k^2x = \mu u_y|_{y=0}$ can now be combined with this solution for $u(x,y,t)$ to recast the governing equation as

$$W\frac{d^2x}{dt^2} + r\frac{dx}{dt} + k^2x = \mu\left[\int_0^t \dot{x}(s)\frac{ye^{-\frac{y^2}{4\nu(t-s)}}}{2\sqrt{\pi\nu}(t-s)^{\frac{3}{2}}}ds\right]_y |_{y=0} \tag{5.111}$$

Since the limits of integration are not dependent on y we can bring the differentiation (with respect to y) inside the integral. We have

$$u_y = -\frac{1}{4\nu\sqrt{\pi\nu}}\int_0^t \dot{x}(s)\frac{e^{\frac{-y^2}{4\nu(t-s)}}}{(t-s)^{\frac{5}{2}}}(y^2 - 2\nu(t-s))ds. \tag{5.112}$$

To evaluate this integral we will try integration by parts.

$$\int_0^t X\frac{dY}{ds} = [XY]_0^t - \int_0^t Y\frac{dX}{ds}ds$$

with $X = \dot{x}(s)$ and $\frac{dY}{ds} = \frac{e^{\frac{-y^2}{4\nu(t-s)}}}{(t-s)^{\frac{5}{2}}}(y^2 - 2\nu(t-s))$. So Y becomes

$$\begin{aligned} Y &= 2y^2\left[-\frac{2\nu e^{\frac{-y^2}{4\nu(t-s)}}}{y^2\sqrt{(t-s)}} + \frac{2\nu^{\frac{3}{2}}erf\sqrt{\pi}\left(\frac{y}{2\sqrt{\nu(t-s)}}\right)}{y^3}\right] - \frac{4\nu^{\frac{3}{2}}erf\sqrt{\pi}\left(\frac{y}{2\sqrt{\nu(t-s)}}\right)}{y} \\ &= -\frac{4\nu e^{\frac{-y^2}{4\nu(t-s)}}}{\sqrt{(t-s)}} \end{aligned} \tag{5.113}$$

We can substitute the expressions for X,Y,$\frac{dX}{ds}$ and $\frac{dY}{ds}$, to give

$$\begin{aligned} -4\nu\sqrt{\pi\nu}u_y(x,y,t) &= \int_0^t \dot{x}(s)\frac{ye^{-\frac{y^2}{4\nu(t-s)}}}{2\sqrt{\pi\nu}(t-s)^{\frac{3}{2}}}ds \\ &= \left[-\dot{x}(s)\frac{4\nu e^{-\frac{y^2}{4\nu(t-s)}}}{\sqrt{(t-s)}}\right]_0^t - \int_0^t -\frac{4\nu e^{-\frac{y^2}{4\nu(t-s)}}}{\sqrt{(t-s)}}\frac{d^2x(s)}{ds^2}ds \quad (5.114) \end{aligned}$$

But we can see that $[XY]_0^t = 0$ since $\dot{x}(0) = 0$ and as $s \to 0$, $e^{-\frac{y^2}{4\nu(t-s)}} \to 0$ quicker than $\sqrt{(t-s)} \to 0$, hence

$$-4\nu\sqrt{\pi\nu}u_y(x,y,t) = \int_0^t \frac{4\nu e^{-\frac{y^2}{4\nu(t-s)}}}{\sqrt{(t-s)}}\frac{d^2x(s)}{ds^2}ds. \quad (5.115)$$

We now wish to take the limit of u_y as y tends to 0.

$$\begin{aligned} \lim_{y=0}\left[\frac{du}{dy}\right] &= \lim_{y=0}\left[-\frac{1}{4\nu\sqrt{\pi\nu}}4\nu\int_0^t \frac{e^{-\frac{y^2}{4\nu(t-s)}}}{\sqrt{t-s}}\frac{d^2x(s)}{ds^2}ds\right] \\ &= -\frac{1}{\sqrt{\pi\nu}}\int_0^t \frac{\frac{d^2x(s)}{ds^2}}{\sqrt{t-s}}ds. \quad (5.116) \end{aligned}$$

Substituting this back into equation (5.111) we get

$$W\frac{d^2x}{dt^2} + r\frac{dx}{dt} + k^2x = -\frac{\mu}{\sqrt{\pi\nu}}\int_0^t \frac{\frac{d^2x(s)}{ds^2}}{\sqrt{t-s}}ds, \quad (5.117)$$

which can be simplified using our previous notation to give

$$\frac{d^2x}{dt^2} + \mathsf{A}\frac{dx}{dt} + \mathsf{B}x = -\frac{\mathsf{E}}{\sqrt{\pi}}\int_0^t \frac{\frac{d^2x(s)}{ds^2}}{\sqrt{t-s}}ds. \quad (5.118)$$

It is possible to check to see whether this agrees with our earlier analysis by taking the Laplace transform of each side.

$$\begin{aligned} s^2\hat{x} - \dot{x}(0) - sx(0) + \mathsf{A}s\hat{x} - \mathsf{A}x(0) + \mathsf{B}\hat{x} &= -\frac{\mathsf{E}}{\sqrt{\pi}}L\left[\int_0^t \frac{d^2x(s)}{ds^2}(\sqrt{t-s})^{-1}ds\right] \\ &= -\frac{\mathsf{E}}{\sqrt{\pi}}\frac{\sqrt{\pi}}{\sqrt{s}}(s^2\hat{x} - \dot{x}(0) - sx(0)). \quad (5.119) \end{aligned}$$

If we let $\dot{x}(0) = 0$ and $x(0) = X$ then

$$\begin{aligned} s^2\hat{x} - sX + \mathsf{A}s\hat{x} - \mathsf{A}X + \mathsf{B}\hat{x} &= -\frac{\mathsf{E}}{\sqrt{s}}(s^2\hat{x} - sX) \\ \hat{x}(s^2 + \mathsf{A}s + \mathsf{B} + \mathsf{E}s^{\frac{3}{2}}) &= X(s + \mathsf{A} + \mathsf{E}\sqrt{s}) \\ \Rightarrow \hat{x} = X\left(\frac{s + \mathsf{A} + \mathsf{E}\sqrt{s}}{s^2 + \mathsf{A}s + \mathsf{B} + \mathsf{E}s^{\frac{3}{2}}}\right). \end{aligned} \tag{5.120}$$

This is identical to (5.87).

Before solving equation (5.118) numerically it is worth pointing out that it can also be considered to be a fractional differential equation. This may be done by observing that the fractional derivative of a suitably well behaved function may be defined for non integer values of λ by

$$D^{\lambda}[f(x)] = \frac{1}{\Gamma(1-\lambda)}\int_0^x \frac{1}{(x-\xi)^{\lambda}}\frac{df(\xi)}{d\xi}d\xi.$$

A whole theory exists for such equations (see for example [47]), but we will not pursue this further here: in particular a suitable specification of boundary conditions depends on exactly which definition of the fractional derivative is used (see [47]).

We now solve equation (5.118) numerically. We define x_i to be the value of $x(t)$ at time $t = t_i$ with $i = 1..n$, and define Δt to be the mesh size for t between 0 and t_n. The initial conditions are that the plate starts from a stationary position (with zero velocity) at a distance X from the origin.

$$\frac{dx(0)}{dt} = 0, \tag{5.121}$$

$$x(0) = X. \tag{5.122}$$

We will define the first and second differential of x with respect to t using difference formulae [46]. We use a central difference method since it is more accurate than the forward or backward difference methods. For a comparison of difference methods and associated accuracies, see appendix B.

$$\frac{dx}{dt} \Rightarrow x'(i) = \frac{x_{i+1} - x_{i-1}}{2\Delta t}, \tag{5.123}$$

$$\frac{d^2x}{dt^2} \Rightarrow x''(i) = \frac{x_{i+1} - 2x_i + x_{i-1}}{(\Delta t)^2}. \tag{5.124}$$

The left hand side of equation (5.118) may now be written as

$$\frac{x_{i+1} - 2x_i + x_{i-1}}{(\Delta t)^2} + \frac{\mathsf{A}(x_{i+1} - x_{i-1})}{2\Delta t} + \mathsf{B}x_i.$$

We assume that x_i'' is constant on $t = t_i$, so that we can use the trapezium rule to integrate $x''(t)$.

$$\int_0^{t_i} x'' d\tau \Rightarrow \sum_{j=1}^{i} \left(\frac{x_j'' + x_{j-1}''}{2} \right) (\Delta t)$$

For the left hand side we treat the integral as a sum of areas beneath a curve.

$$\begin{aligned}
-\frac{\mathsf{E}}{\sqrt{\pi}} \int_0^t \frac{x''(\tau)}{\sqrt{t-\tau}} d\tau &= -\frac{\mathsf{E}}{\sqrt{\pi}} \sum_{j=1}^{i} \int_{(j-1)\Delta t}^{j\Delta t} \frac{x''(j) + x''(j-1)}{2\sqrt{i\Delta t - \tau}} d\tau \\
&= -\frac{\mathsf{E}}{\sqrt{\pi}} \sum_{j=1}^{i} \frac{x''(j) + x''(j-1)}{2} [-2\sqrt{i\Delta t - \tau}]_{j\Delta t}^{(j-1)\Delta t} \\
&= -\frac{\mathsf{E}}{\sqrt{\pi}} \sum_{j=1}^{i} (x''(j) + x''(j-1)) \sqrt{\Delta t} (\sqrt{i-j+1} - \sqrt{i-j}).
\end{aligned}$$

One can see that due to the summation, we can use an iterative process to find x_{i+1} for all terms from $i \geq 2$. We will need to work out x_2 independently. We note here that $x_1 = x_{-1}$ due to the original condition $x'(0) = 0$, and our assumption is that $x_1 = x_{-1} = x_0 = X$. Thence

$$\begin{aligned}
\int_0^t \frac{x''(\tau)}{\sqrt{t-\tau}} d\tau &= \sum_{j=1}^{i} \frac{x_{j+1} - 2x_j + x_{j-1} + x_j - 2x_{j-1} + x_{j-2}}{(\Delta t)^{\frac{3}{2}}} (\sqrt{i-j+1} - \sqrt{i-j}) \\
&= \sum_{j=1}^{i} \frac{x_{j+1} - x_j - x_{j-1} + x_{j-2}}{(\Delta t)^{\frac{3}{2}}} (\sqrt{i-j+1} - \sqrt{i-j}) \qquad (5.125) \\
&= \sum_{j=1}^{i-1} \frac{x_{j+1} - x_j - x_{j-1} + x_{j-2}}{(\Delta t)^{\frac{3}{2}}} (\sqrt{i-j+1} - \sqrt{i-j}) \\
&\quad + \frac{x_{j+1} - x_j - x_{j-1} + x_{j-2}}{(\Delta t)^{\frac{3}{2}}}.
\end{aligned}$$

Substituting this into (5.118) gives us the right hand side of the equation, so that we can now rewrite (5.118) as

$$\begin{aligned}
&\frac{x_{i+1} - 2x_i + x_{i-1}}{(\Delta t)^2} + \mathsf{A}\frac{x_{i+1} - x_{i-1}}{2\Delta t} + \mathsf{B}x_i + \frac{\mathsf{E}}{\sqrt{\pi}} \frac{x_{j+1} - x_j - x_{j-1} + x_{j-2}}{(\Delta t)^{\frac{3}{2}}} \\
&\qquad = -\frac{\mathsf{E}}{\sqrt{\pi}} \sum_{j=1}^{i-1} \frac{x_{j+1} - x_j - x_{j-1} + x_{j-2}}{(\Delta t)^{\frac{3}{2}}} (\sqrt{i-j+1} - \sqrt{i-j}) \qquad (5.126)
\end{aligned}$$

We can rearrange equation (5.126) to get a solution for x_{i+1} in terms of x_i, x_{i-1} and x_{i-2} so that we can use an explicit finite difference method to find all values of x for $i \geq 2$.

$$\begin{aligned} x_{i+1} &= \left(\frac{2\sqrt{\pi}(\Delta t)^2}{2\sqrt{\pi}+\mathsf{A}\sqrt{\pi}\Delta t+2\mathsf{E}\sqrt{\Delta t}}\right)\left[x_i\left(\frac{2}{(\Delta t)^2}-\mathsf{B}+\frac{\mathsf{E}}{\sqrt{\pi}(\Delta t)^{\frac{3}{2}}}\right)\right. \\ &\quad +x_{i-1}\left(\frac{\mathsf{E}}{\sqrt{\pi}(\Delta t)^{\frac{3}{2}}}+\frac{\mathsf{A}}{2\Delta t}-\frac{1}{(\Delta t)^2}\right)-x_{i-2}\left(\frac{\mathsf{E}}{\sqrt{\pi}(\Delta t)^{\frac{3}{2}}}\right) \\ &\quad \left.-\frac{\mathsf{E}}{\sqrt{\pi}}\sum_{j=1}^{i-1}\frac{x_{j+1}-x_j-x_{j-1}+x_{j-2}}{(\Delta t)^{\frac{3}{2}}}(\sqrt{i-j+1}-\sqrt{i-j})\right] \end{aligned} \tag{5.127}$$

To allow us to begin calculating each value of x_i, we need to know x_0, x_1 and x_2. As previously discussed, x_0 is known from our first initial condition (5.121). Following from the second initial condition (5.122), we assume that $x_1 = x_{-1} = x_0$. We now evaluate equation (5.125) with $i = 1$ to determine the value of x_2.

$$\begin{aligned} \frac{x_{i+1}-2x_i+x_{i-1}}{(\Delta t)^2}+\mathsf{A}\frac{x_{i+1}-x_{i-1}}{2\Delta t}+\mathsf{B}x_i &= -\frac{\mathsf{E}}{\sqrt{\pi}}\sum_{j=1}^{i}(x''(j)+ \\ &\quad x''(j-1))\sqrt{\Delta t}(\sqrt{i-j+1}-\sqrt{i-j}) \\ \frac{x_2-2x_1+x_0}{(\Delta t)^2}+\mathsf{A}\frac{x_2-x_0}{2\Delta t}+\mathsf{B}x_1 &= -\frac{\mathsf{E}}{\sqrt{\pi}}\frac{x_2-x_1-x_0+x_{-1}}{(\Delta t)^{\frac{3}{2}}}(\sqrt{1}-\sqrt{0}) \\ x_2\left(1+\frac{\mathsf{A}\Delta t}{2}+\frac{\mathsf{E}\sqrt{\Delta t}}{\sqrt{\pi}}\right) &= x_0\left(1+\frac{\mathsf{A}\Delta t}{2}-\mathsf{B}(\Delta t)^2+\frac{\mathsf{E}\sqrt{\Delta t}}{\sqrt{\pi}}\right) \\ x_2 &= X\left(1-\frac{2\sqrt{\pi}\mathsf{B}(\Delta t)^2}{2\sqrt{\pi}+\mathsf{A}\sqrt{\pi}\Delta t+2\mathsf{E}\sqrt{\Delta t}}\right) \end{aligned}$$

We would expect the solution to behave such that $x_i \to 0$ as $i \to \infty$ and $|x_{i+1}| < |x_i|$, since the plate should have a decaying oscillatory motion which should stop at some time $t = T$.

The complete numerical scheme for x_i is thus

$$\begin{aligned}
x_{-1} &= X \\
x_0 &= X \\
x_1 &= X \\
x_2 &= X\left(1-\frac{2\sqrt{\pi}\mathsf{B}(\Delta t)^2}{2\sqrt{\pi}+\mathsf{A}\sqrt{\pi}\Delta t+2\mathsf{E}\sqrt{\Delta t}}\right) \\
x_{i+1} &= \left(\frac{2\sqrt{\pi}(\Delta t)^2}{2\sqrt{\pi}+\mathsf{A}\sqrt{\pi}\Delta t+2\mathsf{E}\sqrt{\Delta t}}\right)[x_i\left(\frac{2}{(\Delta t)^2}-\mathsf{B}+\frac{\mathsf{E}}{\sqrt{\pi}(\Delta t)^{\frac{3}{2}}}\right) \\
&\quad +x_{i-1}\left(\frac{\mathsf{E}}{\sqrt{\pi}(\Delta t)^{\frac{3}{2}}}+\frac{\mathsf{A}}{2\Delta t}-\frac{1}{(\Delta t)^2}\right)-x_{i-2}\left(\frac{\mathsf{E}}{\sqrt{\pi}(\Delta t)^{\frac{3}{2}}}\right) \\
&\quad -\frac{\mathsf{E}}{\sqrt{\pi}}\sum_{j=1}^{i-1}\frac{x_{j+1}-x_j-x_{j-1}+x_{j-2}}{(\Delta t)^{\frac{3}{2}}}(\sqrt{i-j+1}-\sqrt{i-j})]. \qquad (5.128)
\end{aligned}$$

We can also carry out some asymptotic approximations of the original equation (5.118), for large and small time, to see if they correspond with the pole and branch cut analysis and our new numerical solution.

Small time solution

The equation to be solved for small time is

$$x''(t)+\mathsf{A}x'(t)+\mathsf{B}x(t)=-\frac{\mathsf{E}}{\sqrt{\pi}}\int_0^t\frac{x''(\tau)}{\sqrt{t-\tau}}d\tau. \qquad (5.129)$$

We assume a solution of the form

$$x(t)\sim\frac{\alpha t^{n+2}}{(n+1)(n+2)}+x_0$$

so that

$$x'(t)\sim\frac{\alpha t^{n+1}}{n+1}$$

$$x''(t)\sim\alpha t^n$$

Using the substitution $\tau=tu$, the right hand side of the equation may be written as

$$\begin{aligned}
-\frac{\mathsf{E}}{\sqrt{\pi}}\int_0^t\frac{\alpha\tau^n}{\sqrt{t-\tau}}d\tau &= -\frac{\mathsf{E}}{\sqrt{\pi}}\int_0^1\frac{\alpha t^n u^n t}{\sqrt{t-tu}}du \\
&= -\frac{\mathsf{E}\alpha t^{n+\frac{1}{2}}}{\sqrt{\pi}}\int_0^1\frac{u^n du}{\sqrt{1-u}}
\end{aligned}$$

Substituting this back into equation (5.129) we are left with

$$\alpha t^n + \mathsf{A}\frac{\alpha t^{n+1}}{n+1} + \mathsf{B}\left(\frac{\alpha t^{n+2}}{(n+1)(n+2)} + x_0\right) = -\frac{\mathsf{E}\alpha t^{n+\frac{1}{2}}}{\sqrt{\pi}}\int_0^1 \frac{u^n du}{\sqrt{1-u}} \tag{5.130}$$

We need to find a balance between the two dominant terms in the equation. Since every term apart from $\mathsf{B}x_0$ contains a different power of t, there is no n for which these terms can balance,

$$t^n \neq t^{n+1} \neq t^{n+2} \neq t^{n+\frac{1}{2}}$$

hence the balance must involve $\mathsf{B}x_0$.

If $\mathsf{B}x_0$ balances $\frac{\mathsf{B}\alpha t^{n+2}}{(n+1)(n+2)}$, this would imply that $n = -2$. However, if $n = -2$ then αt^n would become the dominant term at small time.

For $\mathsf{B}x_0$ to balance $\frac{\mathsf{A}\alpha t^{n+1}}{n+1}$ we would need $n = -1$. Once again this leads to a contradiction, since if $n = -1$ then αt^n would become the dominant term.

If $\mathsf{B}x_0$ balances $-\frac{\mathsf{E}\alpha t^{n+\frac{1}{2}}}{\sqrt{\pi}}\int_0^1 \frac{u^n du}{\sqrt{1-u}}$ then we would need $n = -\frac{1}{2}$, which also leads to a similar contradiction.

The only remaining possibility therefore is to have $\mathsf{B}x_0$ balanced with αt^n, such that $n = 0$. This means that we would need the following value for α.

$$\begin{aligned} \alpha t^n &= -\mathsf{B}x_0 \\ \Rightarrow \alpha &= -\mathsf{B}x_0 \end{aligned} \tag{5.131}$$

Substituting $n = 0$ and (5.131) back into our assumed solution for $x(t)$ gives us the small time approximation.

$$x(t) \sim -\frac{\mathsf{B}x_0}{2}t^2 + x_0 \tag{5.132}$$

This corresponds exactly with the first two terms of the small time approximation from the pole and branch cut analysis (5.102).

We need to check that this small time solution satisfies the boundary conditions at $t = 0$.

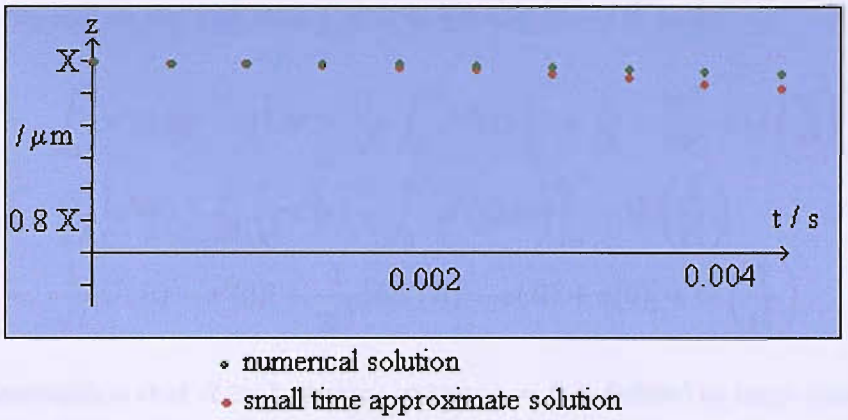

Figure 5.14: Comparison between numerical solution and small time approximation

Setting $t = 0$ in (5.132) gives us

$$x(0) \sim -\frac{\mathsf{B}x_0}{2}0^2 + x_0 = x_0$$

which satisfies the initial condition (5.121). Differentiating $x(t)$ with respect to t, then setting $t = 0$ gives

$$\begin{aligned} x'(t) &\sim -\mathsf{B}x_0 t \\ x'(0) &\sim -\mathsf{B}x_0 0 = 0. \end{aligned}$$

so that the second initial condition (5.122) is also satisfied.

Large time solution

To find the large time solution for (5.129) we first assume a solution of the form

$$x(t) \sim \alpha t^n \tag{5.133}$$

such that

$$x'(t) \sim n\alpha t^{n-1},$$

$$x''(t) \sim n(n-1)\alpha t^{n-2}.$$

We can rewrite the integral on the right hand side as a sum of two integrals, with $1 \ll R < t$.

$$\begin{aligned} -\frac{\mathsf{E}}{\sqrt{\pi}}\int_0^t \frac{x''(\tau)}{\sqrt{t-\tau}}d\tau &= -\frac{\mathsf{E}}{\sqrt{\pi}}\left[\int_0^R \frac{x''(\tau)d\tau}{\sqrt{t-\tau}} + \int_R^t \frac{x''(\tau)d\tau}{\sqrt{t-\tau}}\right] \\ &= -\frac{\mathsf{E}}{\sqrt{\pi}}[I_1 + I_2]. \end{aligned} \tag{5.134}$$

Since $R < t$, we can us the fact that $\frac{\tau}{t} \ll 1$ to expand $(t-\tau)^{\frac{1}{2}}$ in I_1.

$$\begin{aligned} I_1 &= \int_0^R x''(\tau)(t-\tau)^{\frac{1}{2}} d\tau = \frac{1}{\sqrt{t}} \int_0^R x''(\tau) \left[1 + \frac{\tau}{2t} + \frac{3\tau^2}{8t^2} + O\left(\frac{1}{t^3}\right)\right] d\tau \\ &= \frac{1}{\sqrt{t}} \left[x'(\tau) + \frac{1}{2t}\left(\tau x'(\tau) - \int_0^R x'(\tau) d\tau\right)\right]_0^R + O\left(\frac{1}{t^{\frac{5}{2}}}\right) \\ &= \frac{1}{\sqrt{t}}[x'(R) - x'(0)] + \frac{1}{2t^{\frac{3}{2}}}[Rx'(R) - x(R) + x(0)] + O\left(\frac{1}{t^{\frac{5}{2}}}\right). \end{aligned} \tag{5.135}$$

Due to the assumption that $R \gg 1$, motion at time $t = R$ is defined as large time behaviour, hence $x(R) = \alpha R^n$ and $x'(R) = n\alpha R^{n-1}$. From our initial conditions we have that $x'(0) = 0$ and $x(0) = x_0$, simplifying I_1.

$$I_1 = \frac{\alpha n}{\sqrt{t}} R^{n-1} + \frac{\alpha(n-1)}{2t^{\frac{3}{2}}} R^n + \frac{x_0}{2t^{\frac{3}{2}}} + O\left(\frac{1}{t^{\frac{5}{2}}}\right). \tag{5.136}$$

In the second integral, I_2, we can let $x''(\tau) = \alpha\tau^n$ since $r \gg 1$ and $t \gg 1$ so the limits of the integral are both in large time.

$$\begin{aligned} I_2 &= \alpha \int_R^t \frac{\tau^n d\tau}{\sqrt{t-\tau}} \\ &= \alpha t^{n+\frac{1}{2}}(1+n)\sqrt{\pi}\Gamma(1+n) - \frac{\alpha R^{n+1}}{\sqrt{t}} \left[\Gamma(n+\frac{3}{2}) + \frac{(n+1)\Gamma(n+\frac{3}{2})R}{(n+2)2t} + O\left(\frac{R}{t}\right)^2\right]. \end{aligned}$$

This is a general form of I_2 which holds true when $n \neq -\frac{j}{2}$ for all $j \in \mathbb{N} \neq 0$, where Γ is the gamma function, see appendix B.

From the analysis of the poles and branch cut, we found that the curve behaved like $x(t) \sim t^{-\frac{3}{2}}$ at large time. We can check if this holds true here by trying $n = -\frac{3}{2}$, so that I_2 becomes

$$\begin{aligned} I_2 &= \alpha \int_R^t \frac{\tau^n d\tau}{\sqrt{t-\tau}} = \frac{15\alpha}{4} \int_R^t \frac{\tau^{-\frac{7}{2}} d\tau}{\sqrt{t-\tau}} \\ &= \frac{15\alpha}{4} \left[\frac{-2\sqrt{t-\tau}}{5t(\tau^{\frac{5}{2}})} + \frac{4\left(\frac{-2\sqrt{t-\tau}}{3t(\tau^{\frac{3}{2}})} - \frac{4\sqrt{t-\tau}}{3t^2\sqrt{\tau}}\right)}{5t}\right]_R^t \\ &= \frac{\alpha}{4}\left[\frac{2\sqrt{t-R}(3t^2+4Rt+8R^2)}{t^3 R^{\frac{5}{2}}}\right] \\ &= \frac{\alpha}{4}\left[\frac{2\left(1-\frac{R}{t}\right)^{\frac{1}{2}}\left(3+\frac{4R}{t}+\frac{8R^2}{t}\right)}{t^{\frac{1}{2}}R^{\frac{5}{2}}}\right] \end{aligned}$$

We can now use a binomial expansion on $\left(1-\frac{R}{t}\right)^{\frac{1}{2}}$ so that

$$\left(1-\frac{R}{t}\right)^{\frac{1}{2}} = 1-\frac{1}{2}\frac{R}{t}-\frac{1}{8}\left(\frac{R}{t}\right)^2-\frac{1}{16}\left(\frac{R}{t}\right)^3-\dots \tag{5.137}$$

This can be substituted into (5.137) to give

$$\begin{aligned} I_2 &= \frac{\alpha}{4}\left[\frac{8}{R^{\frac{3}{2}}t^{\frac{3}{2}}}-\frac{3}{R^{\frac{3}{2}}t^{\frac{3}{2}}}+\frac{6}{R^{\frac{5}{2}}\sqrt{t}}+\frac{16}{t^{\frac{5}{2}}\sqrt{R}}-\frac{3}{4t^{\frac{5}{2}}\sqrt{R}}-\frac{4}{\sqrt{R}t^{\frac{5}{2}}}\right]+O\left(\frac{1}{t^{\frac{7}{2}}}\right) \\ &= \alpha\left[\frac{3}{2R^{\frac{5}{2}}\sqrt{t}}+\frac{5}{4R^{\frac{3}{2}}t^{\frac{3}{2}}}+\frac{45}{16\sqrt{R}t^{\frac{5}{2}}}\right]+O\left(\frac{1}{t^{\frac{7}{2}}}\right). \end{aligned}$$

When we sum I_2 and I_1 we see that most of the terms will cancel out leaving us with

$$I_1+I_2=\frac{x_0}{2t^{\frac{3}{2}}}+O\left(\frac{1}{t^{\frac{5}{2}}}\right). \tag{5.138}$$

We can now determine the large time approximate solution of (5.129) for $n=-\frac{3}{2}$.

$$\frac{15}{4}\alpha t^{-\frac{7}{2}}+\mathsf{A}\left(\frac{-3\alpha}{2}\right)t^{-\frac{5}{2}}+\mathsf{B}\alpha t^{-\frac{3}{2}}=-\frac{\mathsf{E}x_0}{2\sqrt{\pi}}t^{-\frac{3}{2}} \tag{5.139}$$

Here we can see that there is a balance between $\mathsf{B}\alpha t^{-\frac{3}{2}}$ and $-\frac{\mathsf{E}x_0}{2\sqrt{\pi}}t^{-\frac{3}{2}}$. In this case, these two terms are also the dominant terms for large time behaviour so the balance holds true. This gives us the following value for α.

$$\begin{aligned} \mathsf{B}\alpha &= -\frac{\mathsf{E}x_0}{2\sqrt{\pi}} \\ \Rightarrow \alpha &= -\frac{\mathsf{E}x_0}{2\mathsf{B}\sqrt{\pi}}. \end{aligned}$$

Substituting this back into (5.133) gives us a general large time approximation for $x(t)$.

$$x(t)\sim-\frac{\mathsf{E}x_0}{2\mathsf{B}\sqrt{\pi}}t^{-\frac{3}{2}}. \tag{5.140}$$

This approximation has the same t-behaviour as the analysis done on the poles and branch cut, thus confirming that after a very long period of time the plate decays algebraically. This is a bit of a surprise since most viscometers of this sort decay exponentially.

Non-dimensionalising the problem

We can non-dimensionalise (5.118) in order to simplify the equation and carry out some simple stability analysis on the numerical solution. First we let $x = X\tilde{x}$

$$X\frac{d^2\tilde{x}}{dt^2} + X\mathsf{A}\frac{d\tilde{x}}{dt} + X\mathsf{B}\mathbf{x} = -\frac{X\mathsf{E}}{\sqrt{\pi}}\int_0^t \frac{\frac{d^2\tilde{x}(s)}{ds^2}}{\sqrt{t-s}}ds. \tag{5.141}$$

with $\mathsf{A} = \frac{r}{W}$, $\mathsf{B} = \frac{k^2}{W}$, $\mathsf{E} = \frac{2\sqrt{\mu\rho}Ba}{W}$ and $W = \rho_s dBa$. Next we scale time using $t = \frac{\sqrt{W}}{k}\tilde{t}$ and $s = \frac{\sqrt{W}}{k}\tilde{s}$, allowing us to re-write (5.141) as

$$\begin{aligned}
\frac{k^2}{W}\frac{d^2\tilde{x}}{d\tilde{t}^2} + \mathsf{A}\frac{k}{\sqrt{W}}\frac{d\tilde{x}}{d\tilde{t}} + \frac{k^2}{W}\tilde{x} &= -\frac{\mathsf{E}}{\sqrt{\pi}}\int_0^t \frac{\frac{k^2}{W}\frac{d^2\tilde{x}(\tilde{s})}{d\tilde{s}^2}\frac{\sqrt{W}}{k}}{\sqrt{\frac{\sqrt{W}}{k}(\tilde{t}-\tilde{s})}}d\mathbf{s} \\
\frac{d^2\tilde{x}}{d\tilde{t}^2} + \frac{r}{k\sqrt{W}}\frac{d\tilde{x}}{d\tilde{t}} + \tilde{x} &= \frac{-2\sqrt{\mu\rho}Ba}{\sqrt{\pi}kW^{\frac{3}{4}}}\int_0^{\tilde{t}} \frac{\frac{d^2\tilde{x}(\tilde{s})}{d\tilde{s}^2}}{\sqrt{(\tilde{t}-\tilde{s})}}d\mathbf{s}.
\end{aligned}$$

We now choose to write the non-dimensionalised equation in the following form

$$\frac{d^2\tilde{x}}{d\tilde{t}^2} + \alpha\frac{d\tilde{x}}{d\tilde{t}} + \tilde{x} = -\beta\int_0^{\tilde{t}} \frac{\frac{d^2\tilde{x}(\tilde{s})}{d\tilde{s}^2}}{\sqrt{(\tilde{t}-\tilde{s})}}d\tilde{s}. \tag{5.142}$$

where α and β are dimensionless variables dependent on the material properties of the plate and the viscosity and density of the surrounding fluid. To determine the effect α and β will have on the solution we can multiply the equation by x' and then integrate.

$$\int_0^t \tilde{x}'\left(\tilde{x}'' + \alpha\tilde{x}' + \tilde{x} = -\beta\int_0^{\tilde{t}} \frac{\tilde{x}''(\tilde{s})}{\sqrt{\tilde{t}-\tilde{s}}}d\tilde{s}\right)dz$$

$$\int_0^{\tilde{t}} \tilde{x}'\tilde{x}''dz + \int_0^{\tilde{t}} \tilde{x}'\tilde{x}dz = -\alpha\int_0^{\tilde{t}} (\tilde{x}')^2dz - \beta\int_0^{\tilde{t}} \tilde{x}\int_0^{\tilde{t}} \frac{\tilde{x}'(\tilde{s})}{\sqrt{\tilde{t}-\tilde{s}}}d\tilde{s}dz$$

$$\frac{1}{2}[(\tilde{x}')^2]_0^{\tilde{t}} + \frac{1}{2}[\tilde{x}^2]_0^{\tilde{t}} = -\alpha\int_0^{\tilde{t}} (\tilde{x}')^2dz - \beta\int_0^{\tilde{t}} \tilde{x}\int_0^{\tilde{t}} \frac{\tilde{x}'(\tilde{s})}{\sqrt{\tilde{t}-\tilde{s}}}d\tilde{s}dz$$

$$\frac{1}{2}(\tilde{x}')^2 + \frac{1}{2}\tilde{x}^2 - \frac{\tilde{x}(0)^2}{2} = -\alpha\int_0^{\tilde{t}} (\tilde{x}')^2dz - \beta\int_0^{\tilde{t}} \tilde{x}\int_0^{\tilde{t}} \frac{\tilde{x}'(\tilde{s})}{\sqrt{\tilde{t}-\tilde{s}}}d\tilde{s}dz.$$

Note that we now use the non-dimensional boundary conditions

$$\tilde{x}'(0) = 0$$

$$\tilde{x}(0) = 1$$

On the left hand side of this equation, $\frac{1}{2}(\tilde{x}')^2$ is the kinetic energy term, $\frac{1}{2}(\tilde{x})^2$ is the potential energy, and $\frac{\tilde{x}(0)^2}{2}$ represents the initial potential energy. Since $\alpha > 0$ and $\beta > 0$, both terms on the right hand side are dissipating energy from the system, hence α and β are both damping terms. The sum of these two terms is negative which indicates the oscillations will decrease as time progresses, as required. We require α and β to be small so that the system is not overdamped to the extent that decay occurs too rapidly for any oscillations to be seen. We also need α to be much smaller than β so that the main damping is dependent on the term containing viscosity and density, since these are the variables we wish to measure. For this reason we specify that

$$0 < \alpha << \beta < 1.$$

Using (5.123), (5.124), (5.125) and our new boundary conditions, we can rewrite the numerical solution for x_{i+1} in non-dimensionalised form as

$$\begin{aligned}
\tilde{x}_0 &= 1 \\
\tilde{x}_1 &= 1 \\
\tilde{x}_2 &= 1 - \frac{2(\Delta\tilde{t})^2}{2 + \alpha\Delta\tilde{t} + 2\beta\sqrt{\Delta\tilde{t}}} \\
\tilde{x}_{i+1} &= \left(\frac{2(\Delta\tilde{t})^2}{2 + \alpha\Delta\tilde{t} + 2\beta\sqrt{\Delta\tilde{t}}}\right)[\tilde{x}_i\left(\frac{2}{(\Delta\tilde{t})^2} - 1 + \frac{\beta}{(\Delta\tilde{t})^{\frac{3}{2}}}\right) \\
&\quad + \tilde{x}_{i-1}\left(\frac{\beta}{(\Delta\tilde{t})^{\frac{3}{2}}} + \frac{\alpha}{2\Delta\tilde{t}} - \frac{1}{(\Delta\tilde{t})^2}\right) - \tilde{x}_{i-2}\left(\frac{\beta}{(\Delta\tilde{t})^{\frac{3}{2}}}\right) \\
&\quad - \beta\sum_{j=1}^{i-1}\frac{\tilde{x}_{j+1} - \tilde{x}_j - \tilde{x}_{j-1} + \tilde{x}_{j-2}}{(\Delta\tilde{t})^{\frac{3}{2}}}(\sqrt{i-j+1} - \sqrt{i-j})].
\end{aligned} \tag{5.143}$$

Numerical Stability Analysis

Although the numerical scheme that has been posed clearly gives credible results, it is obviously of interest to show if possible that the scheme is numerically stable. If we consider the exact solution as a sum of our numerical approximation and an error term $\tilde{x}_{exact} = \tilde{x} + e_r$, then since (5.142) is a linear equation the numerical solution and the error term (e_r) must both satisfy the same system of equations. This error will also depend on the time step $\Delta\tilde{t}$. For the numerical solution to be a good approximation we can analyse the absolute stability of the system, finding when the error term is growing and shrinking. The numerical solution will be useful when the error term gives a stable solution and is thus converging. The details of this analysis can be found in appendix D.

Conclusions

Since r is small, we can choose to simplify the non-dimensional numerical scheme (5.143) further by neglecting terms containing internal damping, thus letting $\alpha = 0$. Our simplified non-dimensional numerical solution for $\tilde{x}_i$ is thus

$$\begin{aligned}
\tilde{x}_0 &= 1 \\
\tilde{x}_1 &= 1 \\
\tilde{x}_2 &= 1 - \frac{2(\Delta\tilde{t})^2}{2 + 2\beta\sqrt{\Delta\tilde{t}}} \\
\tilde{x}_{i+1} &= \left(\frac{2(\Delta\tilde{t})^2}{2 + 2\beta\sqrt{\Delta\tilde{t}}}\right)\left[\tilde{x}_i\left(\frac{2}{(\Delta\tilde{t})^2} - 1 + \frac{\beta}{(\Delta\tilde{t})^{\frac{3}{2}}}\right)\right. \\
&\quad + \tilde{x}_{i-1}\left(\frac{\beta}{(\Delta\tilde{t})^{\frac{3}{2}}} - \frac{1}{(\Delta\tilde{t})^2}\right) - \tilde{x}_{i-2}\left(\frac{\beta}{(\Delta\tilde{t})^{\frac{3}{2}}}\right) \\
&\quad \left. -\beta\sum_{j=1}^{i-1}\frac{\tilde{x}_{j+1} - \tilde{x}_j - \tilde{x}_{j-1} + \tilde{x}_{j-2}}{(\Delta\tilde{t})^{\frac{3}{2}}}(\sqrt{i-j+1} - \sqrt{i-j})\right] \qquad (5.144)
\end{aligned}$$

The key parameter in this system is β and this will let us know how the plate will oscillate. Using equation (??) to find the vacuum frequency of the plate and comparing this to plots of the numerical solution with $\mu = 0$, we can calculate the spring constant to be approximately $k = 95$. This gives us $\beta = 0.051\sqrt{\mu\rho}$. Analysis of the numerical solution shows us that when $\beta > 1$, the system will be too greatly damped to produce a measurable amount of oscillations (see figure 5.15). For a reasonable number of oscillations we require

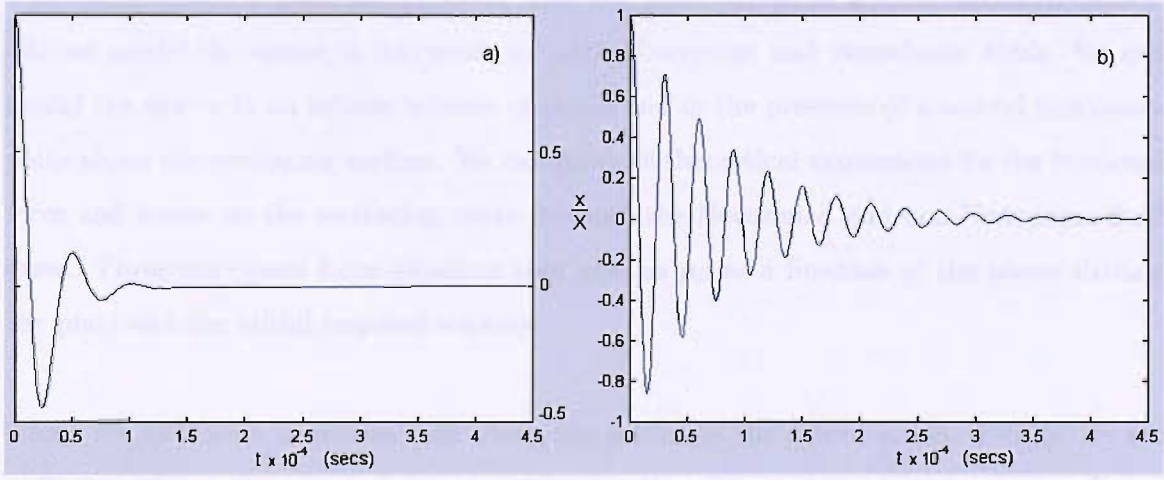

Figure 5.15: a) numerical solution for $\beta = 1$; b) numerical solution for $\beta = 0.1$

$0.001 < \beta < 0.1$. Hence, using the decaying oscillations method, this MEMS viscometer would be suitable for fluids in the range $0.01957 < \mu\rho/\text{Pa}^2\cdot\text{s} < 1.957$.

5.4 Summary of the Spider

The transversely oscillating MEMS device discussed in this chapter is designed for use as an in situ viscometer in oil exploration. An advantage of the MEMS sensor is that it is small and can be integrated into existing tools used down-hole. Amplitude of motion is typically measured in micrometers. Due to the geometric design of the sensor there will be a relatively large fluid mass on the small device making it sensitive to fluid properties. The device is relatively easy to produce, using integrated circuit techniques, fabricated using material deposition and etching onto a silicon wafer.

The sensor can be modelled for use in Newtonian and non-Newtonian fluids. In the modelling of the viscometer, certain assumptions need to be made. The device oscillates in its own plane and we assume that oscillation results only in a deformation of the legs connecting the vibrating plate to the surrounding stationary frame. Having looked at the heat equation (5.1) we concluded that thermal dissipation is unimportant in the modelling of this device.

The viscometer can be operated in two different modes, forced or plucked, and it was of interest to discover which mode would be the most practical experimentally.

Forced mode

The forced model is time-independent, with the plate driven at a fixed forced frequency. We can model the sensor in this mode for both Newtonian and viscoelastic fluids. We can model the device in an infinite volume of liquid and in the presence of a second stationary plate above the oscillating surface. We can produce theoretical expressions for the frictional force and power on the oscillating plate for both the Newtonian and non-Newtonian fluid cases. These are closed form solutions that give us $\mu\rho$ as a function of the power driving the plate and the initial imposed velocity.

There are two main problems with using the sensor in the forced mode. Firstly, we are unlikely to know the value of the power driving the plate and the initial velocity. In experimentation, these parameters are not always measured. This means that our theoretical result will have no practical value. Secondly, the first resonance frequency of the sensor is at approximately 16.9 kHz. At this frequency the legs of the spider have a tendency to break!

We can overcome the first of these problems by recasting the model in terms of alternative parameters. For Newtonian fluids we can determine $\mu\rho$ as a function of resonance frequency and quality factor. Both of these parameters are determined from the in-phase and quadrature voltage of the system that are measured experimentally. The second problem is more serious and can not be overlooked. This implies that the forced mode will never really be of practical use since the devices are destroyed whenever they reach their first resonance frequency.

Plucked mode

The plucked model is time-independent, where the amplitude of oscillation varies with time, decaying gradually after an initial perturbation. When placed in a fluid, the decay in amplitude of oscillation allows us to infer the fluid properties in terms of things that we are able to measure. Operation in this mode seems a lot more promising, however the solution is not easily written down and the result is a Laplace transform problem that can not be solved simply.

There are two ways to tackle this problem. The first is to solve the inverse Laplace transform problem asymptotically, analysing the poles and branch cut. This allows us to determine the long and short time behaviours of the plate. This is relatively straightforward but will not give us a complete time picture for the plate behaviour.

The second way to proceed is to solve the problem numerically. This requires us to recast the inverse Laplace transform as a differential/integral equation. We can also do some asymptotic analysis on this form of the problem to find short and long time behaviours. Solving the problem numerically allows us to identify a parameter that would indicate the practical value of the sensor. For the sensor to be successful we require a certain number of measurable oscillations. This means that the oscillations must not decay too quickly or continue to vibrate at the same amplitude forever. The parameter that will tell us this is $\beta = 0.051\sqrt{\mu\rho}$, dependent on the fluid properties. For a successful device we require $0.001 < \beta < 0.1$.

β is a dimensionless variable, also dependent on the material properties of the plate, $\beta = \frac{2\sqrt{\mu\rho}Ba}{\sqrt{\pi}kW^{\frac{3}{4}}}$. If we know an approximate range of viscosity and density values for a fluid then β will allow us to decide on the properties of the sensor needed.

Experiments have not yet been successfully carried out with the spider in the plucked mode, but it is clear that the issue of the robustness of the model, with respect to any experimental errors that might occur, should be considered. It seems most likely that the device will not be too sensitive to experimental errors since only the decay rate needs to be measured. However in the absence of experiments this is only conjecture.

The model deals with an infinite plate, therefore assuming that any edge effects are negligible. This is a reasonable assumption when the viscous penetration depth is small compared with the dimensions of the plate. For a plate oscillating in the third mode, using dimensions for kinematic viscosity as given in table (5.1), the viscous penetration depth, δ, can be calculated as

$$\delta = \sqrt{\frac{2\nu}{\omega}} = \sqrt{\frac{2 \times 10^{-6}}{35 \times 10^{3}}} = 7.6 \times 10^{-6}$$

The sensors produced have a width of 1.6×10^{-3} and length of 2.4×10^{-3}, so this would appear be a reasonable assumption.

In conclusion, the transversely oscillating MEMS device should be operated in the plucked mode in a fluid satisfying the criteria allowing for a measurable number of oscillations.

Chapter 6

The Flexion

6.1 The cantilever plate

We will now move on to study a different MEMS sensor produced and tested by Schlumberger. As with the spider, the cantilever plate is modelled as an elastic solid oscillating in a fluid [37]. This device is based on a vibrating plate, with dimensions on the order of 1 mm and a mass of about 0.3 mg, clamped along one edge. The plate is set in motion when an alternating current is passed through the coil mounted on the plate in the presence of a magnetic field. At resonance the plate motion is observed using a strain gauge. The in vacuo resonance frequency of the first bending mode is about 5 kHz, at a temperature of 298 K, with a quality factor of about 2900.

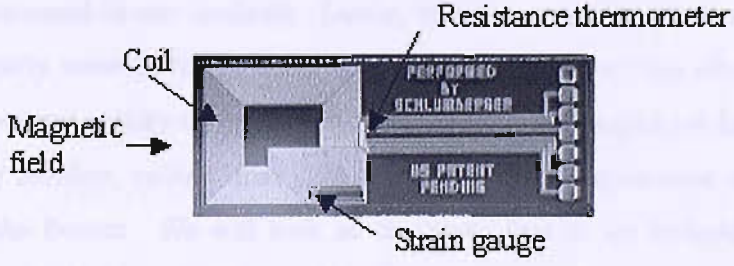

Figure 6.1: Photograph of the upper surface of the 'flexion'

The method adopted in the past has been to study the mechanical behaviour of the plate in a vacuum to obtain the resonance frequencies. The interaction with the fluid is then carried out once the mechanics is fully understood. Due to the small amplitudes of oscillation, the problem can be simplified by applying linear theory. A similar problem has been solved in [48] for the case of a densitometer plate clamped at both ends in an inviscid fluid. J.E. Sadar modelled a similar design of sensor [49] describing a cantilever beam of arbitrary cross section, excited by an arbitrary driving force, immersed in a fluid, regarding

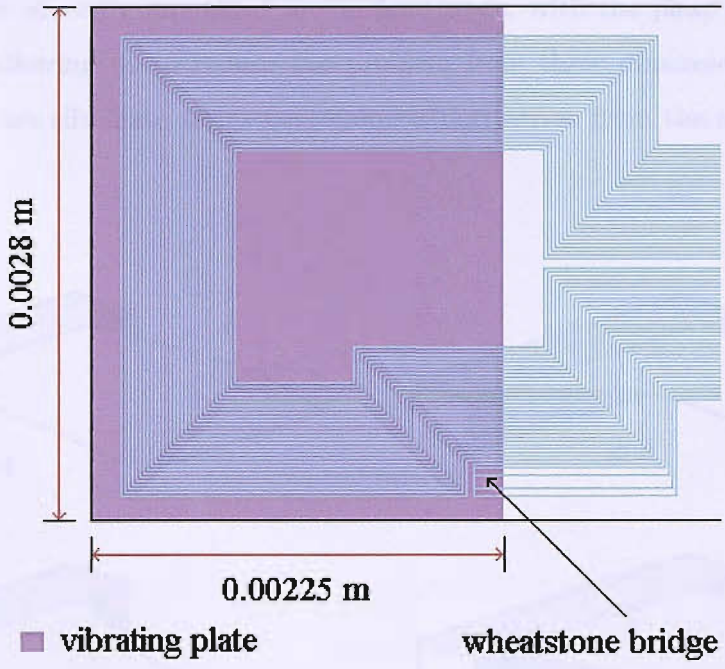

Figure 6.2: Dimensions of the 'flexion'

application to the atomic force microscope. The theory is restricted by limitations to the geometry of the beam, which disagrees with our MEMS design. The equations derived by Sadar involving viscosity and density rely on three main assumptions. The first is that the amplitude of oscillation of the beam is considerably smaller than any length scale in the beam geometry. Due to the dimensions of the flexion, this would mean an amplitude of less than 2.8 mm, a realistic requirement. The second assumption is that the fluid is incompressible, also assumed in our analysis. Lastly, Sadar's equations require that the length of the beam greatly exceeds its breadth. On the flexion sensor, the vibrating portion of the armature does not satisfy this final condition. Sadar uses impulsive formula, assuming a high Reynolds number, rather than slow flow, again in disagreement with the analysis carried out on the flexion. We will look at the plate first in an inviscid fluid, as in the densitometer case, and then in a viscous fluid where viscosity can be determined. We hope then to introduce a different method for formulating the fluid flow and the motion of the plate as a coupled problem to be solved simultaneously.

6.1.1 The mechanics of an oscillating cantilever plate, clamped at one end

As with other MEMS sensors, the cantilever plate oscillates in a number of different modes, see figure (6.3). Experimentally Schlumberger have found that the first mode occurs in vacuum at 5.3 kHz. The second mode is at 11.8 kHz, the third at 30.3 kHz and the fourth

at 33.6 kHz. We are only interested in the first mode, with the plate oscillating in one direction only, allowing us to reduce the problem from three dimensions to two. This means that we can eliminate terms containing x derivatives from the equation for plate motion.

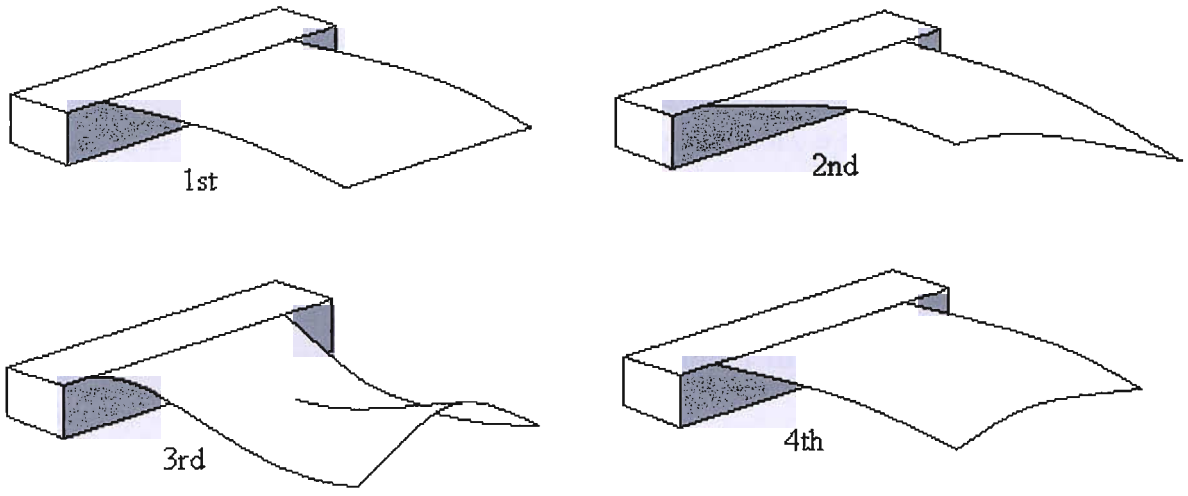

Figure 6.3: Modes of oscillation for the 'flexion' (diagrams reproduced from Maria Manrique de Lara's analysis using ANSYS [40])

The plate is initially modelled as a cantilever plate clamped at one end, $z = 0$, $y = 0$, as shown in figure (6.4).

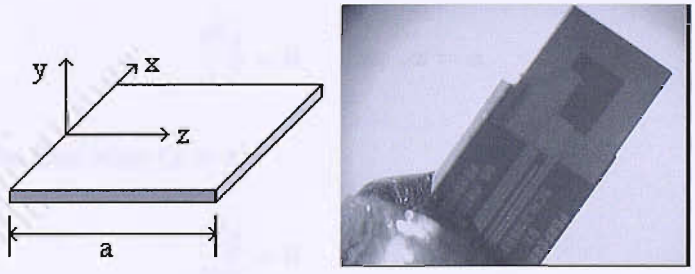

Figure 6.4: Schematic for the 'flexion' with a photograph of the clamped plate

The transverse displacement of the plate normal to the x-z plane is given by:

$$y = q(x, z, t)$$

We assume that longitudinal strains vary linearly across the plate's depth and the bending moment at any cross section is proportional to a local radius of curvature. Given these assumptions and due to the dimensions of the plate, we can state that the partial differential

equation for q follows the Bernoulli-Euler bending theory of thin plates:

$$\rho_s d\frac{\partial^2 q}{\partial t^2} + D\nabla^4 q = F \tag{6.1}$$

$$0 < z < a$$

$$0 < x < B$$

Where $a \equiv$ length of plate, $B \equiv$ breadth of plate, $D = Ed^3/12(1-\sigma^2) \equiv$ flexural rigidity of plate, $\rho_s \equiv$ density of plate material, $E \equiv$ Youngs modulus, $\sigma \equiv$ Poisson ratio of plate, $d \equiv$ thickness of plate and $F \equiv$ force per unit area applied normal to plate surface.

We assume the plate is infinitely long in the x direction to simplify the problem to only two dimensions. It is now necessary to solve (6.1) subject to the following clamped edge conditions:
no deflection at the clamped edge

$$q = 0 \qquad \text{at} \quad z = 0 \tag{6.2}$$

no slope at the clamped edge

$$\frac{\partial q}{\partial z} = 0 \qquad \text{at} \quad z = 0 \tag{6.3}$$

no bending moment at the free edge ($z = a$)

$$\frac{\partial^2 q}{\partial z^2} = 0 \qquad \text{at} \quad z = a \tag{6.4}$$

no shear force at the free edge ($z = a$)

$$\frac{\partial^3 q}{\partial z^3} = 0 \qquad \text{at} \quad z = a \tag{6.5}$$

This will give us the equation of motion for the cantilever plate subject to an external force F. We can define F to be the retarding force on the plate due to the surrounding fluid so that we can couple the fluid and plate equations.

6.1.2 Solving equations of the plate in vacuum

Before defining F, the first step is to solve the homogeneous form of (6.1) subject to conditions (6.2) through to (6.5). At this stage we define that there is no force (external

driving force or retarding force due to surrounding fluid) acting on the plate which is assumed to be in vacuum, $F = 0$. We assume that the plate oscillates with harmonic motion of the form $q = Z(z)e^{-i\omega t}$ where $Z(z)$ is a function of z only. Using the separation of variables method [50] this results in the following equation for q:

$$q = \frac{A_0}{2}\cos\omega_n t\left[\frac{(\sinh b_n a + \sin b_n a)(\cosh b_n z - \cos b_n z) - (\sinh b_n z - \sin b_n z)(\cosh b_n a + \cos b_n a)}{\cosh b_n a \sin b_n a - \cos b_n a \sinh b_n a}\right] \tag{6.6}$$

where $A_0 \equiv$ arbitrary initial amplitude, $\omega_n \equiv$ natural frequency of oscillation of plate and $b_n = \sqrt{\omega_n}(\frac{\rho_s d}{D})^{\frac{1}{4}}$. This equation satisfies the boundary conditions subject to $1 + \cos(b_n a)\cosh(b_n a) = 0$.

The fundamental value is found to be $b_n \equiv b_f = \frac{1.8751}{a}$

The solution to the homogeneous form of (6.1) can be plotted to show the position of the surface of the plate at different times. Here we can see a plot of one complete period in steps of $\frac{\Pi}{8}$, and for values of z across the length of the plate from 0 to a. It is evaluated with $\omega_v = 1$ and $b_f = 1.87$.

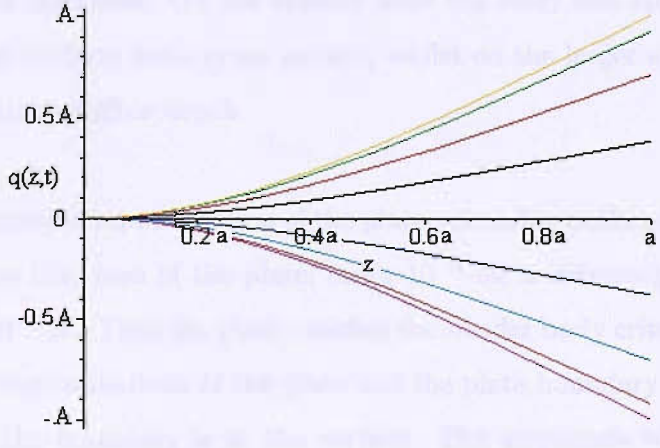

Figure 6.5: Plate position through one complete period of vibration

The next step is to find out how the plate acts due to the presence of the fluid as described by the force, F. This force will be discussed further in the next section.

6.2 Densitometer - Inviscid Flow

We will first consider an inviscid fluid, so that the cantilever plate acts as a densitometer only. This will allow us to see how the plate motion changes in the presence of a fluid without the added complication of viscosity. Schlumberger have been using the sensors as densitometers in various gases, where the effects of viscosity are much smaller than that of density. Experimentally, the fluid surrounding the plate is initially at rest. To simplify our model we assume the fluid is inviscid and incompressible ($\nabla.\mathbf{v} = \mathbf{0}$) and that the flow is irrotational. This implies that the fluid velocity $\mathbf{v}$ is the gradient of a potential

$$\mathbf{v} = \nabla\Phi$$

where Φ satisfies

$$\frac{\partial\Phi}{\partial x} = u \qquad \text{and} \qquad \frac{\partial\Phi}{\partial y} = v \tag{6.7}$$

$$\nabla^2\Phi = 0. \tag{6.8}$$

6.2.1 Slender body theory

Long bodies can be considered to have two naturally occurring length scales and asymptotic expansions can be made for each of them. The two scales in this case are the length of the body and its thickness. On the smaller scale the body can appear to have infinite length with a quasi-uniform finite cross section, whilst on the larger scale it can appear to be finitely long with negligible depth.

Taking a two-dimensional representation of the plate, assuming uniformity along the breadth, it is shown that the thickness of the plate, order 10^{-6} m, is extremely small compared to the length, order 10^{-3} m. Thus the plate satisfies the slender body criteria. This theory can also be applied to the oscillations of the plate and the plate boundary. The plate oscillates harmonically and the boundary is at the surface. The amplitude of this wave is of the same order as the thickness of the plate. We define that the position of this surface varies only slightly with the perturbation quantity ϵ. If the plate oscillates around the centre line $y = 0$ then since the boundary only moves a small amount we define that any particle on the surface $y = q(x, z, t)$ is assumed to be at [51]

$$y = \epsilon\bar{q}(x, z, t)$$

with $\epsilon << 1$ and $\bar{q}$ of order 1. Since ϵ is small, $y = \epsilon\bar{q}(x, z, t)$ gives no order 1 contribution to the boundary therefore to leading order we can express the boundary conditions on $y = 0$ [52].

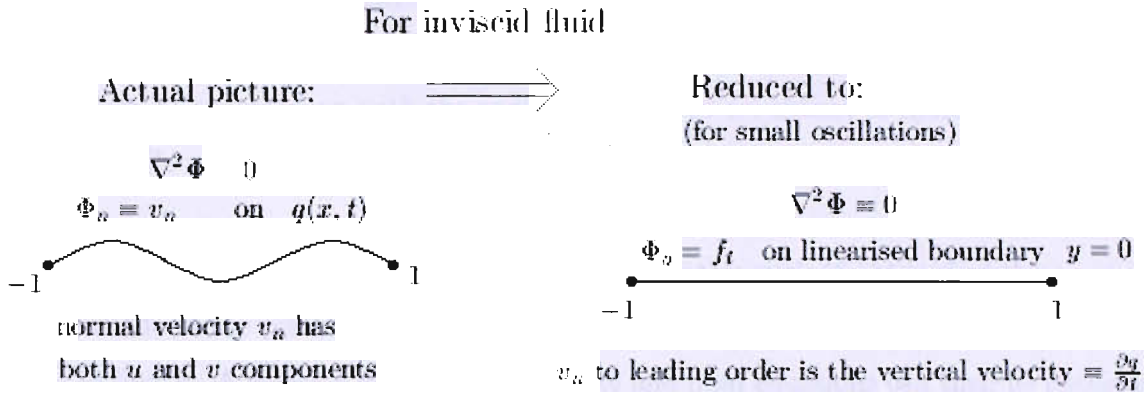

Figure 6.6: Linearising the boundary for an inviscid fluid

6.2.2 Fluid-plate interaction

We assume that the transverse displacements of the plate are sufficiently small that the plate surface can be linearised to $y = 0$. We imply that the normal velocity of the plate is equal to the fluid velocity in the y-direction at this surface.

$$\frac{\partial q}{\partial t} = \frac{\partial \Phi}{\partial y} \qquad \text{at} \quad y = 0 \tag{6.9}$$

Also defined is that the force on the plate, F, is a result of the pressure difference either side of the plate surface

$$F = (p^- - p^+) \tag{6.10}$$

where $p^{+-} \equiv$ fluid pressure at $y = 0^{+-}$.

For an inviscid fluid we can find these pressures using other fluid flow quantities. The Bernoulli equation, neglecting the gravity and square of velocity term (using standard values from table 5.1 it can be seen that these terms are negligible), gives

$$p = -\rho\frac{\partial \Phi}{\partial t} \tag{6.11}$$

where ρ is the fluid density.

We should also impose the boundary conditions $\Phi^{\pm} \to 0$ as $y \to^{\pm} \infty$ to represent the pertubations in the fluid decaying to zero far from the plate surface. Here we will need to approximate because an inviscid solution which also satisfies these conditions will be much more complicated. Experimentally, the flexion will be positioned inside a tube but the geometry of this arrangement is difficult to model. Due to the small size of oscillations of the plate in comparrison with the radius of the tube we choose to ignore the effects of the tube walls and do not impose the extra boundary conditions.

We can solve (6.8) for Φ subject to (6.9) and combine this with (6.11) to find the pressure at either side of the plate surface. The pressure at $y = 0^{+-}$ can then be substituted into (6.10) to find F. A solution satisfying both plate and fluid equations can then be obtained by substituting F with q into (6.1).

Solving the equations

The first step is to use our homogeneous solution for q (6.6) in (6.9) to get definitions for Φ^+ and Φ^-.

$$\begin{aligned}\Phi^+ &= \frac{A_0 \sin(\omega t)\omega}{2b(\cosh(ba)\sin(ba) - \cos(ba)\sinh(ba))}((\cos(by) - \sin(by))(S\cosh(bz) \\ &\quad -C\sinh(bz)) + e^{-by}(C\sin(bz) - S\cos(bz))) \qquad (6.12)\end{aligned}$$

$$\begin{aligned}\Phi^- &= -\frac{A_0 \sin(\omega t)\omega}{2b(\cosh(ba)\sin(ba) - \cos(ba)\sinh(ba))}((\cos(by) + \sin(by))(S\cosh(bz) \\ &\quad -C\sinh(bz)) + e^{by}(C\sin(bz) - S\cos(bz))) \qquad (6.13)\end{aligned}$$

with $C = \cosh(ba) + \cos(ba)$ and $S = \sinh(ba) + \sin(ba)$. As anticipated from the discussion above, concerning the tube in which the flexion is placed, Φ^+ and Φ^- do not tend to zero as $y \to \pm\infty$ respectively. They are however, not exponentially large. Φ^+ and Φ^- are now substituted into (6.11) resulting in two equations for the pressure above and below the plate, p^+ and p^-.

$$\begin{aligned}p^+ &= -\frac{\rho A_0 \cos(\omega t)\omega^2}{2b(\cosh(ba)\sin(ba) - \cos(ba)\sinh(ba))}((\cos(by) - \sin(by))(S\cosh(bz) \\ &\quad -C\sinh(bz)) + e^{-by}(C\sin(bz) - S\cos(bz))) \qquad (6.14)\end{aligned}$$

$$p^- = \frac{\rho A_0 \cos(\omega t)\omega^2}{2b(\cosh(ba)\sin(ba) - \cos(ba)\sinh(ba))}((\cos(by) + \sin(by))(S\cosh(bz) - C\sinh(bz)) + e^{by}(C\sin(bz) - S\cos(bz))) \quad (6.15)$$

Next we can determine the force, F, using (6.14) and (6.15) in equation (6.10).

$$F = \frac{\rho A_0 \cos(\omega t)\omega^2(S(\cosh(bz) - \cos(bz)) + C(\sin(bz) - \sinh(bz)))}{2b(\cosh(ba)\sin(ba) - \cos(ba)\sinh(ba))} \quad (6.16)$$

This new expression for F is substituted, along with our homogeneous solution for q, into our initial equation (6.1) which can now be re-solved. At this stage we redefine the frequency ω to be $2\pi f$ and rearrange the solution to get a definition of the fluid density in terms of frequency f, the determined constant b and plate material constants.

$$\rho = \frac{Db^5}{(2\pi f)^2} - \rho_s db \quad (6.17)$$

This equation can be used to determine fluid density in an inviscid fluid. Since D and b are both positive this tells us that as you increase the density of the surrounding fluid, the frequency of oscillation of the plate will decrease, as expected physically.

6.2.3 Comparison with data

This is all very well theoretically, but the plate is not pure silicon, so the density of the plate and its elastic properties are relatively unknown. We re-write equation (6.17) in terms of two constants, K_2 and K_1, which can be calibrated from known data.

$$\rho = \frac{K_2 b^5 d^3}{(2\pi f)^2} - K_1 db \quad (6.18)$$

with $K_1 \equiv \rho_s$ and $K_2 \equiv \frac{E}{12(1-\sigma^2)}$, where E, σ and ρ_s are unknown. This equation can be modified further by adding in a temperature dependence to the length scales to account for thermal expansion at high temperatures, once again assuming the plate to be pure silicon. The plate depth, d, is now written as

$$d(T/\mathrm{K}) = d \times (1.000002366975533 \times (T - 273.16)^2 + 0.0000000100192 \times (T - 273.16))$$

and b, which is a function of $\frac{1}{a}$, becomes

$$\begin{aligned} b(T/\mathrm{K}) &= b/(1.000002366975533 \times (T - 273.16)^2 \\ &\quad +0.0000000100192 \times (T - 273.16)) \end{aligned}$$

The parameter representing plate density , K_1, becomes

$$K_1(T/\mathrm{K}) = (K_1 - 0.00002859446 \times (T - 273.16)^2 - 0.016541425 \times (T - 273.16))$$

This gives us a temperature dependent equation for fluid density (6.19).

$$\rho = \frac{K_2 b(T)^5 d(T)^3}{(2\pi f)^2} - K_1(T) db \tag{6.19}$$

Two sets of experimental data have been analysed using different flexion plates. The first viscometer was tested in argon at a range of temperatures and pressures. The constants were calibrated at a temperature of 323 K and resulted in $K_1 = 2130.661146$ kg·m^{-3} and $K_2 = 462902788.8$ kg·m^{-1}·s^{-2}. It was expected that the constant representing silicon density, K_1, would be lower than the true density for pure silicon due to the layers on the plate consisting of other materials. These values were then put back into equation (6.19) and this was used to calculate densities at the other temperatures. This produced density values accurate to within 2 % of the true value, see graph (6.7).

The second flexion plate was tested in several different fluids at varying temperatures. Using an uncalibrated model, equation (6.19) with $K_1 = \rho_s$ and $K_2 = \frac{D}{d^3}$, the density was determined to within 20 % of the true value over the entire range. Some of the fluids tested showed an accuracy of less than 2 %, see plot (6.9). All data used in these plots can be seen in appendix A.

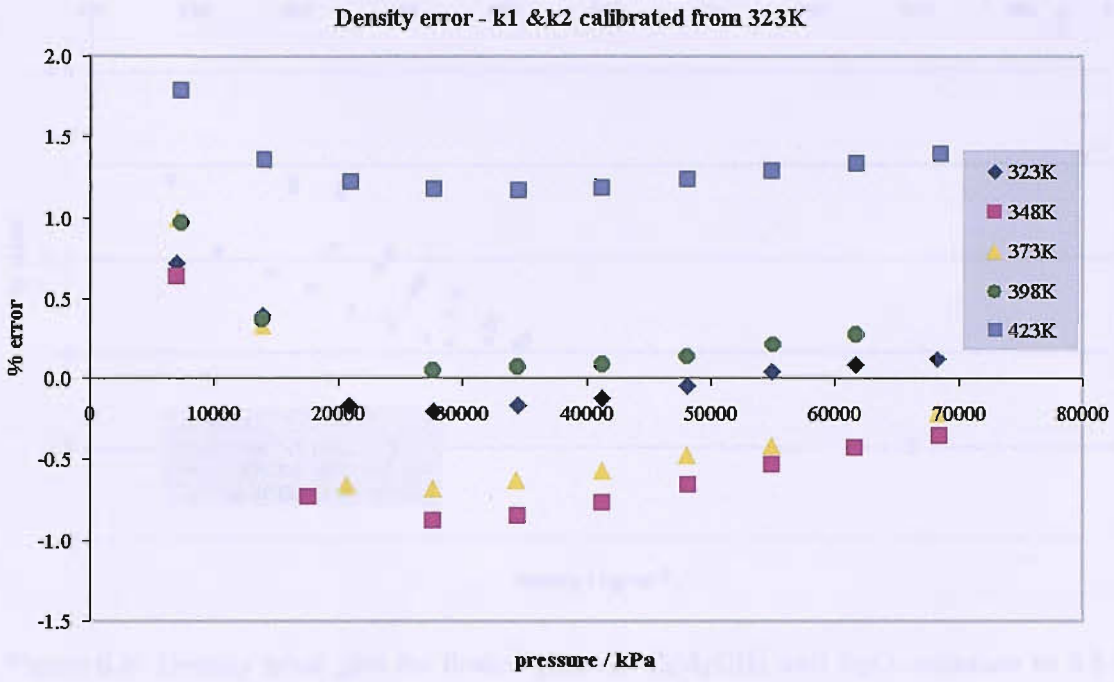

Figure 6.7: Density error plot for flexion plate in argon, accurate to 2 %

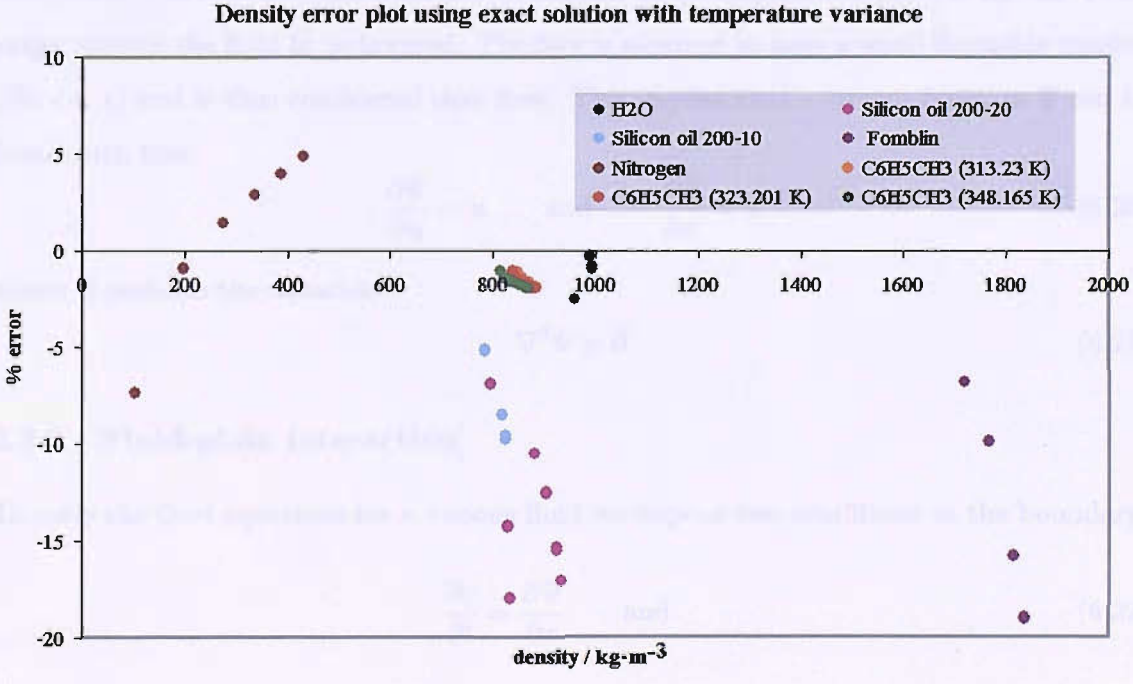

Figure 6.8: Density error plot for flexion plate in assorted fluids, accurate to 20 %

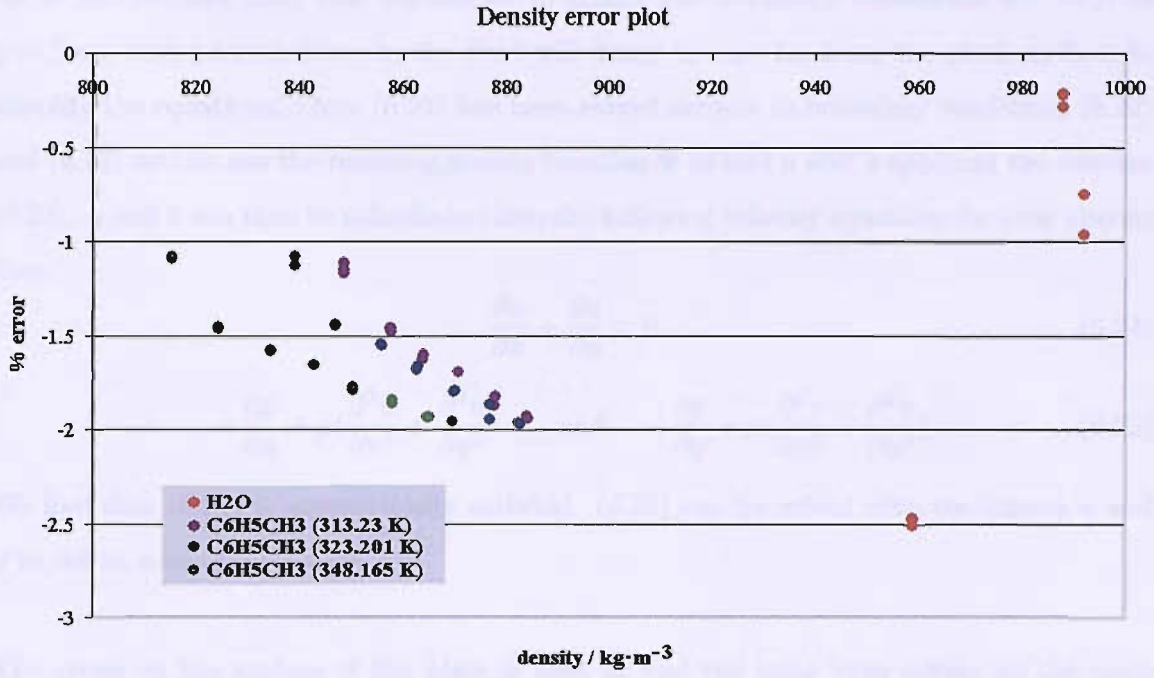

Figure 6.9: Density error plot for flexion plate in $C_6H_5CH_3$ and H_2O, accurate to 2.5 %

6.3 Viscometer - Slow Viscous Flow

The MEMS sensors are intended to measure density and viscosity so we will next consider oscillations in a viscous fluid to introduce viscosity into the fluid equations. For the more complicated viscous case the fluid is still defined as incompressible ($\nabla.\mathbf{v} = \mathbf{0}$) but we no longer assume the fluid to be inviscid. The flow is assumed to have a small Reynolds number ($Re << 1$) and is thus considered slow flow. This implies that a stream function Ψ can be found such that

$$\frac{\partial \Psi}{\partial y} = u \qquad \text{and} \qquad -\frac{\partial \Psi}{\partial x} = v \tag{6.20}$$

where Ψ satisfies the equation

$$\nabla^4 \Psi = 0 \tag{6.21}$$

6.3.1 Fluid-plate interaction

To solve the fluid equations for a viscous fluid we impose two conditions at the boundary:

$$\frac{\partial q}{\partial t} = \frac{\partial \Psi}{\partial x} \qquad \text{and} \tag{6.22}$$

$$\frac{\partial \Psi}{\partial y} = 0 \qquad \text{at} \quad y = 0 \tag{6.23}$$

As in the inviscid fluid case we choose to ignore the boundary conditions $\Psi^{\pm} \to 0$ as $y \to^{\pm} \infty$, that perturbations in the fluid will decay to zero far from the plate surface, to simplify the equations. Once (6.21) has been solved subject to boundary conditions (6.22) and (6.23) we can use the resulting stream function Ψ to find u and v applying the relation (6.20). u and v can then be substituted into the following velocity equations for slow viscous flow.

$$\frac{\partial u}{\partial x} + \frac{\partial v}{\partial y} = 0 \tag{6.24}$$

$$-\frac{\partial p}{\partial x} + \mu\left(\frac{\partial^2 u}{\partial x^2} + \frac{\partial^2 u}{\partial y^2}\right) \quad \text{and} \quad -\frac{\partial p}{\partial y} + \mu\left(\frac{\partial^2 v}{\partial x^2} + \frac{\partial^2 v}{\partial y^2}\right) \tag{6.25}$$

We find that (6.24) is automatically satisfied. (6.25) can be solved with the known u and v to define a unique pressure.

The stress on the surface of the plate is used to find the total force acting on the plate due to the presence of the fluid. This is shown diagramatically in figure (6.10).

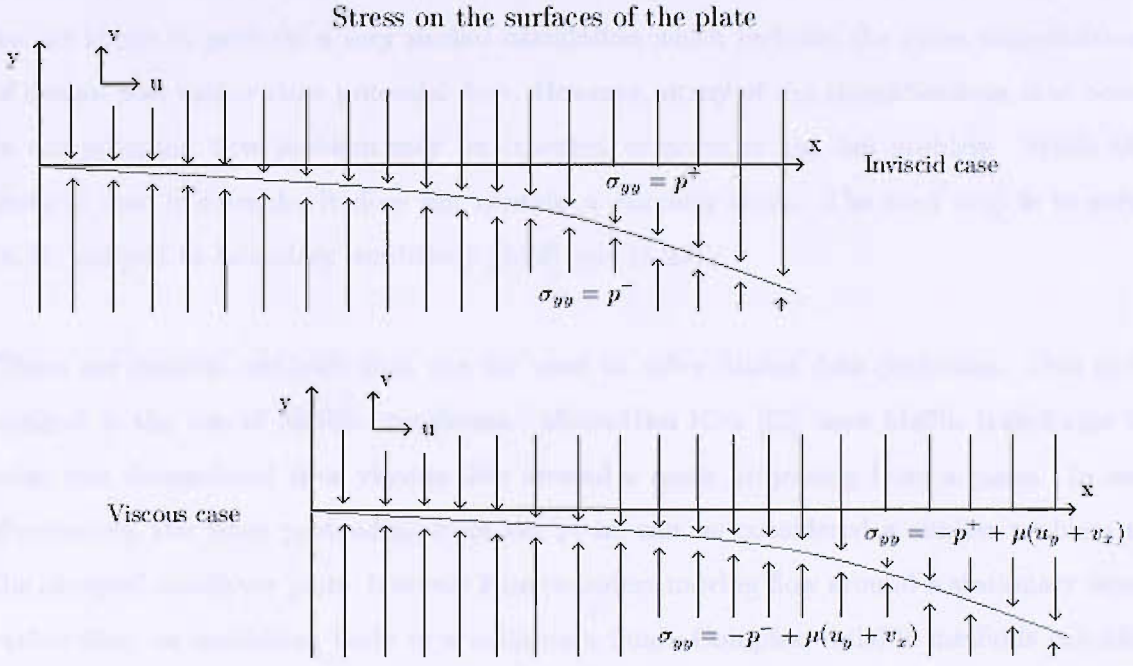

Figure 6.10: Stress in an inviscid and viscous fluid

We define that the force on the plate, F, is a result of the difference in stress normal to the surface of the plate top and bottom.

$$F = F^- - F^+ = (-p^- + \mu(\frac{\partial u^-}{\partial y} + \frac{\partial v^-}{\partial x}) - (-p^+ + \mu(\frac{\partial u^+}{\partial y} + \frac{\partial v^+}{\partial x})) \tag{6.26}$$

where $p^{+-} \equiv$ fluid pressure at $y = 0^{+-}$. F can thus be determined using this unique pressure and substituted with q into (6.1) in a similar way to the inviscid case. This time the resulting problem will be a lot harder to solve since F is likely to be a function of q.

Inviscid fluid analogy

Before we solve the viscous fluid equations it helps to consider the inviscid fluid analogy. For the inviscid fluid case we could view the plate as a system of sources acting on the fluid. A fundamental solution to (6.8) exists of the form

$$\Phi = \frac{\epsilon}{\pi} \int_{-1}^{1} f_t \log[(x-\zeta)^2 + y^2] d\zeta \tag{6.27}$$

which is subject to the boundary condition

$$\frac{\partial f}{\partial t} = \frac{\partial \Phi}{\partial y} \qquad \text{on} \quad y = 0 \tag{6.28}$$

where $f(x,t)$ is the function defining the position of a particle at the surface of the plate. The first term, f_t, is equivalent to the source strength. The value of this analogy is that we are about to perform a very similar calculation which includes the extra complications of Stokes flow rather than potential flow. However, many of the simplifications that occur in the potential flow problem may be expected to occur in the full problem. While the inviscid case is solvable, it does not contain a viscosity term. The next step is to solve (6.21) subject to boundary conditions (6.22) and (6.23).

There are various methods that can be used to solve Stokes flow problems. One such method is the use of Mellin transforms. Moon-Uhn Kim [53] uses Mellin transforms to solve two dimensional slow viscous flow around a fence projecting from a plane. In two dimensions, the fence protruding from the plane can be considered a similar problem to the clamped cantilever plate, however Kim considers moving flow around a stationary fence rather than an oscillating body in a stationary fluid. Complex variable methods can also be used to solve Stokes flow problems and many authors have used this to analyse the bi-harmonic equation [54].

Solving the viscous fluid equation

We chose to solve the Stokes flow problem using the method of Stokeslets. Similar methods have been use to analyse the swimming motions of microscopic organisms such as flagellum.

Examples of this can be seen in the work of Lighthill [55] [56], Hancock [57] and Taylor [58]. More recently a numerical method for computing Stokes flows using stokeslets has been explained in a paper by Cortez [59]. He presents a more general case of Stokes flows driven by external forcing, allowing the method to be applied to any moving body that interacts with the fluid.

The main assumption made is that the Reynolds number of the fluid is small enough that inertial effects on the fluid or the plate can be neglected. The resultant and the moment of all forces acting on the plate will be zero [56]. The fluid will satisfy the equations

$$\mu \triangle^2 \mathbf{v} = \nabla p - F \tag{6.29}$$

$$\nabla . \mathbf{v} = 0 \tag{6.30}$$

where μ is the fluid viscosity, $\mathbf{v}$ is velocity, and p is pressure. In a similar fashion to the inviscid case, a fundamental solution of these equations can be found which is called a stokeslet field. Every flow field at very low Reynolds number can be defined as a superposition of stokeslet fields distributed along a surface.

Refering back to figure (6.4), we are modelling the sensor as a cantilever plate clamped at one end. We now chose to introduce an infinite, flat solid wall at the clamped edge, perpendicular to the sensor plate. This is to more closely represent the true geometry of the sensor. The equations of motion for the flow are the Stokes equations (6.24) and (6.25), and the boundary conditions are that the fluid velocity is zero on the wall $z = 0$ and is equal to the velocity of the oscillating plate wherever the fluid and the plate are in contact.

6.3.2 The Method of Stokeslets

A stokeslet is the name given to the Stokes flow due to a point force. We will seek to model the flow around the plate using an infinite regular array of stokeslets all with equal strength. Techniques for arrays of stokeslets are given by Blake [60] and Liron & Mochon [61].

In this chapter we will begin by considering the equation for a single stokeslet near a flat plane wall. This idea will then be extended for the modelling of the plate viscometer by considering three problems.

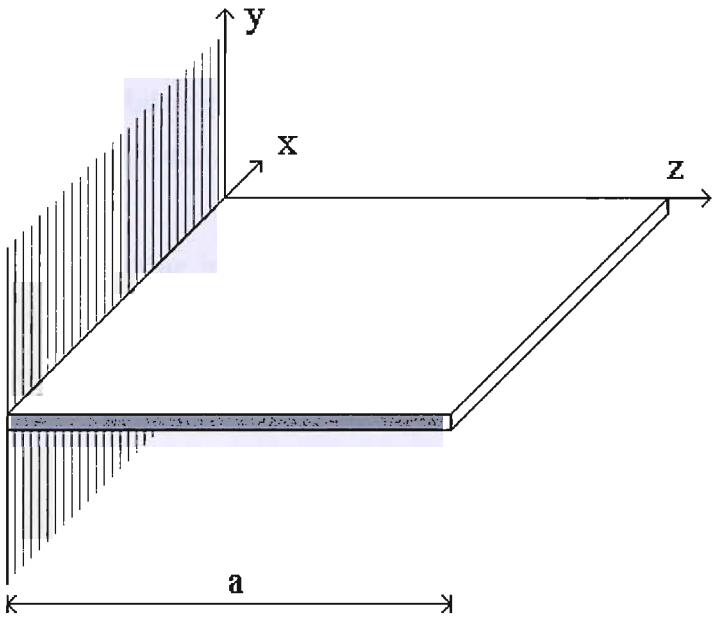

Figure 6.11: Flexion with infinite wall at $z = y = 0$

1) Firstly the solution to an infinite continuous distribution of stokeslets on a line above a flat plane wall.
2) This will lead to the consideration of a double array of stokeslets above the plane, infinite in one direction and finite in the other, representing the plate itself.
3) Finally the idea of dipoles will be introduced to allow the no-slip condition on the plate surface to be satisfied.
The culmination of these problems should result in a complete fluid-plate model.

To understand stokeslets in general it is useful to look at them in three dimensions. This will allow us to pose the full boundary value problem with the plate having finite edges. Although this is possible, ultimately we will assume the edge effects are negligible to reduce the problem to equations in only two dimensions.

A Single Stokeslet and the Image System

The equation for a stokeslet in an infinite viscous fluid is found by considering Stokes flow past a sphere. The fundamental singular solution is given by Lighthill [55] and Blake [62], obtained using a three dimensional Fourier transform on the equations of motion in an infinite viscous fluid. The velocity and pressure field components respectively can be written as

$$u_j = \frac{F_k}{8\pi\mu}\left[\frac{\delta_{jk}}{|\mathbf{x}-\boldsymbol{\gamma}|} + \frac{(x_j-\gamma_j)(x_k-\gamma_k)}{|\mathbf{x}-\boldsymbol{\gamma}|^3}\right] \tag{6.31}$$

$$p = \frac{F_k}{4\pi} \frac{x_k - \gamma_k}{|\mathbf{x} - \boldsymbol{\gamma}|^3} \tag{6.32}$$

where $\mathbf{x} = (x, y, z)$ is an arbitrary point in the fluid, $\boldsymbol{\gamma} = (\gamma_1, \gamma_2, \gamma_3)$ is the position of the stokeslet and $|\mathbf{x} - \boldsymbol{\gamma}|$ is the distance between the two points.

Now consider a stokeslet acting in the y direction situated at $\boldsymbol{\gamma}$, a distance $\gamma_3 = h$ from a plane $z = 0$, see diagram (6.12). A Greens function is constructed for the pressure and velocity fields associated with this point force, F_k, satisfying the no-slip condition on the plane boundary.

$$U_j = u_j + v_j \qquad (j = 1, 2, 3) \tag{6.33}$$

$$P = p + q \tag{6.34}$$

Here u_j and p are the fundamental singular solutions (6.31) and (6.32) respectively. The problem of obtaining the complementary solutions v_j and q is carried out by Blake [62]. The terms satisfy the creeping flow equations

$$\nabla q = \mu \nabla^2 \mathbf{v}$$

$$\nabla . \mathbf{v} = 0 \tag{6.35}$$

subject to $\mathbf{v} = -\mathbf{u}$ at all points in the plane $z = 0$. The resulting entire velocity field for a point force in the y-direction near the plane $z = 0$ can be written

$$U_j = \frac{F_k}{8\pi\mu} \left[(\frac{1}{r} - \frac{1}{R}) \delta_{jk} + \frac{r_j r_k}{r^3} - \frac{R_j R_k}{R^3} + \right.$$

$$\left. 2h(\delta_{k\alpha}\delta_{\alpha l} - \delta_{k3}\delta_{3l}) \frac{\partial}{\partial R_l} \left\{ \frac{hR_j}{R^3} - (\frac{\delta_{j3}}{R} + \frac{R_j R_3}{R^3}) \right\} \right] \tag{6.36}$$

and the pressure field as

$$P = \frac{F_k}{\pi} \left[\frac{r_k}{r^3} - \frac{R_k}{R^3} - 2h(\delta_{k\alpha}\delta_{\alpha l} - \delta_{k3}\delta_{3l}) \frac{\partial}{\partial R_l} \left\{ \frac{R_3}{R^3} \right\} \right] \tag{6.37}$$

where α assumes the value 1 or 2, $\mathbf{r} = \mathbf{x} - \boldsymbol{\gamma}$, $\mathbf{R} = \mathbf{x} - \boldsymbol{\gamma}'$, $r = |\mathbf{r}|$ and $R = |\mathbf{R}|$, with $\boldsymbol{\gamma}' = (\gamma_1, \gamma_2, -h)$. The term $(\delta_{k\alpha}\delta_{\alpha l} - \delta_{k3}\delta_{3l})$ only has a non-zero value when $k = l$ and is positive when $k = 1$ or 2 but has a negative sign when $k = 3$.

Blake describes these equations using an image system of singularities below the plane for two distinct cases, when the stokeslet points normal to the plane and when the axis of

the stokeslet is aligned parallel to the plane. We are only concerned with the latter and this system can be seen in diagram (6.12).

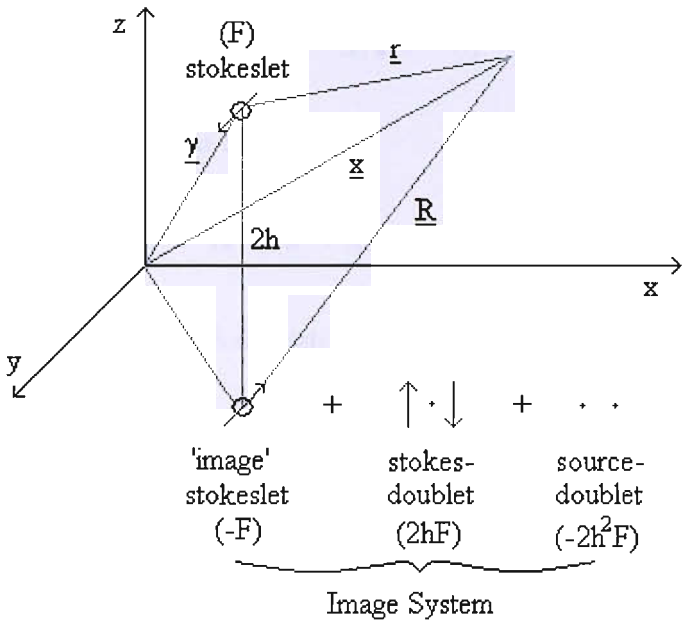

Figure 6.12: Image system for a stokeslet aligned parallel to the plane $z = 0$, with $k = 2$

This system consists of a stokeslet equal in strength and opposite in sign to the original, a stokes-doublet of strength $2hF_k$ and a source-doublet of strength $2h^2F_k$ where k is 1 or 2. We are interested in what happens when $k = 2$. For this case the stokes-doublet is defined by the equations

$$u'_i = \frac{2hF_2}{8\pi\mu}\left[-\frac{r_i}{r^3} + \frac{3r_ir_jr_k}{r^5} + \frac{r_k\delta_{ij} - r_j\delta_{ik}}{r^3}\right]$$

$$p' = \frac{2hF_2}{8\pi\mu}\frac{3r_jr_k}{r^5} \tag{6.38}$$

The stokes-doublet contains two stokeslets pointing normal to the plane boundary, equal in strength and opposite in direction. The source doublet contains two sources, equal in strength and opposite in direction, at an infinitessimal distance apart. This image system is satisfactory for local flow but in the far field the effect of the two stokeslets is to introduce a far field stokes-doublet. This will be located at $\frac{1}{2}(\gamma + \gamma')$ and will have strength $4hF_2$.

Line of stokeslets above a flat plane

As explained earlier we wish to extend the single stokeslet solution to an array of stokeslets to begin to construct the model of the plate surface. To do this we consider an infinite line

array of identical stokeslets situated at points $\gamma = (\gamma_1, 0, h)$, $-\infty < \gamma_1 < \infty$. The radius vector from the stokeslet γ to $\mathbf{x}$ is given by

$$\mathbf{r} = (x - \gamma_1, y, z - h)$$

and from the image stokeslet γ' to $\mathbf{x}$ is

$$\mathbf{R} = (x - \gamma_1, y, z + h)$$

This problem has been done in the discrete array case by Liron [63].

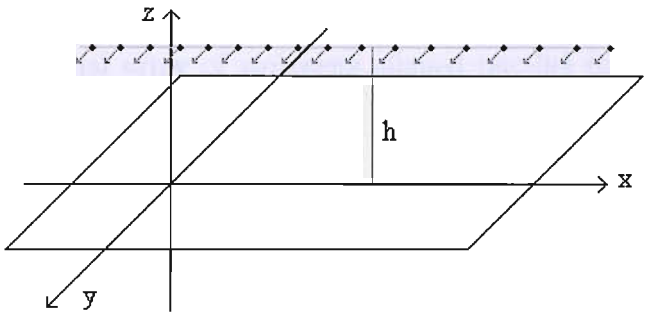

Figure 6.13: Line array of identical $k = 2$ stokeslets

To obtain the velocity at $\mathbf{x}$ due to the infinite line of stokeslets at γ we need to integrate (6.36) with respect to γ_1 in the limits $-\infty < \gamma_1 < \infty$.

$$U^*{}_j = \int_{-\infty}^{\infty} U_j^k(\mathbf{x}, \gamma) d\gamma_1 \tag{6.39}$$

Double array of stokeslets above the plane

Once the solutions for a line array have been found, these results are extended to a double array, infinite in the x direction and finite in the z direction. This will now represent the basic shape of the oscillating plate. The length of the array in the z direction will correspond with the length of the oscillating plate viscometer. Again, the discrete case is covered by Liron [63]. The 2-dimensional array of stokeslets can be seen in diagram (6.14). In this case the radius vector from the stokeslet γ to $\mathbf{x}$ is given by

$$\mathbf{r} = (x - \gamma_1, y, z - \gamma_3)$$

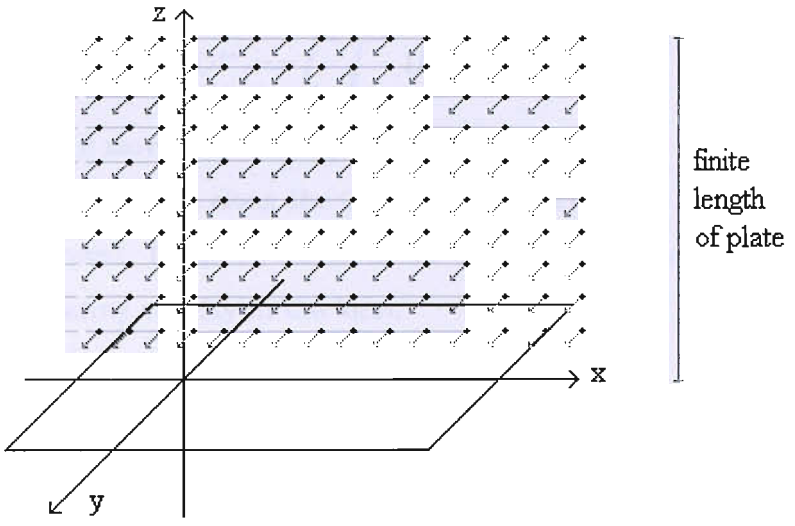

Figure 6.14: 2-dimensional array of stokeslets aligned parallel to the plane boundary at $z = 0$

and from the image stokeslet $\boldsymbol{\gamma}'$ to $\mathbf{x}$ is

$$\mathbf{R} = (x - \gamma_1, y, z + \gamma_3)$$

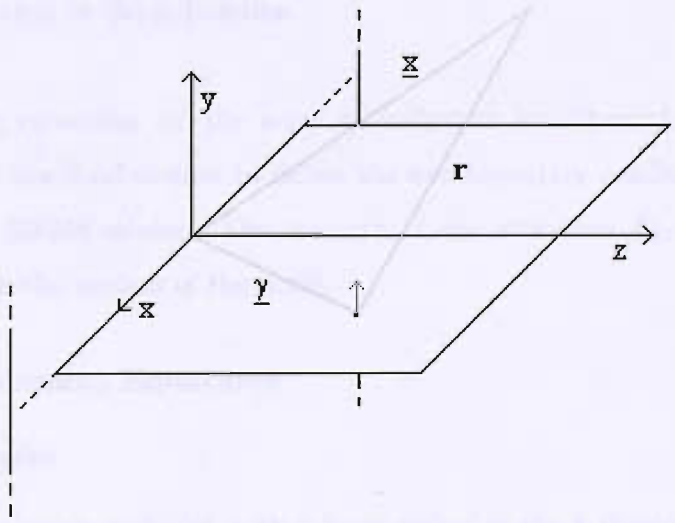

Figure 6.15: Identifying a stokeslet in the 2-dimensional plate array

To obtain the velocity at $\mathbf{x}$ due to the double array of stokeslets at $\boldsymbol{\gamma}$ we need to do a double integration on (6.36). The first is with respect to γ_1 in the limits $-\infty < \gamma_1 < \infty$ and secondly with respect to γ_3 in the limits $0 < \gamma_1 < a$, where a is the length of the MEMS

device.

$$U^{**}{}_j = \int_0^a \int_{-\infty}^{\infty} U_j^k(\mathbf{x}, \boldsymbol{\gamma}) d\gamma_1 d\gamma_3 \tag{6.40}$$

To create the effect of movement in the plate we need to define the force F to be a function of both time and the distance along the plate, γ_3. This makes the next step of integration much more complicated. It will be shown in the working equations that we can write the components of the array velocity in the form:

$$U^{**}{}_2 = \int_0^a F(t, \gamma_3) K_v(y, z, \gamma_3) d\gamma_3 \tag{6.41}$$

$$U^{**}{}_3 = \int_0^a F(t, \gamma_3) K_w(y, z, \gamma_3) d\gamma_3 \tag{6.42}$$

Boundary conditions

We now have an array of stokeslets representing our plate which can be used to model the fluid motion caused by the oscillating device. The next problem is the boundary condition on the surface of the plate itself. The fluid must satisfy the no-slip condition on this surface. A similar problem is solved by Lighthill [55] defining flagellum motion. He couples a stokeslet with a corresponding dipole to create the effect of a solid spherical boundary. In our case the no-slip condition on the surface of the plate can be incorporated by defining the force F to act only in the y direction.

Once the working equations for the array of stokeslets have been found (6.40) we can use this model for the fluid motion to define the two boundary conditions for the motion of the oscillating MEMS device. The strength of the stokeslets F_k can then be varied corresponding with the motion of the plate.

6.3.3 The Stokeslets Equations

The single stokeslet

The equation for a single stokeslet with a force acting in the k direction situated at $\boldsymbol{\gamma}$, a distance $\gamma_3 = h$ from the plane $z = 0$, was given by equation (6.36). The problem that we are interested in will eventually be an array of stokeslets each with force in the $k = 2$ direction. We will first write down the individual stokeslet's velocity components for $k = 2$, with $\mathbf{F} = (0, F, 0)$. The remaining velocity terms will all be zero since $F_1 = 0 = F_3$,

therefore if k is equal to 1 or 3 we will get $U_1 = U_2 = U_3 = 0$. When $k = 2$ we get

$$U_1 = \frac{F}{8\pi\mu}\left[\frac{y(x-\gamma_1)}{r^3} - \frac{y(x-\gamma_1)}{R^3} + 2h\frac{\partial}{\partial y}\left\{\frac{h(x-\gamma_1)}{R^3} - \frac{(x-\gamma_1)(z+h)}{R^3}\right\}\right] \tag{6.43}$$

$$U_2 = \frac{F}{8\pi\mu}\left[(\frac{1}{r} - \frac{1}{R}) + \frac{y^2}{r^3} - \frac{y^2}{R^3} + 2h\frac{\partial}{\partial y}\left\{\frac{hy}{R^3} - \frac{y(z+h)}{R^3}\right\}\right] \tag{6.44}$$

$$U_3 = \frac{F}{8\pi\mu}\left[\frac{y(z-h)}{r^3} - \frac{y(z+h)}{R^3} + 2h\frac{\partial}{\partial y}\left\{\frac{h(z+h)}{R^3} - \frac{1}{R} - \frac{(z+h)^2}{R^3}\right\}\right] \tag{6.45}$$

with

$$r = \sqrt{(x-\gamma_1)^2 + y^2 + (z-h)^2}$$

$$R = \sqrt{(x-\gamma_1)^2 + y^2 + (z+h)^2}.$$

Removing the derivatives we can rewrite these equations as:

$$\frac{8\pi\mu}{F}U_1 = \left[\frac{y(x-\gamma_1)}{r^3} - \frac{y(x-\gamma_1)}{R^3} + \frac{6hyz(x-\gamma_1)}{R^5}\right] \tag{6.46}$$

$$\frac{8\pi\mu}{F}U_2 = \left[\frac{1}{r} - \frac{1}{R} + \frac{y^2}{r^3} - \frac{y^2}{R^3} + 2h\frac{z}{R^5}\left\{3y^2 - R^2\right\}\right] \tag{6.47}$$

$$\frac{8\pi\mu}{F}U_3 = \left[\frac{y(z-h)}{r^3} - \frac{y(z+h)}{R^3} + 2h\frac{y}{R^5}\left\{R^2 + 3z(z+h)\right\}\right] \tag{6.48}$$

The continuous line of stokeslets

To find a line of stokeslets aligned parallel to the plane boundary with force in the k=2 direction we now need to integrate each of (6.46), (6.47) and (6.48) with respect to γ_1 over the interval $-\infty < \gamma_1 < \infty$. For the velocity at a point on this line we need to divide through by the breadth of the plate, in this case B.

$$\frac{B8\pi\mu}{F}U^*{}_1 = \int_{-\infty}^{\infty}\left[\frac{y(x-\gamma_1)}{r^3} - \frac{y(x-\gamma_1)}{R^3} + \frac{6hyz(x-\gamma_1)}{R^5}\right]d\gamma_1 \tag{6.49}$$

$$\frac{B8\pi\mu}{F}U^*{}_2 = \int_{-\infty}^{\infty}\left[\frac{1}{r} - \frac{1}{R} + \frac{y^2}{r^3} - \frac{y^2}{R^3} + 2h\frac{z}{R^5}\left\{3y^2 - R^2\right\}\right]d\gamma_1 \tag{6.50}$$

$$\frac{B8\pi\mu}{F}U^*{}_3 = \int_{-\infty}^{\infty}\left[\frac{y(z-h)}{r^3} - \frac{y(z+h)}{R^3} + 2h\frac{y}{R^5}\left\{R^2 + 3z(z+h)\right\}\right]d\gamma_1 \tag{6.51}$$

To simplify calculations we break the equations up into smaller integrals to be solved, such that

$$\frac{B8\pi\mu}{F}U^*{}_1 = yT2 + 6hzyT5$$

$$\frac{B8\pi\mu}{F}U^*{}_2 = T6 + y^2T1 + 6hzy^2T3 - 2hzT4$$

$$\frac{B8\pi\mu}{F}U^*{}_3 = (2hy - y(z+h))T4 + 6hyz(z+h)T3 + y(z-h)T7$$

$$T1 = \int_{-\infty}^{\infty}\left[\frac{1}{r^3} - \frac{1}{R^3}\right]d\gamma_1 = -2\left[\frac{\alpha^2-\beta^2}{\alpha^2\beta^2}\right] \tag{6.52}$$

$$T2 = \int_{-\infty}^{\infty}\left[\frac{x-\gamma_1}{r^3} - \frac{x-\gamma_1}{R^3}\right]d\gamma_1 = 0 \tag{6.53}$$

$$T3 = \int_{-\infty}^{\infty}\left[\frac{1}{R^5}\right]d\gamma_1 = \frac{4}{3\beta^4} \tag{6.54}$$

$$T4 = \int_{-\infty}^{\infty}\left[\frac{1}{R^3}\right]d\gamma_1 = \frac{2}{\beta^2} \tag{6.55}$$

$$T5 = \int_{-\infty}^{\infty}\left[\frac{x-\gamma_1}{R^5}\right]d\gamma_1 = 0 \tag{6.56}$$

$$T6 = \int_{-\infty}^{\infty}\left[\frac{1}{r} - \frac{1}{R}\right]d\gamma_1 = \ln(\frac{\beta^2}{\alpha^2}) \tag{6.57}$$

$$T7 = \int_{-\infty}^{\infty}\left[\frac{1}{r^3}\right]d\gamma_1 = \frac{2}{\alpha^2} \tag{6.58}$$

with α and β given by the following expressions

$$\alpha^2 = y^2 + (z-h)^2 \qquad \text{and} \qquad \beta^2 = y^2 + (z+h)^2$$

We can now write down equations for the velocity at $\mathbf{x}$ due to a continuous, infinite sequence of stokeslets at γ.

$$U^*{}_1 = 0 \tag{6.59}$$

$$U^*{}_2 = \frac{F}{B8\pi\mu}\left[\ln(\frac{\beta^2}{\alpha^2}) - 2y^2\left[\frac{\alpha^2-\beta^2}{\alpha^2\beta^2}\right] + \frac{8hzy^2}{\beta^4} - \frac{4hz}{\beta^2}\right] \tag{6.60}$$

$$U^*{}_3 = \frac{F}{B8\pi\mu}\left[\frac{2y(z-h)}{\alpha^2} - \frac{2y(z+h)}{\beta^2} + \frac{8hzy(z+h)}{\beta^4} + \frac{4hy}{\beta^2}\right] \tag{6.61}$$

These expressions are independent of x and hence our problem is reduced to a two dimensional system of equations.

For equations (6.59), (6.60) and (6.61) to be of use they must satisfy the conditions originally prescribed. They must be a solution of the two-dimensional Stokes equations, they must satisfy no-slip at the plane boundary $z = 0$ and the velocities must tend to zero as $\mathbf{x}$ tends to ∞. The velocities do indeed all tend to zero with increasing $\mathbf{x}$ so it just remains

to check the other two conditions.

The first condition is satisfied since the following expressions hold true

$$\frac{\partial U^*{}_2}{\partial y} + \frac{\partial U^*{}_3}{\partial z} = 0$$

$$\frac{\partial^2 P}{\partial y \partial z} - \frac{\partial^2 P}{\partial z \partial y} = 0$$

It can next be shown that the no-slip condition is satisfied given that

$$U^*{}_2 = 0 = U^*{}_3 \qquad \text{on} \quad z = 0$$

The continuous array of stokeslets

As mentioned in the previous chapter, this step of integration is made more complicated by the definition that F is a function of t and h (γ_3). To find the velocity due to an array of stokeslets protruding from the plane boundary with force in the k=2 direction we need to integrate each of (6.59), (6.60) and (6.61) with respect to h over the interval $0 < h < a$. To find the velocity at a point due to the array we must divide through by the length of the plate, a. It now helps to write the fluid velocity at x due to the continuous array of stokeslets, in component form.

$$u = U^{**}{}_1 = 0 \tag{6.62}$$

$$v = U^{**}{}_2 = \int_0^a F(t,h) K_v(y,z,h) dh \tag{6.63}$$

$$w = U^{**}{}_3 = \int_0^a F(t,h) K_w(y,z,h) dh \tag{6.64}$$

with K_v and K_w given by the following expressions

$$K_v = \frac{1}{8aB\pi\mu}\left[\ln(\frac{\beta^2}{\alpha^2}) - 2y^2\left[\frac{\alpha^2-\beta^2}{\alpha^2\beta^2}\right] + \frac{8hzy^2}{\beta^4} - \frac{4hz}{\beta^2}\right] \tag{6.65}$$

$$K_w = \frac{1}{8aB\pi\mu}\left[\frac{2y(z-h)}{\alpha^2} - \frac{2y(z+h)}{\beta^2} + \frac{8hzy(z+h)}{\beta^4} + \frac{4hy}{\beta^2}\right] \tag{6.66}$$

Boundary conditions

Referring back to the original plate equation (6.1) for the velocity of the plate, q, we can use equations (6.63) and (6.64) to define our two necessary boundary conditions.

$$q_t = \int_0^a F(t,h)K_v(0,z,h)dh \tag{6.67}$$

$$0 = \int_0^a F(t,h)K_w(0,z,h)dh \tag{6.68}$$

The first condition states that the velocity of the plate is equal to the fluid velocity at the surface $y = 0$.

$$q_t = \int_0^a \frac{F(t,h)}{4aB\pi\mu}\left[\ln(\frac{z+h}{z-h}) - \frac{2hz}{(z+h)^2}\right]dh \tag{6.69}$$

The second condition satisfies the no-slip condition on the surface, hence $w = 0$ on $y = 0$. It becomes apparent that for our choice of stokeslets, acting in the $k = 2$ direction only, condition (6.68) is automatically satisfied. This can be proven by identifying that the limit of w is 0 as y tends to 0.

$$\lim_{y\to 0}(w) = \int_0^a F(t,h)\lim_{y\to 0}[K_w(y,0,h)]dh \tag{6.70}$$

$$= \int_0^a \frac{F(t,h)}{8aB\pi\mu}\lim_{y\to 0}[\frac{2y(z-h)}{y^2+(z-h)^2}]dh - \int_0^a \frac{F(t,h)}{8aB\pi\mu}\lim_{y\to 0}[\frac{2y(z+h)}{y^2+(z+h)^2}]dh$$

$$+\int_0^a \frac{F(t,h)}{8aB\pi\mu}\lim_{y\to 0}[\frac{8hyz(z+h)}{(y^2+(z+h)^2)^2}]dh + \int_0^a \frac{F(t,h)}{8aB\pi\mu}\lim_{y\to 0}[\frac{4hy}{y^2+(z+h)^2}]dh$$

As y approaches 0 the limit of the third and fourth term will be reduced to 0. It is shown that this is also true for the first two terms using dirac-delta function relationships.

$$\lim_{\psi\to 0}\frac{\psi}{\psi^2+\chi^2} = \pi\delta(\chi)$$

$$\begin{aligned}\int_a^b \delta(\psi-\psi_0)f(t,h)d\psi &= (-1)f(\psi_0) \quad \text{for} \quad a<\psi_0<b \\ &= 0 \quad \text{for} \quad a>\psi_0 \quad \text{or} \quad b<\psi_0\end{aligned}$$

provided $f(\psi)$ exists at $\psi = \psi_0$. If we next define $F(t,h) = e^{i\omega t} f(h)$, this allows us to write the remaining terms in equation (6.70) as

$$\begin{aligned}\int_0^a \frac{e^{i\omega t}}{8aB\pi\mu} f(h) \lim_{y\to 0}[\frac{2y(z-h)}{y^2+(z-h)^2}]dh &= \int_0^a \frac{e^{i\omega t}}{8aB\pi\mu} f(h) 2(z-h)\pi\delta(h-z)dh \\ &= \frac{-2e^{i\omega t}}{8aB\pi\mu} f(z)(z-z)\pi = 0\end{aligned}$$

$$\begin{aligned}\int_0^a \frac{e^{i\omega t}}{8aB\pi\mu} f(h) \lim_{y\to 0}[\frac{-2y(z+h)}{y^2+(z+h)^2}]dh &= \int_0^a \frac{-e^{i\omega t}}{8aB\pi\mu} f(h) 2(z+h)\pi\delta(h+z)dh \\ &= \frac{2e^{i\omega t}}{8aB\pi\mu} f(-z)(z-z)\pi = 0\end{aligned}$$

Hence the velocity component w is zero on the boundary $y = 0$ for all $f(h)$.

$$\lim_{y\to 0}(w) = 0$$

This leaves us with just the single boundary condition (6.67).

Now consider the velocity component v, equation (6.63), on the boundary $y = 0$. Taking the first derivative of v with respect to y gives

$$\begin{aligned}\frac{dv}{dy} &= \int_0^a \frac{e^{i\omega t}}{8aB\pi\mu} f(h) \left[\frac{16hzy}{\beta^4} - 4y\frac{\alpha^2-\beta^2}{\alpha^2\beta^2}\right] dh \\ &= y\int_0^a \frac{e^{i\omega t}}{2aB\pi\mu} f(h) \left[\frac{4hz}{\beta^4} - \frac{\alpha^2-\beta^2}{\alpha^2\beta^2}\right] dh\end{aligned}$$

Hence $\frac{dv}{dy} \to 0$ as $y \to 0$, since $\frac{dv}{dy}$ is proportional to y, which shows that there is no discontinuous jump on the boundary $y = 0$.

Pressure on the plate

As mentioned previously, we define the force, F, in equation (6.1) to be the jump in force from above to below the vibrating plate. Since the force is only acting in the y direction, F is given as the difference in the corresponding component of the stress tensor σ_{yy} at the upper plate surface, $y = 0^+$, and at the lower plate surface, $y = 0^-$.

$$[\sigma_{yy}]_{0^-}^{0^+} = \left[-P + \mu\frac{\partial v}{\partial y}\right]_{0^-}^{0^+} = [-P]_{0^-}^{0^+} + \mu\left[\frac{\partial v}{\partial y}\right]_{0^-}^{0^+}$$

where P is the pressure. The term $\frac{\partial v}{\partial y}$ does not produce a discontinuous jump at the boundary, $y = 0$, so any difference between ${\sigma_{yy}}^{0^+}$ and ${\sigma_{yy}}^{0^-}$ will be as a result only of pressure differences.

$$[\sigma_{yy}]_{0^-}^{0^+} = [-P]_{0^-}^{0^+} \tag{6.71}$$

Equation (6.37) gives us the pressure field for a point force in the k direction. Considering the force is defined to be $\mathbf{F} = (0, F, 0)$, we can rewrite this equation in a simpler form.

$$p = p^{k=2} = \frac{F}{\pi}\left[\frac{y}{r^3} - \frac{y}{R^3} - 2h\frac{\partial}{\partial y}\left(\frac{z+h}{R^3}\right)\right] \tag{6.72}$$

In a similar way to the velocity equations, we now integrate over the breadth of the plate (assumed infinite for integration) and divide through by B.

$$\begin{aligned} p^* = \frac{1}{B}\int_{-\infty}^{\infty}[p]d\gamma_1 &= \frac{1}{B}\int_{-\infty}^{\infty}\frac{F}{\pi}\left[\frac{y}{r^3} - \frac{y}{R^3} + \frac{6hy(z+h)}{R^5}\right]d\gamma_1 \\ &= \frac{F}{B\pi}\left[\frac{2y}{\alpha^2} - \frac{2y}{\beta^2} + \frac{8hy(z+h)}{\beta^4}\right] \end{aligned} \tag{6.73}$$

We now integrate over the length of the plate ($0 < h < a$) and divide through by a to give us our pressure for the array of stokeslets. If we write $F(t,h) = e^{i\omega t}f(h)$ then our equation for pressure becomes:

$$p^{**} = \frac{1}{a}\int_0^a [p^*]d\gamma_1 = \frac{e^{i\omega t}}{aB\pi}\int_0^a \left[\frac{2yf(h)}{\alpha^2} - \frac{2yf(h)}{\beta^2} + \frac{8hy(z+h)f(h)}{\beta^4}\right]dh \tag{6.74}$$

This equation for the pressure ($P = p^{**}$) is not continuous across the plate boundary at $y = 0$, hence we will have a jump in pressure between the upper and lower surface. To find the value of $[-P]_{0^-}^{0^+}$ we need to find the limits of P as y approaches the boundary from above and below the plate, denoted $[-P]^{0^+}$ and $[-P]^{0^-}$ respectively. We can write the limit of P as y tends to 0^+ as

$$[-P]^{0^+} = -\frac{e^{i\omega t}}{aB\pi}\left[\lim_{y\to 0^+}(I_1) - \lim_{y\to 0^+}(I_2) + \lim_{y\to 0^+}(I_3)\right] \tag{6.75}$$

with I_1, I_2 and I_3 defined as

$$I_1 = \int_0^a \frac{2yf(h)}{y^2 + (z-h)^2}dh$$

$$I_2 = \int_0^a \frac{2yf(h)}{y^2 + (z+h)^2}dh$$

$$I_3 = \int_0^a \frac{8yh(z+h)f(h)}{(y^2+(z+h)^2)^2}dh$$

To find the limits for the individual integrals we need to define new variables, $g = h - z$ and $\Psi = \frac{g}{y}$. Firstly, making these substitutions into our integral (I_1) gives

$$\begin{aligned}\lim_{y\to 0^+}(I_1) &= \lim_{y\to 0^+}\left(2\int_{-\frac{z}{y}}^{\frac{a-z}{y}} \frac{yf(z+\Psi y)}{(1+\Psi^2)y^2}yd\Psi\right) \\ &= \lim_{y\to 0^+} 2f(z)\int_{-\frac{z}{y}}^{\frac{a-z}{y}} \frac{1}{(1+\Psi^2)}d\Psi\end{aligned} \tag{6.76}$$

we can split the integral (6.76) into two parts from which we will be able to take limits.

$$\lim_{y\to 0^+}(I_1) = \lim_{y\to 0^+} 2f(z)\left[\int_0^{\frac{a-z}{y}} \frac{1}{(1+\Psi^2)}d\Psi - \int_0^{-\frac{z}{y}} \frac{1}{(1+\Psi^2)}d\Psi\right] \tag{6.77}$$

We can now solve this limit, which will vary depending on the value of z.

$$\begin{aligned}\lim_{y\to 0^+}(I_1) &= 2f(z)\left[\int_0^{\infty} \frac{1}{(1+\Psi^2)}d\Psi - \int_0^{-\infty} \frac{1}{(1+\Psi^2)}d\Psi\right] \\ &= 2f(z)\left[\frac{\pi}{2} - \left(\frac{-\pi}{2}\right)\right] = 2\pi f(z) \qquad \text{for} \quad 0 < z < a\end{aligned}$$

$$\begin{aligned}\lim_{y\to 0^+}(I_1) &= 2f(z)\left[\int_0^{-\infty} \frac{1}{(1+\Psi^2)}d\Psi - \int_0^{-\infty} \frac{1}{(1+\Psi^2)}d\Psi\right] \\ &= 2f(z)\left[\frac{-\pi}{2} - \left(\frac{-\pi}{2}\right)\right] = 0 \qquad \text{for} \quad z > a\end{aligned}$$

Also we can see that a singularity occurs at $z = a$.

$$\begin{aligned}\lim_{y\to 0^+}(I_1) &= 2f(z)\left[\int_0^{0} \frac{1}{(1+\Psi^2)}d\Psi - \int_0^{-\infty} \frac{1}{(1+\Psi^2)}d\Psi\right] \\ &= 2f(z)\left[-\left(\frac{-\pi}{2}\right)\right] = \pi f(z) \qquad \text{for} \quad z = a\end{aligned}$$

In a similar way we can write

$$\lim_{y\to 0^+}(I_2) = \lim_{y\to 0^+} 2\int_{\frac{-z}{y}}^{\frac{a-z}{y}} \frac{yf(z+\Psi y)}{y^2+(2z+\Psi y)^2}yd\Psi = 0 \tag{6.78}$$

$$\lim_{y\to 0^+}(I_3) = \lim_{y\to 0^+} 8\int_{\frac{-z}{y}}^{\frac{a-z}{y}} \frac{y(z+\Psi y)f(z+\Psi y)(2z+\Psi y)}{(y^2+(2z+\Psi y)^2)^2}yd\Psi = 0 \tag{6.79}$$

Substituting these limits back into equation (6.75) gives us the pressure at the upper surface

of the plate.

$$\begin{aligned}[-P]^{0^+} &= -\frac{e^{i\omega t}}{aB\pi}[2\pi f(z) - 0 + 0] = -\frac{2e^{i\omega t}}{aB}f(z) \qquad \text{for} \quad 0 < z < a \\ &= 0 \qquad \text{for} \quad z > a \end{aligned} \tag{6.80}$$

Using the same method we can determine the pressure at the lower plate surface to be

$$\begin{aligned}[-P]^{0^-} &= -\frac{e^{i\omega t}}{aB\pi}[-2\pi f(z) - 0 + 0] = \frac{2e^{i\omega t}}{aB}f(z) \qquad \text{for} \quad 0 < z < a \\ &= 0 \qquad \text{for} \quad z > a \end{aligned} \tag{6.81}$$

Since $[P]_{0^-}^{0^+} = [P]^{0^+} - [P]^{0^-}$, we can substitute the solutions (6.80) and (6.81) into equation (6.71). Assuming that $f(z) \neq 0$ for all $z \in [0, a]$, and that $(y^2 + (z+h)^2) \neq 0$ for all $z \in [0, a], y \in [0, y_{max}]$, we can now write the force F as

$$\begin{aligned}F = \frac{1}{2}[\sigma_{yy}]_{0^-}^{0^+} = \frac{1}{2}[-P]_{0^-}^{0^+} &= -\frac{2e^{i\omega t}}{aB}f(z) \qquad \text{for} \quad 0 < z < a \\ &= 0 \qquad \text{for} \quad z > a \end{aligned} \tag{6.82}$$

Starting with the equations for a single stokeslet near a flat plane wall, (6.46) to (6.48), we have extended these results to determine the equations for an infinite continuous distribution of stokeslets on a line above the wall, (6.61) to (6.61). This led to the equations of a double array of stokeslets perpendicular to the plane, infinite in one direction and finite in the other, representing the plate itself, (6.62) to (6.64). By then considering the boundary conditons on the plate, we used these solutions to define F such that a complete fluid-plate model could be determined.

6.3.4 Complete problem

We now consider the original problem (6.1) with the force being defined by the equation (6.82). This allows us to write the initial problem within the area of the plate, $0 < z < a$, in the form

$$\frac{\rho_s d}{D}q(z,t)_{tt} + q(z,t)_{zzzz} = -\frac{2e^{i\omega t}}{aBD}f(z) \tag{6.83}$$

where $f(z)$ is the known, measurable driving force. If we define $q(z,t) = e^{i\omega t}q(z)$ we can now write equation (6.83) and the boundary condition (6.69) respectively as

$$q(z)_{zzzz} - \frac{\rho_s d\omega^2}{D}q(z) = -\frac{2f(z)}{aBD} \tag{6.84}$$

$$q(z) = \frac{1}{4aB\pi\mu i\omega}\int_0^a \left[f(h)\left(\ln(\frac{z+h}{z-h}) - \frac{2hz}{(z+h)^2}\right)\right]dh \tag{6.85}$$

The remaining conditions specified earlier by the plate movement become

$$\begin{aligned} q(0) &= 0 && \text{deflection} = 0 \text{ at } \quad z = 0 \\ q(0)_z &= 0 && \text{slope} = 0 \text{ at } \quad z = 0 \\ q(a)_{zz} &= 0 && \text{bending moment} = 0 \text{ at } \quad z = a \\ q(a)_{zzz} &= 0 && \text{shear force} = 0 \text{ at } \quad z = a \end{aligned}$$

We now introduce a forcing term (per unit area) of the form $\kappa e^{i\omega t}$ to represent the external driving force of the plate so that our equation (6.84) becomes

$$q(z)_{zzzz} - \frac{\rho_s d\omega^2}{D}q(z) = -\frac{2f(z)}{aBD} + \frac{\kappa}{D} \tag{6.86}$$

Non-dimensionalising the equations

The next step is to non-dimensionalise the coupled equations (6.85) and (6.86). We define

$$z = \tilde{z}a \qquad q(z) = \frac{\kappa}{D}a^4\tilde{q}(\tilde{z}) \qquad \text{and} \qquad f(z) = \frac{-4\pi\kappa\mu\omega a^4 B}{D}\tilde{f}(\tilde{z})$$

such that the set of equations and boundary conditions become

$$\tilde{q}_{\tilde{z}\tilde{z}\tilde{z}\tilde{z}} - \xi_1\tilde{q} - \xi_2\tilde{f} = 1 \tag{6.87}$$

$$i\int_0^1 \tilde{f}(h)\left[\ln\left(\frac{\tilde{z}+h}{\tilde{z}-h}\right) - \frac{2\tilde{z}h}{(\tilde{z}+h)^2}\right]dh - \tilde{q} = 0 \tag{6.88}$$

$$\begin{aligned} \tilde{q}(0) &= 0 \\ \tilde{q}(0)_{\tilde{z}} &= 0 \\ \tilde{q}(1)_{\tilde{z}\tilde{z}} &= 0 \\ \tilde{q}(1)_{\tilde{z}\tilde{z}\tilde{z}} &= 0 \end{aligned}$$

involving two real dimensionless constants $\xi_1 = \frac{\rho_s d\omega^2 a^4}{D}$ and $\xi_2 = \frac{8\pi\omega\mu a^3}{D}$.

6.3.5 Solving the problem numerically

We now need to solve the system of equations numerically. We define q_i and f_i to be the value of $\tilde{q}(\tilde{z})$ and $\tilde{f}(\tilde{z})$ respectively at a distance $\tilde{z} = z_i$ from the origin, with $i = 0 \ldots N$.

We set a mesh size Δz for $\tilde{z}$ between 0 and z_N. We define the derivatives of $\tilde{q}$ with respect to $\tilde{z}$ using the central difference formulae [46]. The boundary conditions are that the plate has no deflection at $\tilde{z} = 0$

$$\tilde{q}(0) = 0 \Rightarrow q_0 = 0 \tag{6.89}$$

no slope at $\tilde{z} = 0$

$$\tilde{q}(0)_{\tilde{z}} = 0 \Rightarrow \frac{q_1 - q_{-1}}{2\Delta z} = 0 \Rightarrow q_1 = q_{-1} \qquad \text{with} \qquad q_{-1} = \tilde{q}(-1) \tag{6.90}$$

no bending moment at $\tilde{z} = 1$

$$\tilde{q}(1)_{\tilde{z}\tilde{z}} = 0 \Rightarrow \frac{q_{N+1} - 2q_N + q_{N-1}}{\Delta z^2} = 0 \Rightarrow q_{N+1} = 2q_N - q_{N-1} \tag{6.91}$$

and no shear force at $\tilde{z} = 1$

$$\tilde{q}(1)_{\tilde{z}\tilde{z}\tilde{z}} = 0 \Rightarrow \frac{q_{N+2} - 2q_{N+1} + 2q_{N-1} - q_{N-2}}{\Delta z^3} = 0 \Rightarrow q_{N+2} = 4q_N - 4q_{N-1} + q_{N-2} \tag{6.92}$$

Again using the central difference method, the fourth differential in (6.87) is written as

$$q_{n\tilde{z}\tilde{z}\tilde{z}\tilde{z}} = \frac{q_{n+2} - 4q_{n+1} + 6q_n - 4q_{n-1} + q_{n-2}}{\Delta z^4}$$

Combining this with the boundary conditions gives us the numerical solution for equation (6.87).

$$\begin{aligned}
n = 0: &\quad q_2\tfrac{2}{\Delta z^4} - q_1\tfrac{8}{\Delta z^4} + q_0(\tfrac{6}{\Delta z^4} - \xi_1) - \xi_2 f_0 = 1 \\
n = 1: &\quad q_3\tfrac{1}{\Delta z^4} - q_2\tfrac{4}{\Delta z^4} + q_1(\tfrac{7}{\Delta z^4} - \xi_1) - \xi_2 f_1 = 1 \\
2 \le n \le N-2: &\quad q_{n+2}\tfrac{1}{\Delta z^4} - q_{n+1}\tfrac{4}{\Delta z^4} + q_n(\tfrac{6}{\Delta z^4} - \xi_1) - q_{n-1}\tfrac{4}{\Delta z^4} + q_{n-2}\tfrac{1}{\Delta z^4} - \xi_2 f_n = 1 \\
n = N-1: &\quad -q_N\tfrac{2}{\Delta z^4} + q_{N-1}(\tfrac{5}{\Delta z^4} - \xi_1) - q_{N-2}\tfrac{4}{\Delta z^4} + q_{N-3}\tfrac{1}{\Delta z^4} - \xi_2 f_{N-1} = 1 \\
n = N: &\quad q_N(\tfrac{2}{\Delta z^4} - \xi_1) - q_{N-1}\tfrac{4}{\Delta z^4} + q_{N-2}\tfrac{2}{\Delta z^4} - \xi_2 f_N = 1
\end{aligned}$$

In equation (6.88), we assume that f_i is constant on $\tilde{z} = z_i$, so that we can use the trapezium rule to integrate $\tilde{f}(\tilde{z})$, treating the integral as a sum of areas beneath a curve.

$$\int_0^1 \tilde{f}(h)dh \Rightarrow \sum_{j=1}^{N} \frac{f_j + f_{i-1}}{2}$$

$$
\begin{aligned}
\text{Let} \quad I_{01} &= i\int_0^1 \tilde{f}(h)\left[\ln\left(\frac{\tilde{z}+h}{\tilde{z}-h}\right)-\frac{2\tilde{z}h}{(\tilde{z}+h)^2}\right]dh \qquad (6.93)\\
\text{then} \quad I_{01} &= i\sum_{j=1}^{N}\int_{(j-1)\Delta z}^{j\Delta z}\frac{f_j+f_{j-1}}{2}\left[\ln\left(\frac{n\Delta z+h}{n\Delta z-h}\right)-\frac{2n\Delta z h}{(n\Delta z+h)^2}\right]dh\\
&= i\sum_{j=1}^{N}\frac{f_j+f_{j-1}}{2}\int_{(j-1)\Delta z}^{j\Delta z}\left[\ln\left(\frac{n\Delta z+h}{n\Delta z-h}\right)-\frac{2n\Delta z h}{(n\Delta z+h)^2}\right]dh\\
&= \sum_{j=1}^{N}(f_j+f_{j-1})\tilde{k}(j,n)
\end{aligned}
$$

with $\tilde{k}(j,n)$ defined by

$$
\begin{aligned}
\tilde{k}(j,n) = \frac{i}{2}\{&\frac{-1}{n\Delta z+j\Delta z}[2n^2\Delta z^2+2n\Delta z(n\Delta z+j\Delta z)\ln|2n\Delta z^2(n+j)|\\
&-(n\Delta z+j\Delta z)^2\ln|n\Delta z+j\Delta z|-(n^2\Delta z^2-j^2\Delta z^2)\ln|n\Delta z-j\Delta z|]\\
&+\frac{1}{n\Delta z+(j-1)\Delta z}[2n\Delta z(n\Delta z(n\Delta z+(j-1)\Delta z)\ln|2n\Delta z^2(n+(j-1))|\\
&+2n^2\Delta z^2-(n\Delta z+(j-1)\Delta z)^2 ln|n\Delta z+(j-1)\Delta z|\\
&-(n^2\Delta z^2-(j-1)^2\Delta z^2)\ln|n\Delta z-(j-1)\Delta z|]\} \qquad (6.94)
\end{aligned}
$$

which holds for $n \neq j$ and $n \neq (j-1)$. In these two cases we have respectively

$$
\tilde{k}(n,n) = \tilde{k}_0(n) = \frac{i}{2}\left(\frac{2n^2\Delta z^2}{2n\Delta z+\Delta z}+\Delta z\ln|2n-1|-n\Delta z\right) \qquad (6.95)
$$

$$
\tilde{k}(n+1,n) = \tilde{k}_1(n) = \frac{i}{2}\left(\frac{-2n^2\Delta z^2}{2n\Delta z+\Delta z}+\Delta z\ln|2n+1|+n\Delta z\right) \qquad (6.96)
$$

This allows us to write the numerical solution for equation (6.88).

$$
\begin{aligned}
n=1: \quad & f_0\tilde{k}_0(1)+f_1(\tilde{k}_0(1)+\tilde{k}_1(1))+f_2(\tilde{k}_1(1)+\tilde{k}(3,1))+ \\
& \textstyle\sum_{j=3}^{N-1} f_j(\tilde{k}(j,1)+\tilde{k}(j+1,1))+f_N\tilde{k}(N,1)-q_1=0 \\
n=2: \quad & f_0\tilde{k}(1,2)+f_1(\tilde{k}(1,2)+\tilde{k}_0(2))+f_2(\tilde{k}_0(2)+\tilde{k}_1(2))+f_3(\tilde{k}_1(2)+\tilde{k}(4,2)) \\
& +\textstyle\sum_{j=4}^{N-1} f_j(\tilde{k}(j,2)+\tilde{k}(j+1,2))+f_N\tilde{k}(N,2)-q_2=0 \\
3\le n\le N-3: \quad & f_0\tilde{k}(1,n)+\textstyle\sum_{j=1}^{n-2} f_j(\tilde{k}(j,n)+\tilde{k}(j+1,n))+f_{n-1}(\tilde{k}(n-1,n)+\tilde{k}_0(n)) \\
& +f_n(\tilde{k}_0(n)+\tilde{k}_1(n))+f_{n+1}(\tilde{k}_1(n)+\tilde{k}(n+2,n)) \\
& +\textstyle\sum_{j=n+2}^{N-1} f_j(\tilde{k}(j,n)+\tilde{k}(j+1,n))+f_N\tilde{k}(N,n)-q_n=0 \\
n=N-2: \quad & f_0\tilde{k}(1,N-2)+\textstyle\sum_{j=1}^{N-4} f_j(\tilde{k}(j,N-2)+\tilde{k}(j+1,N-2)) \\
& +f_{N-3}(\tilde{k}(N-3,N-2)+\tilde{k}_0(N-2))+f_{N-2}(\tilde{k}_0(N-2)+\tilde{k}_1(N-2)) \\
& +f_{N-1}(\tilde{k}_1(N-2)+\tilde{k}(N,N-2))+f_N\tilde{k}(N,N-2)-q_{N-2}=0 \\
n=N-1: \quad & f_0\tilde{k}(1,N-1)+\textstyle\sum_{j=1}^{N-3} f_j(\tilde{k}(j,N-1)+\tilde{k}(j+1,N-1)) \\
& +f_{N-2}(\tilde{k}(N-2,N-1)+\tilde{k}_0(N-1))+f_{N-1}(\tilde{k}_0(N-1)+\tilde{k}_1(N-1)) \\
& +f_N\tilde{k}(N,N-1)-q_{N-1}=0 \\
n=N: \quad & f_0\tilde{k}(1,N)+\textstyle\sum_{j=1}^{N-2} f_j(\tilde{k}(j,N)+\tilde{k}(j+1,N)) \\
& +f_{N-1}(\tilde{k}(N-1,N)+\tilde{k}_0(N))+f_N\tilde{k}_0(N)-q_N=0
\end{aligned}
$$

We now have $2N+1$ equations for $2N+2$ unknowns (q_i, f_i, $i=0\ldots N$). As the extra necessary equation we use the boundary condition $q_0=0$. We can now solve this system of equations using matrix operations (carried out in MATLAB, see appendix C).

$$
\begin{bmatrix} q_0 \\ q_1 \\ q_2 \\ \vdots \\ q_n \\ \vdots \\ q_{N-2} \\ q_{N-1} \\ q_N \\ f_0 \\ f_1 \\ f_2 \\ \vdots \\ f_n \\ \vdots \\ f_{N-2} \\ f_{N-1} \\ f_N \end{bmatrix} = \begin{bmatrix} & & & & \\ & & & & \\ & & & & \\ & & & & \\ & A & & -\xi_2 \begin{bmatrix} I \end{bmatrix} & \\ & & & & \\ & & & & \\ & & & & \\ & & & & \\ & & & & \\ & & & & \\ & & & & \\ & & & & \\ & -\begin{bmatrix} I \end{bmatrix} & & D & \\ & & & & \\ & & & & \\ & & & & \\ & & & & \end{bmatrix}^{-1} \begin{bmatrix} 1 \\ 1 \\ 1 \\ 1 \\ 1 \\ 1 \\ 1 \\ 1 \\ 1 \\ 0 \\ 0 \\ 0 \\ 0 \\ 0 \\ 0 \\ 0 \\ 0 \\ 0 \end{bmatrix}
$$

where $\begin{bmatrix} I \end{bmatrix}$ is the $(N+1) \times (N+1)$ identity matrix and C and D are $(N+1) \times (N+1)$ square matrices. We choose to define $\tilde{\delta} = \frac{1}{\Delta z^4}$.

$$\left[A \right] = \begin{bmatrix}
6\tilde{\delta}-\xi_1 & -8\tilde{\delta} & 2\tilde{\delta} & & & & & & \\
 & 7\tilde{\delta}-\xi_1 & -4\tilde{\delta} & \tilde{\delta} & & & & & \\
\tilde{\delta} & -4\tilde{\delta} & 6\tilde{\delta}-\xi_1 & -4\tilde{\delta} & \tilde{\delta} & & & & \\
 & \tilde{\delta} & -4\tilde{\delta} & 6\tilde{\delta}-\xi_1 & -4\tilde{\delta} & \tilde{\delta} & & & \\
 & & \ddots & \ddots & \ddots & \ddots & \ddots & & \\
 & & & \ddots & \ddots & \ddots & \ddots & \ddots & \\
 & & & & \tilde{\delta} & -4\tilde{\delta} & 6\tilde{\delta}-\xi_1 & -4\tilde{\delta} & \tilde{\delta} \\
 & & & & & \tilde{\delta} & -4\tilde{\delta} & 6\tilde{\delta}-\xi_1 & -4\tilde{\delta} \\
 & & & & & & \tilde{\delta} & -4\tilde{\delta} & 5\tilde{\delta}-\xi_1 \\
 & & & & & & & 2\tilde{\delta} & -4\tilde{\delta}
\end{bmatrix}
\begin{matrix} \\ \\ \\ \\ \\ \\ \\ \\ -2\tilde{\delta} \\ 2\tilde{\delta}-\xi_1 \end{matrix}$$

$$\left[D \right] = \begin{bmatrix}
0 & \cdots & 0 & \cdots & 0 \\
\tilde{k}_0(1) & \cdots & (\tilde{k}(j,1)+\tilde{k}(j+1,1)) & \cdots & \tilde{k}(N,1) \\
\tilde{k}(1,2) & \cdots & (\tilde{k}(j,2)+\tilde{k}(j+1,2)) & \cdots & \tilde{k}(N,2) \\
\vdots & & \vdots & & \vdots \\
\tilde{k}(1,n) & \cdots & (\tilde{k}(j,n)+\tilde{k}(j+1,n)) & \cdots & \tilde{k}(N,n) \\
\vdots & & \vdots & & \vdots \\
\tilde{k}(1,N-2) & \cdots & (\tilde{k}(j,N-2)+\tilde{k}(j+1,N-2)) & \cdots & \tilde{k}(N,N-2) \\
\tilde{k}(1,N-1) & \cdots & (\tilde{k}(j,N-1)+\tilde{k}(j+1,N-1)) & \cdots & \tilde{k}_1(N-1) \\
\tilde{k}(1,N) & \cdots & (\tilde{k}(j,N)+\tilde{k}(j+1,N)) & \cdots & \tilde{k}_0(N)
\end{bmatrix}$$

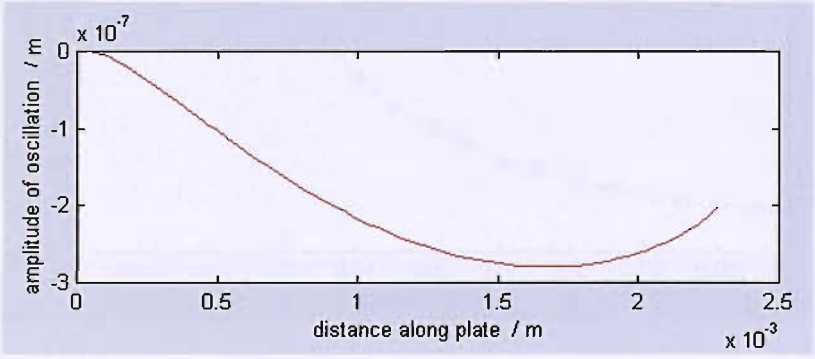

Figure 6.16: Numerical solution for $\mu = 0.04$ Pa·s and $\kappa = 1$ kg·m^{-1}·s^{-2}

The numerical solution gives an increasing maximum amplitude of oscillation with increased driving force and a decreasing amplitude with increased viscosity, as expected. A driving force of zero also gives us no motion as required. Due to inaccuracies brought about by

the unknown material properties of the plate, calibration will be necessary. Using a fluid of known viscosity we can set the plate in motion using a fixed driving force and measure the maximum amplitude achieved by the oscillations. This should give us a value for κ by matching the maximum amplitude to the viscosity in our numerical solution. Keeping

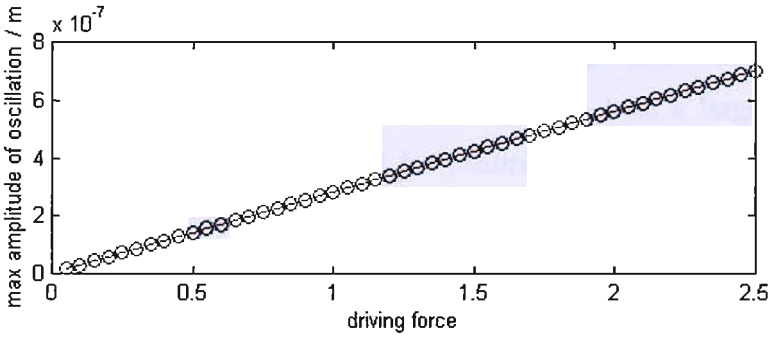

Figure 6.17: Plot of κ against maximum amplitude for $\mu = 0.04$, where the red curve shows the numerical solution and the line of blue circles is a fitted polynomial

this fixed driving force, and κ value, we can then use the plate to determine the viscosity of other fluids. Using the numerical solution, a graph can be plotted of viscosity against maximum amplitude for a fixed value of κ (red line in figure (6.18)). A polynomial can

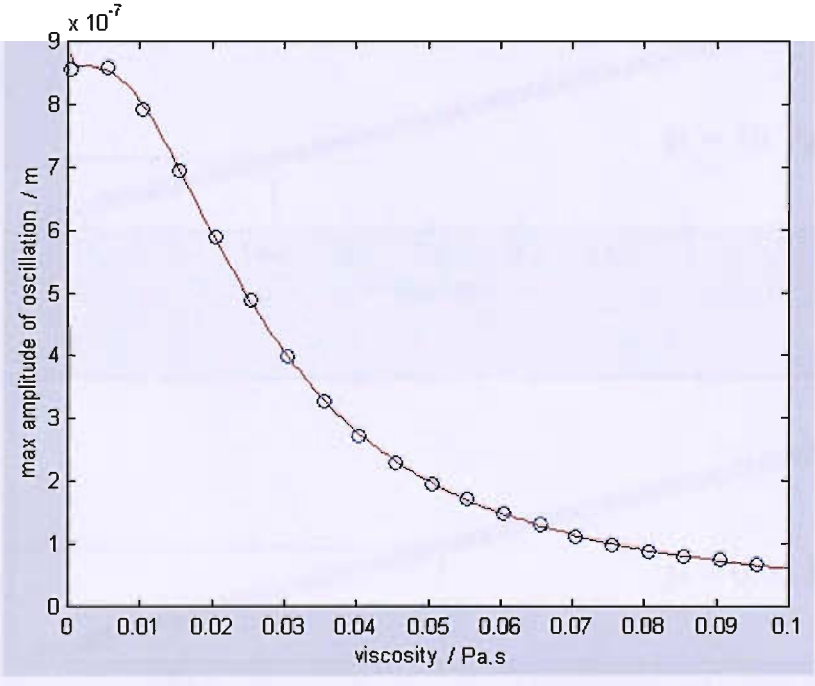

Figure 6.18: Plot of μ against maximum amplitude for $\kappa = 1$ kg·m^{-1}·s^{-2}, where the red curve shows the numerical solution and the line of blue circles is a fitted polynomial

then be fitted to this curve (blue circles). We can then use the equation of this polynomial to determine the viscosity.

We now have a method of determining the viscosity of a fluid using two parameters, the force driving the plate and the maximum amplitude achieved by oscillations in the fluid. The constant in the driving force, κ, can be found from calibration in a known fluid and an oscilloscope or alternate method of measuring oscillations can be used to determine the maximum amplitude. Unfortunately we do not have any experimental data for these parameters to compare the numerical solution with. κ can take a large range of values dependent on the viscosity of the fluid used for calibration. To achieve an amplitude of 0.000001 m in a fluid of viscosity μ =0.01 we would use $\kappa \approx 1.25$, whereas in a fluid of viscosity μ =10 we would use $\kappa \approx 16000$. If we were testing a fluid with a viscosity thought to be of the order of $\mu = 0.1$ we can see from figure (6.20) that to use the driving force that gave us $\kappa \approx 160000$ would result in a maximum amplitude of 1 cm, a physical impossibility for a sensor of the cantilever's size. To maximise accuracy in fitting the polynomial to the numerical solution it is therefore beneficial to calibrate in a fluid with viscosity close to that expected from the unknown fluid being tested.

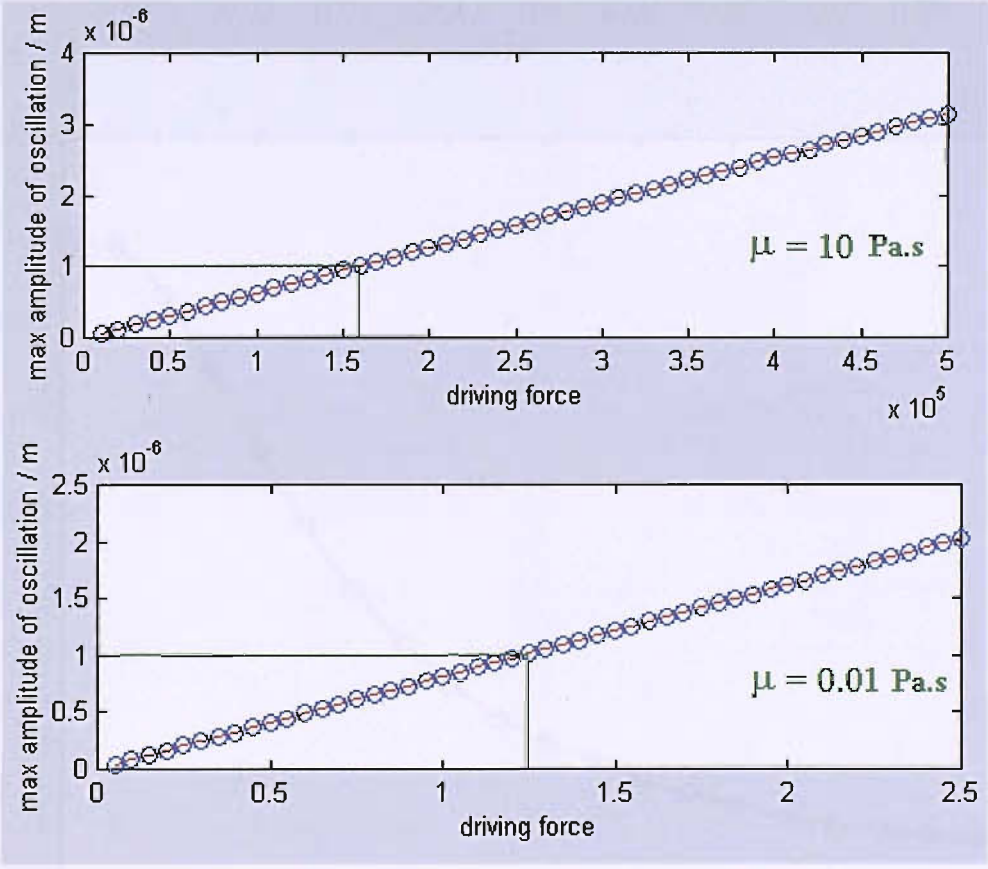

Figure 6.19: Determining κ for the cantilever driven to a maximum amplitude of 1μm in two fluids with different viscosities

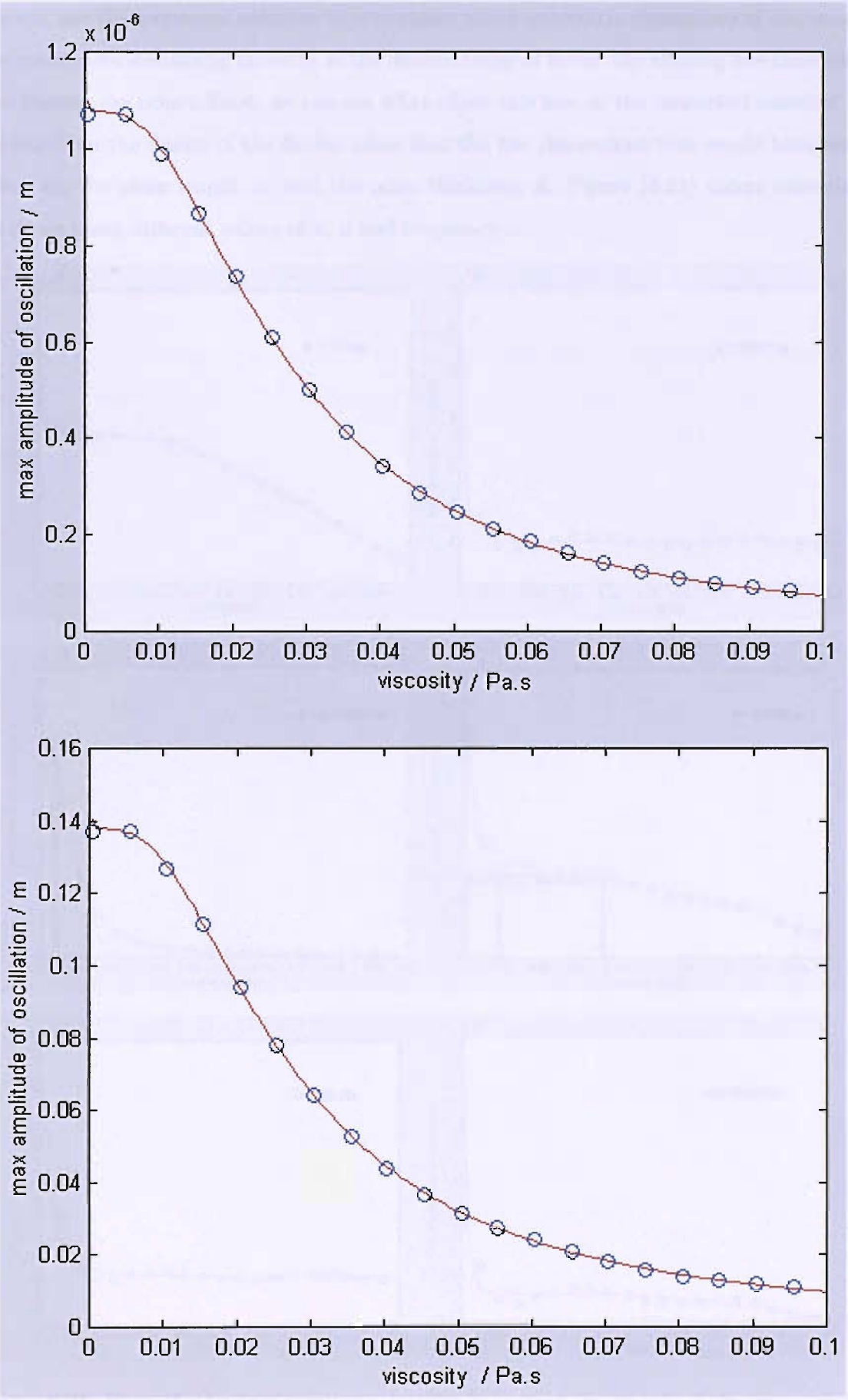

Figure 6.20: Plot of μ against maximum amplitude for $\kappa = 1.25$ and $\kappa = 160000$, where the red curve shows the numerical solution and the line of blue circles is a fitted polynomial

We can use the numerical solution to investigate which geometric dimensions of the sensor are optimal for measuring viscosity in the desired range of fluids. By altering one dimension and leaving the others fixed, we can see what effect this has on the numerical solution. It is clear from the design of the flexion plate that the two dimensions that would have most effect are the plate length, a, and the plate thickness, d. Figure (6.21) shows numerical solutions using different values of a, d and frequency ω.

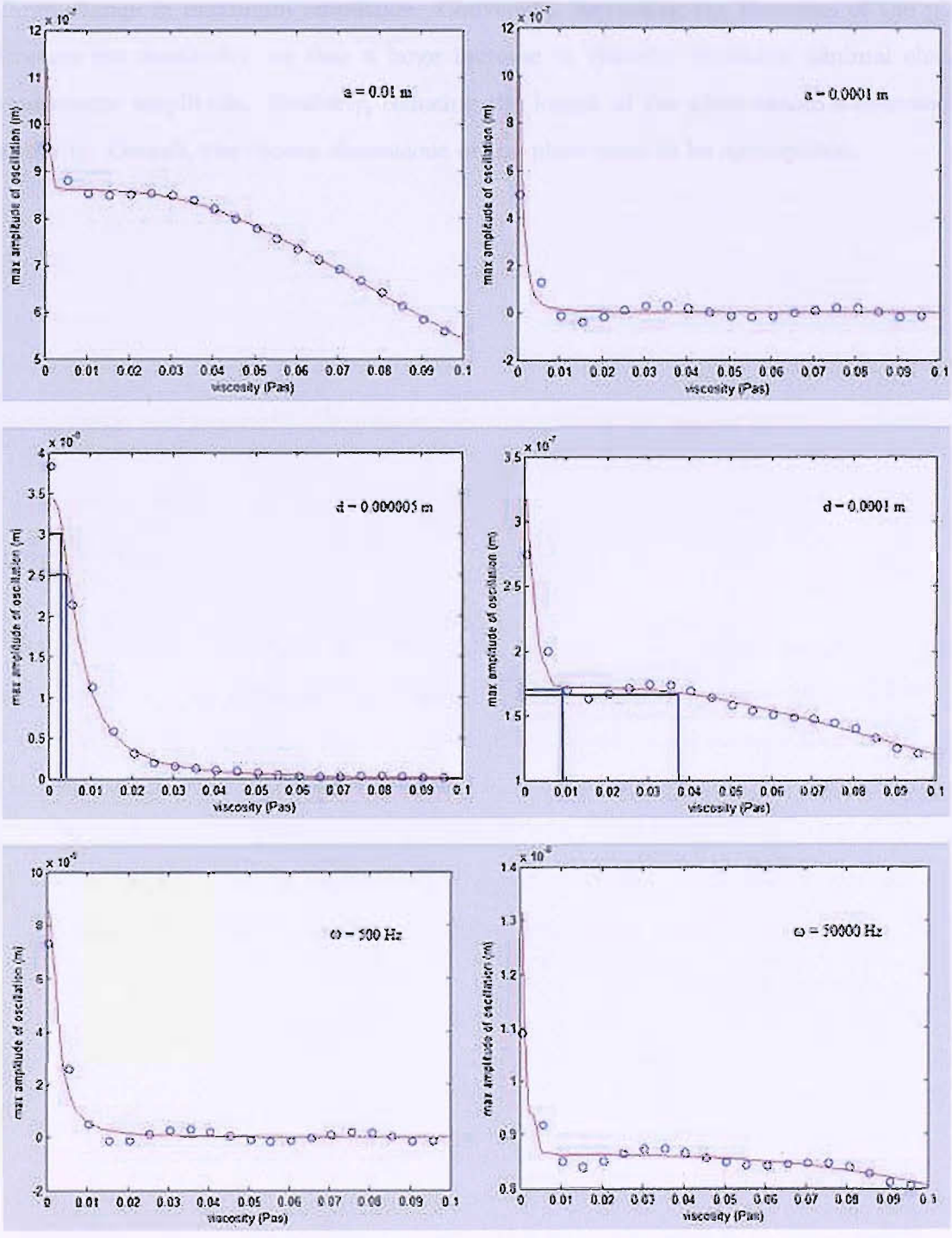

Figure 6.21: Plots of μ against maximum amplitude varying dimensions of the plate, where the red curve shows the numerical solution and the line of blue circles is a fitted polynomial

Using the actual dimensions of the plate in the numerical solution produces a graph that is easily readable, as in figure (6.20). The curve illustrates a clear relationship between maximum amplitude and viscosity that is measurable for a range of viscosities. When we alter the dimensions of the plate the flexion varies in sensitivity to changes in viscosity which affects the usability of the device. Intuitively, making the plate thinner (decreasing d) results in an increased sensitivity to viscosity. A small change in viscosity produces a large change in maximum amplitude. Conversely, increasing the thickness of the plate decreases the sensitivity, so that a large increase in viscosity produces minimal change to maximum amplitude. Similarly, reducing the length of the plate causes a decrease in sensitivity. Overall, the chosen dimensions of the plate seem to be appropriate.

6.4 Summary of the Flexion

Similar to the Spider, this MEMS device is also small and relatively easy to make. The geometry of the sensor results in a large fluid mass on a small oscillating surface, making it more sensitive to fluid properties. In theory we could increase this sensitivity yet further by making the plate even thinner, but this will make the device less robust and more prone to breakage. The sensor must be able to survive and operate in down hole conditions.

The sensor is modelled as a cantilever plate, clamped at one end. It oscillates in a direction perpendicular to its own plane. It is driven by passing an alternating current through the aluminium coil mounted on the surface of the sensor.

We can model the device as a densitometer. Due to the small amplitudes of oscillation, the problem can be simplified by applying linear theory. For Newtonian fluids, we can get ρ as a function of plate properties, frequency and temperature. Two sets of experimental data have been analysed using flexion sensors. When calibrated to determine plate properties, the resulting values for ρ were accurate to within 2 % of the true value. Using an uncalibrated model, assuming the device is pure silicon, density was determined to within 20% of the true value over a range of fluids.

We can also model the device as a viscometer although this is more complicated. The flow around the plate is assumed to have a small Reynolds number (Re $<<$ 1) and is thus considered slow flow. Using the method of stokeslets we can write the viscous fluid problem as a system of equations in a form that can be solved numerically. The numerical solution allows us to determine viscosity as a function of driving force and maximum amplitude of oscillation. This requires us to solve a polynomial equation for μ. Whilst the numerical solution gives us a resulting viscosity term, it appears to be unstable for $\mu < 0.001$ Pa·s.

Chapter 7

Conclusions

Our intention was to model the development of new viscometers that will remain sufficiently accurate in hostile down-hole conditions and reflect both Newtonian and non-Newtonian fluid motion. The analysis of past viscometer designs indicated that conventional viscometers were unsuitable for measurements in situ in oil wells. Despite the accuracy of falling body viscometers such as the falling needle, the free moving parts make it inappropriate for in situ measurements. A capillary viscometer would need constant fluid flow and could also suffer problems due to the high pressures. Extreme pressure environments are also problematic for oscillating body viscometers, often causing distortions in the dimensions of the body. The vibrating wire viscometer is able to work in the hostile conditions but is limited to measuring Newtonian fluids due to the use of Navier Stokes equations in the modelling of the device. The in situ capabilities of the MEMS sensor, due to its small size and robust design which can be readily integrated into existing tools, will reduce the time required for analysis, decrease errors caused by transferring fluids from the well to the testing facilities and give a clearer picture of fluid properties at reservoir conditions. The geometrical design of the sensors make them particularly sensitive to the added mass of the fluid during oscillations, due to the large surface to volume ratio of the vibrating armature.

A petroleum reservoir can exhibit temperatures up to 473 K and pressures up to 200 MPa. The upper operating temperature for the sensor is dependent on two main components, the strain gauges and the adhesive used in the packaging. The adhesive is predicted to become unstable at 423 K. Assuming an alternate adhesive could be found, the piezoresistive gauges that make up the wheatstone bridge would be the next thing expected to fail, at a temperature of 493 K, which is in excess of that required for reservoir measurements. During laboratory testing of the sensors, an upper operating pressure of 68 MPa was deter-

mined by the positive displacement pump which was generating the pressures. The sensors appear to work consistently at this pressure and there is currently no prediction as to what pressure the sensors could withstand. Physically the MEMS have proven to be sturdy and resilient to extreme temperatures and pressures, as required for down-hole viscometers.

For our simple fluid models, we assumed that the fluid was an incompressible homogeneous liquid. We first considered the "forced" spider, driven with a constant external driving force. For the "forced" spider model we produced theoretical expressions for the frictional force and power on the oscillating plate. These were closed form solutions and could be rearranged to give an expression for viscosity or density in terms of plate properties, power and the initial velocity of the plate. The oscillating plate will typically have a viscous penetration depth in the order of micrometers. This small distance means that even in the presence of the stationary added top plate, as long as $h >> \delta$ the armature will oscillate as in an unbounded fluid. For the Newtonian case we also produced equation (5.60) for $\mu\rho$ in terms of maximum recorded frequency, ω_m, vacuum frequency, ω_v, plate density, ρ_s, and plate depth, d.

We then moved on to the decaying oscillations model of the spider. In this model the plate was either plucked or driven to a constant speed and then allowed to decay by removing the external driving force. Our analysis of the "plucked" spider problem led us to the key parameter β which allowed us to determine how the plate will oscillate. β is a function of the material properties of the plate and the viscosity and density of the surrounding fluid.

$$\beta = \frac{2\sqrt{\mu\rho}Ba}{\sqrt{\pi k}W^{\frac{3}{4}}}$$

For a reasonable number of oscillations we require $0.001 < \beta < 0.1$ and hence it was found that the viscometer would be suitable for fluids within the range $0.01957 < \mu\rho/\mathrm{Pa^2{\cdot}s} < 1.957$. Unfortunately we did not have sufficient reliable experimental data for the spider sensor to enable us to compare the theoretical models with the real physical behaviour of the plate.

The second MEMS design we considered was the cantilever plate. For the flexion densitometer model, we produced an equation, (6.19), allowing us to find density as a function of the plate properties, frequency and temperature. When compared with experimental results, this equation produced density values accurate to within 2 % of the true value.

Small errors due to the inaccuracy of equipment will lead to uncertainties in our results. The pressure gauge has an inaccuracy of up to 0.029 MPa and the precision thermometer is accurate to 3 mK. The sum of these small uncertainties should have a negligible effect on the viscosity and density values. Unfortunately errors due to the unknown material properties of the plate, which is not pure silicon as assumed in the theory, cause calibration to be necessary.

Using the method of stokeslets, we derived a numerical solution for the viscosity of the fluid. This allowed us to write the viscosity in terms of driving force and maximum amplitude of oscillation as a polynomial to be solved. Once again however, calibration would be necessary. The numerical solution appears to lose stability for $\mu < 0.001$ Pa·s. A petroleum reservoir can contain liquids with viscosities in the range $0.00005 < \mu\ /\text{Pa·s} < 1$ so the viscometer will be useful for a significant part of this range. Unfortunately there are no experimental results in terms of maximum amplitude of oscillation. An oscilloscope or alternate method for measuring this amplitude would be needed for future experiments before comparisons could be made.

The theoretical work behind the two MEMS devices show that it is possible to measure viscosity and density in a wide range of fluids. The sensors themselves are robust and resilient to extreme conditions making them suitable for hostile down-hole conditions. The flexion has been shown to produce reasonable experimental results, a trade off in accuracy deemed acceptable for the ability to wishstand the harsh conditions of petroleum reservoirs.

Three papers have been written up as a result of this work which should be considered for further reading on this topic [37], [67] and [68].

Recommendations for future work

The spider sensor could be analysed more thoroughly with the addition of the stationary top plate, to see whether this would add any practical advantages other than stopping large particles from reaching the plate surface. More theoretical work can be done considering the spider in a number of other non-Newtonian fluids such as Bingham fluids, possibly a more accurate model for reservoir fluids.

A full experimental program is needed for the spider sensor, using the plucked method

to overcome the problem of breakages in the plate legs which have occurred during previous experiments. It would also be useful to test the flexion plate in a wider variety of fluids and gases.

The MEMS designs could both be investigated using computational fluid dynamics software. This would produce two dimensional quasi-steady or three dimensional unsteady full numerical solutions for the problems. Although the software is not simple to use, the advantage is we would not have any geometrical limitations.

Other MEMS designs have also been produced by Schlumberger. One example is a torsionally oscillating plate. It would be interesting to compare these geometrically different sensors to see which would be the most efficient viscometer for reservoir fluids.

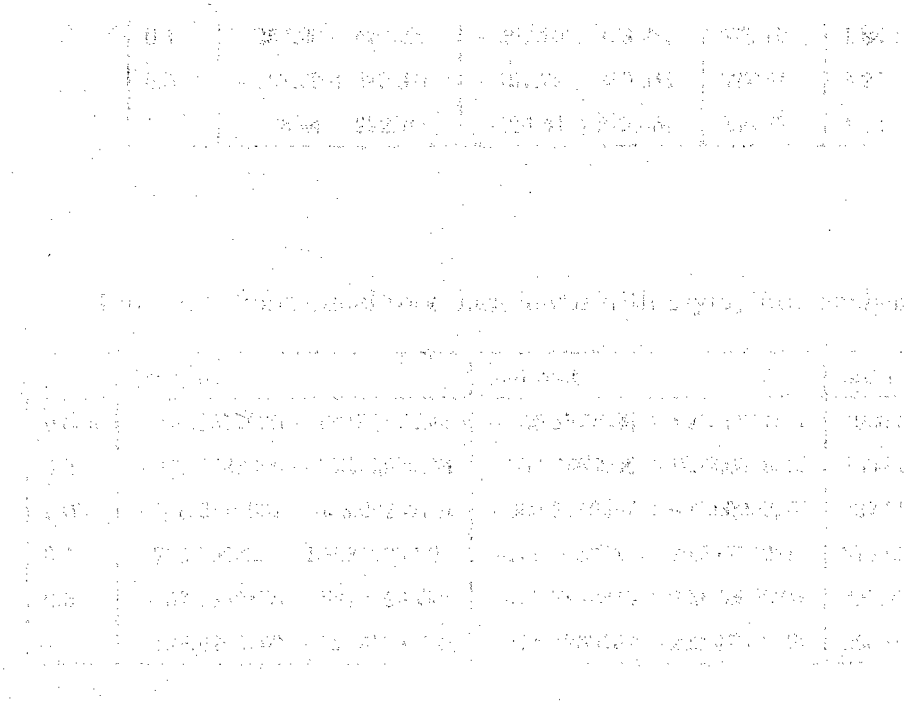

appendix A

Data

Spider - Pole analysis data

The following results correspond to the four roots found using exact evaluation and asymptotic analysis of the polynomial $f = s^4 - \frac{4(Ba)^2\mu\rho}{W^2}s^3 + \frac{2k^2}{W}s^2 + \frac{k^4}{W^2}$, with $\rho = 1000$ and $W = 1.78944 \times 10^{-7}$. The lines on graphs (5.11) and (5.12) correspond to these roots.

Table 7.1: Polynomial root data found exactly (k=1)

μ	1st root	2nd root	3rd root	4th root
0.005	$-453.10 - 1211.31i$	$-453.10 + 1211.31i$	2428.86	7.69×10^3
0.01	$-428.29 - 997.29i$	$-428.29 + 997.29i$	1490.52	1.78×10^4
0.05	$-310.45 - 600.77i$	$-310.45 + 600.77i$	742.46	9.20×10^4
0.1	$-257.20 - 478.28i$	$-257.20 + 478.28i$	575.10	1.84×10^5
0.5	$-157.79 + 280.31i$	$-157.79 - 280.31i$	327.81	9.21×10^5
1	$-126.44 - 222.46i$	$-126.44 + 222.46i$	258.95	1.84×10^6

Table 7.2: Polynomial root data found with asymptotic analysis (k=1)

μ	1st root	2nd root	3rd root	4th root
0.005	$-346.6577626 - 1301.067466i$	$-346.6577626 + 1301.067466i$	1906.86	1234.50
0.01	$-393.9483906 - 1032.657932i$	$-393.9483906 + 1032.657932i$	1394.67	633.18
0.05	$-308.2116062 - 603.9020225i$	$-308.2116062 + 603.9020225i$	737.78	166.51
0.1	$-256.508308 - 479.3173527i$	$-256.508308 + 479.3173527i$	573.69	128.65
0.5	$-157.7898875 - 280.3064884i$	$-157.7898875 + 280.3064884i$	327.72	117.57
1	$-126.4259762 - 222.4794072i$	$-126.4259762 + 222.4794072i$	258.92	109.43

$f_0(=\frac{\omega_0}{2\pi})$	$2g$	ρ (Pa)	μ (Pa·s)	$Q(=\frac{f_0}{2g})$
31288				
31452	55	33.9349	11.6604×10^{-6}	571.854
31499	61	42.3007	11.9558×10^{-6}	516.377
31572	71	55.95	12.4879×10^{-6}	444.676
31611	76	63.999	12.8334×10^{-6}	415.934
31657	81	71.4608	13.1683×10^{-6}	390.827
31697	90	80.3001	13.5952×10^{-6}	391.320
31725	96	88.2751	14.0057×10^{-6}	330.468
31762	105	97.438	14.5081×10^{-6}	302.495

Table 7.3: Experimental data for spider in methane

T (K)	p (kPa)	known ρ (kg/m^3)	f_0 ($= \frac{\omega_0}{2\pi}$)	$2g$	Q ($= \frac{f_0}{2g}$)	ρ (eq 6.19) (kg/m^3)	% error
323.162	7005.81	106.48	7592.46	90.06	84.30	107.24	0.72
323.162	13877.00	212.30	5982.62	72.93	82.03	213.13	0.39
323.162	20898.79	316.28	5116.16	62.77	81.51	315.76	-0.17
323.162	27679.46	408.29	4594.23	56.64	81.12	407.47	-0.20
323.162	34458.51	489.94	4243.09	52.97	80.10	489.11	-0.17
323.162	41249.47	561.37	3993.48	50.75	78.69	560.69	-0.12
323.162	48119.29	624.19	3806.22	49.31	77.20	623.89	-0.05
323.162	54885.41	678.21	3664.06	48.37	75.74	678.48	0.04
323.162	61689.92	726.03	3551.05	47.74	74.38	726.63	0.08
323.162	68311.73	767.42	3461.19	47.34	73.12	768.34	0.12
348.15	6977.88	97.41	7802.74	95.87	81.39	98.04	0.64
348.15	17495.87	242.66	5706.09	73.38	77.76	240.88	-0.73
348.15	27652.58	371.08	4799.62	61.23	78.38	367.81	-0.88
348.15	34469.49	447.41	4428.44	56.77	78.01	443.61	-0.85
348.15	41287.72	515.41	4160.31	53.85	77.26	511.44	-0.77
348.15	48153.53	576.07	3957.12	51.93	76.21	572.28	-0.66
348.15	54879.42	628.80	3801.96	50.66	75.05	625.45	-0.53
348.15	61689.74	676.41	3676.29	49.72	73.95	673.55	-0.42
348.15	68529.36	719.29	3573.40	48.72	73.34	716.76	-0.35
373.12	7080.44	91.52	7939.69	98.32	80.75	92.44	1.00
373.12	13847.52	177.90	6392.50	85.27	74.97	178.49	0.33
373.12	20678.94	261.52	5538.20	76.06	72.82	259.79	-0.66
373.12	27683.47	341.49	4966.40	69.26	71.71	339.17	-0.68
373.12	34426.07	411.89	4585.54	64.07	71.58	409.30	-0.63
373.12	41254.58	476.37	4303.50	59.68	72.11	473.66	-0.57
373.12	48098.62	534.48	4088.39	56.33	72.57	531.96	-0.47
373.12	54892.36	586.31	3921.77	54.27	72.26	583.86	-0.42
373.12	68432.68	675.01	3676.23	51.39	71.54	673.59	-0.21
398.11	7359.81	88.63	8014.97	99.04	80.93	89.49	0.97
398.11	13876.07	165.50	6560.92	84.83	77.34	166.11	0.37
398.11	27718.55	316.95	5107.47	67.31	75.88	317.11	0.05
398.11	34448.48	382.72	4718.13	62.70	75.25	382.96	0.06
398.11	41293.58	443.88	4425.78	59.79	74.03	444.26	0.08
398.11	48139.56	499.49	4201.61	57.26	73.37	500.17	0.14
398.11	54948.68	549.73	4025.36	55.47	72.57	550.85	0.20
398.11	61784.51	595.59	3882.16	54.14	71.71	597.21	0.27
423.11	7271.58	82.03	8174.18	114.68	71.28	83.50	1.79
423.11	14123.87	157.30	6657.65	97.73	68.12	159.43	1.36
423.11	21056.11	230.05	5782.56	85.68	67.49	232.86	1.22
423.11	27785.88	296.48	5225.75	77.38	67.53	299.97	1.18
423.11	34604.92	359.06	4825.15	71.40	67.58	363.28	1.18
423.11	41249.24	415.32	4533.83	67.56	67.11	420.24	1.18
423.11	48197.29	469.32	4297.79	64.51	66.63	475.13	1.24
423.11	48188.85	469.26	4298.06	64.35	66.79	475.06	1.24
423.11	55017.87	517.85	4114.13	62.34	65.99	524.53	1.29
423.11	61833.70	562.30	3964.93	60.66	65.36	569.82	1.34
423.11	68620.39	603.14	3840.91	59.50	64.56	611.55	1.39

Table 7.4: Experimental data for flexion plate in argon

Fluid	T (K)	p (Pa)	known ρ (kg/m^3)	f_0 ($= \frac{\omega_0}{2\pi}$)	$2g$	Q ($= \frac{f_0}{2g}$)	ρ (6.17) (kg/m^3)	error %
H_2O	313.234	100.8	992.18	3590.16	132.66	27.06	1001.71	-0.96
	313.234	100.8	992.18	3593.61	139.72	25.72	999.66	-0.75
	323.205	100.9	988.01	3609.76	132.31	27.28	990.13	-0.21
	323.205	100.9	988.01	3608.66	135.77	26.58	990.77	-0.28
	323.205	100.9	988.01	3609.71	136.43	26.46	990.16	-0.22
	373.115	102.7	958.95	3622.56	122.69	29.53	982.72	-2.48
	373.115	102.7	958.92	3622.63	122.38	29.60	982.65	-2.47
	373.115	102.7	958.89	3622.12	123.45	29.34	982.95	-2.51
Silicon oil 200-20	313.234	102.7	935.67	3442.09	503.71	6.83	1095.76	-17.11
	313.234	102.7	935.67	3442.61	500.01	6.89	1095.41	-17.07
	323.205	102.7	926.73	3480.05	482.81	7.21	1070.51	-15.51
	323.205	102.7	926.73	3482.45	481.38	7.23	1068.94	-15.34
	348.172	102.6	904.59	3562.27	390.51	9.12	1018.56	-12.60
	348.172	102.6	904.59	3563.89	395.15	9.02	1017.57	-12.49
	373.115	102.4	882.62	3634.65	341.51	10.64	975.71	-10.55
	373.115	102.4	882.62	3634.93	343.38	10.59	975.55	-10.53
	313.234	99.8	836.67	3613.85	549.80	6.57	987.73	-18.06
	313.234	99.8	836.67	3615.12	541.62	6.68	986.99	-17.97
	323.205	101.4	830.27	3683.49	467.10	7.89	948.18	-14.20
	323.205	101.4	830.27	3683.21	467.33	7.88	948.34	-14.22
	323.205	101.4	830.27	3681.68	465.72	7.91	949.18	-14.32
	373.115	103.2	798.24	3868.06	262.80	14.72	853.51	-6.92
	373.115	103.2	798.24	3867.24	264.34	14.63	853.90	-6.97
Silicon oil 200-10	313.234	99.8	826.55	3763.05	362.40	10.38	905.64	-9.57
	313.234	99.8	826.55	3759.51	357.05	10.53	907.48	-9.79
	313.234	99.8	826.55	3759.39	358.98	10.47	907.54	-9.80
	323.205	101	819.97	3793.21	325.42	11.66	890.23	-8.57
	323.205	101	819.97	3793.95	327.32	11.59	889.85	-8.52
	373.115	103.1	787.01	3922.59	211.95	18.51	828.06	-5.22
	373.115	103.1	787.01	3923.83	213.96	18.34	827.50	-5.14
Fomblin	313.234	102.2	1834.90	2473.50	438.78	5.64	2186.00	-19.13
	313.234	102.2	1834.90	2474.87	460.63	5.37	2183.50	-19.00
	323.205	102.3	1815.72	2519.95	375.52	6.71	2103.65	-15.86
	323.205	102.3	1815.72	2520.77	377.20	6.68	2102.25	-15.78
	348.172	102.3	1767.69	2618.99	279.16	9.38	1942.50	-9.89
	348.172	102.3	1767.69	2618.73	273.40	9.58	1942.90	-9.91
	373.115	101.7	1719.69	2690.41	216.09	12.45	1837.17	-6.83
	373.115	101.7	1719.69	2690.44	216.98	12.40	1837.13	-6.83
Nitrogen	323.205	10148.5	104.02	8751.68	70.77	123.66	111.71	-7.39
	323.205	10140.9	103.94	8753.97	71.65	122.18	111.61	-7.38
	323.205	10137.8	103.91	8754.77	70.87	123.53	111.58	-7.38
	323.205	20488.4	199.02	7156.22	64.86	110.33	200.96	-0.97
	323.205	20490.3	199.04	7157.33	64.77	110.50	200.87	-0.92
	323.205	30311.1	274.09	6382.24	60.12	106.16	270.24	1.40
	323.205	30322.2	274.17	6382.20	59.15	107.90	270.24	1.43
	323.205	40321.9	336.31	5909.13	56.93	103.80	326.63	2.88
	323.205	40330.6	336.36	5908.54	57.63	102.53	326.71	2.87
	323.205	50401.3	387.44	5596.11	56.61	98.86	372.06	3.97
	323.205	60476.8	429.88	5375.68	55.20	97.39	408.92	4.88

Table 7.5: Experimental data for flexion in different fluids

Fluid	T (K)	p (Pa)	known ρ (kg/m^3)	f_0 ($= \frac{\omega_0}{2\pi}$)	$2g$	Q ($= \frac{f_0}{2g}$)	ρ (6.17) (kg/m^3)	error %
$C_6H_5CH_3$	313.23	103.9	848.69	3857.40	111.80	34.50	858.58	-1.17
	313.232	103.9	848.69	3857.34	111.82	34.50	858.61	-1.17
	313.231	103.9	848.69	3858.34	112.53	34.29	858.13	-1.11
	313.231	104	848.69	3857.69	111.98	34.45	858.44	-1.15
	313.231	11217.7	857.74	3832.94	116.11	33.01	870.45	-1.48
	313.23	11216.8	857.74	3833.36	115.97	33.05	870.24	-1.46
	313.231	11178.8	857.71	3833.38	116.33	32.95	870.23	-1.46
	313.232	19593.9	864.07	3817.84	119.53	31.94	877.89	-1.60
	313.23	19270.7	863.83	3817.84	118.81	32.13	877.89	-1.63
	313.23	29339.5	870.96	3802.14	123.55	30.78	885.72	-1.69
	313.231	29308	870.94	3802.21	122.34	31.08	885.69	-1.69
	313.231	39937.6	877.97	3785.86	127.91	29.60	893.95	-1.82
	313.231	39689.5	877.81	3785.26	126.49	29.93	894.25	-1.87
	313.231	49859	884.14	3771.71	130.18	28.97	901.18	-1.93
	313.231	50213.5	884.35	3771.06	130.86	28.82	901.51	-1.94
$C_6H_5CH_3$	323.201	103.6	839.3	3878.82	108.03	35.91	848.38	-1.08
	323.201	103.6	839.3	3878.03	108.08	35.88	848.75	-1.13
	323.202	8941	847	3856.09	110.23	34.98	859.22	-1.44
	323.202	9084.2	847.12	3855.69	110.93	34.76	859.41	-1.45
	323.201	199998.7	855.86	3835.71	114.26	33.57	869.10	-1.55
	323.202	20208.5	856.03	3835.26	114.65	33.45	869.32	-1.55
	323.201	29507	862.91	3819.10	117.40	32.53	877.27	-1.66
	323.201	29373.7	862.81	3818.99	117.01	32.64	877.32	-1.68
	323.201	39805.9	870.03	3802.2	121.87	31.20	885.70	-1.80
	323.201	39974.3	870.15	3802.15	121.13	31.39	885.72	-1.79
	323.201	50254.3	876.8	3786.03	124.87	30.32	893.86	-1.95
	323.201	50585.9	877.01	3787.03	125.34	30.22	893.35	-1.86
	323.201	59628.5	882.52	3774.35	128.56	29.36	899.83	-1.96
	323.201	59852.1	882.66	3773.89	128.76	29.31	900.06	-1.97
$C_6H_5CH_3$	348.165	103.8	815.37	3930.85	98.58	39.88	824.28	-1.09
	348.165	103.8	815.37	3931.09	97.88	40.16	824.17	-1.08
	348.165	103.8	815.37	3930.87	98.60	39.87	824.27	-1.09
	348.165	9080.7	824.45	3904.10	100.68	38.78	836.56	-1.47
	348.165	9136.2	824.51	3904.28	100.85	38.71	836.47	-1.45
	348.165	19988.9	834.45	3880.34	104.42	37.16	847.67	-1.58
	348.165	20142.9	834.59	3880.20	104.85	37.01	847.74	-1.58
	348.165	30000.9	842.82	3861.22	107.78	35.83	856.77	-1.65
	348.165	30149.4	842.94	3860.89	108.04	35.74	856.92	-1.66
	348.165	30315.4	843.07	3860.70	107.95	35.76	857.01	-1.65
	348.165	39999.6	850.54	3842.86	110.98	34.63	865.63	-1.77
	348.165	39843.7	850.42	3842.79	110.03	34.93	865.66	-1.79
	348.165	50469.7	858.04	3825.76	113.45	33.72	873.99	-1.86
	348.165	50539.7	858.09	3825.67	114.92	33.29	874.04	-1.86
	348.165	50620.4	858.15	3825.91	113.18	33.80	873.92	-1.84
	348.165	60456.7	864.74	3810.69	117.24	32.50	881.46	-1.93
	348.165	61131.9	865.18	3809.76	117.8	32.34	881.93	-1.94
	348.165	60601.2	864.83	3810.54	117.06	32.55	881.54	-1.93
	348.165	68295.7	869.72	3800.11	118.71	32.01	886.76	-1.96

Table 7.6: Continuation of table (7.5)

appendix B

Bessel Functions

Bessel function of the first kind

$$\text{zero order:} \qquad J_0(x) = 1 - \frac{(\frac{x}{2})^2}{(1!)^2} + \frac{(\frac{x}{2})^4}{(2!)^2} - \frac{(\frac{x}{2})^6}{(3!)^2} + \dots$$

$$\text{first order:} \qquad J_1(x) = \frac{x}{2}\left[1 - \frac{(\frac{x}{2})^2}{2(1!)^2} + \frac{(\frac{x}{2})^4}{3(2!)^2} - \frac{(\frac{x}{2})^6}{4(3!)^2} + \dots\right] = -\frac{d}{dx}[J_0(x)]$$

Modified Bessel function of the first kind

$$\text{zero order:} \qquad K_0(x) = 1 + \frac{(\frac{x}{2})^2}{(1!)^2} + \frac{(\frac{x}{2})^4}{(2!)^2} + \frac{(\frac{x}{2})^6}{(3!)^2} + \dots$$

$$\text{first order:} \qquad K_1(x) = \frac{x}{2}\left[1 + \frac{(\frac{x}{2})^2}{2(1!)^2} + \frac{(\frac{x}{2})^4}{3(2!)^2} + \frac{(\frac{x}{2})^6}{4(3!)^2} + \dots\right] = \frac{d}{dx}[K_0(x)]$$

Modified Bessel function of the second kind

$$\text{zero order} \qquad I_0(x) = -\left[\left(\ln\frac{x}{2} + C\right)K_0(x) - \frac{2}{1}K_2(x) - \frac{2}{2}K_4(x) - \frac{2}{3}K_6(x) - \dots\right]$$

Difference formulae

The difference formula used in the numerics included in this thesis is the 3-point central difference formula. We will show the error involved in using this formula and will give an example of some other difference formula for comparison. The forward difference method follows from rearranging the Taylor series of $x(t_i + \Delta t)$,

$$\begin{aligned} x(t_i + \Delta t) &= x(t_i) + x'(t_i)\Delta t + x''(\Sigma)\frac{\Delta t^2}{2} \qquad \text{with} \qquad \Sigma \in [t_i, t_i + \Delta t] \\ \Rightarrow x'_i &= \frac{x_{i+1} - x_i}{\Delta t} - x''(\Sigma)\frac{\Delta t}{2} \end{aligned} \tag{7.1}$$

so it has an error term of order Δt.

The central difference method comes from combining two Taylor series for $x(ti + \Delta t)$ and

$x(t_i - \Delta t)$ to give

$$x'_i = \frac{x_{i+1} - x_{i-1}}{2\Delta t} - x'''(\Sigma)\frac{\Delta t^2}{6} \qquad \text{with} \qquad \Sigma \in [t_i - \Delta t, t_i + \Delta t] \tag{7.2}$$

which is more accurate since it has a smaller error term of order Δt^2.

We can increase the accuracy further by increasing the number of points used in the formula. Equation (7.1) is a two point method and (7.2) is an example of a three point method (although the central point can not be seen). In a similar way we can use five points to get a more accurate version of the forward difference method

$$x_i' = \frac{-3x_{i+4} + 16x_{i+3} - 36x_{i+2} + 48x_{i+1} - 25x_i}{12\Delta t} + x''''(\Sigma)\frac{\Delta t^4}{5} \qquad \text{with} \qquad \Sigma \in [t_i, t_{i+4}]$$

and the central difference method.

$$x_i' = \frac{-x_{i+2} + 8x_{i+1} - 8x_{i-1} + x_{i-2}}{12\Delta t} + x''''(\Sigma)\frac{\Delta t^4}{30} \qquad \text{with} \qquad \Sigma \in [t_{i-2}, t_{i+2}]$$

We could have used the forward difference method for the second derivative but again this would have been less accurate.

$$\text{3 point forward} \qquad x_i'' = \frac{x_{i+2} - 2x_{i+1} + x_i}{\Delta t^2} + x''''(\Sigma)\Delta t \qquad \text{with} \qquad \Sigma \in [t_i, t_{i+2}]$$

$$\text{3 point central} \qquad x_i'' = \frac{x_{i+1} - 2x_i + x_{i-1}}{\Delta t^2} + x''''(\Sigma)\frac{\Delta t^2}{12} \qquad \text{with} \qquad \Sigma \in [t_{i-1}, t_{i+1}]$$

We chose to use the three point central difference method for both the first and second derivatives which then both have an error term of order Δt^2.

Binomial series

For $|x| < 1$, the binomial series expansion [64] of $(1 + x)^r$ is

$$\begin{aligned}(1+x)^r &= 1 + rx + \frac{r(r-1)}{2!}x^2 + \frac{r(r-1)(r-2)}{3!}x^3 + \ldots \\ &= 1 + \sum_{n=1}^{\infty} \frac{r(r-1)(r-2)\ldots(r-n+1)}{n!}x^n \qquad (-1 < x < 1)\end{aligned}$$

Gamma function

The definition of the gamma function is based on the Euler Intergral

$$\Gamma(n) = \int_0^\infty x^{n-1} e^{-x} dx \qquad n > 0$$

and converges for positive n, such that

$$\Gamma(0) = \infty \qquad \Gamma(\frac{1}{2}) = \sqrt{\pi} \qquad \Gamma(1) = 1 \qquad \Gamma(\frac{3}{2}) = \frac{\sqrt{\pi}}{2} \qquad \Gamma(2) = 1$$

$$\Gamma(z+1) = z\Gamma(z) \qquad z > 0$$

$$\Gamma(m+1) = m! \qquad m > 0 \qquad m \in N$$

Letting $x = st$, this function is comparable to Laplace-transform integrals in the following manner:

$$\frac{\Gamma(n)}{s^n} = \int_0^\infty e^{-st} t^{n-1} dt \equiv L(t^{n-1})$$

appendix C

MATLAB code

Non-dimensionalised numerical solution for the plucked spider

$N = 1000; dt = 1; X = 1; k = 1; mu = 0.004; rho = 1000;$

$a = 0.002; B = 0.004; d = 0.00002;$

$W = 2330 * a * B * d; beta = (2 * sqrt(mu * rho) * B * a)/(sqrt(pi * k) * W \wedge (3/4));$

$x = zeros(1, N); s = zeros(1, (N-4)); p = zeros(1, (N-4)); q = zeros(1, (N-4));$

$x(1) = X; x(2) = x(1); x(3) = x(1); x(4) = 1 - ((dt \wedge 2)/(1 + beta * sqrt(dt)));$

$s(1) = x(4) - x(3) - x(2) + x(1); p(1) = (sqrt(2) - sqrt(1)) * s(1);$

$$\begin{aligned} x(5) \;=\; & ((dt \wedge 2)/(1 + beta * sqrt(dt))) * (x(4) * ((2/(dt \wedge 2)) - 1 + \ldots \\ & (beta/(dt \wedge (3/2)))) + x(3) * ((beta/(dt \wedge (3/2))) - (1/(dt \wedge 2))) \ldots \\ & -x(2) * (beta/(dt \wedge (3/2))) - (beta/(dt \wedge (3/2))) * p(1)); \end{aligned}$$

$for \quad j = 2 : 1 : (N-4)$

$for \quad i = 1 : 1 : (j-1)$

$s(j-i+1) = s(j-i); \qquad q(j-i+1) = (sqrt(j-i+2) - sqrt(j-i+1)) * s(j-i+1);$

end

$s(1) = x(j+3) - x(j+2) - x(j+1) + x(j); q(1) = (sqrt(2) - sqrt(1)) * s(1);$

$p(j) = sum(q(1 : j));$

$$\begin{aligned} x(j+4) \;=\; & ((dt \wedge 2)/(1 + beta * sqrt(dt))) * (x(j+3) * ((2/(dt \wedge 2)) - 1 + \ldots \\ & (beta/(dt \wedge (3/2)))) + x(j+2) * ((beta/(dt \wedge (3/2))) \ldots \\ & -(1/(dt \wedge 2))) - x(j+1) * (beta/(dt \wedge (3/2))) - (beta/(dt \wedge (3/2))) * p(j)); \end{aligned}$$

end

$plot(x)$

Small time solution to plucked spider problem

$k = 1; a = 0.002; B = 0.004; d = 0.00002;$

$W = 2330 * a * B * d; BB = (k \wedge 2)/W;$

$NN = 0.001; nn = 0.00001;$

$t = (0 : nn : NN);$

$for \quad i = 1 : 1 : ((NN/nn) + 1)$

$xs(i) = 1 - (BB/2) * (t(i) \wedge 2);$

end

$plot(t, xs)$

$xlabel('time'); ylabel('xs/X');$

Large time solution to plucked spider problem

$N = 1000; dt = 1; X = 1; k = 1; mu = 0.004; rho = 1000;$

$a = 0.002; B = 0.004; d = 0.00002; W = 2330 * a * B * d;$

$SSS = 100; NNN = 200; nnn = 1;$

$t = (SSS : nnn : NNN);$

$for \quad i = 1 : 1 : (((NNN - SSS)/nnn) + 1)$

$xl(i) = (2 * B * a * sqrt(mu * rho * pi))/((k \wedge 2) * (t(i) \wedge (3/2)));$

end

$plot(t, xl)$

$xlabel('time'); ylabel('xl/X');$

Numerical solution for the vibrating 'flexion' plate

$N = 63; r = 1/N; mu = 0.04; a = 0.00225; B = 0.0028; omega = 5000; d = 0.00002;$

$rhos = 2330; E = 150; sigma = 0.17; D = (E * (d^3))/(12 * (1 - sigma^2));$

$alpha = (rhos * d * (omega^2) * (a^4))/D; beta = (8 * pi * mu * omega * (a^3))/D; k = 1;$

$x = zeros(2 * N + 2, 1); s = zeros(1, 2 * N + 2); Q = zeros(1, N + 1); F = zeros(1, N + 1);$

$q = zeros(1, N + 1); f = zeros(1, N + 1);$

$p = zeros(N + 1, N + 1); pp = zeros(N + 1, N + 1); ppp = zeros(N, N + 1);$

$pppp = zeros(N, N + 1); P = zeros(2 * N + 2, 2 * N + 2); PP = zeros(2 * N + 2, 2 * N + 2);$

$K0 = zeros(1, N); K1 = zeros(0, N); K = zeros(N, N);$

$z = zeros(1, N + 1); t = zeros(1, N + 1);$

$p(1,1) = 6 * r - alpha; p(1,2) = -8 * r; p(1,3) = 2 * r;$

$p(2,2) = 7 * r - alpha; p(2,3) = -4 * r; p(2,4) = r;$

$p(N, N-2) = r; p(N, N-1) = -4 * r; p(N, N) = 5 * r - alpha; p(N, N+1) = -2 * r;$

$p(N+1, N-1) = 2 * r; p(N+1, N) = -4 * r; p(N+1, N+1) = 2 * r - alpha;$

$for \quad j = 3 : 1 : N - 1$

$p(j, j-2) = r; p(j, j-1) = -4 * r; p(j, j) = 6 * r - alpha; p(j, j+1) = -4 * r; p(j, j+2) = r;$

end

$for \quad j = 1 : 1 : (N + 1)$

$pp(j, j) = -beta; s(j) = 1;$

end

$for \quad j = 1 : 1 : N$

$ppp(j, j+1) = -1;$

end

$for \quad j = 1 : 1 : N$

$K0(j) = ((2 * j^2 * r^2)/(2 * j * r - r) + (r * log(abs(2 * j - 1))) - (j * r));$

$K1(j) = ((-2 * j^2 * r^2)/(2 * j * r + r) + (r * log(abs(2 * j + 1))) + (j * r));$

$for \quad v = 1 : 1 : j - 2$

$K(j, v) = ((-1/(v * r + j * r)) * (2 * v^2 * r^2 + 2 * v * r * (v * r + j * r) * log(abs(2 * v * r^2 *$

$(v + j))) - (v * r + j * r)^2 * log(abs(v * r + j * r)) - \ldots$

$(v^2 * r^2 - j^2 * r^2) * log(abs(v * r - j * r))) + (1/(v * r + (j - 1) * r)) * (2 * v^2 * r^2 + 2 * v * r *$

$(v * r + (j - 1) * r) * log(abs(2 * v * r^2 * (v + j - 1))) - \ldots$

$(v*r+(j-1)*r)^2 * log(abs(v*r+(j-1)*r)) - (v^2 * r^2 - (j-1)^2 * r^2) * log(abs(v*r-(j-1)*r))));$

end

$for \quad v = j+1:1:N$

$K(j,v) = ((-1/(v*r+j*r))*(2*v^2*r^2+2*v*r*(v*r+j*r)*log(abs(2*v*r^2*$

$(v+j))) - (v*r+j*r)^2*log(abs(v*r+j*r)) - \ldots$

$(v^2*r^2-j^2*r^2)*log(abs(v*r-j*r))) + (1/(v*r+(j-1)*r))*(2*v^2*r^2+2*v*r*$

$(v*r+(j-1)*r)*log(abs(2*v*r^2*(v+j-1))) - \ldots$

$(v*r+(j-1)*r)^2*log(abs(v*r+(j-1)*r)) - (v^2*r^2-(j-1)^2*r^2)*log(abs(v*r-(j-1)*r))));$

end

end

$pppp(1,1) = (i/2)*K0(1); pppp(1,2) = (i/2)*(K0(1)+K1(1));$

$pppp(1,3) = (i/2)*(K1(1)+K(3,1)); pppp(1,N+1) = (i/2)*K(N,1);$

$for \quad v = 4:1:N$

$pppp(1,v) = (i/2)*(K(v-1,1)+K(v,1));$

end

$pppp(2,1) = (i/2)*K(1,2); pppp(2,2) = (i/2)*(K(1,2)+K0(2)); pppp(2,3) = (i/2)*$

$(K0(2)+K1(2)); pppp(2,4) = (i/2)*(K1(2)+K(4,2)); pppp(2,N+1) = (i/2)*K(N,2);$

$for \quad v = 5:1:N$

$pppp(2,v) = (i/2)*(K(v-1,2)+K(v,2));$

end

$pppp(N-2,1) = (i/2)*K(1,N-2); pppp(N-2,N-2) = (i/2)*(K(N-3,N-2)+$

$K0(N-2)); pppp(N-2,N-1) = (i/2)*(K0(N-2)+K1(N-2));$

$pppp(N-2,N) = (i/2)*(K1(N-2)+K(N,N-2)); pppp(N-2,N+1) = (i/2)*K(N,N-2);$

$for \quad v = 2:1:N-3$

$pppp(N-2,v) = (i/2)*(K(v-1,N-2)+K(v,N-2));$

end

$pppp(N-1,1) = (i/2)*K(1,N-1); pppp(N-1,N-1) = (i/2)*(K(N-2,N-1)+$

$K0(N-1)); pppp(N-1,N) = (i/2)*(K0(N-1)+K1(N-1));$

$pppp(N-1,N+1) = (i/2)*K1(N-1);$

$for \quad v = 2:1:N-2$

$pppp(N-1,v) = (i/2)*(K(v-1,N-1)+K(v,N-1));$

end

$pppp(N,1) = (i/2)*K(1,N); pppp(N,N) = (i/2)*(K(N-1,N)+K0(N)); pppp(N,N+1) =$

$(i/2)*K0(N);$

$for \quad v = 2:1:N-1$

$pppp(N,v) = (i/2) * (K(v-1,N) + K(v,N));$

end

$for \quad j = 3:1:N-3$

$pppp(j,1) = (i/2) * K(1,j); pppp(j,j) = (i/2) * (K(j-1,j) + K0(j)); pppp(j,j+1) = (i/2) *$

$(K0(j) + K1(j)); pppp(j,j+2) = (i/2) * (K1(j) + K(j+2,j)); pppp(j,N+1) = (i/2) * K(N,j);$

$for \quad v = 2:1:j-1$

$pppp(j,v) = (i/2) * (K(v-1,j) + K(v,j));$

end

$for \quad v = j+3:1:N$

$pppp(j,v) = (i/2) * (K(v-1,j) + K(v,j));$

end

end

$P(N+2,1) = 1;$

$for \quad v = 1:1:N+1$

$for \quad j = 1:1:N+1$

$P(j,v) = p(j,v); P(j,N+1+v) = pp(j,v);$

end

$for \quad j = 1:1:N$

$P(N+2+j,v) = ppp(j,v); P(N+2+j,N+1+v) = pppp(j,v);$

end

end

$PP = inv(P); x = PP * (s');$

$for \quad j = 1:1:N+1$

$Q(j) = x(j); F(j) = x(N+1+j);$

$z(j) = j * r * a; t(j) = (j-1) * r * 2 * pi/omega;$

end

$for \quad j = 1:1:N+1$

$q(j) = k * a^4 * Q(j)/D; f(j) = -4 * pi * k * mu * omega * a^4 * B * F(j)/D;$

$for \quad v = 1:1:(N+1)$

$qq(j,v) = q(j) * exp(i * omega * t(v));$

end

end

appendix D

Numerical Stability Analysis

No damping

Assuming α and β are small, we begin with some simple stability analysis on the numerical form of (5.142) by taking $\alpha = \beta = 0$.

$$\begin{aligned} e_r{}'' + e_r &= 0 \\ \Rightarrow \frac{e_{ri+1} - 2e_{ri} + e_{ri-1}}{(\Delta\tilde{t})^2} + e_{ri} &= 0 \end{aligned}$$

Trying the solution $e_{ri} = a\mathsf{p}^i$, this becomes

$$a\mathsf{p}^2 + a((\Delta\tilde{t})^2 - 2)\mathsf{p} + a = 0$$

which gives us the following value for p

$$\mathsf{p} = 1 - \frac{(\Delta\tilde{t})^2}{2} \pm \frac{\sqrt{(\Delta\tilde{t})^4 - 4(\Delta\tilde{t})^2}}{2}.$$

Considering the root in this value, we see that p will be complex when $(\Delta\tilde{t})^4 - 4(\Delta\tilde{t})^2 < 0$, hence when $\Delta\tilde{t} < 2$. Alternatively, p will be real when $(\Delta\tilde{t})^4 - 4(\Delta\tilde{t})^2 \geq 0$, hence when $\Delta\tilde{t} \geq 2$. The system will be stable when $a\mathsf{p}^i \rightarrow 0$ as $i \rightarrow 0$, hence when $|\mathsf{p}| < 1$. We will consider the stability of the three separate cases, $\Delta\tilde{t} > 2$, $\Delta\tilde{t} = 2$ and $\Delta\tilde{t} < 2$.

$|\mathsf{p}| < 1$ gives

$$-1 < \frac{2 - (\Delta\tilde{t})^2 \pm \sqrt{(\Delta\tilde{t})^4 - 4(\Delta\tilde{t})^2}}{2} < 1$$

which reduces to

$$(\Delta\tilde{t})^2 - 4 < \pm\sqrt{(\Delta\tilde{t})^2}\sqrt{(\Delta\tilde{t})^2 - 4} < (\Delta\tilde{t})^2 \tag{7.3}$$

For the first case, looking at the positive root, this holds true since $\Delta\tilde{t} > 2$ implies that $\sqrt{(\Delta\tilde{t})^2} > \sqrt{(\Delta\tilde{t})^2 - 4}$, and rearranging $|\mathsf{p}| < 1$ gives us:

$$\sqrt{(\Delta\tilde{t})^2 - 4}\sqrt{(\Delta\tilde{t})^2 - 4} < \sqrt{(\Delta\tilde{t})^2}\sqrt{(\Delta\tilde{t})^2 - 4} < \sqrt{(\Delta\tilde{t})^2}\sqrt{(\Delta\tilde{t})^2}$$

If we look at the negative root of (7.3), this does not hold true since $\Delta\tilde{t} > 2$ gives us that $(\Delta\tilde{t})^2 - 4 > 0$ and $-\sqrt{(\Delta\tilde{t})^2}\sqrt{(\Delta\tilde{t})^2 - 4} < 0$. Hence this leads to the contradiction

$$(\Delta\tilde{t})^2 - 4 < -\sqrt{(\Delta\tilde{t})^2}\sqrt{(\Delta\tilde{t})^2 - 4}$$

The system is therefore unstable when $\Delta\tilde{t} > 2$.

In the second case, when $\Delta\tilde{t} = 2$, the value for $|\mathsf{p}|$ becomes

$$|\mathsf{p}| = \left|1 - \frac{4}{2} \pm \frac{\sqrt{16 - 16}}{2}\right| = |-1| = 1.$$

Hence $|\mathsf{p}| = 1$ with repeated roots indicating that the system is unstable in this case. If only one of the roots had been equal to 1 the system would have been marginally stable.

For the third case we need to re-write p in complex form as $\mathsf{p} = 1 - \frac{(\Delta\tilde{t})^2}{2} \pm i\frac{\sqrt{4(\Delta\tilde{t})^2 - (\Delta\tilde{t})^4}}{2}$. When we take the modulus of p we get

$$\begin{aligned} |\mathsf{p}| &= \sqrt{\left(\frac{1 - (\Delta\mathbf{t})^2}{2}\right)^2 + \left(\frac{\pm\sqrt{4(\Delta\tilde{t})^2 - (\Delta\tilde{t})^4}}{2}\right)^2} \\ &= \sqrt{1 - (\Delta\tilde{t})^2 + \frac{(\Delta\tilde{t})^4}{4} + (\Delta\tilde{t})^2 - \frac{(\Delta\tilde{t})^4}{4}} \\ &= 1. \end{aligned}$$

Hence once again we get $|\mathsf{p}| = 1$ with repeated roots leading to marginal instability, the error term will neither grow nor shrink. Therefore, this analysis shows that when no damping is present ($\alpha = \beta = 0$), the numerical system is always unstable or marginally unstable for any choice of time step $\Delta\tilde{t}$.

Including the effects of damping

We now try introducing some damping into the system. This time we assume $\beta = 0$ but $\alpha \neq 0$ which leaves us with

$$e_r'' + \alpha e_r' + e_r = 0$$

This will give a solution of the form

$$e_r = a_1 e^{\mathsf{p}_1 \tilde{t}} + a_2 e^{\mathsf{p}_2 \tilde{t}}$$

where p_1 and p_2 are the two roots of the polynomial $\mathsf{p}^2 + \alpha\mathsf{p} + 1 = 0$. Hence,

$$\mathsf{p} = \frac{-\alpha \pm \sqrt{\alpha^2 - 4}}{2}$$

For e_r to be a stable solution we require the real parts of both p_1 and p_2 to be negative so that $e_r = a_1 e^{\mathsf{p}_1 \tilde{t}} + a_2 e^{\mathsf{p}_2 \tilde{t}} \to 0$ as $\tilde{t} \to \infty$.

When $\alpha < -2$, we have that $\alpha^2 - 4 > 0$ and $\sqrt{\alpha^2 - 4} < \alpha$, so both p_1 and p_2 are real and positive. When $\alpha > 2$, again the roots of p will be real but this time they will both be negative. When $-2 < \alpha < 0$, we get $\alpha^2 - 4 < 0$ and $-\alpha > 0$, so the roots of p will be complex. The real part for both roots is $\frac{-\alpha}{2} > 0$, which is positive. When $0 < \alpha < 2$, again p will have complex roots but this time $-\alpha < 0$ so the real part will be negative.

This means that the first condition for a stable solution is $\alpha > 0$, which is as we would expect. There should be a positive damping term for oscillations to decay.

Now we consider the numerical system again.

$$\begin{aligned} e_r'' + \alpha e_r' + e_r &= 0 \\ \Rightarrow \frac{e_{ri+1} - 2e_{ri} + e_{ri-1}}{(\Delta\tilde{t})^2} + \frac{\alpha(e_{ri+1} - e_{ri-1})}{2\Delta\tilde{t}} + e_{ri} &= 0 \\ \Rightarrow e_{ri+1} + e_{ri}\left(\frac{\Delta\tilde{t}^2 - 2}{1 + \frac{\alpha}{2}\Delta\tilde{t}}\right) + e_{ri-1}\left(\frac{1 - \frac{\alpha}{2}\Delta\tilde{t}}{1 + \frac{\alpha}{2}\Delta\tilde{t}}\right) &= 0 \end{aligned} \tag{7.4}$$

As in the example with no damping, we assume a solution of the form $e_{ri} = a\mathsf{p}^i$ so that we can write (7.4) as

$$a\mathsf{p}^2 + a\mathsf{p}\left(\frac{\Delta\tilde{t}^2 - 2}{1 + \frac{\alpha}{2}\Delta\tilde{t}}\right) + a\left(\frac{1 - \frac{\alpha}{2}\Delta\tilde{t}}{1 + \frac{\alpha}{2}\Delta\tilde{t}}\right) = 0. \tag{7.5}$$

This is a quadratic expression which can be solved for p to give

$$\begin{aligned}\mathsf{p} &= \frac{\left(\frac{2-\Delta \mathbf{t}^2}{1+\frac{\alpha}{2}\Delta\tilde{t}} \pm \sqrt{\left(\frac{\Delta \mathbf{t}^2-2}{1+\frac{\alpha}{2}\Delta\tilde{t}}\right)^2 - 4\left(\frac{1-\frac{\alpha}{2}\Delta\tilde{t}}{1+\frac{\alpha}{2}\Delta\tilde{t}}\right)}\right)}{2} \\ &= \frac{2-\Delta \mathbf{t}^2 \pm \Delta\tilde{t}\sqrt{\Delta\tilde{t}^2-4+\alpha^2}}{2+\alpha\Delta\tilde{t}}. \end{aligned} \tag{7.6}$$

When $\Delta\tilde{t} << 1$, to leading order we get $\mathsf{p} = \frac{2}{2} = 1$. This tells us that when $\Delta\tilde{t}$ is small the solution will be neutrally stable for all choices of α. As before, the system will be stable when $a\mathsf{p}^i \to 0$ as $i \to 0$, hence when $|\mathsf{p}| < 1$. Once again will consider the stability of the three separate cases, $\Delta\tilde{t} = 2$, $0 < \Delta\tilde{t} < 2$ and $\Delta\tilde{t} > 2$.

Looking first at $\Delta\tilde{t} = 2$, substituting this value into (7.6) allows us to rewrite p as

$$\mathsf{p} = \frac{2-2^2 \pm 2\sqrt{2^2-4+\alpha^2}}{2+\alpha 2} = \frac{-1 \pm \alpha}{1+\alpha}. \tag{7.7}$$

For the positive root

$$\mathsf{p}_1 = \frac{\alpha-1}{\alpha+1}$$

we have that $-1 < \mathsf{p}_1 < 1$ for all choices of $\alpha > 0$. The negative root is

$$\mathsf{p}_2 = \frac{-(\alpha+1)}{\alpha+1} = -1$$

so that p_2 is only marginally stable. Hence, overall $\Delta\tilde{t} = 2$ gives us an error term which is marginally stable.

Next we look at $0 < \Delta\tilde{t} < 2$. Since $\Delta\tilde{t}^2 - 4 < 0$ there will be cases when p will have complex roots. We therefore need to split this further into two parts:
$\Delta\tilde{t}^2 + \alpha^2 - 4 < 0 \longrightarrow$ complex p,
$\Delta\tilde{t}^2 + \alpha^2 - 4 < 0 \longrightarrow$ real p.

For the complex roots, the modulus of p becomes

$$\begin{aligned} |\mathsf{p}| &= \sqrt{\left[\left(\frac{2-\Delta\tilde{t}^2}{2+\alpha\Delta\tilde{t}}\right)^2 + \frac{\Delta\tilde{t}^2(4-\Delta\tilde{t}^2-\alpha^2)}{(2+\alpha\Delta\tilde{t})^2}\right]} \\ &= \frac{\sqrt{4-\alpha^2\Delta\tilde{t}^2}}{2+\alpha\Delta\tilde{t}} = \sqrt{\left(\frac{2-\alpha\Delta\tilde{t}}{2+\alpha\Delta\tilde{t}}\right)} \end{aligned} \tag{7.8}$$

We know that $-1 < \frac{2-\alpha\Delta\tilde{t}}{2+\alpha\Delta\tilde{t}} < 1$ for all $\alpha > 0$ with $0 < \Delta\tilde{t} < 2$, so $|\mathsf{p}| < 1$ and the complex roots of p are stable.

For the real roots of p we write $|\mathsf{p}|$ in the following form,

$$\begin{aligned} |\mathsf{p}_1| < 1 \quad &: \quad -\alpha\Delta\tilde{t} < 4 - \Delta\tilde{t}^2 + \Delta\tilde{t}\sqrt{\Delta\tilde{t}^2+\alpha^2-4} < 4 + \alpha\Delta\tilde{t} \\ |\mathsf{p}_2| < 1 \quad &: \quad -\alpha\Delta\tilde{t} < 4 - \Delta\tilde{t}^2 - \Delta\tilde{t}\sqrt{\Delta\tilde{t}^2+\alpha^2-4} < 4 + \alpha\Delta\tilde{t} \end{aligned} \tag{7.9}$$

First considering $|\mathsf{p}_1| < 1$, we now use the following inequality relation

$$\sqrt{a-b} < \sqrt{a} \qquad \text{for} \qquad a > 0 \qquad \text{and} \qquad b > 0 \tag{7.10}$$

Since $\Delta\tilde{t}^2 - 4 < 0$ we can say that $\Delta\tilde{t}\sqrt{\Delta\tilde{t}^2+\alpha^2-4} < \Delta\tilde{t}\sqrt{\alpha^2}$ and thus

$$4 - \Delta\tilde{t}^2 + \Delta\tilde{t}\sqrt{\Delta\tilde{t}^2+\alpha^2-4} < 4 + \alpha\Delta\tilde{t}$$

as required to satisfy the second half of the inequality. Concentrating on the first half of the inequality

$$-\alpha\Delta\tilde{t} < 4 - \Delta\mathbf{t}^2 + \Delta\tilde{t}\sqrt{\Delta\tilde{t}^2+\alpha^2-4}$$

we can see that the left hand side is negative and, since $4 - \Delta\tilde{t}^2 > 0$, the right hand side is positive, so the inequality is true. Now we can look at $|\mathsf{p}_2| < 1$. The second half of the inequality

$$4 - \Delta\tilde{t}^2 - \Delta\tilde{t}\sqrt{\Delta\tilde{t}^2+\alpha^2-4} < 4 + \alpha\Delta\tilde{t}$$

is true due to the fact that $\sqrt{\Delta\tilde{t}^2+\alpha^2-4} > 0$. If we subtract 4 from each side we are left with a negative left hand side and a positive right hand side. It was shown previously that $\Delta\tilde{t}\sqrt{\Delta\tilde{t}^2+\alpha^2-4} < \Delta\tilde{t}\alpha$ which implies that $-\Delta\tilde{t}\alpha < -\Delta\tilde{t}\sqrt{\Delta\tilde{t}^2+\alpha^2-4}$. Also using the

fact that $4 - \Delta\tilde{t}^2 < 0$ we get

$$-\alpha\Delta\tilde{t} < 4 - \Delta\tilde{t}^2 + \Delta\tilde{t}\sqrt{\Delta\tilde{t}^2 + \alpha^2 - 4}$$

as required to satisfy the remaining half of the inequality.

This confirms that $|\mathsf{p}| < 1$ for the case of real or complex roots, so the error term is stable for all $\alpha > 0$ when $0 < \Delta\tilde{t} < 2$.

Finally we will analyse $\Delta\tilde{t} > 2$. Due to the fact that $\sqrt{\Delta\tilde{t}^2 + \alpha^2 - 4} > 0$, p will always have real roots, so once again p_1 and p_2 will satisfy the inequalities (7.9). First we look at $|\mathsf{p}_1| < 1$, for the error term to be stable we need

$$-\alpha\Delta\tilde{t} < 4 - \Delta\tilde{t}^2 + \Delta\tilde{t}\sqrt{\Delta\tilde{t}^2 + \alpha^2 - 4}$$

which can be rewritten as

$$-\alpha\Delta\tilde{t} < -(\sqrt{\Delta\tilde{t}^2 - 4}\,)^2 + \Delta\tilde{t}\sqrt{(\Delta\tilde{t}^2 - 4) + \alpha^2}$$

We can show that this inequality is true by proving that the right hand side is greater than zero. Using another simple inequality relation

$$\sqrt{a+b} > \sqrt{a} \qquad \text{for} \qquad a > 0 \qquad \text{and} \qquad b > 0 \tag{7.11}$$

we define $\sqrt{(\Delta\tilde{t}^2 - 4) + \alpha^2} > \sqrt{\Delta\tilde{t}^2 - 4}$. Since (7.10) gives us $\sqrt{\Delta\tilde{t}^2 - 4} < \Delta\tilde{t}$ we can therefore say that

$$-(\sqrt{\Delta\tilde{t}^2 - 4}\,)^2 + \Delta\tilde{t}\sqrt{(\Delta\tilde{t}^2 - 4) + \alpha^2} > \sqrt{\Delta\tilde{t}^2 - 4}(\Delta\tilde{t} - \sqrt{\Delta\tilde{t}^2 - 4}) > 0$$

which completes the proof. Hence p_1 leads to a stable error term. Now we will look at $|\mathsf{p}_2| < 1$. Using (7.11) and the knowledge that $\Delta\tilde{t}^2 - 4 > 0$, leads to $-\Delta\tilde{t}\sqrt{\Delta\tilde{t}^2 + \alpha^2 - 4} < -\Delta\tilde{t}\alpha$. The assumption $\Delta\tilde{t} > 2$ implies that $2 - \Delta\tilde{t}^2 < -2$. Adding these together results in

$$2 - \Delta\tilde{t}^2 - \Delta\tilde{t}\sqrt{\Delta\tilde{t}^2 + \alpha^2 - 4} < -2 - \alpha\Delta\tilde{t}$$

which contradicts the original inequality (7.9). Hence p_2 leads to an unstable error term. This means that the system is unstable when $\Delta\tilde{t} > 2$.

To summarise:

$$\Delta\tilde{t} = 2 \longrightarrow \begin{cases} |p_1| < 1 & \text{real root} \\ |p_2| = 1 & \text{real root} \quad \text{error term marginally stable} \end{cases}$$

$$0 < \Delta\tilde{t} < 2 \longrightarrow \begin{cases} |p| < 1 & \text{complex roots} \\ |p_1| < 1 & \text{real root} \quad \text{error term stable} \\ |p_2| < 1 & \text{real root} \end{cases}$$

$$\Delta\tilde{t} > 2 \longrightarrow \begin{cases} |p_1| < 1 & \text{real root} \\ |p_2| > 1 & \text{real root} \quad \text{error term unstable} \end{cases}$$

Bibliography

[1] Private communication, Schlumberger Cambridge Research

[2] Berkley, *Sir Isaac Newton's Mathematical Principles of Natural Philosophy and his System of the World*, University of California Press: 5th printing (1962)

[3] Ockendon, H. & Ockendon, J.R. *Viscous Flow*, Cambridge University Press, 1-13, (1995)

[4] Bird, R.B. Armstrong, R.C. & Hassager, O. *Dynamics of Polymeric Liquids Vol 1, Fluid Mechanics*, John Wiley & Sons, Inc, (1987)

[5] Besq, A. Malfoy, C. Pantet, A. Monnet, P. Righi, D. Physiochemical characterisation and flow properties of some bentonite muds, *Applied Clay Science*, **23**, 275-286, (2003)

[6] Alderman, N.J. Maitland, G.C. Rheology of water-based muds at high temperatures and pressures, Scientific report, Schlumberger, Cambridge, (1988)

[7] Parlaktuna, O. *Introduction to petroleum engineering*, (2002)

[8] Kawata, M. Kurase, K. Yoshida, K.*Proc. 5th Int. Congr. on Rheology*, **1**, 293-295, (1969)

[9] Joseph, D.D. Liu, Y.J. Poletto, M. & Feng, J. Aggregation and dispersion of spheres falling in viscoelastic liquids, *J. Non-Newt. Fluid Mech.*, **54**, 45-86, (1994)

[10] Maude, A.D. End effects in a falling-sphere viscometer, *Brit. J. Appl. Phys.*, **12**, 453, (1961)

[11] Davis, A.M.J. & Brenner, H. The falling-needle viscometer, *Phys of Fluids*, **13**, 3086-3088, (2001)

[12] Oliveira, C.M.B.P *Viscosity of Liquid Hydrocarbons at High Pressure*, thesis, Imperial College of London, (1991)

[13] Kestin, J. & Persen, L.N. Proceedings ninth itern. Congress of Appl. Mech., Brussels, **v3**, 326, (1956)

[14] Newell, G.F. *Z. angew. Math. Phys.* (1959)

[15] Kestin, J. & Leidenfrost, W. An absolute determination of the viscosity of eleven gases over a range of pressures, *Physica* **25**, 1033-1062

[16] Dipippo, R. Kestin, J. & Whitelaw, J.H. A high-temperature oscillating-disc viscometer, *Physica* **32**, 2064-2080, (1966)

[17] Diller, D.E. Measurements of the Viscosity of Parahydrogen, *J Chem Phys*, **42**, 2089-2096, (1965)

[18] Tadros, Th.F. *Solid/Liquid Dispersions*, Academic Press Inc, (1987)

[19] Stokes, Sir G.G. *Mathematical and Physical Papers, Vol. 3*, Cambridge University Press, 38-55, (1901)

[20] Tough, J.T McCormick W.D. & Dash, J.G. Viscosity of Liquid He II, *Phys. Rev.*, **132**, 2373-2378, (1963)

[21] Karnus, A.I. Slyusar, V.P. Rudento, N.S. & Vinokurov, E.I. High-Pressure String Viscometer with Wide Working Temperature Range, *Kharkov Institute of Technical Physics*, Academy of Sciences of the Ukrainian SSR. Translated from Pribory i Tekhnika Eksperimenta, **1**, 256-266, (1977)

[22] Charles, E. Molenat, J. Abachi, H. Michel, J. & Malbrunot, P. The Use of a Vibrating Wire Viscometer in Liquids, *J. Phys. E: Sci. Instrum.*, **13**, 829-834, (1980)

[23] Mostert, R. Van der Gulik, P.S. & Van den Berg, H.R. The Working Equations of a Vibrating Wire Viscometer, *Physica A*, **156**, 909-920, (1989)

[24] Retsina, T. Richardson, S.M. & Wakeham, W.A. The theory of a vibrating-rod viscometer, *Appl. Sci. Res.*, **43**, 325-346, (1987)

[25] Assael, M.J. Oliveira, C.P. Papadaki, M. & Wakeham, W.A. Vibrating-wire viscometers for liquids at high pressures, *Int. J. Thermophys.*, **13**, 593-615, (1992)

[26] Sittel, K. Rouse, P.E. & Bailey, E.D. Method for determining the viscoelastic properties of dilute polymer solutions at audio-frequencies, *J. Appl. Phys.*, **23**, 1312-1320, (1954)

[27] Diller, D.E. Measurements of the viscosity of parahydrogen, *J. Chem. Phys.*, **42**, 2089-2093, (1965)

[28] Konno, A. Makino, S. & Kaneko, M. Measurements of the mechanical properties of a polymer solution, *Japan. J. Appl. Phys.*, **7**, 89-90, (1998)

[29] Schrag, J.L. & Johnson, R.M. Application of the Birnboim multiple lumped resonator principle to viscoelastic measurements of dilute macromolecular solutions, *Rev. Sci. Instrum.*, **42**, 224-232, (1971)

[30] Torklep, K. & Oye, H.A. An absolute oscillating-cylinder (or cup) viscometer for high temperatures, *J. Phys. E: Sci. Instrum.*, **12**, 875-885, (1979)

[31] Assael, M.J. Oliveira, C.P. Papadaki, M. & Wakeham, W.A. An absolute vibrating-wire viscometer for liquids at high pressures, *Int. J. Thermophys.*, **12**, 231-243, (1991)

[32] Stokich, T.M. Radtke, D.R. White, C.C. & Schrag, J.L. An instrument for precise measurement of viscoelastic properties of low-viscosity dilute macromolecular solutions at frequencies from 20 to 500 kHz, *J. Rheol.*, **38**, 1195-1210, (1994)

[33] Gourgouillon, D. Avelino, H.M.N.T. Fareleira, J.M.N.A. & Nunes da Ponte, M. Simultaneous viscosity and density measurement of supercritical CO2-saturated PEG 400, *J. Supercritical Fluids*, **13**, 177-185, (1998)

[34] Martin, S.J. Butler, M.A. Spates, J.J. Mitchell, M.A. & Schubert, W.K. Flexural plate wave resonator excited with Lorentz forces, *J. Appl. Phys.*, **83**, 4589-4601, (1998)

[35] Teston, F. Feuillard, G. Tessier, L. Tran Hu Hue, L.P. & Lethiecq, M. Analysis of the coupling between shear horizontal plate waves and liquids: Application to the measurement of the shear rigidity modulus of glycerol solutions, *J. Appl. Phys.*, **87**, 689-694, (2000)

[36] Romoscanu, A.I. Sayir, M.B. Hausler, K. & Servais, C. High frequency probe for the measurement of the complex viscosity of liquids, *Meas. Sci. Technol.*, **14**, 451-462, (2003)

[37] Goodwin, A.R.H. Donzier, E.P. Vancauwenberghe, O. Fitt, A.D. Ronaldson, K.A. Wakeham, W.A. Manrique de Lara, M. Marty, F. & Mercier, B. A vibrating edge supported plate, fabricated by the methods of micro electro mechanical system for the silmultaneous measurement of density and viscosity: Results for methylbenzene and octane at temperatures between (323 and 423) K and pressures in the range (0.1 to 68) MPa, *J. Chem. Eng. Data*, **51**, 190-208, (2006)

[38] Spiering, V.L. Bouwstra, S. Spiering, R. On chip decoupling zone for package-stress reduction, *Sensors and Actuators*, **A.39**, 149-156, (1993)

[39] Petersen, K.E. Silicon as a mechanical material, *Proc. IEEE.* Vol. 70, No. 5, (1982)

[40] Claire Jakeways, Anthony R. H. Goodwin and Maria Manrique de Lara, Private communication, Schlumberger Cambridge Research

[41] Goodwin, A.R.H. Meeten, G.H. Research note, Schlumberger Cambridge Research, (2000)

[42] Jensenius, H. et al., *Phys. Rev. Lett.*, (1997)

[43] Landau, L.D., Lifshitz, E.M. *Fluid Mechanics*, Pergamon Press Ltd, (1959)

[44] Acheson, D.J. *Elementary Fluid Dynamics*, Clarendon Press, 33-38, (1990)

[45] Moiseiwitsch, B.L. *Integral equations*, Longman Mathematical Texts, (1977)

[46] Wheatley, G. *Applied Numerical Analysis*, World student series, (1997)

[47] Luchko, Y. F. Srivastava, H.M. The exact solution of certain differential equations of fractional order by using operational calculus, *Computers Math. Applic.*, **29**, (1995)

[48] Cumberbatch, E. & Fitt, A. *Mathematical Modelling*, Cambridge University Press, 66-79, (2001)

[49] Sadar, J.E. Fequency response of cantilever beams immersed in viscous fluids with applications to the atomic force microscope, *J. Appl. Phys.*, Vol. 84, No. 1, 64-76 , (1998)

[50] Evans, G., Blackledge, J. & Yardley, P. *Analytic Methods for Partial Differential Equations*, Springer-Verlag London Limited, (2000)

[51] Hinch, E.J. *Perturbation Methods*, Cambridge University Press, 87-90, (1991)

[52] Van Dyke, M. *Perturbation Methods in Fluid Mechanics*, Academic Press, 87-90, (1964)

[53] Kim, M.U Slow Viscous Flow around a Vertical Fence on a Plane, *J. Phys. Soc. Jpn.*, **49**, 2387-2391, (1980)

[54] Langois, W.E. *Slow viscous flow*, MacMillon New York, 1964

[55] Lighthill, J. Flagellar Hydrodynamics, *SIAM Rev*, **18**, 161-231, (1976)

[56] Lighthill, J. Reinterpreting the basic theorem of flagellar hydrodynamics, *J. Eng. Math*, **30**, 25-34, (1996)

[57] Hancock, G.J. The self-propulsion of microscopic organisms through liquids, *Proc. Roy. Soc. Ser. A*, **217**, 96-121, (1973)

[58] Taylor, Sir G. Flagellar Hydrodynamics, *Proc. Roy. Soc. Ser. A*, **209**, 447-461, (1951)

[59] Cortez, R. The Method of Regularized Stokeslets, *SIAM J. Sci.Comput.*, **23**, 1204-1225, (2001)

[60] Blake, J.R. A model for the micro-structure in ciliated organisms, *J. Fluid Mech.*, **55**, 1-23, (1972)

[61] Liron, N. Mochon, S. The discrete-cilia approach to propulsion of ciliated micro-organisms, *J. Fluid Mech.*, **75**, 593-607, (1976)

[62] Blake, J.R. A note on the image system for a stokeslet in a no-slip boundary, *Proc. Camb. Phil. Soc.*, **70**, 303-310, (1971)

[63] Liron, N. Stokes flow due to infinite arrays of stokeslets in three dimensions, *J. Eng. Math.*, **30**, 267-297, (1996)

[64] Adams, R.A. *Calculus, A Complete Course*, Addison-Wesley Publishers Limited, (1995)

[65] Goodwin, A.R.H. Manrique de Lara, M. Meeten, G.H. and Pelham, S.E. Private communication, Schlumberger Cambridge Research, (2000)

[66] Gilat, A. *MATLAB, An Introduction With Applications*, John Wiley & Sons Inc, (2005)

[67] Goodwin, A.R.H. Fitt, A.D. Ronaldson, K.A. and Wakeham, W.A. A Vibrating Plate Fabricated by the Methods of Microelectromechanical Systems (MEMS) for the Simultaneous Measurement of Density and Viscosity: Results for Argon at Temperatures Between 323 and 423K at Pressures up to 68 MPa, *Int. J. Thermophys.*, **27**, 1650-1676, (2006)

[68] Ronaldson, K.A. Fitt, A.D. Goodwin, A.R.H. and Wakeham, W.A. Transversely Oscillating MEMS Viscometer: The Spider, *Int. J. Thermophys.*, **27**, 1677-1695, (2006)